

Self-Organizing n-type Perylene Derivatives for  
Organic Photovoltaics –  
Synthesis, Characterization and Application

DISSERTATION

zur Erlangung des akademischen Grades  
eines Doktors der Naturwissenschaften (Dr. rer. nat.)  
im Fach Chemie der Fakultät für  
Biologie, Chemie und Geowissenschaften der Universität Bayreuth

vorgelegt von

**André Dominik Wicklein**

geboren in München / Deutschland

Bayreuth, 2010



Die vorliegende Arbeit wurde in der Zeit von November 2006 bis April 2010 am Lehrstuhl für Angewandte Funktionspolymere/Makromolekulare Chemie I der Universität Bayreuth unter der Betreuung von Prof. Dr. Mukundan Thelakkat angefertigt.

Vollständiger Abdruck der von der Fakultät für Biologie, Chemie und Geowissenschaften der Universität Bayreuth genehmigten Dissertation zur Erlangung des akademischen Grades eines Doktors der Naturwissenschaften (Dr. rer. nat.)

Dissertation eingereicht am:	09. April 2010
Zulassung durch die Promotionskommission:	28. April 2010
Wissenschaftliches Kolloquium:	21. Juli 2010

*Prüfungsausschuss:*

Prof. Dr. Mukundan Thelakkat	(Erstgutachter)
Prof. Dr. Karlheinz Seifert	(Zweitgutachter)
Prof. Dr. Peter Strohriegl	(Vorsitzender)
Prof. Dr. Helmut G. Alt	

Amtierender Dekan: Prof. Dr. Stephan Clemens



*Nicht Kunst und Wissenschaft allein,  
Geduld will bei dem Werke sein.*

(J. W. Goethe, Faust I)



*Für meine Familie*

Corinna, Alfred und Martha



---

**TABLE OF CONTENTS**

<b>SUMMARY / ZUSAMMENFASSUNG</b>	<b>1</b>
<b>1. INTRODUCTION</b>	<b>5</b>
1.1 ORGANIC ELECTRONICS	5
1.2 ORGANIC PHOTOVOLTAICS	6
1.3 SEMICONDUCTING MATERIALS BASED ON SELF-ORGANIZING $\pi$ -CONJUGATED SYSTEMS OF SMALL MOLECULES	11
1.4 OBJECTIVE OF THIS THESIS	25
<b>2. THESIS OVERVIEW</b>	<b>33</b>
INDIVIDUAL CONTRIBUTIONS TO JOINT PUBLICATIONS	51
<b>3. SWALLOW-TAIL SUBSTITUTED LIQUID CRYSTALLINE PERYLENE BISIMIDES – SYNTHESIS &amp; THERMOTROPIC PROPERTIES</b>	<b>55</b>
<b>4. SYNTHESIS AND STRUCTURE ELUCIDATION OF DISCOTIC LIQUID CRYSTALLINE PERYLENE IMIDE BENZIMIDAZOLE</b>	<b>95</b>
<b>5. ROOM TEMPERATURE LIQUID CRYSTALLINE PERYLENE DIESTER BENZIMIDAZOLES WITH EXTENDED ABSORPTION</b>	<b>117</b>
<b>6. SELF-ASSEMBLY OF DONOR/ACCEPTOR DISCOGENS IN BLENDS: A STRUCTURAL STUDY OF BINARY Cu-PHTHALOCYANINE – PERYLENE BISIMIDE SYSTEMS</b>	<b>143</b>
<b>7. SELF-ASSEMBLY OF SEMICONDUCTOR NANOWIRES FOR PHOTOINDUCED CHARGE SEPARATION</b>	<b>161</b>
<b>8. APPENDIX: SOLVENT AND HYDROGEN-BOND DIRECTED SELF-ASSEMBLY OF PERYLENE BISIMIDES</b>	<b>179</b>
<b>LIST OF PUBLICATIONS</b>	<b>197</b>
<b>DANKSAGUNG</b>	<b>199</b>
<b>ERKLÄRUNG</b>	<b>201</b>

---

## **SUMMARY**

This thesis deals with the tailor-made synthesis and characterization of different self-organizing perylene derivatives as electronically active n-type semiconducting dyes for application in organic photovoltaic devices (OPV). Two distinct supramolecular self-organization phenomena of well-defined molecular architectures of perylene dyes are in the focus: Liquid crystalline ordering of discotic shaped molecules (DLCs) and hydrogen-bond or solvent directed self-assembly to organogels or nanostructured networks. Both self-organization principles are promising approaches to improve device efficiency. Columnar liquid crystalline ordering allows for a high intracolumnar charge carrier mobility in these quasi one-dimensional “nanowires” and nanostructured networks provide a large interface area between the acceptor and a suitable donor material, together with well defined charge transport pathways in the bulk. In order to determine self-organization processes, appropriate substitution patterns at the perylene core, including suitable synthetic strategies have to be developed. In this context also the extension of absorption in the visible wavelength region of these dyes is an important aspect with respect to light-harvesting properties. Thermotropic phase behaviour of the synthesized discogens was analyzed extensively by different methods, like differential scanning calorimetry (DSC), temperature-controlled polarization optical microscopy (POM) and temperature-controlled X-ray diffraction (XRD) experiments. Morphology of nanostructured assemblies were studied by a combination of scanning electron microscopy (SEM) and atomic force microscopy (AFM).

In a first part of the dissertation, it was possible to determine a comprehensive structure-property relationship to understand fundamental molecular design requirements to induce liquid crystalline phases in perylene bisimide (PBI) dyes. Therefore, a series of differently *N*-substituted PBIs was synthesized, by two different synthetic routes, which are also suitable for an unsymmetrical *N*-substitution pattern of these molecules. The incorporation of branched oligooxyethylene sidechains, alone or in combination with branched alkyl sidechains, was crucial for generating broad columnar hexagonal ( $Col_h$ ) mesophases with intracolumnar long-range order arising from strong  $\pi$ - $\pi$  interactions between cofacially orientated perylene moieties. Additionally, the melting point to the liquid crystalline phase as well as clearing temperature could be controlled very efficiently by an unsymmetrical *N*-substitution pattern of the PBI dyes.

Subsequently, novel classes of n-type semiconductors with an extended  $\pi$ -conjugation system of the mesogens and an asymmetric substitution pattern, such as perylene imide benzimidazole (PIBI) and perylene diester benzimidazoles (PDBIs), were synthesized via straightforward synthetic strategies and the thermotropic packing behavior characterized thoroughly. It was demonstrated for both classes, that the introduction of a fused benzimidazole moiety on the perylene core significantly extends the absorption in the red wavelength regime up to 680 nm. Additionally, these dyes exhibit for the first time self-organization ability into columnar hexagonal mesophases, even at room temperature. Besides, also compounds with a columnar hexagonal plastic phase ( $Col_{hp}$ ) or crystalline lamellar phases ( $Cr_L$ ) were confirmed. In combination with the outstanding

improvement of absorption properties of PBI and PDBIs, such systems are extremely interesting for applications requiring high order in the molecular arrangement and are thus highly promising candidates for utilization in organic electronics.

In a next step towards organic photovoltaics, supramolecular architectures formed in different discotic, all-liquid crystalline donor/acceptor (D-A) blends consisting of copper phthalocyanine and PBI dyes, were studied, in order to control their miscibility and morphology. Supramolecular organization was adjusted by utilizing hydrophobic-hydrophilic interactions of the sidechains of the discogens. Hence, a blend system with a substantially enhanced  $Col_h$ -phase range combined with extended intracolumnar long-range order of the mesogen as well as a blend with a strong phase separation could be obtained. Both blend systems exhibit strong complementary absorption for efficient light-harvesting and have shown efficient photoinduced charge transfer upon PBI excitation in photoluminescence experiments.

In a second part of the thesis, an universal concept to generate self-assembled D-A interpenetrating nanostructures with inherent morphological stability by an organogel/polymer approach is presented successfully. Therefore, hydrogen bond directed self-assembly of a PBI organogelator in presence of an amorphous hole conducting polymer matrix of poly(vinyl-dimethoxytetraphenylbenzidine) was utilized to generate the active D-A interface layer. Self-assembly process and interface generation were carried out either stepwise or in a single-step methodology. The presence of percolation paths for photogenerated electrons and holes in such organogel/polymer composite material was demonstrated directly in photovoltaic devices, which delivered appreciable photocurrents and photovoltages.

The limitation of this concept is the low content of the active n-type perylene moiety. Therefore, synthesis of newly designed, self-organizing PBIs with an increased chromophore content was performed. In this context, hydrogen-bond directed self-assembly of an amide group containing PBI and solvent directed self-assembly of amphiphilic substituted PBIs were employed. It could be shown, that fibrillar nanostructures of PBIs with a high degree of  $\pi$ - $\pi$  stacking of the chromophores are accessible via both strategies.

To sum up, this work demonstrates successfully the tailor-made molecular design and efficient synthesis of various self-organizing n-type perylene derivatives with outstanding absorption properties and diverse molecular arrangements. Moreover, an elaborate incorporation of such self-assembled functional dyes into organic photovoltaic devices is demonstrated.

## ZUSAMMENFASSUNG

Diese Dissertation beschäftigt sich mit der maßgeschneiderten Synthese und der Charakterisierung verschiedener selbst organisierender Perylen-derivate als n-Typ Halbleiter-Farbstoff zur Anwendung in organischen Photovoltaik-Bauelementen. Dabei liegt der Schwerpunkt auf zwei unterschiedlichen Selbstorganisationsphänomenen von Perylenfarbstoffen mit definierter Molekülstruktur: Zum Einen auf der thermotropen flüssigkristallinen Anordnung diskotisch geformter Moleküle, zum Anderen auf der Selbstanordnung zu Organogelen und nanostrukturierten Netzwerken mit Hilfe von Wasserstoffbrückenbindungen oder geeigneter Lösungsmittel. Beide Formen der Selbstorganisation sind vielversprechende Ansätze zur Erhöhung des Wirkungsgrades von Solarzellen. So werden bei einer kolumnaren flüssigkristallinen Ordnung hohe intrakolumnare Ladungsträgermobilitäten in solch quasi eindimensionalen „Nanodrähten“ ermöglicht. Ein nanostrukturiertes Netzwerk hingegen gewährleistet definierte Ladungstransportwege sowie eine große Grenzfläche zwischen dem Elektronenakzeptor und einem geeigneten Elektronendonator. Zur zielgerichteten Steuerung dieser Selbstorganisationsprozesse wurden geeignete Substitutionsmuster am Perylengerüst sowie adäquate Syntheserouten entwickelt. In diesem Zusammenhang stellte auch die Erweiterung der Absorption im sichtbaren Wellenlängenbereich mit dem Ziel einer effektiven Lichtsammlung einen wichtigen Aspekt dieser Arbeit dar. Das thermotrope Phasenverhalten der synthetisierten, diskotischen Perylenfarbstoffe wurde durch Differentielle Wärmeflusskalorimetrie (DSC), temperaturabhängige Polarisationsmikroskopie sowie temperaturabhängige Röntgendiffraktometrie umfassend untersucht. Morphologien unterschiedlicher Nanostrukturen wurden mittels der Rasterelektronenmikroskopie (REM) und der Rasterkraftmikroskopie (AFM) charakterisiert.

Im ersten Abschnitt dieser Dissertation stand die Ermittlung umfangreicher Struktur-Eigenschafts-Beziehungen bezüglich grundlegender Anforderungen an das molekulare Design zur Erzeugung flüssigkristalliner Phasen in Perylenbisimid (PBI) Farbstoffen im Zentrum. Zu diesem Zweck wurde eine Reihe diverser symmetrisch und unsymmetrisch *N*-substituierter PBIs unter Verwendung zweier unterschiedlicher Synthesewege hergestellt. Der Einsatz verzweigter Oligo(oxyethylen)-Seitenketten, alleine oder in Kombination mit verzweigten Alkyl-Seitenketten, war schließlich entscheidend, um kolumnar hexagonale Mesophasen ( $Col_h$ ) über einen breiten Temperaturbereich zu erhalten. Diese Mesophasen zeichneten sich zudem durch eine weitreichende intrakolumnare Ordnung der cofacial orientierten Peryleneinheiten aus. Des Weiteren konnten durch ein unsymmetrisches *N*-Substitutionsmuster der PBIs sowohl der Schmelzpunkt als auch der Klärpunkt wirksam reguliert werden.

Um den Absorptionsbereich der Farbstoffe zu vergrößern wurde nun das  $\pi$ -Konjugationssystem der mesogenen Einheit durch Einführung einer Benzimidazol-Gruppe erweitert und zwei Perylenklassen mit einem unsymmetrischen Substitutionsmuster am Perylengerüst synthetisiert. Für beide Farbstoffklassen, das Perylen-tetracarbonsäure-imid-benzimidazol (PIBI) und die Perylen-tetracarbonsäure-diester-benzimidazole (PDBIs), konnte gezeigt werden, dass sich auf diese Weise die Absorption im roten Spektralbereich (bis 680 nm) signifikant erweitern lässt.

Ferner ließ sich für diese Klasse von Mesogenen zum ersten Mal die Existenz kolumnar hexagonaler Phasen, welche teilweise auch bei Raumtemperatur existieren, nachweisen. Zudem konnten weitere Anordnungen, wie kolumnar hexagonal plastische ( $\text{Col}_{\text{hp}}$ ) oder kristallin lamellare ( $\text{Cr}_l$ ) Phasen erzeugt werden. Dies und die außerordentliche Verbesserung der Absorptionseigenschaften machen PIBI und PDBIs für Anwendungen interessant, welche ein hohes Maß an molekularer Ordnung erfordern. Für Applikationen im Bereich der organischen Elektronik sind diese Verbindungen somit sehr vielversprechend.

In einem weiteren Schritt auf dem Weg zu organischen Solarzellen wurde die supramolekulare Organisation in verschiedenen flüssigkristallinen Donor/Akzeptor (D-A) Mischungen, bestehend aus Cu-Phthalocyaninen in Kombination mit PBIs, studiert. Diese ließ sich hinsichtlich Mischbarkeit und Morphologie anhand von hydrophob-hydrophilen Wechselwirkungen der Seitenketten der diskotischen Komponenten gezielt beeinflussen. Das Ergebnis war eine Mischung mit Phasenseparation sowie eine Mischung, welche sich durch eine wesentlich erweiterbare  $\text{Col}_h$ -Phase und weitreichende intrakolumnare Ordnung auszeichnet. Beide Systeme weisen eine günstige komplementäre Absorption zur Lichtsammlung auf. Des Weiteren konnte in Photolumineszenz-Experimenten ein photoinduzierter Ladungstransfer durch PBI Anregung nachgewiesen werden.

Der zweite Teil dieser Dissertation beinhaltet ein Konzept zur Ausbildung von selbst anordnenden D-A interpenetrierenden Nanostrukturen mit morphologischer Stabilität mittels eines Organogel/Polymer Ansatzes. Durch Wasserstoffbrücken unterstützte Selbstorganisation eines PBI Organogelators in Gegenwart einer amorphen, polymerbasierten Lochleitermatrix aus Poly(vinylidimethoxytetraphenylbenzidin) konnte eine aktive D-A Grenzfläche zwischen beiden Materialien erzeugt werden. Der Selbstanordnungsprozess und die Erzeugung einer Grenzfläche wurden sowohl schrittweise als auch in einem Einzelschritt ausgeführt. Die Anwesenheit von Ladungstransportwegen für photogenerierte Elektronen und Löcher in diesem Organogel/Polymer Kompositmaterial konnte durch Messung von nennenswerten Photoströmen und Photospannungen direkt in Solarzellen nachgewiesen werden.

Eine Einschränkung in diesem Konzept stellte der geringe Anteil an der aktiven n-Typ Perylenkomponente dar. Deshalb wurden in einem weiteren Schritt neue selbst organisierende PBIs mit erhöhtem Chromophorgehalt synthetisiert. Ein erster Ansatz nutzt die Wasserstoffbrücken gesteuerte Selbstanordnung eines PBI, dessen Seitenkette eine Amidgruppe enthält. Eine weitere Möglichkeit besteht in einer durch Lösungsmittel unterstützten Selbstanordnung von PBIs mit amphiphilem *N*-Substitutionsmuster. Die Ausbildung von fibrillaren Nanostrukturen mit einem hohen Grad an  $\pi$ - $\pi$  Stapel-Wechselwirkung der Chromophore konnte für beide Strategien aufgezeigt werden.

Zusammenfassend dargestellt präsentiert diese Dissertation das zielgerichtete molekulare Design und die effektive Synthese verschiedenartiger, selbst organisierender n-Typ Perylenderivate mit hervorragenden Absorptionseigenschaften und diversen molekularen Anordnungen. Darüber hinaus wurde gezeigt, wie solch selbst anordnende Farbstoffe geschickt in organischen Solarzellen integriert werden können.

## 1. INTRODUCTION

### 1.1 ORGANIC ELECTRONICS

Recently, electronics based upon organic thin-film materials started to make considerably inroads into commercial markets, and if the sector continues its rapid growth, it will strongly influence our technological environment. The scientific field of organic electronics<sup>1,2</sup>, that is in general the use of polymeric as well as low-molecular  $\pi$ -conjugated molecules as active materials in electronic devices, is rapidly growing due to the auspicious prospect of the creation of a completely new industry in consumer electronics. The door towards organic electronics was pushed open with the discovery of conducting polymers by A. Heeger, A. MacDiarmid and H. Shirakawa (nobel prize in chemistry in 2000) in 1977.<sup>3</sup> Since then, organic materials have found manifold potential applications in optoelectronic devices such as organic field effect transistors (OFET)<sup>4,5</sup>, organic light emitting diodes (OLED)<sup>6,7</sup> or organic photovoltaics (OPV)<sup>8,9</sup>. Compared to classical inorganic semiconductors, organic materials offer the advantages of low-cost manufacturing associated with facile solution processability onto flexible, large-area substrates.<sup>10,11</sup> A recent forecast predicted an increase of the market of "Printed, Organic & Flexible Electronics" of about 57 billion US-dollars until 2019.<sup>12</sup> Another striking advantage of organic materials compared to inorganic materials is the possibility of tailoring properties of organic molecules on a molecular level. Thus, devices are also formidable tools in order to probe basic structure-performance relationships that govern the physics and chemistry of organic semiconductors. Nowadays, organic light emitting diodes and displays are already commercially available for small displays or cell phones, whereas for the inverse process - converting photons into electricity - the limited efficiency and limited long-term stability has hindered the path towards commercialization so far.

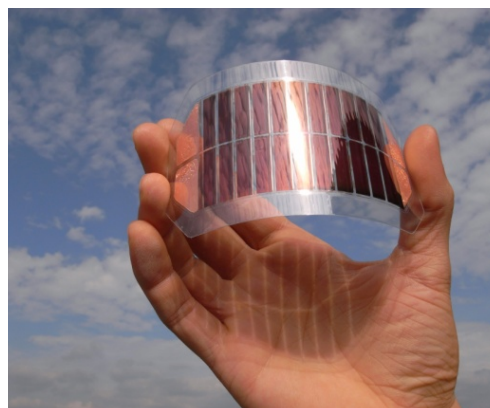


**Figure 1.** Flexible module of organic solar cells (reproduced from Fraunhofer Institute ISE in Freiburg, Germany).

Research in organic photovoltaics<sup>13</sup> as emerging technology is driven by the demand for cost-efficient, renewable and nonpolluting energy sources due to the availability of the quasi indefinite amount of solar energy. One hour of solar irradiation onto the earth's surface provides 14 terawatt-years of energy, corresponding approximately to the world's total annual energy consumption.<sup>14,15</sup> If it would be easy to capture the solar radiation and store the energy efficiently, there would be no global scarcity of renewable and clean energy. Organic solar devices can basically be divided into several classes by different approaches. Today's most efficient, dye-sensitized solar cells (DSSC) with a liquid electrolyte (usually an electrolyte containing

iodide/triiodide redox system) show efficiencies up to 10 - 11.5 %, <sup>16,17</sup> whereas for solid-state dye-sensitized solar cells (SDSC) with a solid-state hole transporting material, efficiencies up to 5.1 % have been reported.<sup>18</sup> For polymer/small molecule bulk heterojunction photovoltaic devices, the power conversion efficiencies have reached 5 - 6.8 %.<sup>19-21</sup> Vapor deposited multi-layer solar cells of small molecules obtained efficiencies up to 5.6 %.<sup>22</sup> All these reported efficiencies are under standard conditions of measurement at AM 1.5 conditions at 1 sun intensity, but in very small area devices.

### 1.2 ORGANIC PHOTOVOLTAICS

Existing types of photovoltaic devices can be divided into two different groups: conventional solar cells, such as inorganic silicon p-n junctions, and excitonic solar cells (XSCs) utilizing donor-acceptor (D-A) interfaces.<sup>23</sup> Most organic-based solar cells, including dye-sensitized solar cells (DSSCs as well as SDSCs), belong to the category of XSCs. In these devices, excitons (electron-hole pairs, bounded by coulombic interactions) are generated upon irradiation with visible light. If these excitons are not created directly at the heterointerface as in DSSCs, they need to diffuse to the D-A interface in order to generate charge carriers. The photogeneration of separated charges in organic photovoltaics consists of multiple steps, starting from light absorption to a detectable photocurrent, which have to be optimized for an efficient device operation.

Basically, active layers suitable for XSCs rely on a heterojunction comprised of an electron conducting acceptor (A) and a hole transporting donor (D) material. The donor material, is generally composed of electron-rich aromatic building moieties and thus characterized by a low ionization potential ( $I_p$ ) in the range of 4-5 eV, whereas the acceptor material is electron-deficient, with an electron affinity ( $E_A$ ) between 3-4 eV. The  $I_p$  is equivalent to the HOMO (highest occupied molecular orbital) energy level and the  $E_A$  is equivalent to the LUMO (lowest unoccupied molecular orbital) energy level. For simplicity, Figure 2 presents the physical processes of a bilayer donor-acceptor heterojunction solar cell. The absorbed light generates excitons which travel in all directions during their lifetime. Depending on the optical properties of the materials involved, this process may occur in both materials. In order to efficiently create excitons, the absorption behavior of the materials should match the solar spectrum and the active layer thickness should be in the range of 200 - 300 nm for complete absorption of visible light, which actually depends on the absorption coefficient. Excitons that reach the donor/acceptor interface within their rather small exciton diffusion length  $L_D$  (typically 5 – 20 nm in organic materials<sup>24</sup>) may dissociate into free charge carriers and can potentially contribute to the photocurrent. Therefore, it is energetically more favourable for the exciton to be separated into an electron and a hole, if a sufficient energy level offset of the two materials to overcome the exciton binding energy (electronic band-gap reduced by the exciton energy  $E_{EX}$ ) is provided. If  $E_{EX} > I_p(D) - E_A(A)$ , an electron transfers into the LUMO of the acceptor and a hole into the HOMO of the donor at the interface. The separated charges are subsequently transported via hopping and finally collected at

the respective electrodes. The charge transport is driven by the built-in potential created by the different work functions of the electrode materials used. A prerequisite is the presence of well-defined continuous pathways of donor and acceptor domains towards the respective electrodes together with a high charge carrier mobility of the materials in order to guarantee an efficient charge transport.

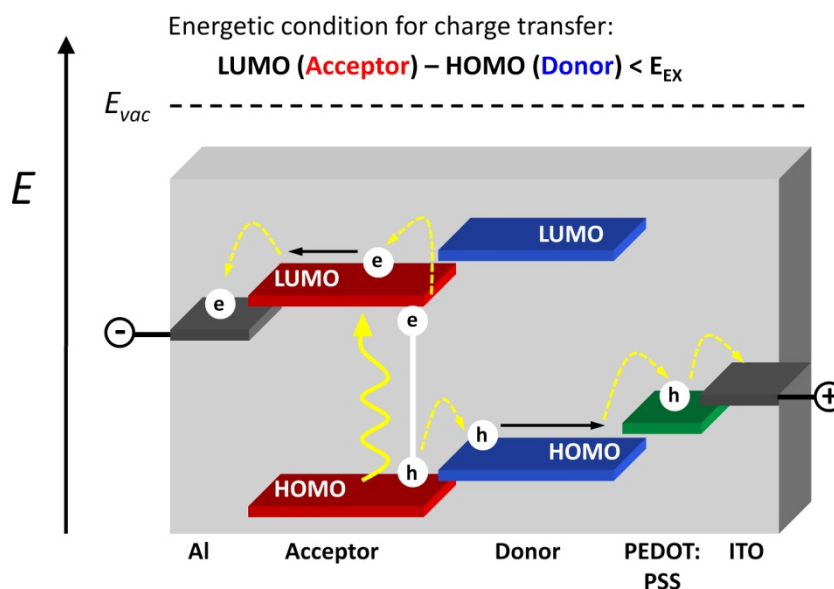


**Figure 2.** Schematic presentation of the individual physical processes in a bilayer donor-acceptor heterojunction solar cell. Absorbed light generates excitons which drift in all directions. Those that reach the donor/acceptor interface may separate into free charges, if a sufficient energy level offset of the two materials is provided to overcome the exciton binding energy. At the donor-acceptor interface an electron transfers into the LUMO of the acceptor and a hole into the HOMO of the donor. The separated charges percolate through the respective material via hopping processes and are collected at the respective electrodes to contribute to the photocurrent.

Accurate efficiency measurements are decisive to evaluate and compare new material systems or processing techniques.<sup>25</sup> In order to maintain internationally accepted testing procedures, devices are measured under simulated sunlight with an intensity of  $100 \text{ mW}\cdot\text{cm}^{-2}$ , which is comparable to a solar irradiation at air mass 1.5 (AM 1.5 designates the photons that pass through 1.5 x the mass of the atmosphere directly overhead and translates to the sun having an angle of  $48.19^\circ$  from the zenith).<sup>26</sup> Organic photovoltaic devices are conventionally characterized by their current density ( $J$ ) - voltage ( $V$ ) characteristics ( $J$ - $V$  curves) and by the external quantum efficiency (EQE). Figure 3a depicts a typical  $J$ - $V$  curve of an organic solar cell. The open circuit voltage ( $V_{oc}$ ), the short circuit current ( $I_{sc}$ ), the fill factor ( $FF$ ) and the power conversion efficiency ( $\eta$ ) can be determined (Fig 4b).<sup>27</sup> The fill factor is an indication of the photodiode quality and is mainly influenced by charge carrier transport and recombination. The EQE represent the conversion efficiency under monochromatic light of a number of photons  $N_{\text{photon}}$  (given by the power of illumination  $P_{\text{light}}$ ) to the number of electrons  $N_{\text{electron}}$  collected in the device (given by  $J_{sc}$ ) in dependence of the wavelength of the incident photons.

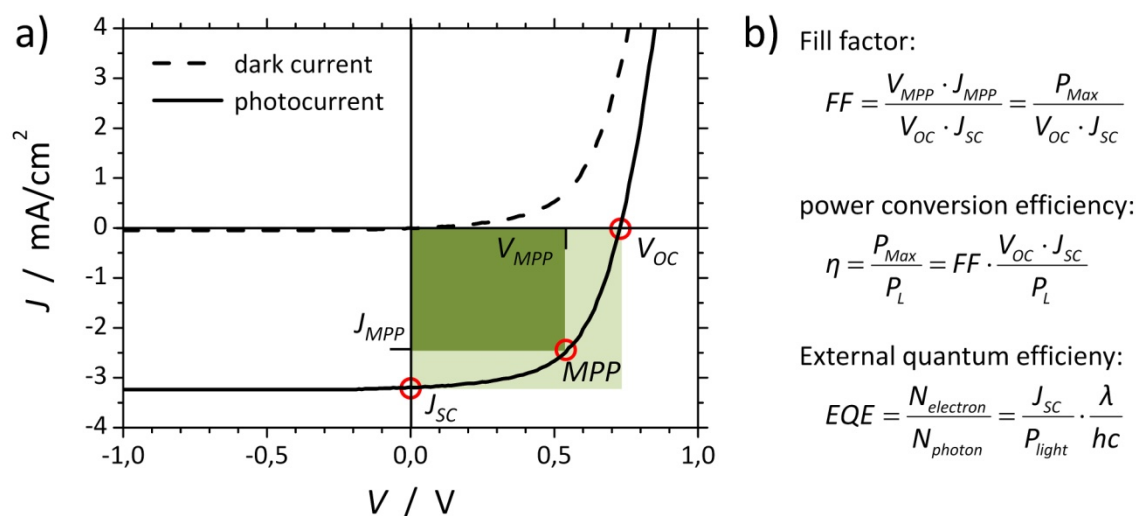


**Figure 3.** Characterization of photovoltaic devices. a) Plot of current density  $J$  versus voltage  $V$  ( $J$ - $V$  characteristics) of a photovoltaic element under dark and under illumination. b) Key parameters for evaluation of solar cells. The fill factor ( $FF$ ) is defined as the ratio (given in percent) of the actual maximum obtainable power ( $V_{MPP} \cdot J_{MPP}$ ) at the maximum power point (MPP) to the theoretically available power ( $V_{OC} \cdot J_{SC}$ ) given by the product of the open circuit voltage ( $V_{OC}$ ) and the short circuit current ( $J_{SC}$ ). The external quantum efficiency ( $EQE$ ) in dependence of the wavelength ( $\lambda$ ) represents the conversion efficiency of a number of photons  $N_{photon}$  (given by the power of illumination  $P_{light}$ ) to the number of electrons  $N_{electron}$  produced in the device (given by  $J_{SC}$ ).

Due to the intrinsically short exciton diffusion length in organic materials, only excitons created in close vicinity of a D/A interface can contribute to the charge separation process. For an ideal heterojunction, an interpenetrating network between an electron-acceptor and -donor material with a suitable concentration gradient in the two materials towards the respective charge collecting electrodes is desirable. This led to the development of the bulk heterojunction concept (BHJ, Fig 4).<sup>9,28,29</sup>

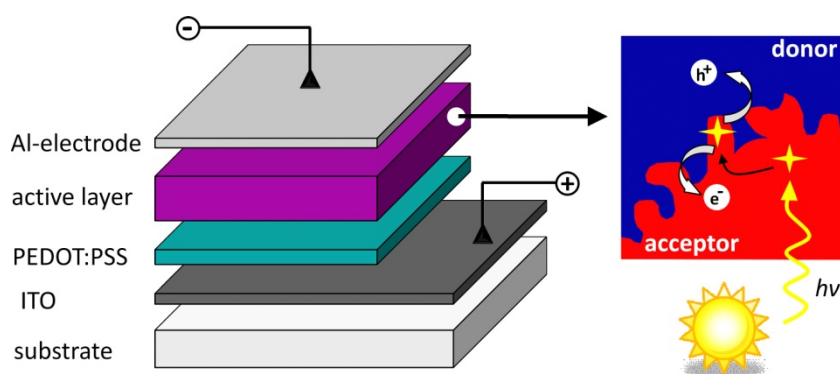


**Figure 4.** Schematic device architecture of a bulk-heterojunction solar cell. An indium tin-oxide (ITO) substrate (glass or plastic foil) covered with poly(3,4-ethylenedioxythiophene):poly(4-styrene sulphonate) (PEDOT:PSS) serves as anode. The active layer may be processed by vapor deposition or preferable from solution (spin coating or doctor-blading). The photovoltaic device is completed by the top-electrode (typically aluminium).

Here, the distance an exciton migrates to reach a D/A interface is significantly reduced and the increased interfacial area assists for exciton dissociation. However, donor and acceptor materials are randomly distributed in such a thermodynamically segregated system. This morphology may lead to charge trapping at cul-de-sacs or bottlenecks in the conducting pathways towards the electrodes. Blending donor and acceptor components has led to highly efficient solar cell systems, even though the desired stable bicontinuous morphology in the nanometer scale in the entire bulk phase is still difficult to achieve.<sup>30</sup> Manifold approaches and material combinations are available to generate organic bulk heterojunction devices.

The most studied and omnipresent material system for BHJ-devices is based on poly(3-hexylthiophene) (P3HT) and the fullerene derivative PCBM, where efficiencies up to 6% have been reported.<sup>20,21</sup>

*M. Thelakkat* et al. have demonstrated that microphase-separated semiconductor D-A block copolymers can elegantly be employed in organic BHJ solar cells.<sup>31</sup> Such block copolymers are capable to microphase separate into domain sizes (several tens of nanometers in size) commensurate to the exciton diffusion length, which makes the morphology in such materials highly suitable for efficient charge separation and charge transport (Fig. 5). Thus, this approach combines all functions required in the active layer, starting from light absorption to charge transport, in only one material. Two different types of complex D-A block copolymer architectures were studied so far, amorphous-crystalline block copolymers,<sup>32</sup> combining different hole transporting poly(triarylamine) blocks with an electron transporting perylene bisimide (PBI) block and crystalline-crystalline block copolymers,<sup>33</sup> combining a hole transporting P3HT-block with a PBI block (P3HT-*b*-PPerAcr). For the latter, outstanding external quantum efficiencies of 31 % could be obtained for a device made up of a high molecular weight P3HT-*b*-PPerAcr.<sup>34</sup>

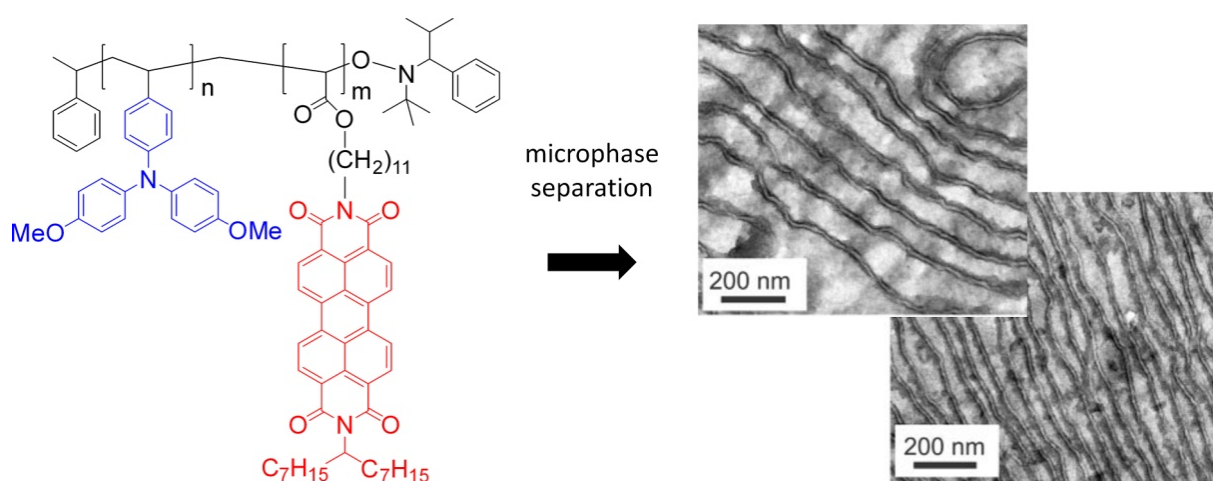


**Figure 5.** Molecular structure of an amorphous-crystalline D/A blockcopolymer poly(bis(4-methoxyphenyl)-4'-vinylphenylamine)-block-poly(perylenediimide acrylate) (PvDMTPA-*b*-PPerAcr) and TEM cross sections of such microphase separated block copolymers. (reproduced from Sommer et al.<sup>32</sup>).

*K. Müllen* and *R. Friend* et al. have demonstrated that also, blends consisting of a liquid crystalline material in combination with a crystal network-forming material can be solution-processed for efficient organic photovoltaic devices. Ordered structures on the basis of alkyl-substituted discotics with a useful morphology for photo-exciton dissociation and charge transport were created via self-organization.<sup>35-37</sup> Room temperature liquid crystalline hexa-perihexabenzocoronene (HBC-PhC<sub>12</sub>) was chosen as a donor in combination with a crystalline perylene bisimide (PBI-C<sub>5</sub>) as the acceptor to produce thin films with vertically segregated PBI-C<sub>5</sub> (crystallites on top) and HBC-PhC<sub>12</sub>, which yield large interfacial surface areas (Fig. 6). Although no device characteristics under solar conditions are provided, these films show high EQEs, of more than 34 % near 490 nm in photodiodes.

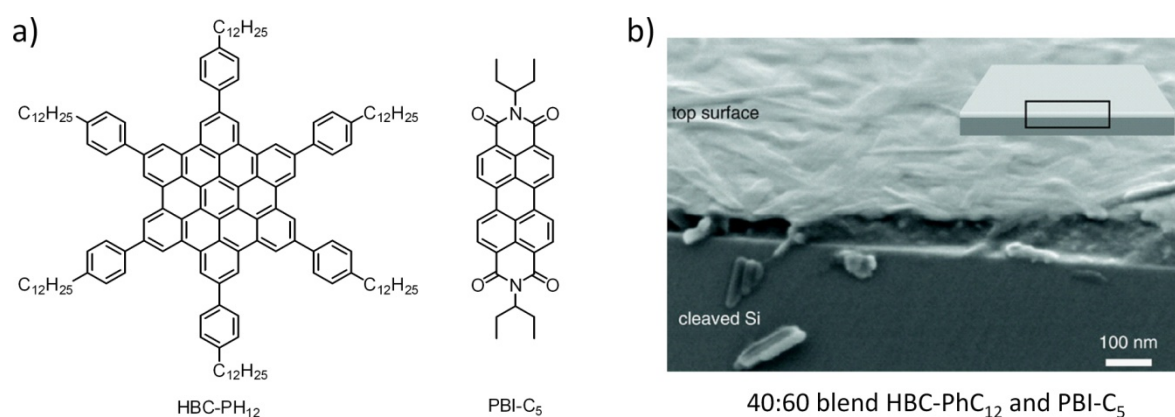


**Figure 6.** (a) Molecular structures of liquid crystalline hexa-perihexabenzocoronene (HBC-PhC<sub>12</sub>) and crystalline perylene bisimide (PBI-C<sub>5</sub>). (b) SEM surface image of a thin film of a 40:60 % HBC-PhC<sub>12</sub> : PBI-C<sub>5</sub> blend sample. (reproduced from Schmidt-Mende et al.<sup>37</sup>).

From a materials chemist's point of view, it is still of fundamental interest to develop new materials as well as new concepts that allow to tune absorption behavior, charge carrier mobility and to control thin film morphology.

### 1.3 SEMICONDUCTING MATERIALS BASED ON SELF-ORGANIZING FUNCTIONAL $\pi$ -CONJUGATED SYSTEMS OF SMALL MOLECULES

The challenging task, to further improve device efficiencies in organic electronics, is accompanied with the development of novel self-organizing semiconducting organic compounds. Active materials for efficient photovoltaics, in particular, need to satisfy a number of criteria, including a high optical density over the visible and near infrared spectral regime, high charge carrier mobilities and a large exciton diffusion length. The conventional approach focuses on  $\pi$ -conjugated polymers or oligomers, which possess the inherent ability to self-organize via crystallization and to conduct electric charges along their backbone as well as via interchain transport.<sup>38,39</sup> These highly processable materials exhibit charge carrier mobilities in the order of  $0.1 \text{ cm}^2 \cdot \text{V}^{-1} \cdot \text{s}^{-1}$ , such as determined for regioregular poly(3-hexylthiophene).<sup>40</sup> Another attractive strategy exploits the hierarchical self-assembly<sup>41,42</sup> of small  $\pi$ -conjugated molecules into supramolecular assemblies by non-covalent interactions as alternative classes of functional materials with innovative design.<sup>43-45</sup> The programmed, supramolecular self-organization of small molecular building blocks into well-defined nanostructural architectures via multiple intermolecular driving forces is recognized as one of the key techniques for the “bottom-up” approach in nanotechnology.<sup>46</sup> Amongst the various new materials for organic electronic applications, **conjugated liquid crystals** (CLCs) are currently contemplated as an auspicious novel class of organic semiconductors because they combine order and dynamics.<sup>47</sup>

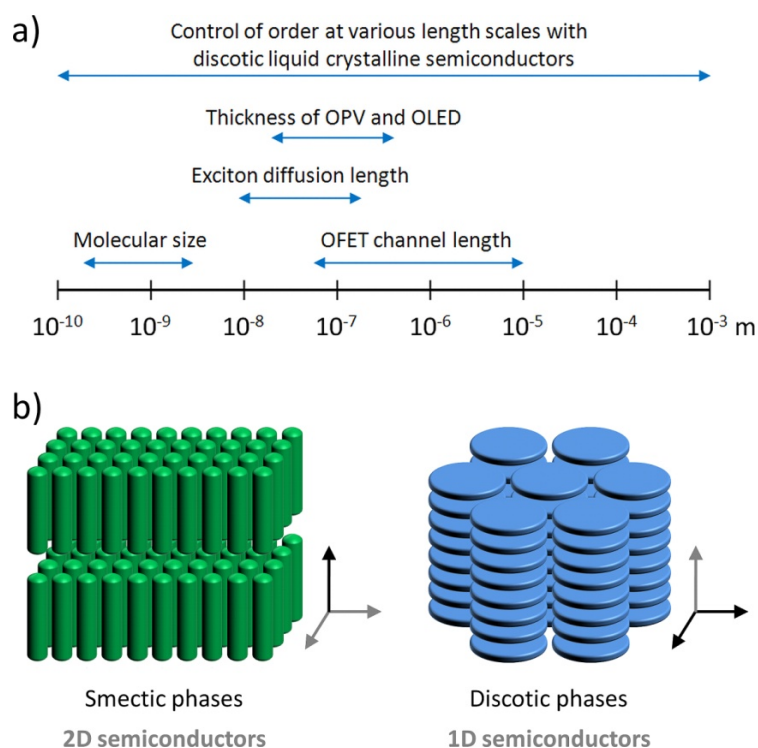


**Figure 7.** (a) Typical length-scales encountered in organic electronics and control of order achievable with conjugated liquid crystalline (CLC) semiconductors. (b) Schematic representation of calamitic and discotic semiconductors. (reproduced from Geerts et al.<sup>47</sup>).

CLCs offer the decisive advantage of controlling order in the bulk as well as at interfaces and at all length-scales from the molecular to the macroscopic scale (Fig. 7). Additionally, liquid crystalline materials possess the unique propensity to form highly organized films, which can be obtained by cheap processing techniques from solution. For conjugated liquid crystals it can be differentiated between calamitic (rod-like) and discotic (disc-like) mesogens. Despite their different molecular shape, they differ basically in the dimensionality of charge transport or exciton migration and in the extent of their orbital overlap. For calamitic mesogens, smectic mesophases with a two-dimensional charge transport and for discotic mesogens columnar mesophases featuring a one-dimensional charge transport are the usually observed phase organizations for contributing towards charge migration.

But also the spatial organization on the mesoscopic length scale (5 - 100nm) of  $\pi$ -conjugated dye-entities as molecular building blocks under a programmed manner by making use of intermolecular interactions such as hydrogen-bonding, dipole-dipole, van der Waals or  $\pi$ - $\pi$  interactions is a topic of particular interest for scientists in this field. It was proposed to call this field of research “*supramolecular electronics*”.<sup>45</sup> In these objects, smallest dimensions are combined with a high degree of order.<sup>48</sup> The hierarchical formation of fibrous nanostructures building up a 3D network under thermodynamic control is controllable and may thus be implemented in various organic device applications. In this context, especially hydrogen bonding motifs or solvophobic effects, e.g. in organogelators<sup>49,50</sup> offer an excellent structure-directing tool to position well-defined objects at predefined positions in order to construct nanotubes,<sup>51</sup> nanowires<sup>52</sup> or xerogels<sup>53</sup> of electronic components in the nanometer range (Fig. 8).

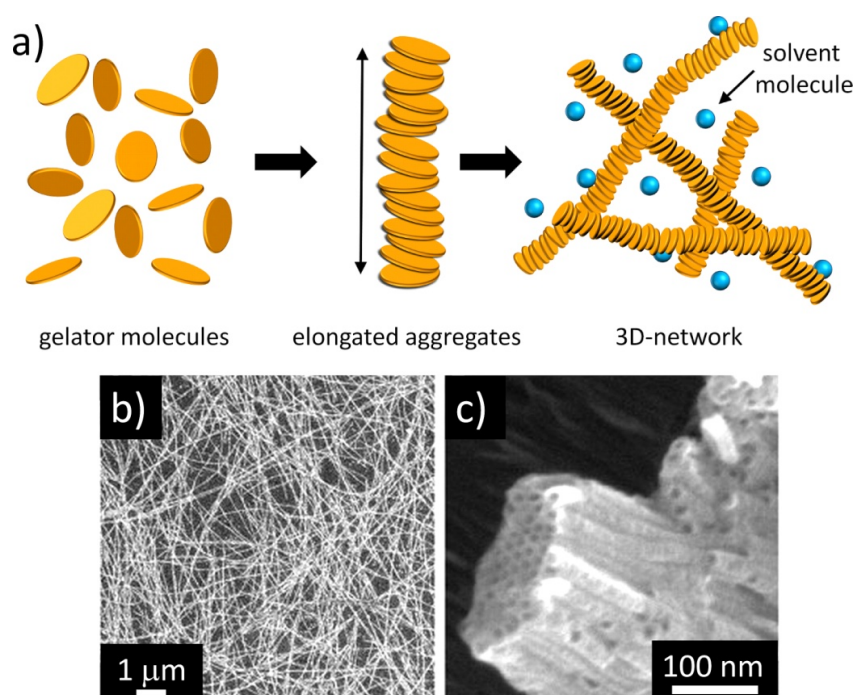


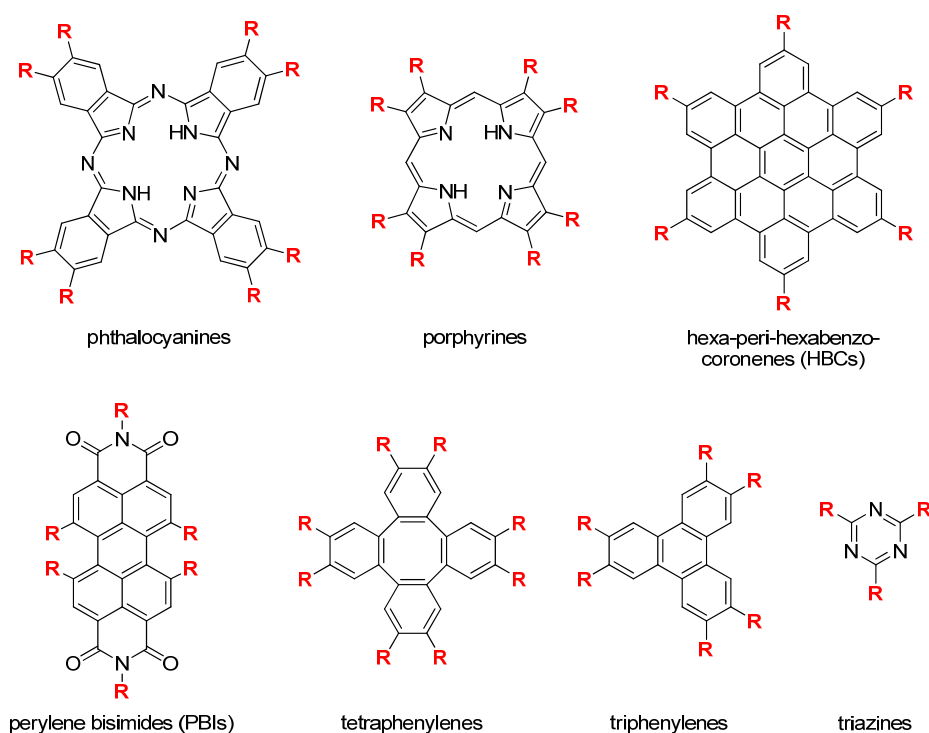
**Figure 8.** (a) Proposed scheme of supramolecular gel formations (reproduced from Hiromitsu et al.<sup>54</sup>). (b, c) Scanning electron microscopy images of the morphology of self-assembled amphiphilic hexabenzocoronene nanotubes (reproduced from Fukushima et al.<sup>51</sup>).

## Columnar Liquid Crystals Formed by $\pi$ -Conjugated Systems

Liquid crystals (LCs) are unique functional soft materials which possess both, mobility and order, ranging from the macroscopic to the molecular level. In addition to the classical states of matter – solid, liquid, gaseous - liquid crystals are accepted as a fourth state of matter.<sup>55</sup> The liquid crystalline phenomenon was described firstly for cholesterol derivatives by *F. Reinitzer* in 1888<sup>56</sup> and recognized as novel state of matter by *O. Lehmann*.<sup>57</sup> Immense efforts in research and development have pushed this topic into a mature field of modern science and many mesophase forming classes of compounds are known nowadays. The special properties of liquid crystals are used in various modern materials, e.g. thermotropic calamitic mesogens in active matrix liquid crystal displays (AM-LCD)<sup>58</sup> or high strength synthetic polyaramid fibers such as Kevlar® which are spun from a lyotropic melt.<sup>59</sup> The liquid crystalline phase of matter can be characterized by attributes in-between those of a conventional, fluid isotropic liquid and those of a solid crystal with orientational and/or positional long-range order co-instantaneously.<sup>60,61</sup> As in liquid crystalline phases, the molecules are able to diffuse like the molecules of a liquid, but still maintain some degree of ordering to a greater or lesser extent, they are also denominated as mesophases (greek: μέσος = middle). Generally, liquid crystals are divided into two categories, thermotropic and lyotropic LCs. Thermotropic LCs exhibit a phase transition into the LC-phase upon temperature change, whereas lyotropic LCs<sup>62</sup> exhibit phase transitions as a function of temperature and concentration of the mesogens in a solvent (a typically example are amphiphilic molecules in water). Besides liquid crystals, also condis-phases<sup>63</sup>, plastic crystals<sup>64</sup> and their corresponding glasses, as well as micro-phase separated copolymers<sup>65</sup> belong to the class of mesomorphic materials. Any compound that is able to form a mesophase is called a mesogene. Mesogenes can consist of only one molecule (molecular mesogene), or they can be build up of several – even different – individual molecules (supramolecular mesomorphism). Liquid crystalline phases can be classified according to the degree of order (1D – 3D) and orientation of the mesogens in the liquid crystalline state into different types of phases as nematic, smectic or columnar. The molecular origin for the formation of a mesophase can mainly be attributed to three different principles: anisotropy, aggregation and segregation. When melting to the liquid crystalline phase, the mesogen must exhibit structural principles in order to maintain parts of its organization or orientation. As molecular shape is an important factor in determining whether certain molecules will self-assemble into liquid crystalline phases, the molecules may usefully be classified according to their anisometric geometry as calamitic- (rod-like) discotic- (disc-like), banana- (bent-like), sanidic- (board-like) or pyramidic- (conical or cone-shaped) mesogens.<sup>66,67</sup>

A prominent class of molecular mesogens, which holds potential for future semiconducting appliances comprises thermotropic liquid crystals with a disc-shaped geometry of the mesogens (DLCs).<sup>68-70</sup> After speculations on the existence of mesomorphism of coin-like mesogens by *D. Vorländer*,<sup>71</sup> the liquid crystalline state of so-called discotic mesogens was discovered by *S. Chandrasekhar* in 1977.<sup>72</sup> Generally, these molecules consist of a disc-shaped rigid  $\pi$ -conjugated core and bear flexible substituents at the periphery, generally hydrocarbon chains which are attached by connecting groups, such as ether, thioether, ester or amide groups.

Scheme 1 presents several prominent examples of discotic molecules, which form columnar superstructures due to  $\pi$ - $\pi$  interactions.



**Scheme 1.** Several prominent discotic liquid crystalline compounds comprising a rigid aromatic central core. The flexible substituents (R) guarantee phase forming properties and solubility of the mesogens.

In most cases, these discotic structures self-assemble into one-dimensional columnar superstructures composed of cofacially stacked mesogens, due to an overlap of orbitals. The core-core distance in columnar mesophases is usually of the order of 3.4-3.5 Å, so that there is considerable overlap of  $\pi$ -orbitals. This is often referred to as  $\pi$ - $\pi$  interactions and is a result of attractive electrostatic forces between the positively charged  $\sigma$ -framework and the negatively charged electron cloud of neighboring moieties.<sup>73</sup> As flexible long aliphatic chains surround the core, the intercolumnar distance usually ranges between 20-40 Å, depending on the appended chain length. The columns are surrounded by the disordered, liquid-like side chains and can further be arranged into regular two-dimensional lattices with the column axes parallel to each other. A proper coverage of the peripheral domains by the side-chains, as well as an optimal space filling in the area of the central core is decisive. The diversity of columnar phases can be thought of as 1D-liquid (along the columns) and 2D-crystalline (along the 2D lattice vectors) structures.<sup>69</sup> There are various types of columnar phases depending on the two-dimensional lattice symmetry of the columnar packing, the degree of order in the molecular stacking, orientation of the molecules along the columnar axis and the dynamics of the discs within the columns. So far, columnar phases of two-dimensional hexagonal (Col<sub>h</sub>), oblique (Col<sub>ob</sub>) and rectangular (Col<sub>r</sub>) symmetry have been distinguished by A. Levelut (Fig. 9 b-c).<sup>74-76</sup> In a simple

description, the phase type depends on the cross-sectional shape of the columns: circular cross-sections (uniaxial) results in hexagonal phases, while elliptical shaped (biaxial) columns will arrange in rectangular symmetry in order to optimize the packing density.<sup>77</sup> Biaxiality can either arise by a tilt of a circular shaped mesogen with respect to the column axis (Fig. 9a) or from a non-circular shaped mesogen.

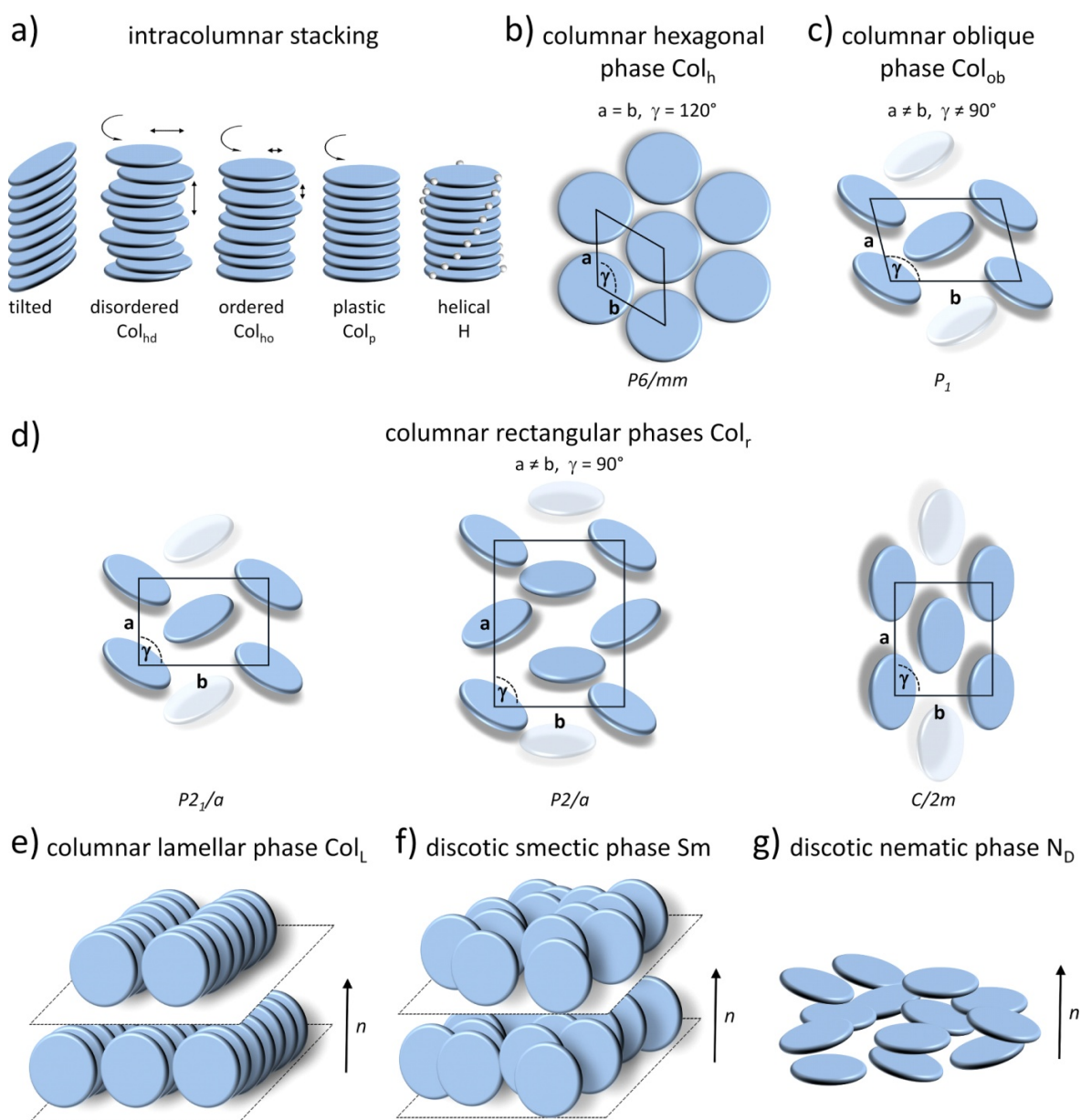


**Figure 9.** Schematic representation of discotic liquid crystalline phases with point-group symmetries in parentheses: (a) types of intracolumnar  $\pi$ - $\pi$  stacking: tilted, disordered, ordered, plastic and helical. (b) Columnar hexagonal mesophase ( $Col_h$ ). (c) Columnar oblique phase ( $Col_{ob}$ ). (d) Columnar rectangular mesophases ( $Col_r$ ). (e) Columnar lamellar phase ( $Col_L$ ). (f) Discotic smectic phase ( $Sm$ ). (g) Discotic nematic phase ( $N_D$ ).

*C. Tschierske* relates the transition from columnar hexagonal via columnar rectangular over to lamellar phases to a change of the shape of the mesogenic unit from disc-like via elliptic to rod-like.<sup>78</sup> In a first step, the rotational disorder around the column long axis is reduced, leading to a non-circular average shape of the columns. Simultaneously, the flexible side chains become non-equivalently distributed around the mesogens. Thus, the majority of these side-chains is segregated in layers, whereas in the other direction the density of side chains between the columns decreases. This leads to a transition from hexagonal to rectangular columnar phases. Col<sub>r</sub>-phases can also be regarded as lamellar arrays of parallel aligned columns, whereby neighbouring columns are orientationally and positionally correlated with each other. If the positional correlation between adjacent layers is lost, arrays of parallel aligned columns are built up in the lamellocolumnar phase (Col<sub>L</sub>, Fig. 9e).<sup>79,80</sup> The Col<sub>L</sub>-phase is described by one lattice parameter, regarding the parallel arrangement of the columns and corresponds to the layer thickness *d*. An additional loss of the long-range positional order of the mesogens within the layers, that means disappearance of the columnar aggregates, leads to discotic smectic phases (Sm, Fig. 9f).<sup>81</sup> Thus, in analogy to smectic phases, only the individual molecules are organized in layers.

Additionally, the intracolumnar stacking in columnar mesophases can be distinguished by two extreme cases: an ordered (Col<sub>xo</sub>) or disordered (Col<sub>xdo</sub>) stacking along the column axis in which fluidity (motion of individual discs, such as longitudinal displacements or rotations around the columnar axis) exists in both cases, but the correlation lengths of the motions are different (Fig. 9a). Ordering of the mesogens along the column axis can be distinguished by wide angle X-ray diffraction. If the molecules are highly ordered, a sharp reflection can be observed and for less ordered packing this peak is diffuse or absent. There exist also columnar plastic phases (Col<sub>p</sub>) in which structural disorders (such as non-parallel arrangement of the discs, longitudinal and lateral displacements and rotation around the columnar axis) can occur, while the motional freedom of the discs is restricted.<sup>82</sup> Hence, the Col<sub>p</sub>-phase is characterized by three-dimensional crystal-like order of the mesogen's centers of gravity while the discs are still able to perform intracolumnar rotations.<sup>83</sup> The occurrence of helical superstructures (H) with strictly 3D-positional order is a special case of plastic phases (Fig. 9a).<sup>84</sup>

In the comparatively least ordered, discotic nematic mesophases (N<sub>d</sub>), the discotic molecules possess full translational and rotational freedom around their disc-normal but on an average, the short molecular axes are oriented in a preferred direction *n* (Fig. 9g).<sup>85</sup> One can say, the short molecular axes of the molecules orient more or less parallel to each other, while their centers of mass are isotropically distributed in the nematic phase. For discotic compounds exhibiting high intracolumnar interactions, the columns itself can act as a mesogenic unit, which may form nematic columnar (N<sub>Col</sub>) phases. However, these columns do not form 2D lattice structures but display a positional short-range order and an orientational long-range order.<sup>86</sup>

### Charge Transport Properties of DLCs

*D. Haarer* et al. reported for the first time the possibility to inject charges into discotic liquid crystal phases of triphenylenes by using a pulse of laser light and have also shown that disk-like organic molecules can exhibit very high mobilities for photoinduced charge carriers, of the order of  $0.1 \text{ cm}^2 \cdot \text{V}^{-1} \cdot \text{s}^{-1}$ .<sup>87</sup> Discotic liquid crystals (DLCs) that are free from impurities behave as insulators and charges have to be injected before electronic conduction can occur.<sup>88</sup> In these systems, the charge carrier mobilities are  $\sim 10^3$  times greater along the column axis than perpendicular to the columns.<sup>89</sup> These highly anisotropic mobilities clearly represent the columnar phases as practical one-dimensional conductors along the column axis. Generally charge carrier mobilities of DLCs are typically a few orders of magnitude lower than those for organic single crystals, but they are easier to process, almost free from grain boundaries which may trap charge carriers, have the tendency to align between electrodes or on surfaces spontaneously and their dynamic self-organization behaviour allows for a self-healing of structural defects (Fig. 10a-c).<sup>90</sup> For photoconducting LCs, two different mechanisms concerning the charge-carrier transport are discussed.<sup>90</sup> Due to the dynamic fluctuations arising from the liquid-like nature of the mesophases, most groups have assumed a hopping mechanism of charge transport between localized states. However, the high bulk mobilities found for highly ordered columnar phases, such as  $\text{Col}_p$  or helical columnar phases, require hopping frequencies in excess of  $10^{13}$ - $10^{14}$  Hz which is much faster than structural phonon vibrations.<sup>91</sup> Therefore, the second, more probable mechanism, describes the formation of conduction bands<sup>92,93</sup> with a delocalized charge across several molecules. This is due to a possible overlap of the  $\pi^* \cdot \pi^*$  LUMOs as a result of the columnar stacking of the  $\pi$ -conjugated systems with typical intercore distances of  $3.5 \text{ \AA}$  (Fig. 10d). Thus, the individual columns can build up molecular wires with conductive channels surrounded by insulating peripheral substituents, so that the columnar liquid crystal may show photoconductivity.<sup>94,95</sup>

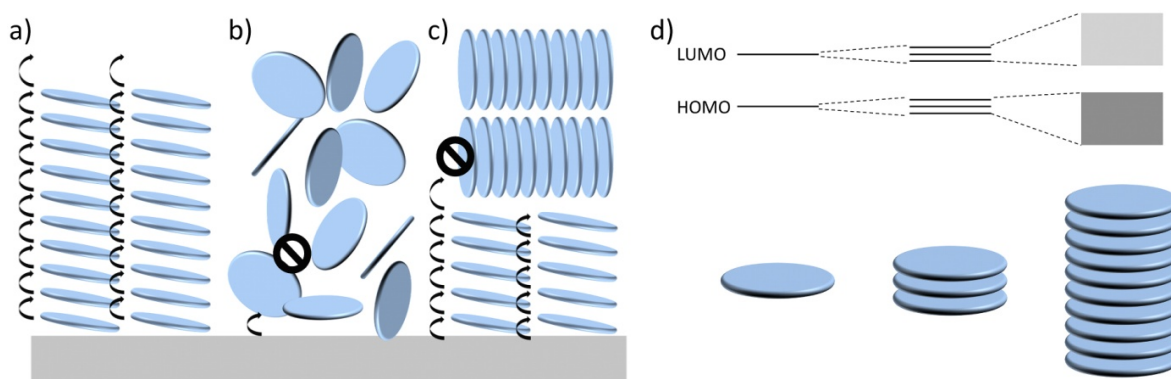


**Figure 10.** Charge transport in different orientations (a) single crystalline – highest charge transport mobility; (b) amorphous materials – charge transport hindered; (c) polycrystalline material – grain boundaries interrupt charge migration (reproduced from Pisula et al.<sup>96</sup>). (d) Electronic band formation from a single molecule to columnar superstructures (reproduced from Laschat et al.<sup>69</sup>).

Additionally, the exciton diffusion length in columnar phases exceeds 70 nm,<sup>97</sup> which is one order of magnitude higher than for most conjugated polymers. Taking these facts into account, columnar liquid crystals turn up as a new class of highly promising charge transport materials. The conductivity in columnar phases is generally limited by the efficiency of the charge-carrier injection process, the order within the mesophase, orientation of molecules and the structure of the mesophase.<sup>98</sup>

The charge carrier mobilities in such materials can be measured by several techniques.<sup>99</sup> The pulse radiolysis time-resolved microwave conductivity (PR-TRMC) method reveals the total local mobilities of both charge carriers that migrate only between a few molecules and is insensitive concerning the sign of charge carriers.<sup>100</sup> Time-of-flight (TOF)<sup>101</sup> or field effect transistor<sup>102</sup> techniques are used in order to determine charge carrier mobilities in the bulk and also to reflect the supramolecular organization with respect to surfaces/the electrodes (Fig. 11). The alignment of DLCs in thin films on the surface of substrates is also of decisive importance for the desired application. There exist various approaches to manipulate the thermodynamically driven and kinetically controlled process of surface alignment of discotic molecules, such as irradiation with polarized light,<sup>103</sup> concentration or temperature gradients<sup>104,105</sup> and specific molecular interface interactions including self-assembled monolayers (SAMs)<sup>106,107</sup> or PTFE-alignment layers.<sup>108-110</sup>

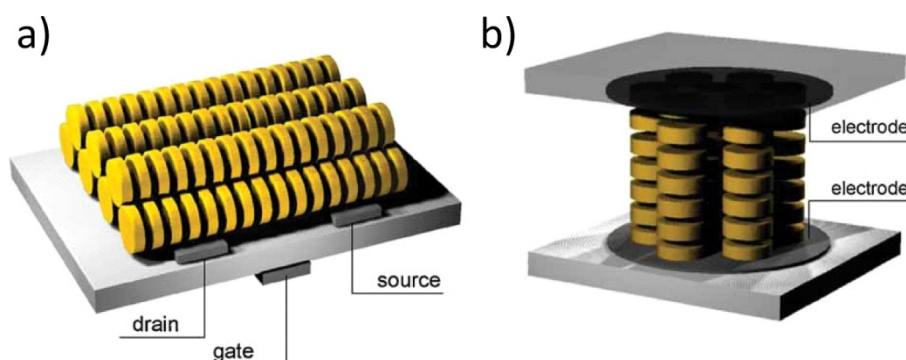


**Figure 11.** Schematic illustration of: (a) edge-on orientation of the discogens in columns lying parallel to the surface. This alignment is suitable for OFETs with lateral charge transport pathways. (b) Face-on (homeotropic) orientation with columns perpendicular to the surface, favorable alignment for applications in organic photovoltaic devices with vertical charge transport in an active layer sandwiched between two electrodes. (reproduced from Pisula et al.<sup>96</sup>)

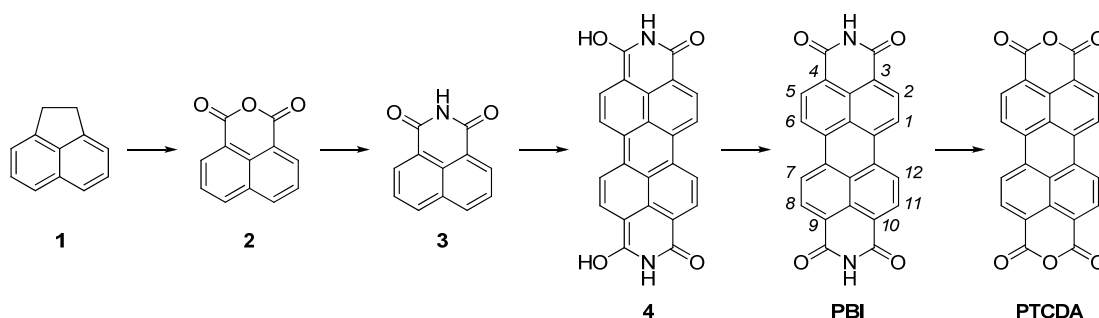
The common criteria towards an application of semiconducting discotic mesogens in photovoltaics are:<sup>111</sup> (i) High solubility of the liquid crystalline derivatives in common organic solvents in order to support solution processing techniques over a wide range of thickness. (ii) Self-assembly of the mesogens into LC phases with a clearing temperature ( $T_c$ ) below 200 °C to enable the formation of preferably homeotropically-aligned single-domain thin films upon slow cooling from the isotropic phase. Therefore, 200 °C is regarded as the upper limit to keep device fabrication compatible with the use of flexible plastic substrates.<sup>112</sup> (iii) The liquid crystalline

mesophase should persist down to room temperature without tendency to crystallization because crystal nucleation and growth occur randomly and turn single-domain LC films into multidomain films with grain boundaries that are detrimental to charge transport.<sup>113</sup> (iv) Additionally, the synthetic pathway of the compounds should be straightforward to allow the synthesis of the materials on the gram-scale.

## Liquid Crystalline Perylene Dyes

The name perylene pigments refers to a class of high-performance pigments made up of *N,N'*-disubstituted perylene-3,4,9,10-tetracarboxylic acid bisimides (perylene bisimides, PBIs) or perylene-3,4,9,10-tetracarboxylic acid dianhydride (PTCDA) (Scheme 2).<sup>114</sup> Additional substituents can be introduced in the bay-area (1, 6, 7, 12-positions) of the perylene core. PBI dyes<sup>115,116</sup> have emerged as an important class of n-type semiconductor materials exhibiting a large molar absorption coefficient and relatively high electron affinity among large band-gap materials.<sup>117-119</sup> PBIs are readily available, inexpensive robust compounds, and they combine high quantum yields of photoluminescence with excellent photochemical and thermal stability.<sup>120,121</sup> Thus, PBIs are promising materials for applications in organic electronic devices.<sup>31,32,37,122</sup> Here, the packing of perylene bisimides in the solid-state decides the morphology in thin films, which plays a major role on the device performance. For instance, an increase in exciton diffusion length and an improvement in charge carrier mobility can be achieved by increased ordering of PBI moieties.<sup>123</sup> As described previously, liquid crystallinity is an elegant way of inducing supramolecular organization, as it promotes  $\pi$ - $\pi$  stacking, allows for dynamic reorganization, and facilitates the processing of thin films.

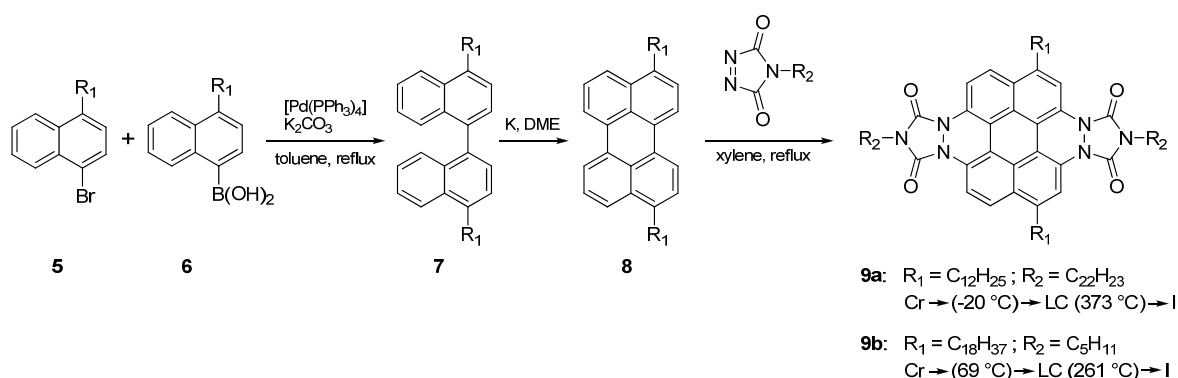
The synthesis of the perylene chromophore is basically unchanged since its discovery in 1913 by *M. Kardos* (Scheme 2).<sup>124</sup> The synthetic sequence starts with a  $V_2O_5$ -catalyzed air oxidation of the coal tar extract acenaphthene 1, to exhibit naphthalic acid anhydride 2. In a next step, 2 is condensed with aqueous ammonia to produce naphthalimide 3.<sup>114</sup> In the following, the perylene chromophore is built up by a fusion reaction of 3 with itself via bimolecular nucleophilic substitution in the presence of molten alkali at temperatures in excess of 200 °C. After precipitation into water perylene is obtained in its reduced (leuco) form 4 or salt, which is then oxidized with air or peroxide to afford perylene-tetracarboxylic acid bisimide (PBI), which can finally be hydrolyzed to the anhydride (PTCDA).



**Scheme 2.** Synthetic route towards perylene-tetracarboxylic acid bisimide (PBI) and perylene-tetracarboxylic acid dianhydride (PTCDA).<sup>114</sup>

In view of the long history of industrial and academic research on perylene dyes and pigments, it is rather surprising that only in the last years liquid crystalline phases of these dyes have been discovered in the condensed phase. In the following, different liquid crystalline derivatives of

perylene reported in literature are summarized; all of them are symmetrically substituted. The first endeavor towards the synthesis of liquid crystalline perylene derivatives was published by *K. Müllen* et al. (Scheme 3).<sup>125,126</sup> Suzuki coupling of boronic acid **5** with the corresponding naphthylbromide **6** gave disubstituted binaphthyl **7**, which was subsequently coupled to form the perylene moiety in **8**. Treatment of 3,10-dialkyl perylenes **8** with an excess of different 4-*n*-alkyl-3,5-dioxotriazoles yielded the Diels-Alder products 2,9-dialkyl-5,6,11,12-tetraaza-5,6,11,12-tetrahydro-coronene-5,6,11,12-tetracarboxylic acid bisalkyl-imides **9a**, **b**. These discotic compounds exhibit liquid crystalline phases over a broad temperature range, but only a vague explanation of the phase structures is provided.

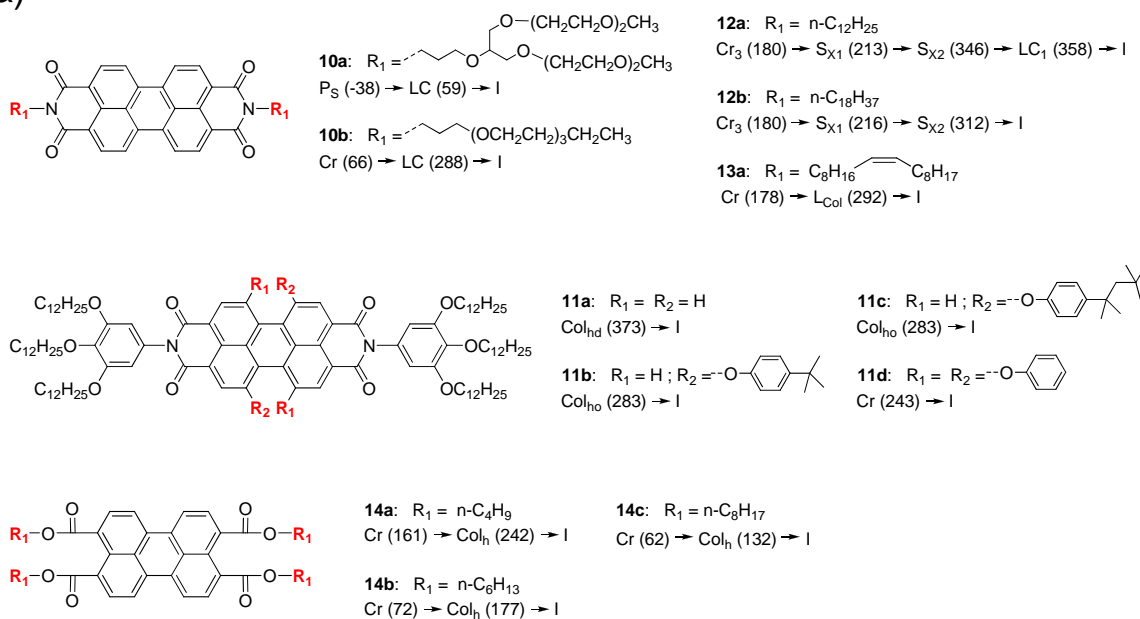


**Scheme 3.** Synthesis of liquid crystalline 2,9-dialkyl-5,6,11,12-tetraaza-5,6,11,12-tetrahydro-coronene-5,6,11,12-tetra-carboxylic acid bisalkylimides **9a**, **b**.

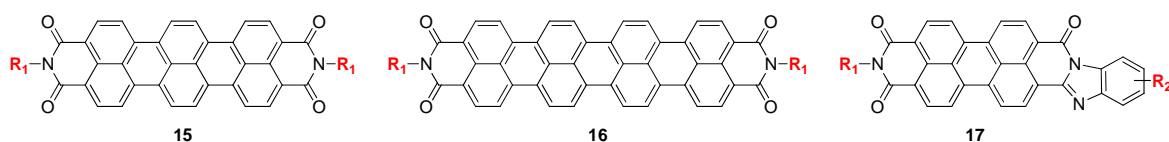
The synthesis of symmetrically *N*-substituted PBIs is generally performed by simple condensation reaction of perylene-tetracarboxylic acid dianhydride (PTCDA) with any primary amine. The first observation of liquid crystalline perylene bisimides **10a**, **b** was reported by *R. Cormier* and *B. Gregg* for several derivatives carrying different propylimid-oligo(oxyethylene) or phenethylimide-oligo(oxyethylene) side-chains as *N*-substituents (Scheme 4a).<sup>127-129</sup> These dyes are liquid crystalline also at room temperature, if branched *N*-substituents are employed. A different approach was conducted by *F. Würthner* et al.<sup>130</sup> Here, columnar liquid crystalline perylene derivatives **11a-d** were prepared from bay-substituted PTCDA and 3,4,5-tridodecyloxyaniline. The phenoxy substituents at the bay positions of the perylene core influence the mesomorphic properties of **11a-d** (Scheme 4a). From investigations of their spectroscopic properties and aggregation behavior in low-polarity solvents it was found that these compounds form fluorescent *J*-type aggregates, which reflect the number and steric demand of the phenoxy substituents. Other reports on symmetrically substituted liquid crystalline PBIs deal with tridodecyloxy gallic acid substituted derivatives without any bay substitution.<sup>121,131</sup> Even PBIs **12a** and **b**, bearing simple aliphatic side-chains have been found to form highly ordered mesophases, which are both smectic and columnar discotic in nature.<sup>117</sup> For **12b** a high charge carrier mobility of  $0.11\text{ cm}^2\cdot\text{V}^{-1}\cdot\text{s}^{-1}$  in the mesophase temperature range was displayed by PR-TRMC. Very recently *K. Müllen* et al. reported on cooperative molecular motion phenomenon

within a symmetrically substituted PBI exhibiting liquid crystalline properties.<sup>132</sup> PBI 13 with linear alkyl chains featuring an internal Z-alkene exhibits a lamella-columnar mesophase ( $L_{Col}$ ).<sup>133</sup> Recent studies report on miscibility between this derivative and a liquid crystalline phthalocyanine derivative.<sup>134</sup> *L. Cisse* et al. reported on a high exciton diffusion length  $L_D = 60$  nm in a homeotropically oriented film of a liquid crystalline PBI derivative.<sup>135</sup> Additionally simple perylene tetracarboxylic acid tetraesters 14 (PTEs) have been recognized to show liquid crystallinity.<sup>136</sup>

a)



b)



**Scheme 4.** (a) Different liquid crystalline perylene bisimide (PBI) and perylene tetraester (PTE) derivatives reported in literature. The corresponding phases transitions and assignments according to the original publications are also presented. (b) Core extended perylene derivatives: terrylene diimides 15, quaterylene diimides 16 and perylenes with a fused benzimidazole moiety 17.

In order to extend the absorption range in the visible wavelength regime, core extended derivatives as terrylene diimides 15 or quaterylene 16 diimides have been developed (Scheme 4b).<sup>137</sup> For this purpose, also perylene derivatives with a fused benzimidazole moiety 17 have been reported, but these dyes are lacking liquid crystalline packing so far.<sup>138</sup>

### Mesoscopic Nanostructures Via Self-Assembly of PBIs

As described previously, the self-assembly of functional semiconductors into well-defined, morphological stable nanostructures is of fundamental interest for electronic and optoelectronic applications. There exist several approaches in order to support self-organization process of perylene bisimide dyes in literature. Generally, solution based self-assembly processes require a balance between molecular interactions and sufficient solubility, which can be tailored by utilizing appropriate sidechain substituents. *K. Balakrishnan* et al. report on one-dimensional nanobelt formation of a propoxyethyl PBI **18**<sup>139</sup> and an amphiphilic substituted PBI **19** (Fig. 12).<sup>140</sup> Here, the self-assembly process is strongly dependent on solvent polarity.

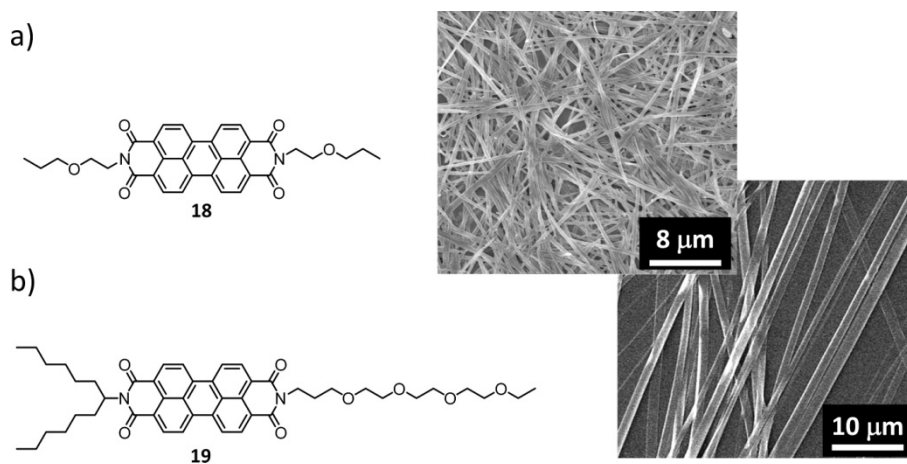


**Figure 12.** (a) Molecular structure of PBI **18** and corresponding SEM image of self-assembled nanobelts. (b) Molecular structure of amphiphilic PBI **19** and corresponding SEM image of self-assembled nanobelts. (reproduced from Balakrishnan et al.<sup>139,140</sup>).

*Y. Che* et al. describe the formation of well-defined nanofibers from a perylene dye by a slow solvent-exchange process, which was realized by vapor diffusion.<sup>141</sup> A different approach for the creation of nanostructures involves PBI organogelators by utilizing hydrogen-bond directed self-assembly. The major advantage of organogelators is that they may form a three-dimensional network superstructure. The first PBI organogelator was presented by *K. Sugiyasu* et al. which carries a cholesterol substituent.<sup>142</sup> *F. Würthner* et al. report on perylene based organogelators with different benzamide functionalities at the imide positions.<sup>143-145</sup> Among them PBI **20** forms *J*-type aggregates and exhibits the most remarkable gelation ability at low concentrations of only 0.1 wt-% (Fig. 13).

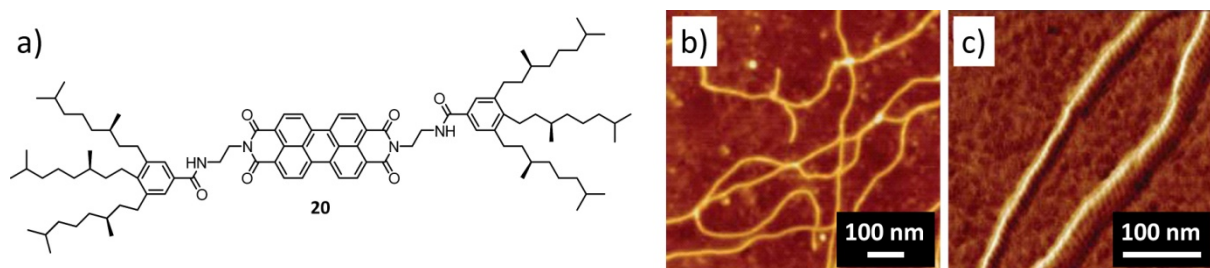


**Figure 13.** (a) Molecular structure of PBI organogelator 20. (b) AFM height image and (c) AFM phase image of spin coated films of 20 from diluted solution. (reproduced from Würthner et al<sup>145</sup>).

It was also shown that urea-functionalized PBIs form organogels by hydrogen-bonding.<sup>146</sup> S. Yagai et al describe the formation of flexible supramolecular polymers based on a perylene bisimide containing melamine hydrogen-bonding units 21. Ribbon-like nanoaggregates capable of gel formation can be obtained by polymerization upon binding with *N*-dodecylcyanurate (CA) (Fig. 14).<sup>147,148</sup>

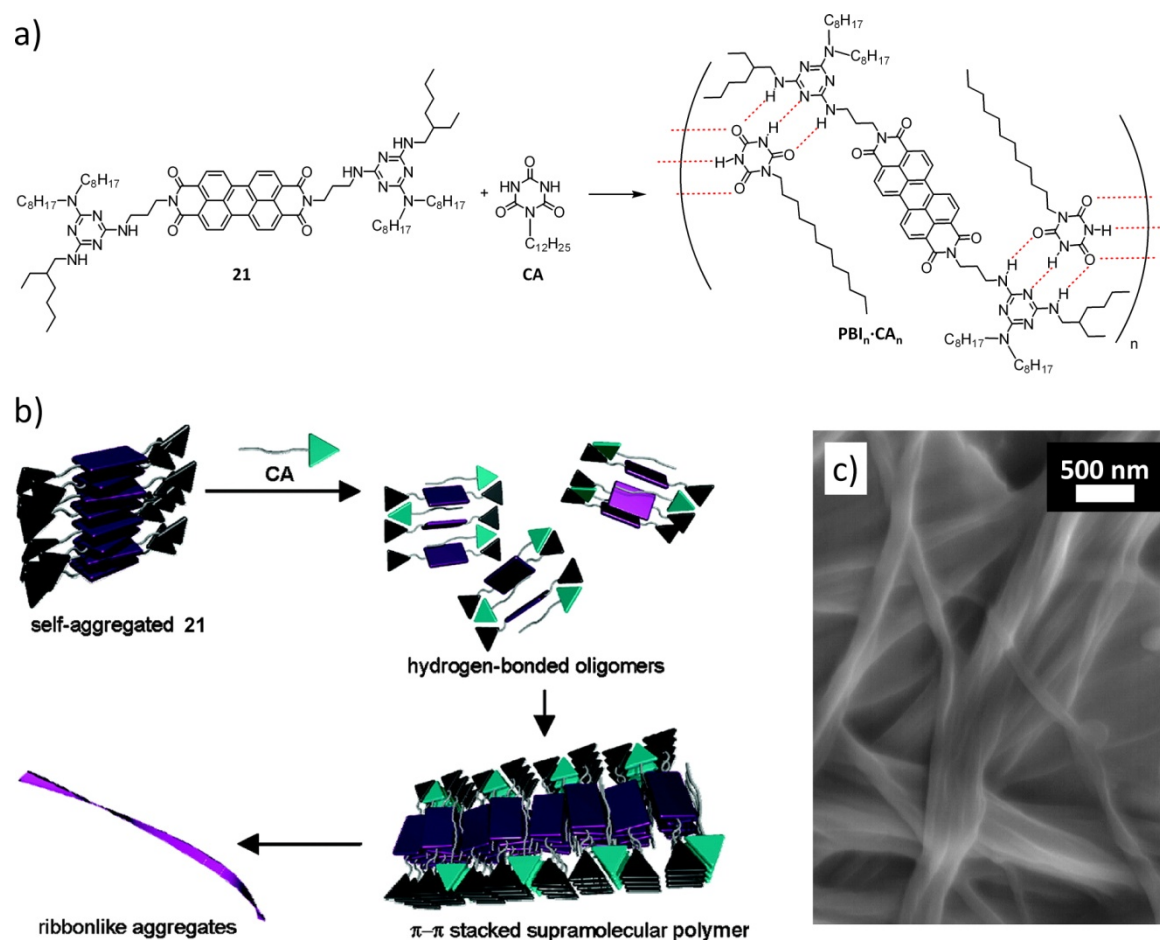


**Figure 14.** (a) Molecular structure of melamine functionalized PBI 21 and *N*-dodecyluracil (CA) with corresponding hydrogen bonded supramolecular polymer  $PBI_n-CA_n$ . (b) Schematic representation of the aggregation of 21 with CA in cyclic alkanes. (c) FE-SEM image of dried filamentous precipitates formed from cyclohexane solution of  $PBI_n-CA_n$ . (reproduced from Yagai et al<sup>148</sup>).

In addition to self-assembly processes from solution, it was also shown that nanobelt self-assembly of PTCDI is feasible from the gas phase.<sup>149</sup>

#### **1.4 OBJECTIVE OF THIS THESIS**

The aim of this thesis is the tailor-made synthesis and characterization of novel self-organizing perylene dyes as electronically active n-type semiconductors for application in organic photovoltaic devices (OPV). In the first part of this thesis, the main focus is set on inducing liquid crystalline phases in different perylene derivatives, along with tuning the mesophase temperature-range as well as packing behaviour. In this context also the extension of absorption in the visible region of these dyes is an important aspect. In order to investigate thermotropic behavior of the synthesized discogens, different methods, like differential scanning calorimetry (DSC), temperature-controlled polarization optical microscopy (POM) and temperature-controlled X-ray diffraction (XRD) experiments should be used. Firstly, a structure-property relationship to understand fundamental molecular design requirements to induce liquid crystalline phases in perylene bisimides (PBIs) is to be accomplished and a library of differently *N*-substituted PBIs to be synthesized. In a next step, the development of perylene derivatives with a mixed substitution pattern and an extended  $\pi$ -conjugation system has to be performed. Therefore, intermediate classes like perylene diester benzimidazoles (PDBIs) or perylene imide benzimidazoles (PIBIs) with appropriate side-chain substituents should be synthesized via suitable synthetic strategies in order to improve absorption in the visible region and solubility as well as maintaining the ability to form thermotropic liquid crystalline mesophases. Moreover, the synthesized PBIs should be characterized in detail in donor/acceptor all-liquid-crystalline blends in combination with copper-phthalocyanine dyes (provided by D. Atilla, Gebze Institute of Technology). In this connection blend morphology and the potential of light-harvesting in such systems should be examined.

In addition to that, in a second part of this thesis, the self-organizing phenomena of a PBI organogelator (provided by S. Ghosh, Universität Würzburg) should be elucidated towards its suitability for the creation of donor-acceptor heterojunctions. Morphology of the nanostructured networks in thin films should be studied by a combination of scanning electron microscopy (SEM) and atomic force microscopy (AFM). Furthermore, the fabrication of prototype organic electronic devices employing this organogelator in combination with a complementary polymeric p-type semiconductor is of major interest. Finally, the development of PBI dyes with an increased chromophore content and self-organization capability into morphological stable nanostructures should be carried out.

## **BIBLIOGRAPHY**

- (1) Forrest, S. R. *Nature* **2004**, *428*, 911-918.
- (2) Klauk, H. *Organic Electronics: Materials, Manufacturing and Applications*; Wiley-VCH: Weinheim, 2006.
- (3) Shirakawa, H.; Louis, E. J.; MacDiarmid, A. G.; Chiang, C. K.; Heeger, A. J. *J. Chem. Soc., Chem. Commun.* **1977**, 578.
- (4) Drury, C. J.; Mutsaers, C. M. J.; Hart, C. M.; Matters, M.; Leeuw, D. M. d. *Appl. Phys. Lett.* **1998**, *73*, 108-110.
- (5) Sirringhaus, H.; Tessler, N.; Friend, R. H. *Science* **1998**, *280*, 1741-1744.
- (6) Tang, C. W.; VanSlyke, S. A. *Appl. Phys. Lett.* **1987**, *51*, 913-915.
- (7) Burroughes, J. H.; Bradley, D. D. C.; Brown, A. R.; Marks, R. N.; Mackay, K.; Friend, R. H.; Burns, P. L.; Holmes, A. B. *Nature* **1990**, *347*, 539-541.
- (8) Tang, C. W. *Appl. Phys. Lett.* **1986**, *48*, 183-185.
- (9) Yu, G.; Gao, J.; Hummelen, J. C.; Wudl, F.; Heeger, A. J. *Science* **1995**, *270*, 1789-1791.
- (10) Brabec, C. J. *Sol. Energy Mater. Sol. Cells* **2004**, *83*, 273-292.
- (11) Brabec, C. J.; Durrant, J. R. *MRS Bull.* **2008**, *33*, 670-675.
- (12) Das, R.; Harrop, P. *Printed, Organic & Flexible Electronics Forecasts, Players & Opportunities 2009-2029* <http://www.idtechex.com/>, 2009.
- (13) Vardeny, Z. V.; Heeger, A. J.; Dodabalapur, A. *Synth. Met.* **2005**, *148*, 1-3.
- (14) Crabtree, G. W.; Lewis, N. S. *Phys. Today* **2007**, *March*, 37.
- (15) Arunachalam, V. S.; Fleischer, E. L. *MRS Bull.* **2008**, *33*, 264 - 276.
- (16) Chen, C.-Y.; Wang, M.; Li, J.-Y.; Pootrakulchote, N.; Alibabaei, L.; Ngoc-le, C.-h.; Decoppet, J.-D.; Tsai, J.-H.; Grätzel, C.; Wu, C.-G.; Zakeeruddin, S. M.; Grätzel, M. *ACS Nano* **2009**, *3*, 3103-3109.
- (17) Nazeeruddin, M. K.; De Angelis, F.; Fantacci, S.; Selloni, A.; Viscardi, G.; Liska, P.; Ito, S.; Takeru, B.; Grätzel, M. *J. Am. Chem. Soc.* **2005**, *127*, 16835-16847.
- (18) Snaith, H. J.; Moule, A. J.; Klein, C.; Meerholz, K.; Friend, R. H.; Grätzel, M. *Nano Lett.* **2007**, *7*, 3372-3376.
- (19) Chen, H.-Y.; Hou, J.; Zhang, S.; Liang, Y.; Yang, G.; Yang, Y.; Yu, L.; Wu, Y.; Li, G. *Nat. Photonics* **2009**, *3*, 649.
- (20) Kim, J. Y.; Lee, K.; Coates, N. E.; Moses, D.; Nguyen, T.-Q.; Dante, M.; Heeger, A. J. *Science* **2007**, *317*, 222-225.

- 
- (21) Peet, J.; Kim, J. Y.; Coates, N. E.; Ma, W. L.; Moses, D.; Heeger, A. J.; Bazan, G. C. *Nat. Mater.* **2007**, *6*, 497-500.
- (22) Xue, J.; Uchida, S.; Rand, B. P.; Forrest, S. R. *Appl. Phys. Lett.* **2004**, *85*, 5757-5759.
- (23) Gregg, B. A. *J. Phys. Chem. B* **2003**, *107*, 4688-4698.
- (24) Hoppe, H.; Sariciftci, N. S. In *Advances in Polymer Science - Photoresponsive Polymers II*; Marder, S. R., Lee, K.-S., Eds.; Springer-Verlag: Heidelberg, 2008, p 1-86.
- (25) Hains, A. W.; Liang, Z.; Woodhouse, M. A.; Gregg, B. A. *Chem. Rev.*
- (26) Case, M. A.; Owusu, Y. A.; Chapman, H.; Dargan, T.; Ruscher, P. *Renewable Energy* **2008**, *33*, 2645-2652.
- (27) Günes, S.; Neugebauer, H.; Sariciftci, N. S. *Chem. Rev.* **2007**, *107*, 1324-1338.
- (28) Halls, J. J. M.; Walsh, C. A.; Greenham, N. C.; Marseglia, E. A.; Friend, R. H.; Moratti, S. C.; Holmes, A. B. *Nature* **1995**, *376*, 498-500.
- (29) Yang, X.; Loos, J. *Macromolecules* **2007**, *40*, 1353-1362.
- (30) Ma, W.; Yang, C.; Gong, X.; Lee, K.; Heeger, A. J. *Adv. Funct. Mater.* **2005**, *15*, 1617-1622.
- (31) Lindner, S. M.; Hüttner, S.; Chiche, A.; Thelakkat, M.; Krausch, G. *Angew. Chem. Int. Ed.* **2006**, *45*, 3364-3368.
- (32) Sommer, M.; Lindner, S. M.; Thelakkat, M. *Adv. Funct. Mater.* **2007**, *17*, 1493-1500.
- (33) Sommer, M.; Lang, A. S.; Thelakkat, M. *Angew. Chem. Int. Ed.* **2008**, *47*, 7901-7904.
- (34) Sommer, M.; Hüttner, S.; Steiner, U.; Thelakkat, M. *Appl. Phys. Lett.* **2009**, *95*, 183308-3.
- (35) Li, J. L.; Kastler, M.; Pisula, W.; Robertson, J. W. F.; Wasserfallen, D.; Grimsdale, A. C.; Wu, J. S.; Müllen, K. *Adv. Funct. Mater.* **2007**, *17*, 2528-2533.
- (36) Schmidt-Mende, L.; Fechtenkötter, A.; Müllen, K.; Friend, R. H.; MacKenzie, J. D. *Physica E* **2002**, *14*, 263-267.
- (37) Schmidt-Mende, L.; Fechtenkötter, A.; Müllen, K.; Moons, E.; Friend, R. H.; MacKenzie, J. D. *Science* **2001**, *293*, 1119-1122.
- (38) Hadziioannou, G.; Malliaras, G. G. *Semiconducting Polymers: Chemistry, Physics and Engineering*; Wiley-VCH: Weinheim, 2006; Vol. 2.
- (39) Heeger, A. J. *Angew. Chem. Int. Ed.* **2001**, *40*, 2591-2611.
- (40) Sirringhaus, H.; Brown, P. J.; Friend, R. H.; Nielsen, M. M.; Bechgaard, K.; Langeveld-Voss, B. M. W.; Spiering, A. J. H.; Janssen, R. A. J.; Meijer, E. W.; Herwig, P.; de Leeuw, D. M. *Nature* **1999**, *401*, 685-688.
- (41) Lehn, J. M.; Atwood, J. L.; Davies, J. E. D.; MacNicol, D. D.; Vögtle, F. *Comprehensive Supramolecular Chemistry*; Pergamon: New York, 1996.
- (42) Whitesides, G. M.; Mathias, J. P.; Seto, C. T. *Science* **1991**, *254*, 1312-1319.

- (43) Hoeben, F. J. M.; Jonkheijm, P.; Meijer, E. W.; Schenning, A. P. H. J. *Chem. Rev.* **2005**, *105*, 1491-1546.
- (44) Simpson, C. D.; Wu, J.; Watson, M. D.; Mullen, K. J. *Mater. Chem.* **2004**, *14*, 494-504.
- (45) Meijer, E. W.; Schenning, A. P. H. J. *Nature* **2002**, *419*, 353-354.
- (46) Whitesides, G. M.; Grzybowski, B. *Science* **2002**, *295*, 2418-2421.
- (47) Sergeyev, S.; Pisula, W.; Geerts, Y. H. *Chem. Soc. Rev.* **2007**, *36*, 1902-1929.
- (48) Schenning, A. P. H. J.; Meijer, E. W. *Chem. Commun.* **2005**, 3245-3258.
- (49) Sangeetha, N. M.; Maitra, U. *Chem. Soc. Rev.* **2005**, *34*, 821-836.
- (50) Terech, P.; Weiss, R. G. *Chem. Rev.* **1997**, *97*, 3133-3160.
- (51) Hill, J. P.; Jin, W.; Kosaka, A.; Fukushima, T.; Ichihara, H.; Shimomura, T.; Ito, K.; Hashizume, T.; Ishii, N.; Aida, T. *Science* **2004**, *304*, 1481-1483.
- (52) Leclere, P.; Surin, M.; Viville, P.; Lazzaroni, R.; Kilbinger, A. F. M.; Henze, O.; Feast, W. J.; Cavallini, M.; Biscarini, F.; Schenning, A. P. H. J.; Meijer, E. W. *Chem. Mater.* **2004**, *16*, 4452-4466.
- (53) Ajayaghosh, A.; George, S. J. *J. Am. Chem. Soc.* **2001**, *123*, 5148-5149.
- (54) Hiromitsu, M. *Chem. Eur. J.* **2008**, *14*, 11274-11282.
- (55) Saeva, F. D. *Liquid Crystals: The Fourth State of Matter*; Marcel Dekker Inc.: New York, 1979.
- (56) Reinitzer, F. *Monatsh. Chem.* **1888**, *9*, 421.
- (57) Lehmann, O. *Z. Phys. Chem.* **1889**, *4*, 462.
- (58) Kirsch, P.; Bremer, M. *Angew. Chem.* **2000**, *39*, 4216-4235.
- (59) Edwards, P. *Modern Plastics* **1989**, 32.
- (60) Chandrasekhar, S. *Liquid Crystals*; 2 ed.; Cambridge University Press: Cambridge, 1993.
- (61) Collings, P. J.; Hird, M. *Introduction to Liquid Crystals, Chemistry and Physics*; Taylor & Francis: London, 1997.
- (62) Israelachvili, J. N.; Mitchel, D. J.; Ninham, B. W. *J. Chem. Soc., Faraday Trans. 2* **1976**, *72*, 1525.
- (63) Wunderlich, B.; Grebowicz, J. *Adv. Polymer Sci.* **1984**, *60/61*, 1.
- (64) Timmermans, J. *J. Phys. Chem. Solids* **1961**, *18*, 1-8.
- (65) Bates, F. S.; Fredrickson, G. H. *Ann. Rev. Phys. Chem.* **1990**, *41*, 525.
- (66) Barón, M.; Stepto, R. F. T. *Pure Appl. Chem.* **2002**, *74*, 493-509.
- (67) Tschierske, C.; Pelzl, G.; Diele, S. *Angew. Chem.* **2004**, *116*, 6340-6368.

- (68) Li, Q.; Li, L. In *Thermotropic Liquid Crystals: Recent Advances*; Ayyalusamy, R., Ed.; Springer: Dordrecht, 2007, p 297.
- (69) Laschat, S.; Baro, A.; Steinke, N.; Giesselmann, F.; Hägele, C.; Scalia, G.; Judele, R.; Kapatsina, E.; Sauer, S.; Schreivogel, A.; Tosoni, M. *Angew. Chem. Int. Ed.* **2007**, *46*, 4832-4887.
- (70) O'Neill, M.; Kelly, S. M. *Adv. Mater.* **2003**, *15*, 1135-1146.
- (71) Vorländer, D. *Z. Phys. Chem.* **1923**, *105*, 211–54.
- (72) Chandrasekhar, S.; Sadashiva, B. K.; Suresh, K. A. *Pramana* **1977**, *9*, 471-480.
- (73) Hunter, C. A.; Sanders, J. K. M. *J. Am. Chem. Soc.* **1990**, *112*, 5525-5534.
- (74) Guillon, D. *Structure & Bonding*; Springer: Berlin / Heidelberg, 1999; Vol. 95.
- (75) Chandrasekhar, S.; Ranganath, G. S. *Rep. Prog. Phys.* **1990**, *53*, 57.
- (76) Levelut, A. M. *J. Chim. Phys. Phys.- Chim. Biol.* **1983**, *80*, 149-161.
- (77) Beginn, U. *Prog. Polym. Sci.* **2003**, *28*, 1049-1105.
- (78) Tschierske, C. *Annu. Rep. R. Soc. Chem. Sect. C. Phys. Chem.* **2001**, *97*, 191-267.
- (79) Davidson, P.; Levelut, A. M.; Strzelecka, H.; Gionis, V. *J. Physique Lett.* **1983**, *44*, 823-828.
- (80) Malehete, J.; Levelut, A.-M.; Liebert, L. *Adv. Mater.* **1992**, *4*, 37-41.
- (81) Shimizu, Y.; Miya, M.; Nagata, A.; Ohta, K.; Matsumura, A.; Yamamoto, I.; Kusabayashi, A. *Chem. Lett.* **1991**, 25.
- (82) Kumar, S. *Chem. Soc. Rev.* **2006**, *35*, 83-109.
- (83) Glüsen, B.; Heitz, W.; Kettner, A.; Wendorff, J. H. *Liq. Cryst.* **1996**, *20*, 627 - 633.
- (84) Heiney, P. A.; Fontes, E.; de Jeu, W. H.; Riera, A.; Carroll, P.; Smith, A. B. *J. Phys. France* **1989**, *50*, 461-483.
- (85) Bisoyi, H. K.; Kumar, S. *Chem. Soc. Rev.* **2010**, *39*, 264-285.
- (86) Praefcke, K.; Singer, D.; Kohne, B.; Ebert, M.; Liebmann, A.; Wendorff, J. H. *Liq. Cryst.* **1991**, *10*, 147 - 159.
- (87) Adam, D.; Schuhmacher, P.; Simmerer, J.; Haussling, L.; Siemensmeyer, K.; Etzbacher, K. H.; Ringsdorf, H.; Haarer, D. *Nature* **1994**, *371*, 141-143.
- (88) Lever, L. J.; Kelsall, R. W.; Bushby, R. J. *Phys. Rev. B: Condens. Matter* **2005**, *72*, 035130.
- (89) Boden, N.; Bushby, R. J.; Clements, J.; Movaghar, B.; Donovan, K. J.; Kreouzis, T. *Phys. Rev. B: Condens. Matter* **1995**, *52*, 13274.
- (90) Bushby, R. J.; Lozman, O. R. *Curr. Opin. Colloid Interface Sci.* **2002**, *6*, 569-578.
- (91) Pecchia, A.; Lozman, O. R.; Movaghar, B.; Boden, N.; Bushby, R. J.; Donovan, K. J.; Kreouzis, T. *Phys. Rev. B: Condens. Matter* **2002**, *65*, 104204.

- (92) Cornil, J.; Lemaury, V.; Calbert, J. P.; Brédas, J. L. *Adv. Mater.* **2002**, *14*, 726-729.
- (93) Wegewijs, B. R.; Siebbeles, L. D. A.; Boden, N.; Bushby, R. J.; Movaghar, B.; Lozman, O. R.; Liu, Q.; Pecchia, A.; Mason, L. A. *Phys. Rev. B: Condens. Matter* **2002**, *65*, 245112.
- (94) Markovitsi, D. *Mol. Cryst. Liq. Cryst.* **2003**, *397*, 1 - 1.
- (95) Ohta, K.; Hatsusaka, K.; Sugibayashi, M.; Ariyoshi, M.; Ban, K.; Maeda, F.; Naito, R.; Nishizawa, K.; van de Craats, A. M.; Warman, J. M. *Mol. Cryst. Liq. Cryst.* **2003**, *397*, 1 - 1.
- (96) Pisula, W.; Zorn, M.; Chang, J. Y.; Müllen, K.; Zentel, R. *Macromol. Rapid Commun.* **2009**, *30*, 1179-1202.
- (97) Markovitsi, D.; Marguet, S.; Bondkowski, J.; Kumar, S. *J. Phys. Chem. B* **2001**, *105*, 1299-1306.
- (98) Bushby, R. J.; Lozman, O. R. *Curr. Opin. Colloid Interface Sci.* **2002**, *7*, 343-354.
- (99) Coropceanu, V.; Cornil, J. r. m.; da Silva Filho, D. A.; Olivier, Y.; Silbey, R.; Brédas, J.-L. *Chem. Rev.* **2007**, *107*, 926-952.
- (100) Schouten, P. G.; Warman, J. M.; de Haas, M. P.; van Nostrum, C. F.; Gelinck, G. H.; Nolte, R. J. M.; Copyn, M. J.; Zwikker, J. W.; Engel, M. K. *J. Am. Chem. Soc.* **1994**, *116*, 6880-6894.
- (101) Brinza, M.; Adriaenssens, G. J. *J. Optoelectron. Adv. Mater.* **2006**, *8*, 2028-2034
- (102) Zaumseil, J.; Sirringhaus, H. *Chem. Rev.* **2007**, *107*, 1296-1323.
- (103) Monobe, H.; Awazu, K.; Shimizu, Y. *Adv. Mater.* **2006**, *18*, 607-610.
- (104) Pisula, W.; Menon, A.; Stepputat, M.; Lieberwirth, I.; Kolb, U.; Tracz, A.; Sirringhaus, H.; Pakula, T.; Müllen, K. *Adv. Mater.* **2005**, *17*, 684-689.
- (105) Tracz, A.; Jeszka, J. K.; Watson, M. D.; Pisula, W.; Mullen, K.; Pakula, T. *J. Am. Chem. Soc.* **2003**, *125*, 1682-1683.
- (106) Boden, N.; Bushby, R. J.; Martin, P. S.; Evans, S. D.; Owens, R. W.; Smith, D. A. *Langmuir* **1999**, *15*, 3790-3797.
- (107) Hoogboom, J.; Garcia, P. M. L.; Otten, M. B. J.; Elemans, J. A. A. W.; Sly, J.; Lazarenko, S. V.; Rasing, T.; Rowan, A. E.; Nolte, R. J. M. *J. Am. Chem. Soc.* **2005**, *127*, 11047-11052.
- (108) Bunk, O.; Nielsen, M. M.; Solling, T. I.; van de Craats, A. M.; Stutzmann, N. *J. Am. Chem. Soc.* **2003**, *125*, 2252-2258.
- (109) Craats, A. M. v. d.; Stutzmann, N.; Bunk, O.; Nielsen, M. M.; Watson, M.; Müllen, K.; Chanzy, H. D.; Sirringhaus, H.; Friend, R. H. *Adv. Mater.* **2003**, *15*, 495-499.
- (110) Zimmermann, S.; Wendorff, J. H.; Weder, C. *Chem. Mater.* **2002**, *14*, 2218-2223.
- (111) Tant, J.; Geerts, Y. H.; Lehmann, M.; De Cupere, V.; Zucchi, G.; Laursen, B. W.; Bjornholm, T.; Lemaury, V.; Marcq, V.; Burquel, A.; Hennebicq, E.; Gardebien, F.; Viville, P.; Beljonne, D.; Lazzaroni, R.; Cornil, J. *J. Phys. Chem. B* **2005**, *109*, 20315-20323.

- (112) MacDonald, W. A. *J. Mater. Chem.* **2004**, *14*, 4-10.
- (113) Méry, S.; Haristoy, D.; Nicoud, J.-F.; Guillon, D.; Diele, S.; Monobe, H.; Shimizu, Y. *J. Mater. Chem.* **2002**, *12*, 37-41.
- (114) Greene, M. In *High Performance Pigments*; Faulkner, E. B., Schwartz, R. J., Eds.; Wiley-VCH: Weinheim, 2009.
- (115) Würthner, F. *Chem. Commun.* **2004**, 1564-1579.
- (116) Langhals, H. *Helv. Chim. Acta* **2005**, *88*, 1309-1343.
- (117) Struijk, C. W.; Sieval, A. B.; Dakhorst, J. E. J.; van Dijk, M.; Kimkes, P.; Koehorst, R. B. M.; Donker, H.; Schaafsma, T. J.; Picken, S. J.; van de Craats, A. M.; Warman, J. M.; Zuilhof, H.; Sudholter, E. J. R. *J. Am. Chem. Soc.* **2000**, *122*, 11057-11066.
- (118) Horowitz, G.; Kouki, F.; Spearman, P.; Fichou, D.; Nagues, C.; Pan, X.; Garnier, F. *Adv. Mater.* **1996**, *8*, 242-245.
- (119) Dimitrakopoulos, C. D.; Malenfant, P. R. L. *Adv. Mater.* **2002**, *14*, 99-117.
- (120) Geissler, G.; Remy, H. *Ger. Pat. Appl., DE 1130099* **1959**.
- (121) Jancy, B.; Asha, S. K. *J. Phys. Chem. B* **2006**, *110*, 20937-20947.
- (122) Yakimov, A.; Forrest, S. R. *Appl. Phys. Lett.* **2002**, *80*, 1667.
- (123) Liu, S.-G.; Sui, G.; Cormier, R. A.; Leblanc, R. M.; Gregg, B. A. *J. Phys. Chem. B* **2002**, *106*, 1307-1315.
- (124) Kardos, M. D. R. P. 276357, 1913.
- (125) Anton, U.; Göltner, C.; Müllen, K. *Chem. Ber.* **1992**, *125*, 2325-2330.
- (126) Göltner, C.; Pressner, D.; Müllen, K.; Spiess, H. W. *Angew. Chem. Int. Ed.* **1993**, *32*, 1660-1662.
- (127) Cormier, R. A.; Gregg, B. A. *J. Phys. Chem. B* **1997**, *101*, 11004-11006.
- (128) Cormier, R. A.; Gregg, B. A. *Chem. Mater.* **1998**, *10*, 1309-1319.
- (129) Gregg, B. A.; Cormier, R. A. *J. Phys. Chem. B* **1998**, *102*, 9952-9957.
- (130) Würthner, F.; Thalacker, C.; Diele, S.; Tschierske, C. *Chem. Eur. J.* **2001**, *7*, 2245-2253.
- (131) Jancy, B.; Asha, S. K. *Chem. Mater.* **2007**, *20*, 169-181.
- (132) Hansen, M. R.; Schnitzler, T.; Pisula, W.; Graf, R.; Müllen, K.; Spiess, Hans W. *Angew. Chem. Int. Ed.* **2009**, *48*, 4621-4624.
- (133) Zucchi, G.; Donnio, B.; Geerts, Y. H. *Chem. Mater.* **2005**, *17*, 4273-4277.
- (134) Zucchi, G. I.; Viville, P.; Donnio, B.; Vlad, A.; Melinte, S.; Mondeshki, M.; Graf, R.; Spiess, H. W.; Geerts, Y. H.; Lazzaroni, R. *J. Phys. Chem. B* **2009**, *113*, 5448-5457.

- (135) Cisse, L.; Destruel, P.; Archambeau, S.; Seguy, I.; Jolinat, P.; Bock, H.; Grelet, E. *Chem. Phys. Lett.* **2009**, *476*, 89-91.
- (136) Benning, S.; Kitzerow, H.-S.; Bock, H.; Achard, M.-F. *Liq. Cryst.* **2000**, *27*, 901 - 906.
- (137) Nolde, F.; Wojciech, P.; Sibylle, M.; Christopher, K.; Klaus, M. *Chem. Mater.* **2006**, *18*, 3715-3725.
- (138) Do, J. Y.; Kim, B. G.; Kwon, J. y.; Shin, W. s.; Jin, S.-H.; Kim, Y.-I. *Macromol. Symp.* **2007**, *249-250*, 461-465.
- (139) Balakrishnan, K.; Datar, A.; Oitker, R.; Chen, H.; Zuo, J.; Zang, L. *J. Am. Chem. Soc.* **2005**, *127*, 10496-10497.
- (140) Che, Y.; Datar, A.; Balakrishnan, K.; Zang, L. *J. Am. Chem. Soc.* **2007**, *129*, 7234-7235.
- (141) Che, Y.; Yang, X.; Loser, S.; Zang, L. *Nano Lett.* **2008**, *8*, 2219-2223.
- (142) Sugiyasu, K.; Fujita, N.; Shinkai, S. *Angew. Chem. Int. Ed.* **2004**, *43*, 1229-1233.
- (143) Ghosh, S.; Li, X.-Q.; Stepanenko, V.; Würthner, F. *Chem. Eur. J.* **2008**, *14*, 11343-11357.
- (144) Li, X.-Q.; Zhang, X.; Ghosh, S.; Würthner, F. *Chem. Eur. J.* **2008**, *14*, 8074-8078.
- (145) Würthner, F.; Bauer, C.; Stepanenko, V.; Yagai, S. *Adv. Mater.* **2008**, *20*, 1695-1698.
- (146) Würthner, F.; Hanke, B.; Lysetska, M.; Lambright, G.; Harms, G. S. *Org. Lett.* **2005**, *7*, 967-970.
- (147) Seki, T.; Yagai, S.; Karatsu, T.; Kitamura, A. *J. Org. Chem.* **2008**, *73*, 3328-3335.
- (148) Yagai, S.; Monma, Y.; Kawauchi, N.; Karatsu, T.; Kitamura, A. *Org. Lett.* **2007**, *9*, 1137-1140.
- (149) Ji, H.-F.; Majithia, R.; Yang, X.; Xu, X.; More, K. *J. Am. Chem. Soc.* **2008**, *130*, 10056-10057.

## 2. THESIS OVERVIEW

This thesis addresses the tailor-made synthesis and characterization of different self-organizing perylene derivatives as electronically active n-type semiconducting dyes for application in organic photovoltaic devices (OPV). The primary question addressed the design of molecular architectures in order to obtain novel self-assembling structures leading to new classes of n-type semiconductors. The central focus of self-assembly was set on two distinct supramolecular self-organization phenomena: 1) liquid crystalline order and 2) hydrogen-bond or solvent directed self-assembly. In this thesis the majority of work was devoted to the liquid crystalline ordering of discotic shaped perylene molecules (DLCs). Additionally, H-bond/solvent directed self-assembly for the creation of nanofibrous networks and their implementation into photovoltaic devices was also examined (Fig. 1).

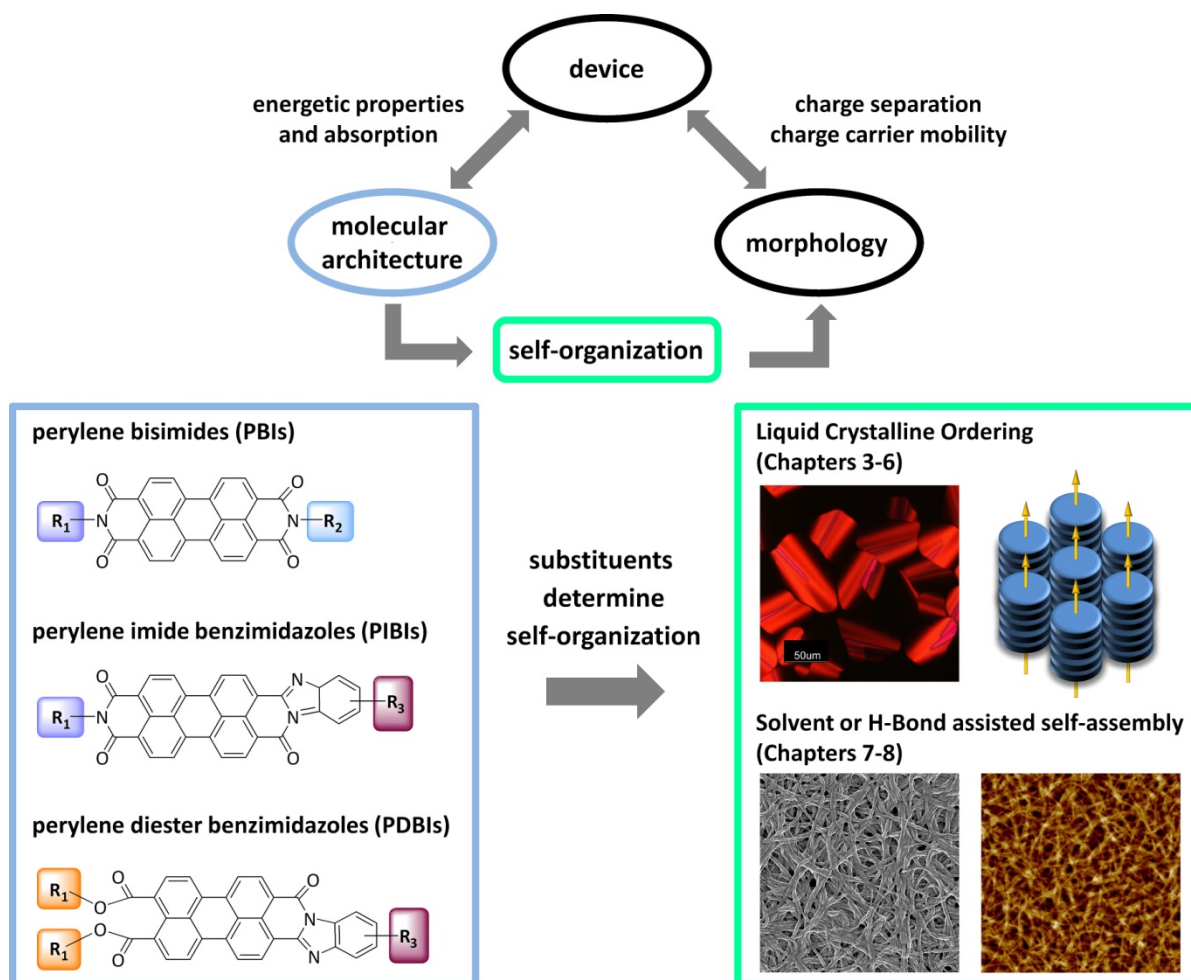
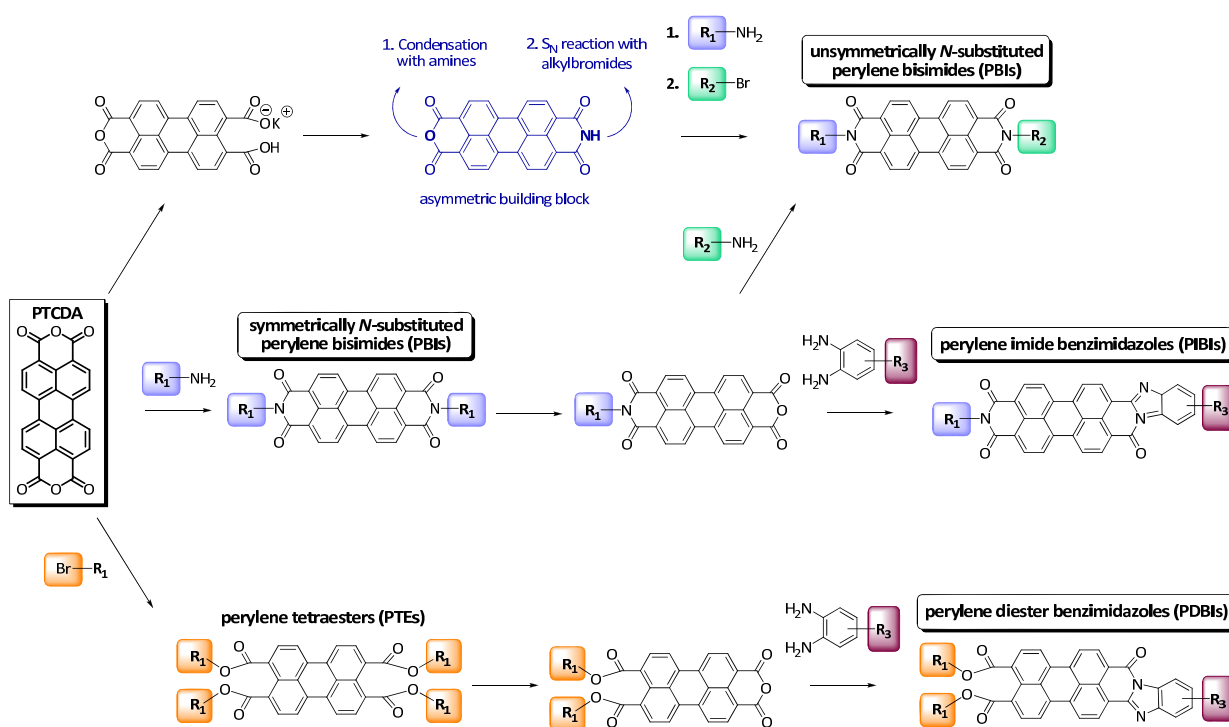


**Figure 1.** Dependency between molecular structure, morphology and device performance. These three main aspects are addressed in this thesis by synthesizing self-organizing perylene derivatives capable of either liquid crystalline ordering which allows for high intracolumnar charge carrier mobility or solvent or hydrogen-bond assisted self-assembly for the formation of nanostructured networks with large interface area and well defined charge carrier pathways.

Both self-organization principles are promising approaches to improve device efficiency. On the one hand, columnar liquid crystalline ordering allows for a high intracolumnar charge carrier mobility in these quasi one-dimensional “nanowires”. On the other hand, a nanostructured fibrous network provides a large interface area between electron acceptor and a suitable donor material, together with well defined charge transport pathways in the bulk. Thus my endeavor addresses fundamental issues in photovoltaic devices, like morphology of the electron accepting component together with optical and electronic properties. The molecular architecture was varied to get new classes of n-type semiconductors with extended absorption in the visible range and to obtain different kinds of ordering or packing such as columnar hexagonal or two-dimensional lamellar structures.

The dissertation contains six manuscripts that focus on different aspects of novel discotic perylene dyes. The chapters can basically be divided into two topics. The first part of the thesis (chapters 3-6) concerns the synthesis and characterization of liquid crystalline perylene dyes with a focus on the extension of absorption in the visible region as well as tailoring the mesophase temperature-width and packing behaviour. In this context, the major challenge was to effectively suppress the inherent tendency of the perylene moieties for crystallization. An overview of the synthetic strategies starting from perylene tetracarboxylic acid dianhydride (PTCDA) for the preparation of various classes of perylene dyes is presented in Scheme 1. A substitution at the bay-positions of the perylene core was avoided in all cases, in order to maintain the planarity and strong  $\pi$ - $\pi$  interactions, which favour intermolecular order and charge carrier transport.



**Scheme 1.** Overview of synthetic strategies starting from perylene tetracarboxylic acid dianhydride (PTCDA) for the synthesis of symmetrically or unsymmetrically N-substituted perylene bisimides (PBIs) and new classes of asymmetric perylene diester benzimidazoles (PDBIs) and perylene imide benzimidazoles (PIBIs) comprising a mixed substitution pattern.

In this work a comprehensive structure-property relationship to understand fundamental molecular design requirements to induce thermotropic liquid crystalline phases in PBIs was accomplished (Chapter 3). The introduction of branched (“swallow-tail”) oligooxyethylene *N*-substituents was crucial for obtaining liquid crystallinity and intracolumnar long-range order. Further, novel classes of *n*-type semiconductors with an extended  $\pi$ -conjugation system and an asymmetric substitution pattern, like perylene imide benzimidazoles (PIBI, chapter 4) and perylene diester benzimidazoles (PDBIs, Chapter 5) were synthesized. Chapter 4 demonstrates the introduction of a fused benzimidazole moiety on the perylene core, resulting in asymmetric perylene imide benzimidazoles (PIBIs). These dyes exhibit a significantly extended absorption to longer wavelengths in the visible spectrum and show for the first time self-organization ability into columnar hexagonal liquid crystalline phases for this special type of material. Chapter 5 takes advantage of this result and expands the concept towards novel asymmetric perylene diester benzimidazoles (PDBIs). Likewise, these dyes exhibit a broad absorption in the visible wavelength regime and additionally exhibit room temperature mesophases. Thermotropic behavior of all novel discogens was investigated thoroughly by differential scanning calorimetry (DSC), polarization optical microscopy (POM) and X-ray diffraction experiments (XRD). By these methods, liquid crystalline packing such as columnar hexagonal mesophases (Col<sub>h</sub>) for all three types of compounds, but as well compounds with a columnar hexagonal plastic phase (Col<sub>hp</sub>) or crystalline lamellar phases (Cr<sub>L</sub>) were confirmed. Such systems are highly interesting for applications requiring high order in the molecular arrangement. Figure 2a illustrates typical X-ray diffractograms for these types of phases.

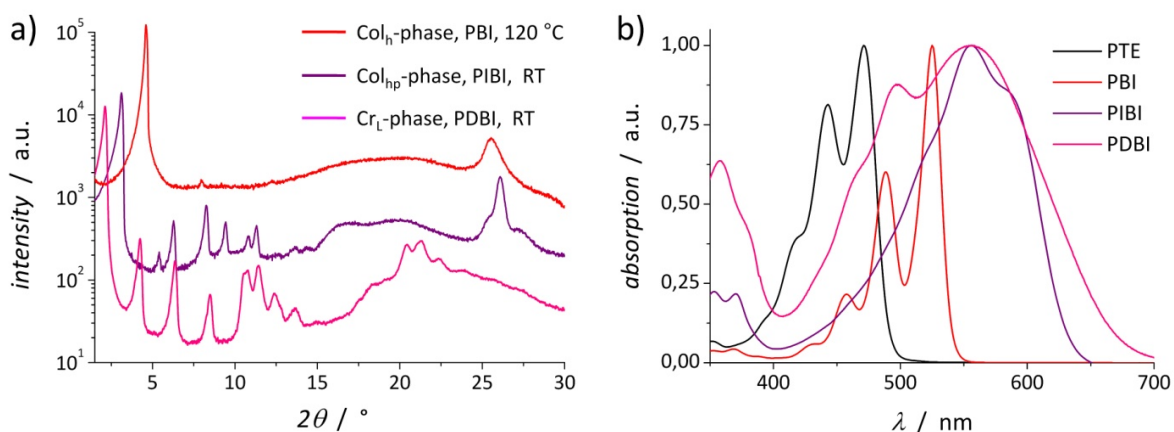


**Figure 2.** (a) X-ray diffractograms for the columnar hexagonal mesophase of a **PBI**, columnar hexagonal plastic phase of a **PIBI** and crystalline lamellar phase of a **PDBI** derivative. (b) UV/Vis absorption spectra of representative **PTE**, **PBI**, **PDBI** and **PIBI** derivatives. The absorption in the visible wavelength regime could be extended up to 680 nm.

The optical and electronic properties were studied via UV/Vis spectroscopy and cyclic voltammetry measurements (CV). Figure 2b gives an overview of absorption spectra of representative candidates of the different classes of perylene dyes. It can clearly be seen that the

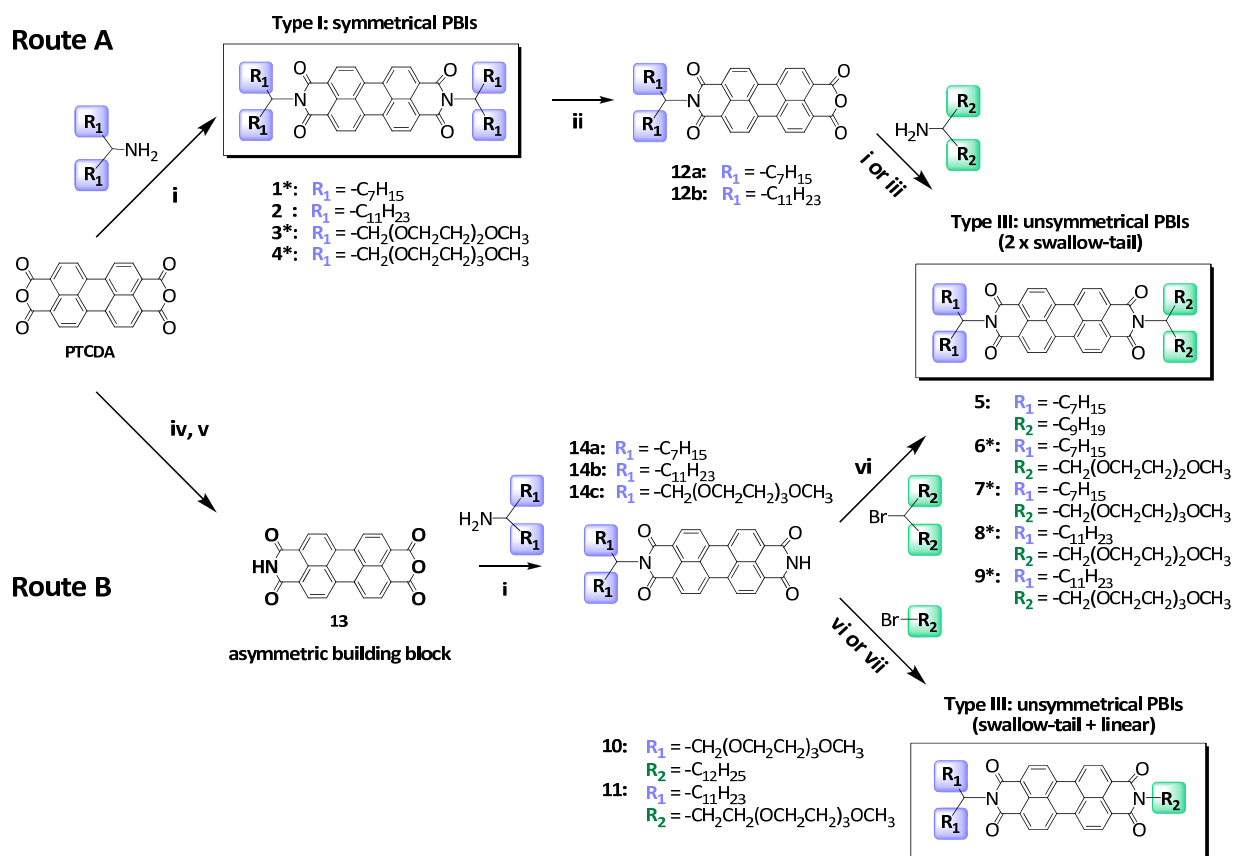
absorption in the visible regime can be red-shifted immensely from PTEs to PIBs and PDBIs due to an extended  $\pi$ -conjugation system. This is also the molecular origin for a decrease of the band-gap in PDBIs and PIBs, which is mainly caused by a raise of the HOMO energy levels. Generally, HOMO values lie in between -5.5 and -6.1 eV and LUMO energy-values between -3.5 eV and -3.8 eV. Finally in chapter 6, a detailed study of donor/acceptor blends of discotic perylene bisimide (based on the results of chapter 3,) and Cu-phthalocyanine (CuPc) binary systems was investigated concerning blend morphology and for the purpose of elucidating their potential for light-harvesting and charge separation.

The second part of this thesis (chapter 7-8) spans the gap towards the second self-organization principle and concentrates on the self-assembly of PBIs into fibrillar nanowires. The morphology of the nanostructures was investigated by Scanning Electron Microscopy (SEM) and Atomic Force Microscopy (AFM). Chapter 7 introduces a novel concept to generate donor-acceptor interpenetrating nanostructures with inherent morphological stability by an organogel/polymer approach. Therefore the hydrogen bond directed self-assembly of a PBI organogelator in presence of an amorphous hole conducting polymer matrix of poly(vinylidimethoxytetraphenylbenzidine) (pvDMTPD) was utilized to successfully generate the active layer for photovoltaic devices (Figure 7a). The presence of percolation paths for photogenerated electrons and holes in such organogel/polymer composite material was demonstrated directly in solar cells, which delivered appreciable photocurrents and photovoltages. These excellent results stimulated for an additional effort in chapter 8, which is directed towards the synthesis of novel self-organizing PBIs with an increased chromophore content to further improve this concept. In this context, hydrogen-bond directed and solvent directed self-assembly of newly designed PBIs were studied (Figure 8).

Subsequently a brief summary of the main results is presented for each publication (Chapters 3-8). For a complete description of a particular topic and experimental details, the reader is referred to the respective chapter.

## SWALLOW-TAIL SUBSTITUTED LIQUID CRYSTALLINE PERYLENE BISIMIDES – SYNTHESIS & THERMOTROPIC PROPERTIES

The focus of investigation was directed towards designing tailor-made liquid crystalline perylene bisimides and to elucidate a structure-property relationship with respect to thermotropic behaviour in *N*-substituted derivatives of PBIs. Therefore, symmetrically and unsymmetrically *N*-substituted PBIs have been synthesized successfully by two different synthetic strategies (Route A and B in Scheme 2). The PBIs were classified into three different types of *N*-substitution patterns, involving swallow-tail and linear alkyl- or oligooxyethylene (OEG) substituents respectively (Scheme 2). Several PBIs exhibiting columnar hexagonal liquid crystalline (Col<sub>h</sub>) packing with broad liquid crystalline temperature-widths were obtained via these approaches.



**Scheme 2.** Overview of symmetrically and unsymmetrically *N*-substituted perylene bisimides (PBIs) classified according to the nature of respective *N*-substituents. Type I: symmetrically *N*-substituted PBIs (2 x swallow-tail), Type II: unsymmetrically *N*-substituted PBIs (2 x swallow-tail) and Type III: unsymmetrically *N*-substituted PBIs (swallow-tail + linear). PBIs exhibiting columnar hexagonal liquid crystalline (Col<sub>h</sub>) packing are labeled by an asterisk. Main synthetic pathways for symmetrical and unsymmetrical *N*-substitution of PBIs. i) imidazole, Zn(OAc)<sub>2</sub>, 2-4 h, 160 °C; ii) KOH, *t*-BuOH, 90 °C 1-1.5 h; iii) DMAc, Zn(OAc)<sub>2</sub>, 20 Min, 160 °C, 200 Watt; iv) 1. KOH, 2. AcOH; v) NH<sub>4</sub>OH, K<sub>2</sub>CO<sub>3</sub>; vi) DMF, K<sub>2</sub>CO<sub>3</sub>, KI, 80 °C, 3-5 d; vii) DMF, NaH, 80 °C, 48 h. Route A: 1-4 and 6-9; Route B: 5, 10 and 11.

The standard procedure for the synthesis of symmetrically *N*-substituted PBIs is the condensation of perylenetetracarboxylic acid dianhydride (PTCDA) with primary amines (Route A). The synthesis of unsymmetrically substituted PBIs is more challenging and there exist two different synthetic strategies suitable for asymmetric *N*-substitution of PBIs. The common method therefore follows a partial saponification of symmetrically *N*-substituted PBIs to afford key intermediates 12. Subsequent condensation of these monoimide-monoanhydrides 12 with a second amine results in unsymmetrically *N*-substituted PBIs (Route A). We also developed a microwave-assisted method for the second condensation reaction of monoimide-monoanhydrides 12 with amines. An alternative synthetic strategy (Route B) makes use of imide anhydride 13 as asymmetric building block. The anhydride moiety allows for condensation reactions with amines in a first step, whereas the imide moiety offers the possibility for introduction of a second *N*-substituent via nucleophilic substitution  $S_N2$  under basic conditions with alkylhalides in a second step. PBIs can be regarded as a closed chromophoric system due to nodes of the HOMO and LUMO orbitals at the imide nitrogens and accordingly, show identical absorption behaviour. Hence, the UV/Vis spectra of these compounds in very dilute  $CHCl_3$  solutions exhibit the characteristic finger-print vibronic fine structure of PBI with peaks at about 525, 490, 460 and 430 nm respectively. Due to the electronic decoupling of the perylene bisimide core and the imide substituents, also the electronic properties are similar, with LUMO energy levels of about -3.8 eV and HOMO energy values of -6.0 eV with respect to the zero energy level. In the following, the three different *N*-substitution patterns with respect to thermotropic behaviour are outlined in brief.

Type I with a symmetric *N*-substitution pattern, utilized different alkyl or OEG swallow-tail substituents to study the influence of sidechains with different spatial requirements or polarity on thermotropic behaviour. It could be shown here, that the symmetrical molecule 1 carrying alkyl substituents ( $R_1 = -C_7H_{15}$ ) exhibits a narrow monotropic hexagonal columnar  $Col_h$  mesophase upon cooling from the isotropic melt with a phase-width of only 8 °C. A simple increase in substituent length for symmetrical analogue 2 ( $R_1 = -C_{11}H_{23}$ ) does not expand the mesophase temperature-width, but surprisingly implicates crystalline behaviour. On the other hand, a change from alkyl swallow-tail to OEG swallow-tail side groups in case of PBIs 3 and 4, results in much broader liquid crystalline phases which are not monotropic. This can be attributed to the higher conformational freedom of the C-O bond as compared to C-C bond allowing for a better space filling around the discotic mesogens.

Type II uses an unsymmetrical *N*-substitution pattern comprising different alkyl swallow-tail substituents in combination with OEG swallow-tail or alkyl swallow-tail substituents with distinct spatial demands. Here an unsymmetrical *N*-substitution is used to study the impact of asymmetry of the substitution profile on thermotropic behavior. Generally, unsymmetrical PBIs with one OEG swallow-tail substituent and one alkyl swallow-tail substituent (6-9) exhibit thermotropic liquid crystalline packing. Moreover, in the unsymmetrical molecules 6-9, an increase in OEG length decreases the clearing temperature considerably, whereas a corresponding increase in alkyl chain length has only a marginal influence in decreasing the clearing temperature. It could also be

shown for these materials, that OEG sidechains pack more tightly than alkyl substituents. It is also interesting to note that unsymmetrical PBI 5 carrying two different alkyl swallow-tail chains remains a crystalline material (Fig. 3b, d and e) with a melting point of 99 °C. Thus a comparison of 1, 2 and 5 clearly shows that the  $Col_h$ -phase observed for 1 could not be broadened for 2 or 5, both by extending the length of alkyl-substituents or by introducing unsymmetrical alkyl *N*-substitution.

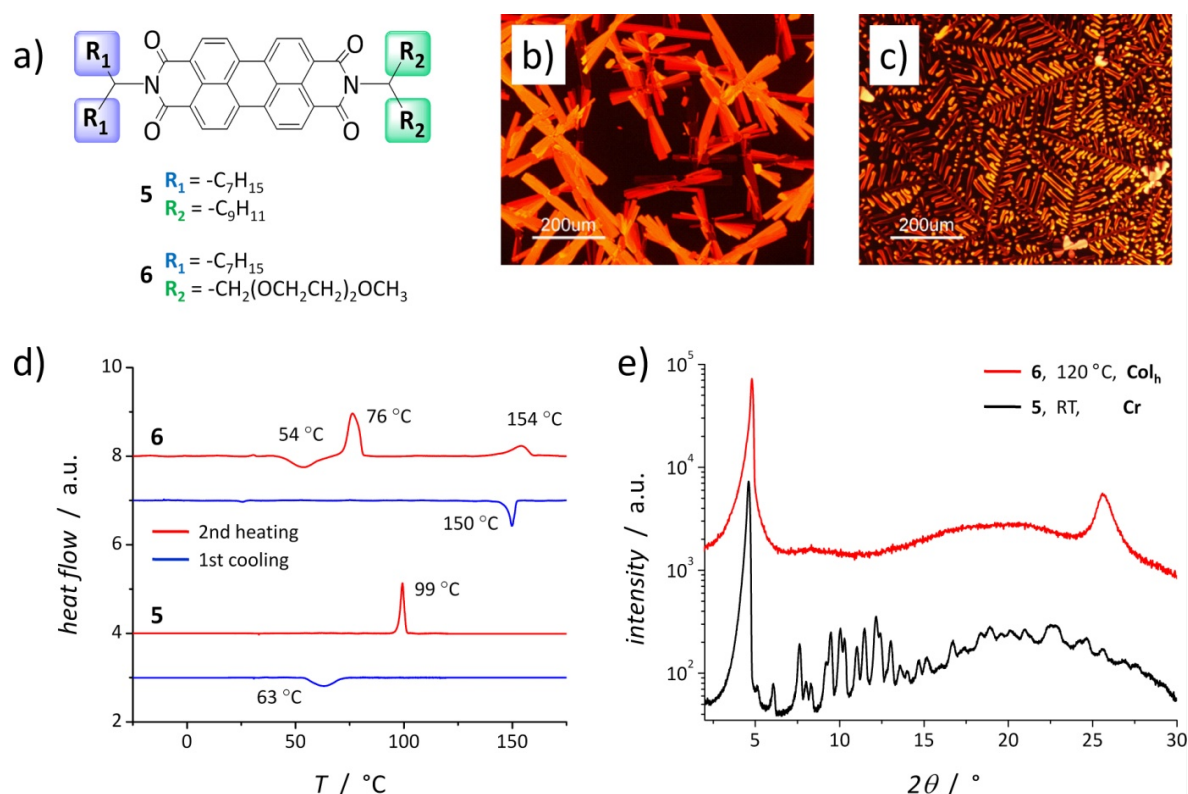


**Figure 3.** (a) Molecular structure of PBIs 5 and 6 with an identical number of sidechain atoms but different flexibility of the  $R_2$ -*N*-substituents. (b-c) Polarization optical microscopy images of 5 and 6 (under crossed polarizers). (b) Crystals of 5 formed upon annealing at 63 °C. (c) Dendritic texture of 6 at 153 °C in the  $Col_h$  phase. (d) DSC-thermograms of 5 and 6 measured at 2 Kmin<sup>-1</sup>. (e) X-ray diffraction patterns of 5 in the crystalline phase (RT) and 6 in the  $Col_h$  phase (120 °C).

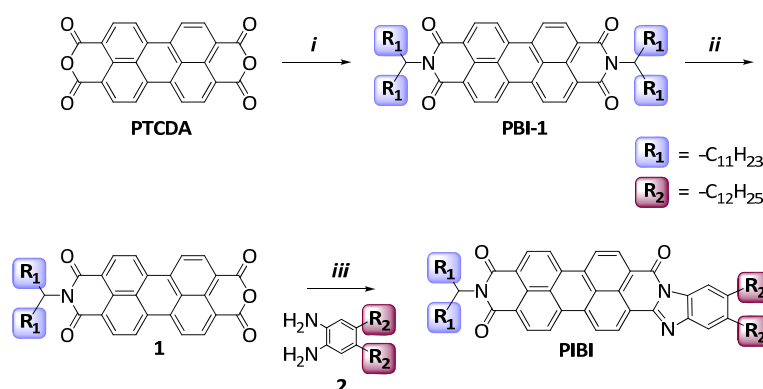
An insightful comparison can be drawn between PBIs 5 and 6, as both bear an identical number of side chain atoms but differ in flexibility of the respective  $R_2$ -substituent (Fig. 3a). As described above, PBI 5 is a crystalline material but on the other hand 6 exhibits a  $Col_h$  mesophase which can only be attributed to the presence of an OEG-substituent. Fig. 3e shows the typical diffraction pattern of a 2D-lattice with  $a_{hex} = 21.23$  nm and a  $\pi$ - $\pi$  stacking distance  $d_{\pi\pi} = 3.48$  Å for 6 in the  $Col_h$  phase at 120 °C. The dendritic texture for 6 observed in POM is consistent with a  $Col_h$ -packing in the mesophase as well (Fig. 3d). In short, the comparison of 5 and 6 clearly indicates the ability of OEG substituents to promote the liquid crystallinity of the perylene bisimide moiety.

The influence of a reduction of branched swallow-tail substituents to linear ones is investigated for PBIs of Type III, as it is of fundamental interest to design PBI semiconductors with a high content of the electronically active perylene chromophore for device applications. Thus, unsymmetrical PBIs 10 and 11 with one swallow-tail and one linear substituent were synthesized. Both 10 and 11 are crystalline materials as can be seen from DSC-thermograms and POM textures. Both compounds recrystallize on cooling and do not exhibit any supercooling effect. The absence of any mesophase indicates that the linear substituents are spatially less demanding and may not be able to fill the space sufficiently around the columnar stacked PBI molecules.

In a nutshell, it could be shown that incorporation of flexible OEG swallow-tail substituents alone or in combination with alkyl swallow-tail substituents, efficiently supports  $\text{Col}_h$  packing arising from  $\pi$ - $\pi$  interactions between cofacially orientated perylene molecules. Thus, both *N*-substituents have to be branched in nature. A reduction to linear *N*-substituents resulted in strongly crystalline behaviour. This molecular design was crucial to obtain liquid crystallinity and intracolumnar long-range order. Additionally, the melting point to the liquid crystalline phase as well as clearing temperature could be controlled very efficiently by an unsymmetrical *N*-substitution pattern. Upon cooling the liquid crystalline phase, the crystallization process of these liquid crystalline PBIs is strongly supercooled. The *N*-substituents did not influence the electronic energy levels and optical properties.

## SYNTHESIS AND STRUCTURE ELUCIDATION OF DISCOTIC LIQUID CRYSTALLINE PERYLENE IMIDE BENZIMIDAZOLE

In this chapter, the synthesis of an asymmetric perylene imide benzimidazole PIBI with an imidazole unit at 3,4 positions and an imide moiety at 9,10 positions of the perylene core is presented.



**Scheme 3.** Synthesis of asymmetric perylene imide benzimidazole PIBI. i) 1-undecyl-dodecylamine,  $\text{Zn}(\text{OAc})_2$ , imidazole, 140 °C, 2 h; ii) KOH, *tert*-BuOH, 90 °C, 1 h; iii) 2, imidazole, 180 °C, 18 h.

The extension of the  $\pi$ -conjugation system is of fundamental interest to investigate its impact on optical and electronic properties as well as on thermotropic phase behaviour. Synthesis of PIBI was carried out by partial hydrolysis of symmetrically *N*-substituted perylene bisimide PBI-1, allowing access to mixed imide-anhydride 1. The desired benzimidazole moiety was subsequently introduced by condensation of 1,2-diaminophenyl 2 with anhydride 1 to afford highly soluble PIBI (Scheme 3). In contrast to perylene bisimides (see PBI-2, Fig. 4a), the introduction of the fused benzimidazole unit on the perylene core significantly extends the absorption of PIBI to longer wavelengths up to 650 nm, with a bathochromic shift of the absorption maximum to 556 nm (Fig. 4b). Thus, the additional absorption range of 100 nm in the visible wavelength regime can be used for efficient light-harvesting in photovoltaic devices. The DSC heating and cooling curves for PIBI in Fig. 4d show two reversible phase transitions. POM-experiments provided evidence for the transition to the isotropic phase at 305 °C and a columnar hexagonal ( $\text{Col}_h$ ) ordering in the high temperature phase (between 302 to 280 °C) as indicated by the formation of typical dendritic growth aggregates (Fig. 4c). From SAXS experiments, we could assign a 2D hexagonal lattice of the columnar structure below and above the phase transition at 283 °C. For instance at 20 °C, the Bragg reflections for a hexagonal lattice with  $a_1 = a_2 = 3.49$  nm were in reasonable agreement with the typical ratios of the  $q$ -values of 1: $\sqrt{3}$ : $\sqrt{4}$ : $\sqrt{7}$ : $\sqrt{9}$ .

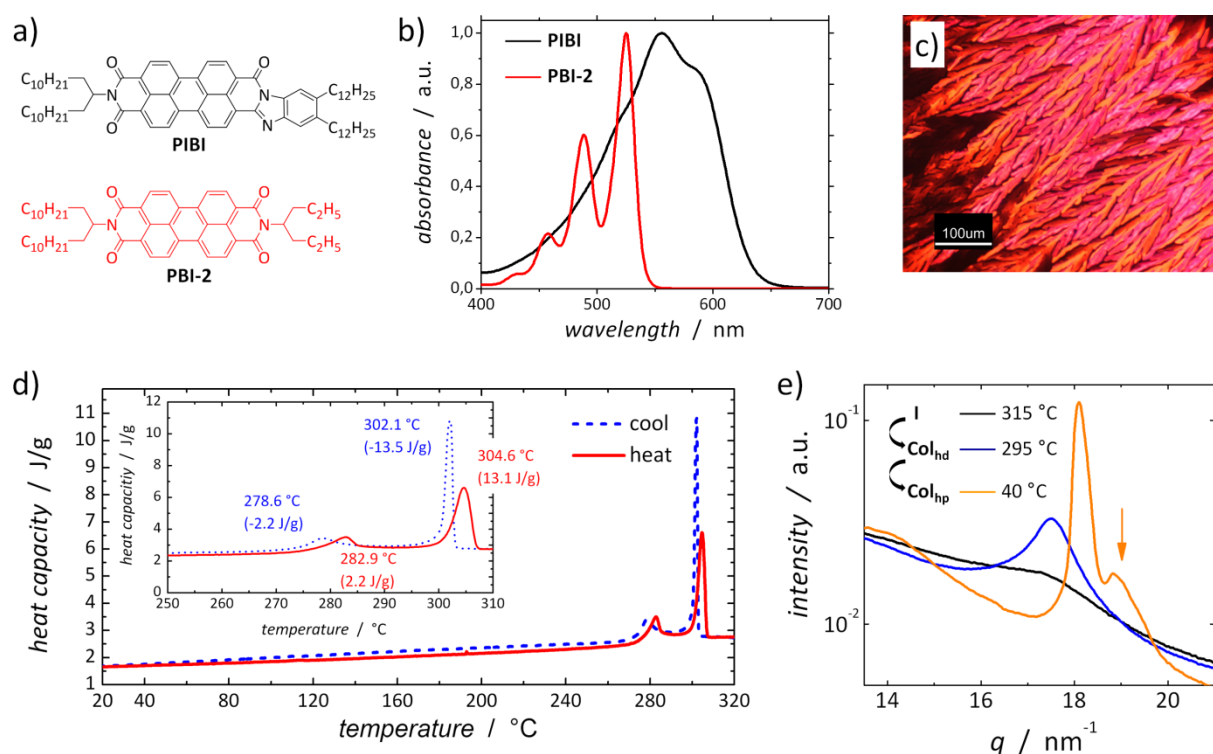


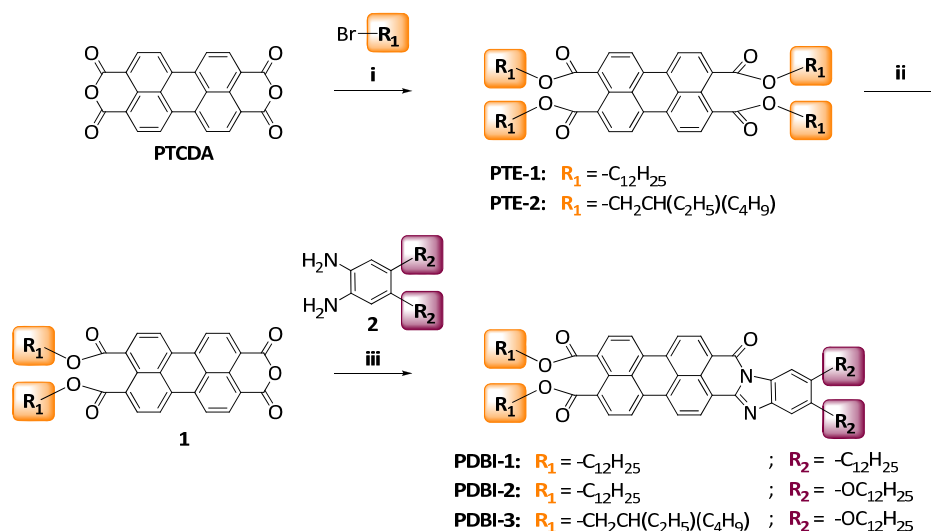
**Figure 4.** (a) Molecular structures of perylene imide benzimidazole PIBI and reference perylene bisimide PBI-2. (b) Normalized UV/Vis absorption spectra of PIBI and PBI-2. (c) Optical microscopic image (under crossed polarizers) of PIBI at 302 °C showing the dendritic texture of Col<sub>hd</sub>-phase. (d) DSC thermograms of PIBI at a scanning rate of 10 Kmin<sup>-1</sup> showing the second heating and first cooling cycle. (e) Wide-angle X-ray scattering curves with the  $q$ -range corresponding to the intracolumnar  $\pi$ - $\pi$  stacking of PIBI in the columnar hexagonal plastic (Col<sub>hp</sub>), columnar hexagonal disordered (Col<sub>hd</sub>) and isotropic (I) phase.

To directly confirm an ordered versus a disordered stacking of the discotic mesogens in both phases, we additionally performed WAXS measurements, as presented in Fig. 4e. At 40 °C, the cores were regularly stacked as can be concluded from the narrow peak at  $q = 18.07 \text{ nm}^{-1}$  and an additional reflection was observed at a higher  $q$ -value (cf. arrow Fig. 4e), which is indicative for a 3D lattice. Such mixed (hkl)-reflections generally occur in crystalline (Cr) or columnar plastic mesophases (Col<sub>p</sub>). We could conclude that PIBI exhibits a columnar plastic phase (Col<sub>hp</sub>) below 280 °C.

In summary, PIBI self-organizes into a hexagonal columnar liquid crystalline phase (Col<sub>hd</sub>) below 305 °C and transforms into a columnar plastic phase (Col<sub>hp</sub>) at lower temperatures. These findings describe for the first time the ability of perylene imide benzimidazoles to self-organize into columnar mesophases. In combination with the outstanding improvement of absorption properties, n-type semiconducting PIBI is a highly promising candidate for applications in organic electronics.

## ROOM TEMPERATURE LIQUID CRYSTALLINE PERYLENE DIESTER BENZIMIDAZOLES WITH EXTENDED ABSORPTION

Taking into consideration the advantageous effects of a fused benzimidazol moiety on the perylene core, we designed discotic molecules based on an asymmetric perylene diester benzimidazole (PDBI) structure. For this novel class of semiconductors, liquid crystalline organization also at room temperature, along with an extended absorption in the red region of visible spectrum was realized. Three derivatives bearing different substituents at the ester and benzimidazole moiety have been synthesized and characterized in detail. Synthesis of PDBIs was carried out by partial hydrolysis of symmetrically substituted perylene tetraesters (PTEs) allowing access to diester-anhydrides **1** (Scheme 4). The benzimidazole moiety was subsequently introduced by condensation of 1,2-diaminophenyls **2** with the respective anhydride **1** under microwave irradiation conditions to afford highly soluble PDBIs 1-3.



**Scheme 4.** Synthesis of asymmetric perylene diester benzimidazoles PDBIs 1-3. i) 1. KOH, H<sub>2</sub>O. 2. HCl, pH 8-9. 3. R<sub>1</sub>-Br, Aliquat 336, KI, 100 °C ii) pT<sub>2</sub>OH·H<sub>2</sub>O, n-dodecane/toluene (5:1), 95 °C. iii) 2, Zn(OAc)<sub>2</sub>, DMAc, 300 Watt, 160 °C, 20 Min.

The PDBIs exhibit extended absorption up to 680 nm, as compared to PTEs (Fig. 5a) and possess high molar extinction coefficients ( $\epsilon$ ); for instance PDBI-2 with  $\epsilon = 3.32 \cdot 10^4 \text{ L} \cdot \text{mol}^{-1} \cdot \text{cm}^{-1}$  at 554 nm. The extension of the  $\pi$ -conjugation system between the perylene core and the benzimidazole unit generally accounts for a narrowing of the HOMO–LUMO gap of the PDBI dyes. Moreover, the lowering of band-gap in PDBIs is mainly caused by a positive shift in HOMO-value rather than a negative shift in LUMO values. This is also desired, if the materials are to be used as acceptors in solar cells. It is well known, that PTEs exhibit columnar mesophases. It could be shown here, that also PDBIs self-organize into liquid crystalline columnar hexagonal phases at higher temperatures (Fig. 5b-e). Thus, the fused benzimidazole unit does not disturb liquid crystalline ordering.

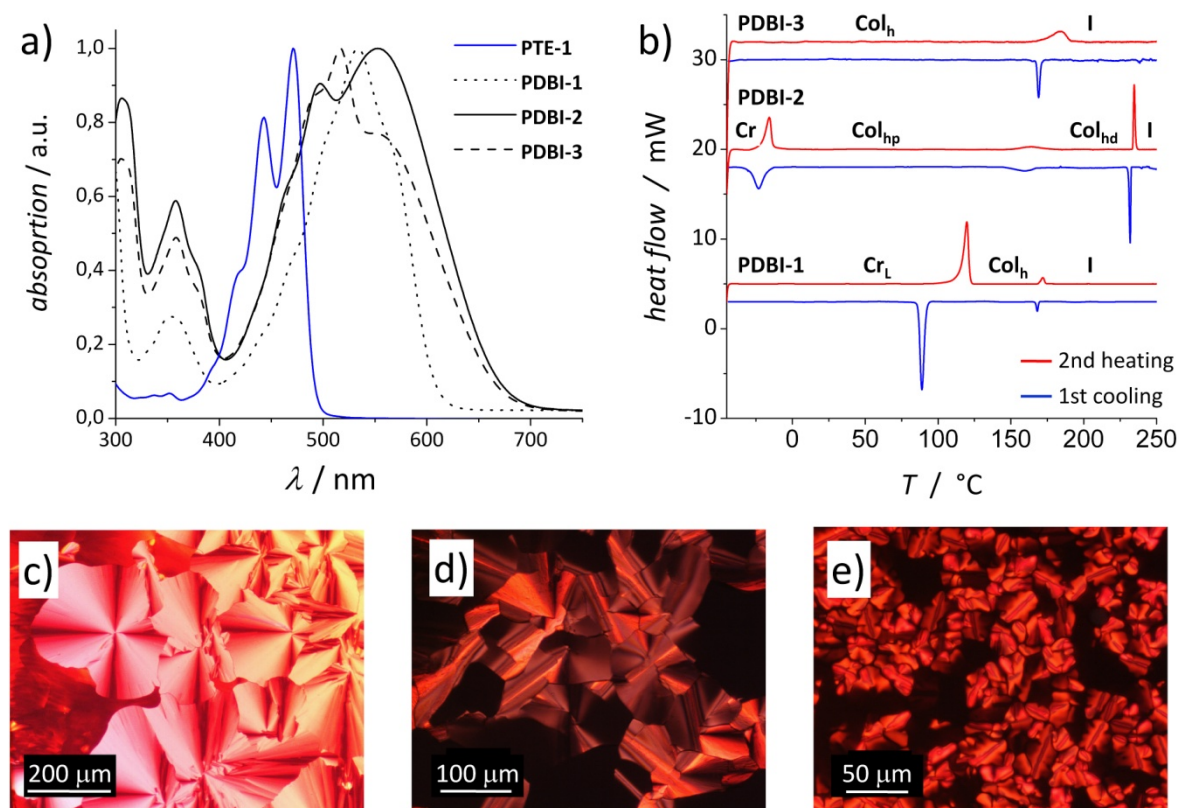


**Figure 5.** (a) UV/Vis absorption spectra of PTE-1 and PDBIs 1-3 displaying a huge extension of absorption. (b) DSC thermograms of PDBIs 1-3 at a scanning rate of  $10 \text{ Kmin}^{-1}$  showing the second heating and first cooling cycle: Cr = crystalline phase; Cr<sub>L</sub> = crystalline lamellar phase; Col<sub>h</sub> = columnar hexagonal mesophase; Col<sub>hd</sub> = disordered columnar hexagonal mesophase; Col<sub>hp</sub> = columnar plastic phase; I = isotropic phase. (c-e) Polarization optical microscopy images (under crossed polarizers). (c) Focal conic texture of PDBI-1 in Col<sub>h</sub> phase at 169 °C. (d) Mixture of mosaic and pseudo focal conic textures of PDBI-2 in Col<sub>hp</sub> phase at 130 °C. (e) Mosaic texture of Col<sub>h</sub> phase of PDBI-3 at 175 °C.

For PDBI-1, we found a lamellar ordering below 120 °C and at 172 °C PDBI-1 melts into a columnar hexagonal mesophase. Also POM observations are in accordance with this packing behavior (Fig. 5c). In contrast, PDBI-2 carrying alkoxy substituents at the benzimidazol moiety, exhibits a columnar plastic phase (Col<sub>hp</sub>, Fig. 5d) at low temperatures which converts to a columnar hexagonal disordered mesophase at 165 °C. For PDBI-3 with branched alkyl-substituents at the ester moieties we found only one reversible phase transition at 183 °C in DSC upon heating. Here, mosaic textures can be observed in POM (Fig. 5e) and also X-ray diffraction gave evidence for the existence of a liquid crystalline columnar hexagonal mesophase over the whole temperature range (-30°C – 183 °C). It is also worthy to note that PDBI-3 shows a partial homeotropic alignment of the columns as observed in POM micrographs employing a  $\lambda/4$  plate. Thus it could be shown, that the introduction of a benzimidazole moiety on the perylene core significantly extends absorption in the visible wavelength regime for PIBI (chapter 4) and PDBIs. Additionally, PDBIs 2 and 3 show liquid crystalline phases at lower temperatures. This fact is highly interesting for applications requiring high order in molecular arrangement.



substantially enhanced columnar hexagonal mesophase ( $Col_h$ ) range combined with extended intracolumnar long-range order was observed for mesogens with similar hydrophilic substituents in case of blend-2. Blend-2 clears at a considerably higher temperature than its discrete components. Furthermore this liquid crystalline phase exists over a broad temperature range, no crystallization was detected in the DSC cooling cycle until 0 °C. These results indicate a high miscibility of the two components and are in line with conclusions from POM experiments (Fig. 6). For PBI-2 dendritic-growth aggregates are observed in the mesophase under crossed polarizers (Fig. 6c) and for CuPc-2, broken fan-shaped textures indicate a  $Col_h$ -ordering between 191 °C and room temperature (Fig. 6b). For the corresponding binary blend-2, entirely new textures developed upon cooling from the isotropic melt at 230 °C (Fig. 6d). As all discogens are compatible in size, the difference in morphology can be attributed to the degree of miscibility between donor and acceptor. Additionally, both blend systems exhibit strong complementary absorption over the whole visible wavelength regime and have shown efficient photoinduced charge transfer upon PBI excitation in photoluminescence experiments. Characterization of these unique blend systems in bulk heterojunction photovoltaic devices is highly interesting for further investigations.

## SELF-ASSEMBLY OF SEMICONDUCTOR NANOWIRES FOR PHOTOINDUCED CHARGE SEPARATION

An innovative concept of general validity based on an organogel/polymer system to generate donor-acceptor nanostructures suitable for charge generation and charge transport was also studied (Fig. 7a). Hence, this work makes use of H-bond directed self-assembly of an n-type PBI organogelator (Fig. 7b), which forms nanowires in suitable solvents during gelation process. This phenomenon was applied for its self-assembly in an amorphous p-type polymer matrix (pvDMTPD, Fig. 7b) to realize an interpenetrating donor-acceptor interface with inherent morphological stability. The self-assembly and interface generation were carried out either step-wise or in a single-step methodology (Fig. 7c).

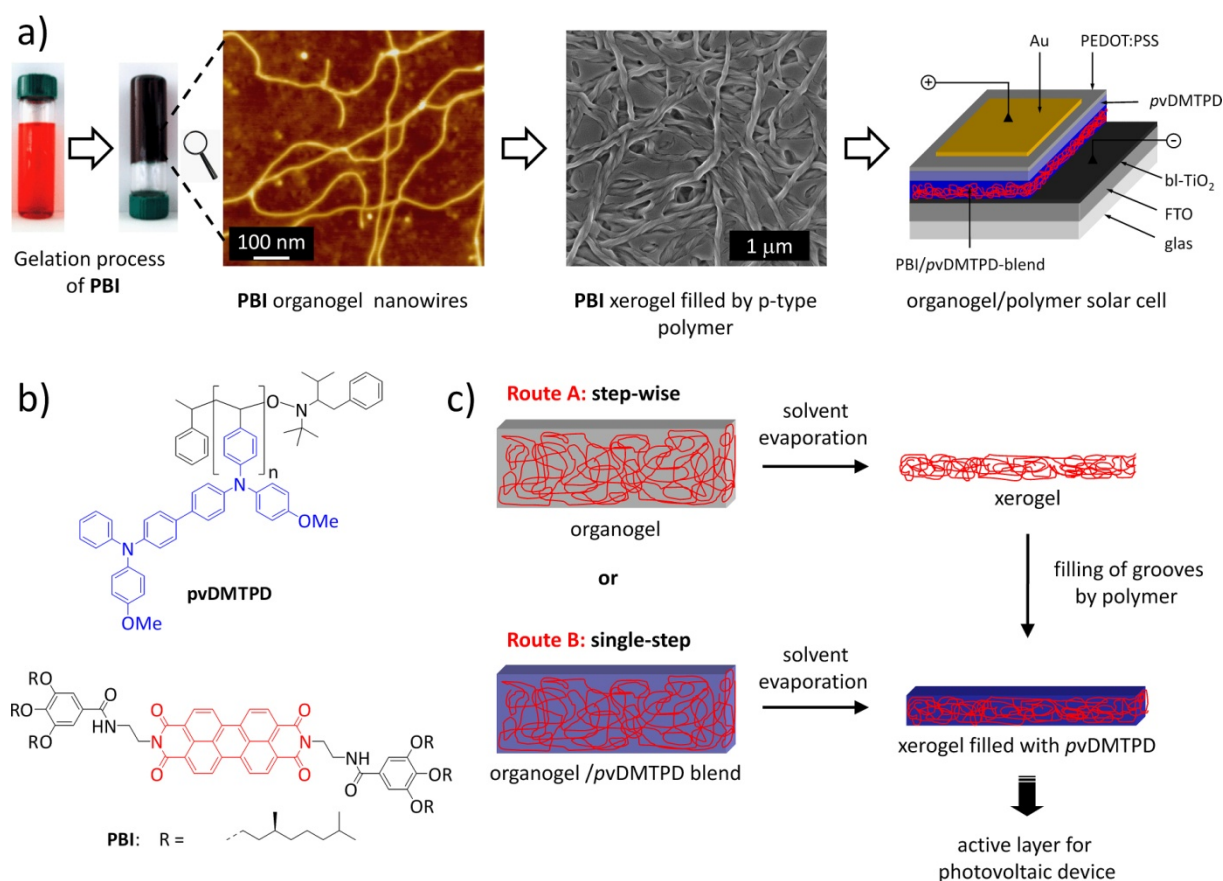


**Figure 7.** (a) Schematic presentation of the organogel/polymer concept for creation of nanostructured donor/acceptor interfaces suitable for charge generation and transport in photovoltaic devices. (b) Molecular structures of perylene bisimide organogelator PBI and hole-transporting polymer pvDMTPD. (c) Schematic representation of two distinct routes for the preparation of donor/acceptor interpenetrating networks: Route A: Formation of n-type xerogel with subsequent filling with p-type polymer. Route B: concomitant embedding of the physical network by a blend approach. Films were prepared by a doctor-blading technique from hot  $\text{CHCl}_3$  solutions.

The outstanding morphology of the network in thin films obtained via both routes was studied by a combination of scanning electron microscopy (SEM) and atomic force microscopy (AFM). The superstructure of PBI-xerogel consists of twisted strands of about 50 nm thickness which are entangled. Even though, the PBI nanofiber morphology formed in dilute solutions is metastable and aggregates over time it could be shown here, that the drying process in route A to obtain the PBI-xerogel and the blending process in route B to fix the xerogel network in a *p*vDMTPD matrix allow us to freeze in the partially aggregated nanofibrous morphology of PBI. The xerogel from route A with its nanometer sized grooves exhibits enough interstitial volume for filling with *p*vDMTPD. Furthermore, the polymer chains hinder individual gel strands from additional sticking or collapsing as compared to the pure xerogel which exhibits thicker fiber strands. Additionally, photoinduced charge separation and charge transport in these systems were tested in organic photovoltaic devices. Fabrication steps of multi-layer organogel/polymer solar cells were optimized with respect to morphology and surface roughness by introducing additional smoothing layers of *p*vDMTPD and charge injection/blocking layers of bil-TiO<sub>2</sub> and PEDOT:PSS (poly(3,4-ethylenedioxythiophene):poly(4-styrene sulphonate)). An inverted cell geometry was used, in which electrons are collected at the bottom FTO-electrode (Fluorine-doped Tin Oxide) and holes at the top Au-electrode (Fig. 7a). The simultaneous preparation of the interface via route B exhibits almost three-fold improvement in device characteristics as compared to the successive method in route A.

## APPENDIX 1: SOLVENT AND HYDROGEN-BOND DIRECTED SELF-ASSEMBLY OF PERYLENE BISIMIDES

The results described above are encouraging, since they demonstrate an universal supramolecular approach to use blends of functional low-molecular weight semiconductors with inherent self-organizing capability into fibrous nanostructures in combination with complementary semiconductor polymers to create donor-acceptor heterojunctions. The limitation in this concept was the low content of the n-type component. Therefore attempts were undertaken to decrease the amount of *N*-substituents in PBI. On the one hand, these substituents are of primary relevance for the self-organization process, but in order to increase the chromophore content, resulting in higher optical densities and better charge transport properties a compromise between active chromophore content and structure determining sidechains has to be accepted. Thus we investigated two different self-assembly strategies: solvent-assisted self-assembly of amphiphilic PBIs (Fig. 8a) or directional hydrogen bond-directed self-assembly of PBIs with an amide functionality between the chromophore core and the solubilizing side group (Fig. 8b). Thus, in analogy to chapter 3, asymmetric PBIs combining hydrophilic and hydrophobic substituents were synthesized via route B (Scheme 2). Additionally, novel amide-bond containing PBIs were synthesized. It could be shown in first experiments, that nanofibrillar structures of PBIs with a high degree of  $\pi$ - $\pi$  stacking of the chromophores are accessible by both strategies. Nevertheless suitable film processing techniques have to be developed for further application of these novel materials and hence aspects for future research are provided.

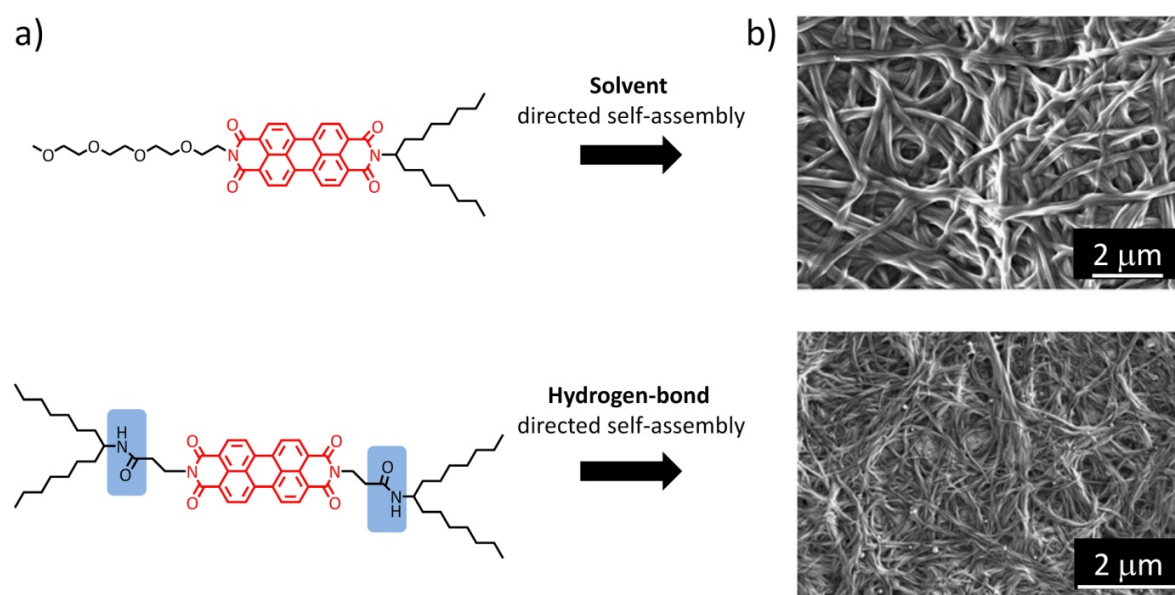


**Figure 8.** Solvent directed self-assembly of an amphiphilic *N*-substituted PBI and hydrogen-bond directed self-assembly of an amide bond-containing PBI derivative which can be utilized in photovoltaic devices. (a) Chemical structures of PBI molecules and (b) SEM images of self-assembled nanostructures thereof.



## **INDIVIDUAL CONTRIBUTIONS TO JOINT PUBLICATIONS**

This thesis consists of six individual manuscripts. Three are already published, one is submitted, one is prepared for submission and another one appears as appendix. In the following, the individual contributions of the authors of the papers are specified in detail.

### **Chapter 3**

This work is published in *Journal of the American Chemical Society* (2009, 131 (40), 1442) under the title:

**“Swallow-tail Substituted Liquid Crystalline Perylene Bisimides - Synthesis & Thermotropic Properties”**

by **André Wicklein**, Andreas Lang, Mathis Muth and Mukundan Thelakkat

I synthesized and characterized all perylene bisimide derivatives, performed the thermotropic characterization of the materials including X-ray diffraction experiments and wrote the manuscript.

Andreas Lang and Mathis Muth helped in the synthesis during their advanced lab course.

Mukundan Thelakkat supervised the project and corrected the manuscript.

### **Chapter 4**

This work is published in *Chemical Communications* (2010, 46, 2328) under the title:

**“Synthesis and Structure Elucidation of Discotic Liquid Crystalline Perylene Imide Benzimidazole”**

by **André Wicklein**, Peter Kohn, Lilit Ghazaryan, Thomas Thurn-Albrecht and Mukundan Thelakkat

I synthesized and characterized the perylene imide benzimidazole derivative, did the optical and thermal characterization and wrote the manuscript exclusive of the X-ray diffraction paragraph.

Peter Kohn performed the structural characterization of the material by X-ray diffraction experiments, was involved in the scientific discussion and wrote the X-ray diffraction paragraph.

Lilit Ghazaryan was involved in the structural characterization of the material by X-ray diffraction experiments during her advanced lab course on the topic.

Mukundan Thelakkat and Thomas Thurn-Albrecht supervised the project and corrected the manuscript.

## Chapter 5

This work is published in *Journal of Materials Chemistry* (DOI:10.1039/C0JM01626H) under the title:

### **“Room Temperature Liquid Crystalline Perylene Diester Benzimidazoles With Extended Absorption”**

by **André Wicklein**, Mathis Muth and Mukundan Thelakkat

I synthesized and characterized one of the perylene diester benzimidazole derivatives, performed the structural characterization of the materials by X-ray diffraction experiments and wrote the manuscript.

Mathis Muth synthesized and characterized two of the perylene diester benzimidazole derivatives with my help, performed the thermotropic characterization and was involved in the scientific discussion during his diploma thesis.

Mukundan Thelakkat supervised the project and corrected the manuscript.

## Chapter 6

This work is prepared for submission under the title:

### **“Self-Assembly of Donor/Acceptor Discogens in Blends: A Structural Study of Binary Cu-Phthalocyanine - Perylene Bisimide Systems”**

by **André Wicklein**, Devrim Atilla, Vefa Ahsen and Mukundan Thelakkat

I synthesized the perylene bisimides derivatives and characterized the thermotropic behaviour of the blends including X-ray diffraction experiments and wrote the manuscript.

Devrim Atilla synthesized the copper-phthalocyanine derivatives and characterized several blends by DSC and POM and was involved in scientific discussions.

Mukundan Thelakkat and Vefa Ahsen supervised the project and corrected the manuscript.

## Chapter 7

This work is published in *ACS Nano* (**2009**, 3 (5), 1107) under the title:

### **“Self-Assembly of Semiconductor Organogelator Nanowires for Photoinduced Charge Separation”**

by **André Wicklein**, Suhrit Ghosh, Michael Sommer, Frank Würthner and Mukundan Thelakkat

I optimized the processing technique for the active layer preparation, performed Scanning Electron Microscopy of thin films and Atomic Force Microscopy of thin films, fabricated and characterized photovoltaic devices and wrote the manuscript.

Suhrit Ghosh provided the perylene bisimide organogelator and was involved in the scientific discussion.

Michael Sommer provided the p-type polymer *pVDMTPD*.

Mukundan Thelakkat and Frank Würthner supervised the project and corrected the manuscript.

## Chapter 8 - Appendix

This work is prepared as a basis for further investigations towards:

### **“Solvent and Hydrogen-Bond Directed Self-Assembly of Perylene Bisimides”**

I synthesized the perylene bisimides and performed all experiments. Mukundan Thelakkat was involved in the scientific discussion and supervised the project.

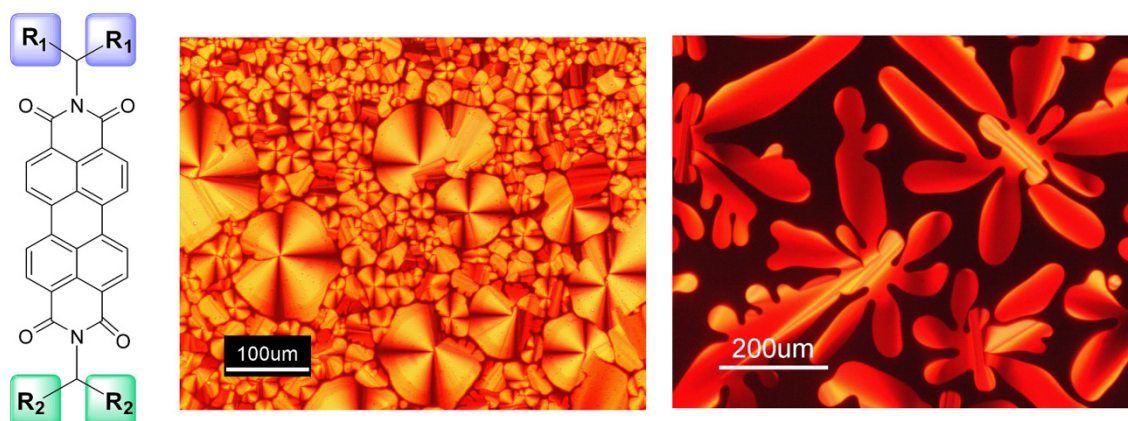


### 3. SWALLOW-TAIL SUBSTITUTED LIQUID CRYSTALLINE PERYLENE BISIMIDES – SYNTHESIS & THERMOTROPIC PROPERTIES

André Wicklein, Andreas Lang, Mathis Muth and Mukundan Thelakkat\*

Department of Macromolecular Chemistry I, Applied Functional Polymers, Universität Bayreuth, Universitätsstr. 30, 95440 Bayreuth, Germany.

Fax: +49-921-55-3206; E-mail: [mukundan.thelakkat@uni-bayreuth.de](mailto:mukundan.thelakkat@uni-bayreuth.de)



Published in *Journal of the American Chemical Society*, **2009**, 131 (40), 14442-14453

## **ABSTRACT**

Tailor-made synthesis and structure-property relationship of several swallow-tail *N*-substituted perylene bisimide (PBI) dyes are presented. PBI derivatives were synthesized by two distinct synthetic approaches, the details being evaluated herein. All the PBIs carry either alkyl swallow-tail or oligoethylenglycoether (OEG) swallow-tail moieties as *N*-substituents, and many of them are unsymmetrically substituted. We avoided substitution at bay-positions of the perylene core in order to maintain the planarity and strong  $\pi$ - $\pi$  interactions, which favour intermolecular order and charge carrier transport. The thermotropic behaviour, which is strongly influenced by the nature of the substituents was investigated using differential scanning calorimetry (DSC), polarization optical microscopy (POM) and X-ray diffraction measurements (XRD). The introduction of OEG swallow-tail units facilitates thermotropic liquid crystalline behavior in most cases and the unsymmetrical substitution allowed the tuning of the mesophase-width. The mesophases exhibit characteristic columnar hexagonal (Col<sub>h</sub>) packing arising from  $\pi$ - $\pi$  interactions between cofacially orientated perylene molecules. Thus the inherent tendency of PBI molecules for crystallization could be effectively suppressed by incorporating flexible OEG swallow-tail units only at imide positions. This molecular design was crucial to obtain liquid crystallinity and intracolumnar long-range order. The substituents did not influence the electronic energy levels such as HOMO and LUMO.

**Keywords:** perylene bisimide / liquid crystalline behaviour / thermotropic mesomorphism / n-type semiconductor.

## INTRODUCTION

Perylene bisimide<sup>1,2</sup> (PBI, perylene tetracarboxylic acid bisimide) derivatives represent an important class of n-type semiconductor materials exhibiting a relatively high electron affinity among large-band-gap materials.<sup>3-5</sup> PBIs are readily available inexpensive robust compounds, and they combine high quantum yields of photoluminescence with excellent photochemical and thermal stability.<sup>6,7</sup> PBIs are promising compounds for application in organic electronic devices.<sup>8-11</sup> The solid-state packing of the perylene bisimides determines the morphology in thin films, which plays a major role in improving the device performance. For instance, an increase in exciton diffusion length and an improvement in charge carrier mobilities can be achieved by increased ordering of PBI molecules.<sup>12,13</sup> In general, inducing liquid crystallinity is an elegant way of improving supramolecular organization, as it promotes  $\pi$ - $\pi$  stacking, allows for dynamic reorganization, and facilitates the processing of thin films, which is not feasible with highly crystalline materials.<sup>14-17</sup> The unique structural and electronic properties of especially discotic liquid crystals,<sup>18,19</sup> also open completely different aspects of possible applications in topical research fields such as molecular electronics and high-efficiency organic photovoltaics.<sup>8,20-22</sup> Most semiconducting discotics are good hole transporting materials (p-type), while only a limited number of good electron transporting materials (n-type) have been reported.<sup>23</sup>

In general, the self-assembly process of PBI in bulk is a complex balance between molecular stacking arising from  $\pi$ - $\pi$  interaction of the perylene core moiety and the flexible nature of appropriate side chains. Thus an optimum balance of rigidity and flexibility that is crucial for inducing liquid crystallinity has to be found. For electronic device applications, the side chains also should be favorably small, so that the dilution of the electronically active perylene moiety with the electronically inactive, insulating side groups is minimal. Hence a compromise between active chromophore content and side groups which influence the morphology has to be met.

To the best of our knowledge, all of the thermotropic liquid crystalline perylene bisimide derivatives reported in literature are symmetrically substituted. Cormier and Gregg report on liquid crystalline PBIs with branched propylimid-oligo(oxyethylene) or phenethylimide-oligo(oxyethylene) side-chains.<sup>24,25</sup> Pioneering work of Würthner and coworkers involves columnar hexagonal PBIs, with tridodecylphenyl or tridodecyloxyphenyl substituents, also in combination with perylene bay substitution.<sup>26,27</sup> Other reports on symmetrically substituted liquid crystalline PBIs deal with tridodecyloxy gallic acid substituted derivatives<sup>6,28</sup> and PBIs with simple aliphatic chains.<sup>3</sup> Very recently Müllen et al reported on cooperative molecular motion phenomenon within a symmetrically substituted PBI exhibiting liquid crystalline properties.<sup>29</sup> It has been observed that for various phthalocyanines and triphenylenes, an unsymmetrical substitution pattern broadens the mesophase and strongly influences liquid crystalline packing.<sup>20,30,31</sup> But this has not been studied in the case of PBIs. In fact there are no unsymmetrically *N*-substituted liquid crystalline PBIs published up to date and therefore, this substitution pattern is also investigated here.

A fundamental question here is, how to efficiently weaken the strong degree of crystallinity which is inherent in PBIs using a suitable synthetic strategy for unsymmetrical *N*-substitution. We report here our successful approach of swallow-tail *N*-substitution employing oligoethylenglycol units (OEG) to accomplish this goal. Thus we report for the first time a systematic study on the effect of an asymmetric *N*-substitution pattern of PBIs on the thermotropic behaviour. The present approach is aimed at understanding the molecular design requirements to introduce liquid crystalline phases in PBIs without any bay substitution. It can be expected that by introducing two swallow-tail *N*-side chains having different spatial dimensions and additionally different polarities, the thermotropic behaviour of PBIs may be tailored. Furthermore, alkyl swallow-tail groups are well-known to induce high solubility in perylene bisimides which allows for the fabrication of solution-processible devices.<sup>32,33</sup> A change from alkyl to oligoxyethylene substituents provides higher conformational flexibility of the C-O bond compared to the C-C bond. Other physical properties, such as optical or redox properties should not be affected by *N*-substitution, as the nodes in the HOMO and LUMO at the imide nitrogen reduce electronic coupling of the perylene bisimide core and the imide substituents to a minimum.<sup>34</sup> This is extremely advantageous if only the thermotropic properties of PBIs should be tailored without altering the electronic properties.

For this purpose, three different types of *N*-substitution patterns were studied (Scheme 1): Type I with a symmetric substitution pattern, utilizing different alkyl or OEG swallow-tail substituents. This approach is used to study the influence of substituents with different spatial requirements or polarity on thermotropic behavior of symmetrically *N*-substituted PBIs. Type II uses an unsymmetrical substitution pattern comprising different alkyl swallow-tail substituents in combination with OEG swallow-tail or alkyl swallow-tail with distinct spatial demands. Here an asymmetric substitution is used to study the impact of asymmetry of the substitution profile on thermotropic behavior. Type III consists of unsymmetrical substitution pattern, utilizing swallow-tail in combination with linear alkyl or OEG substituents. Here the influence of a reduction of branched swallow-tail substituents to linear ones is investigated.

## RESULTS AND DISCUSSION

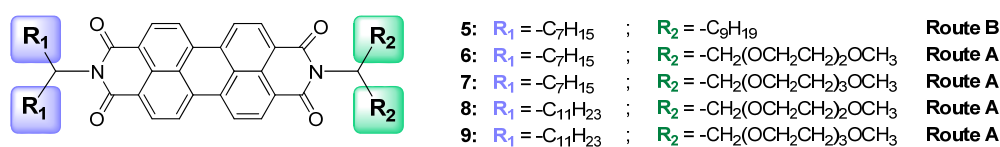
### Synthesis

An overview of the synthesized PBIs **1** to **11** is given in Scheme 1 and the respective synthetic pathway in Scheme 2. The synthesis of PBIs **1** to **11** is based on perylene-3,4,9,10-tetracarboxylic dianhydride **PTCDA** as starting material.

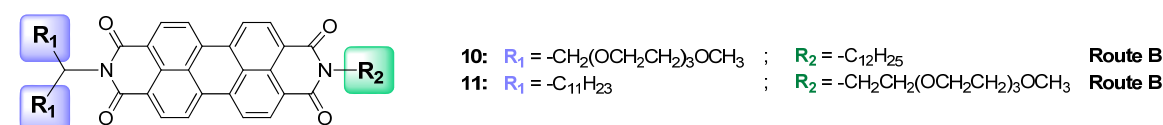
**Type I:** symmetrically *N*-substituted PBIs (2 x swallowtail)



**Type II:** unsymmetrically *N*-substituted PBIs (2 x swallowtail)



**Type III:** unsymmetrically *N*-substituted PBIs (swallowtail + linear)

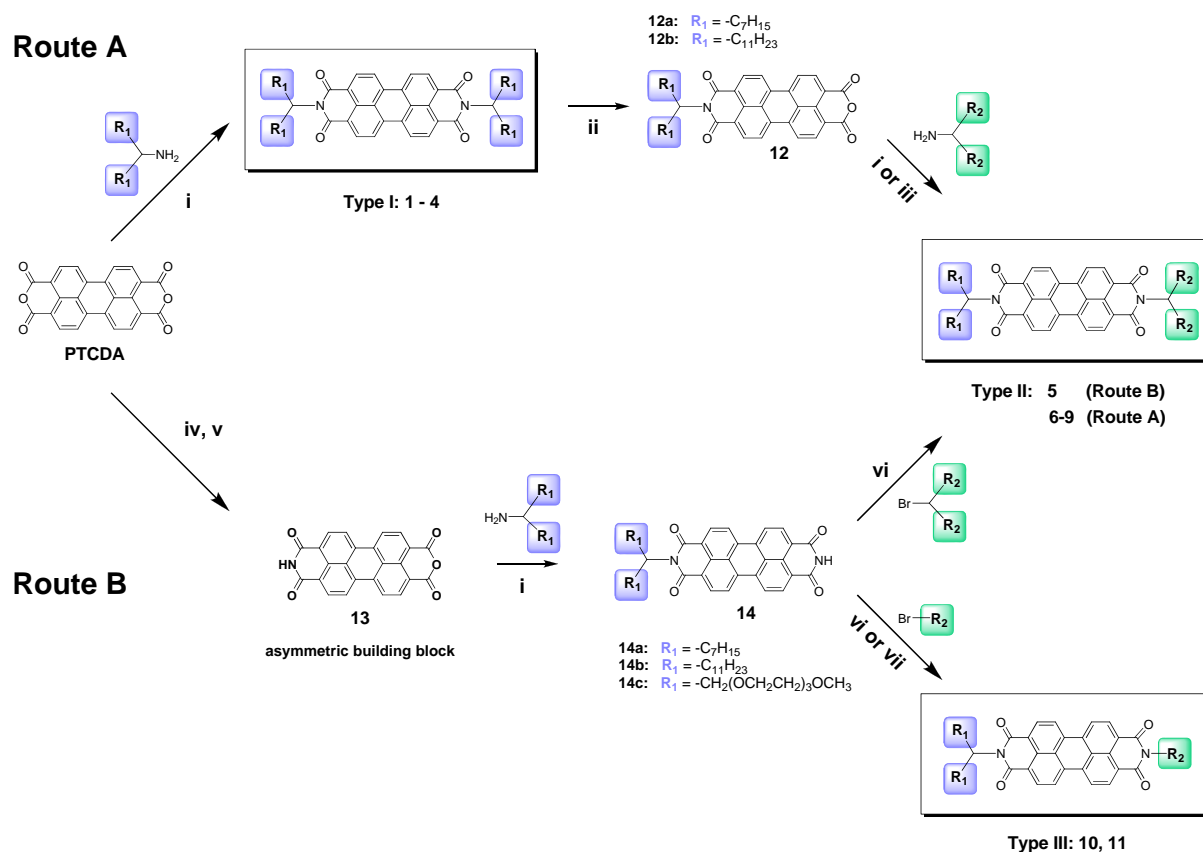


**Scheme 1.** Overview of symmetrically and unsymmetrically *N*-substituted perylene bisimides (**PBIs**) classified according to the nature of respective substituents. PBIs were prepared either by synthetic route A or B.

Generally two different synthetic strategies are feasible for asymmetric *N*-substitution of PBIs (Scheme 2, Route A and B). The common method consists of the condensation of monoimides **12** as key intermediates with some primary amine to unsymmetrical PBIs (Route A).<sup>35,36</sup> Generally, condensation reaction of the dianhydride **PTCDA** with excess of primary amines in molten imidazole or quinoline and zinc acetate as Lewis acid catalyst exclusively allows access to symmetrical bisimides (**1-4**) in high yields but not to key monoimide intermediates **12**. Even substoichiometric amounts of amines usually result in the formation of symmetric bisimides and unreacted perylene dianhydride **PTCDA**. Likewise, the utilization of a mixture of primary amines provides a mixture of two symmetric and one unsymmetric perylene bisimide that is hardly to separate.<sup>35</sup> Nagao and Misono depict a partial saponification of the symmetric bisimides to monoimides **12** with conc. sulphuric acid at high temperatures.<sup>37,38</sup> On the other hand, Langhals

describes a partial saponification under strong basic conditions with KOH in *t*-BuOH as reaction medium.<sup>35</sup> In the following, we prepared PBIs **1-4** and **6-9** using Route A, by saponification of bisimides with KOH and subsequent condensation with a second amine. Additionally a microwave-assisted method for the condensation reaction of mono-imide mono-anhydride **12** with amines was also developed.

An alternative method (Route B) makes use of imide anhydride **13** as asymmetric building block.<sup>39,40</sup> The anhydride moiety allows for condensation reactions with amines in a first step, whereas the imide moiety offers the possibility for introduction of a second *N*-substituent via nucleophilic substitution  $S_N2$  under basic conditions with alkylhalides in a second step. Thus Route B employing asymmetric synthon **13** to attain asymmetric *N*-substituted PBIs was pursued as synthetic strategy for PBIs **5**, **10** and **11**.



**Scheme 2.** Main synthetic pathways for unsymmetrical *N*-substitution of perylene bisimides. i) imidazole,  $\text{Zn}(\text{OAc})_2$ , 2-4 h, 160 °C; ii) KOH, *t*-BuOH, 90 °C 1-1.5 h; iii) DMAc,  $\text{Zn}(\text{OAc})_2$ , 20 Min, 160 °C, 200 Watt; iv) 1. KOH, 2. AcOH; v)  $\text{NH}_4\text{OH}$ ,  $\text{K}_2\text{CO}_3$ ; vi) DMF,  $\text{K}_2\text{CO}_3$ , KI, 80 °C, 3-5 d; vii) DMF, NaH, 80 °C, 48 h. Route A: **1-4** and **6-9**; Route B: **5**, **10** and **11**.

All the required linear and swallow-tail amines and halides were prepared according to conventional synthetic methods already reported in literature. Alkyl swallow-tail amines were

accessible by reductive amination of the corresponding ketones with ammonia and  $\text{NaBH}_3\text{CN}$  as reducing agent in high yields.<sup>41,42</sup> Alkyl swallow-tail bromide was synthesized by bromination of the respective alcohol, which was obtained by a double grignard reaction of the respective alkyl bromide with ethyl formate.<sup>43</sup> OEG swallow-tail amines were derived by a 4 step sequence: OEG swallow-tail secondary alcohols were prepared according to reported procedures,<sup>44,45</sup> converted to the corresponding tosylates<sup>46,47</sup> and then transformed to the azides by nucleophilic substitution.<sup>48</sup> The azides were finally reduced by  $\text{LiAlH}_4$  to the corresponding amines. Linear oligoethylene-bromides were obtained by bromination of the respective alcohol according to literature procedure.<sup>49</sup>

The symmetrically substituted PBIs **1-4** (Type I) were synthesized by simple conversion of perylene dianhydride **PTCDA** with the respective swallow-tail amine (Route A first step). This well-established method allows for high yields of the bisimide products. Due to swallow-tail substituents, the bisimides obtained are highly soluble. For an unsymmetrical substitution, to obtain Type II derivatives, the di-substituted PBIs **1** and **2** were partially hydrolysed to the mono-imide mono-anhydrides **12a, b** respectively by treatment with an excess KOH in *t*-BuOH. Finally these unsymmetrical alkyl swallow-tail OEG swallow-tail PBIs **6, 7, 8** and **9** were obtained by conversion of the respective mono-imide mono-anhydrides (**12a** or **12b**) with the respective OEG swallow-tail amine. The intermediate **12a** was converted to **6** and **7**, whereas **12b** resulted in **8** and **9**. For this synthetic step, microwave irradiation conditions were applied. Under microwave conditions, the reaction time could be reduced drastically from 4 h to 20 minutes and high yields were generally obtained (for example, 96 % for PBI **6**). On the other hand, unsymmetrically substituted PBIs **5, 10** and **11** were obtained via the asymmetric building block **13** according to Route B. After condensation reaction of **13** with the respective alkyl swallow-tail amine, the second substituent was introduced via nucleophilic substitution using the respective bromide in a subsequent step to get **5, 10** and **11**. Both synthetic routes allow for satisfactory yields of the final unsymmetrical PBI products, described under Type II and III. The advantage of Route B is that it is straight forward and there is no unnecessary loss of side chain amine in the bisimide hydrolysis step. Additionally the comparatively mild reaction conditions (< 60 °C) for the nucleophilic substitution allow for introduction of *N*-substituents that are unstable at higher temperatures. A high level of purity was achieved for all PBI compounds by repeated column chromatography purification until they all showed a single chromatogram in gel permeation chromatography (GPC).

All PBIs were fully characterized by means of  $^1\text{H}$ -,  $^{13}\text{C}$ -NMR spectroscopy, IR, GPC, MS and Microanalyses. These PBIs can be regarded as a closed chromophoric system due to the nodes of the HOMO and LUMO orbitals at imide nitrogens.<sup>34</sup> Accordingly, the PBIs under investigation with different substituents show identical absorption behavior. The UV-vis spectra of these compounds in very dilute solutions exhibit the characteristic finger-print vibronic fine structure of PBI with peaks at about 525, 490, 460 and 430 nm respectively. In order to elucidate the electronic energy levels which determine the energy and electron transfer processes, and the reversibility of redox processes, cyclic voltammetry (CV) was used. CV is a common method for studying

electrochemical behavior and to evaluate the relative HOMO and LUMO levels using ferrocene as internal calibration. PBIs possess good electron affinity and so they are easy to be reduced and rather difficult to be oxidized. All PBIs investigated herewith, exhibit two reversible reduction peaks. In order to calculate the absolute values of HOMO and LUMO levels, the redox data was calibrated with respect to ferrocene–ferrocenium couple  $\text{Fc}/\text{Fc}^+$ , which has a quasi-calculated HOMO-energy level of 4.8 eV.<sup>50</sup> The LUMO energy levels of PBIs were obtained from the half-wave reduction potentials. However, the oxidation potentials of most compounds were not observed in the CV measurements window up to +1 V vs.  $\text{Ag}/\text{AgNO}_3$ . Hence the HOMO levels of PBIs were estimated from the optical band gap and the LUMO levels. The optical band gaps of all PBIs were determined from the absorption edge of absorption spectra of diluted solutions. Thus, all compounds exhibit a LUMO of about -3.8 eV and a HOMO value of -6.0 eV with respect to the zero energy level. As expected the differences in electronic properties are negligible for these substitution patterns. This is due to the electronic decoupling of the perylene bisimide core and the imide substituents.<sup>34</sup>

In the following a detailed study of the structure-property relationship of the different substitution patterns Type I-III with respect to thermotropic liquid crystalline behavior is presented. This elucidates the structural requirements for inducing liquid crystalline phases in PBIs.

### **Thermal and thermotropic properties**

The thermal stability of the PBIs was analyzed by means of thermogravimetric analysis (TGA) under nitrogen atmosphere. All compounds are stable up to 300 °C (Table 1). Thermotropic behaviour of the different derivatives was investigated by a combination of differential scanning calorimetry (DSC) and polarization optical microscopy (POM). Additionally the molecular order within observed mesophases was determined using X-ray diffraction studies (XRD). The TGA data and phase transition temperatures with associated enthalpy values obtained from DSC for all PBIs discussed herein are summarized in Table 1. The DSC data was obtained at a scanning rate of 10  $\text{Kmin}^{-1}$  unless indicated otherwise. The first heating cycles of DSC were neglected to exclude influences of the thermal history of the samples. Transition from an isotropic liquid to crystalline or liquid crystalline phases can be monitored by the evolution of characteristic textures. Additionally, liquid-crystalline phases are anisotropic fluids which in general are optically birefringent. The characteristic textures of liquid crystalline materials result not only from the symmetry-dependent elasticity of the liquid-crystalline phase in combination with defects and surface conditions,<sup>18</sup> but also from thickness and cooling rate of the sample, under investigation. Optical polarization microscopic textures for all the compounds are consistent with the phase transition behavior observed in DSC. All unsymmetrical PBIs carrying one alkyl swallow-tail and one OEG swallow-tail exhibit thermotropic liquid crystalline behavior. In contrast, a reduction of the branched substituents to linear ones results in materials without mesophase behaviour. The evidence of a hexagonal ordered stacking ( $\text{Col}_h$ ) with a high order in the individual columns, was

supported by XRD-measurements. The influence of the three different substitution patterns of PBIs under investigation in Type I-III are discussed individually in the following paragraphs.

**Table 1.** Summary of the thermal behaviour, phase transition<sup>[a]</sup> temperatures with corresponding transitions enthalpies and mesophases of investigated **PBIs 1-11** (obtained from TGA and DSC).

PBI	T <sub>dec</sub> <sup>[b]</sup> °C	Phase transitions and corresponding enthalpies ΔH (in parentheses) °C / (kJ·mol <sup>-1</sup> )	
		2 heating cycle	1 cooling cycle
<b>Type I</b>	<b>1</b>	Cr 133.2 (19.5) → I	I 118.3 (-5.0) → Col <sub>h</sub> 110.7 (-11.6) → Cr
	<b>2</b>	Cr <sub>1</sub> 53.8 (6.9) → Cr <sub>2</sub> 76.8 (6.6) → I	I 59.3(-6.2) → Cr <sub>2</sub> 27.2 (-5.2) → Cr <sub>1</sub>
	<b>3</b>	Cr <sub>1</sub> 78.2 (15.8) → Col <sub>h</sub> 145.8 (3.5) → I	I 141.7 (-3.3) → Col <sub>h</sub> 39.8 (-1.8) → Cr <sub>2</sub> 21.9 (-3.7) → Cr <sub>1</sub>
	<b>4</b>	Cr 67.8 (24.0) → Col <sub>h</sub> 126.9 (3.9) → I	I 121.1 (-3.7) → Col <sub>h</sub>
<b>Type II</b>	<b>5</b>	Cr 98.8 (8.5) → I	I 36.3 (-3.7) → Cr
	<b>6</b>	Cr 77.6 (14.8) → Col <sub>h</sub> 154.4 (3.9) → I	I 146.1 (-3.8) → Col <sub>h</sub>
	<b>7</b>	Cr 65.5 (15.0) → Col <sub>h</sub> 148.7 (5.9) → I	I 142.0 (-5.7) → Col <sub>h</sub> 1.7 (-2.2) → Cr
	<b>8</b> <sup>[c]</sup>	Cr 51.0 (10.7) → Col <sub>h</sub> 107.7 (3.0) → I	I 105.0 (-2.9) → Col <sub>h</sub> 23.5 (-7.6) → Cr
	<b>9</b>	Cr 54.3 (12.1) → Col <sub>h</sub> 111.8 (3.3) → I	I 102.1 (-3.3) → Col <sub>h</sub> 1.6 (-3.2) → Cr
<b>Type III</b>	<b>10</b>	Cr 140.1 (10.6) → I	I 129.3 (-10.6) → Cr
	<b>11</b>	Cr 151.8 (14.3) → I	I 142.0 (-14.0) → Cr

[a] Cr = crystal phase; Col<sub>h</sub> = columnar hexagonal mesophase; I = isotropic. [b] Temperature represents 5% weight loss in TGA measurements at a heating rate of 10 Kmin<sup>-1</sup> under nitrogen atmosphere. [c] Measured for a heating and cooling rate at 2.0 Kmin<sup>-1</sup>.

### Thermotropic behaviour of Type I, PBIs 1-4

DSC thermograms of Type I PBIs are summarized in Figure 1. In literature there is a controversial discussion, if symmetrically substituted **1** exhibits liquid crystalline behavior.<sup>51-53</sup> It could be shown here, that the symmetrical molecule **1** carrying alkyl substituents exhibits a narrow monotropic hexagonal columnar Col<sub>h</sub> mesophase upon cooling from the isotropic melt at 118.3 °C with a phase-width of only 8 °C and crystallizes upon further cooling at 110.7 °C. The evidence of a Col<sub>h</sub> ordering was confirmed by polarization microscopy, here typical focal conic textures can be observed under crossed polarizers (Fig. 2a). Also a symmetrical analogue **2** with longer alkyl chains (R<sub>1</sub> = -C<sub>11</sub>H<sub>23</sub>), shows two phase transitions upon heating, and cooling cycle. But here, the first transition in cooling cycle corresponds to a crystallization process that cannot be attributed to a liquid crystalline phase as evidenced by polarization microscopy, where needle-like crystalline aggregates are formed upon annealing the sample at 61 °C (Fig. 2b). The second transition at 27 °C corresponds to a crystalline-crystalline transition, but no difference in the optical texture can be observed here. Hence a simple increase in substituent length does not help

to increase the mesophase temperature-width of compound **1**, but even results in crystalline behaviour.

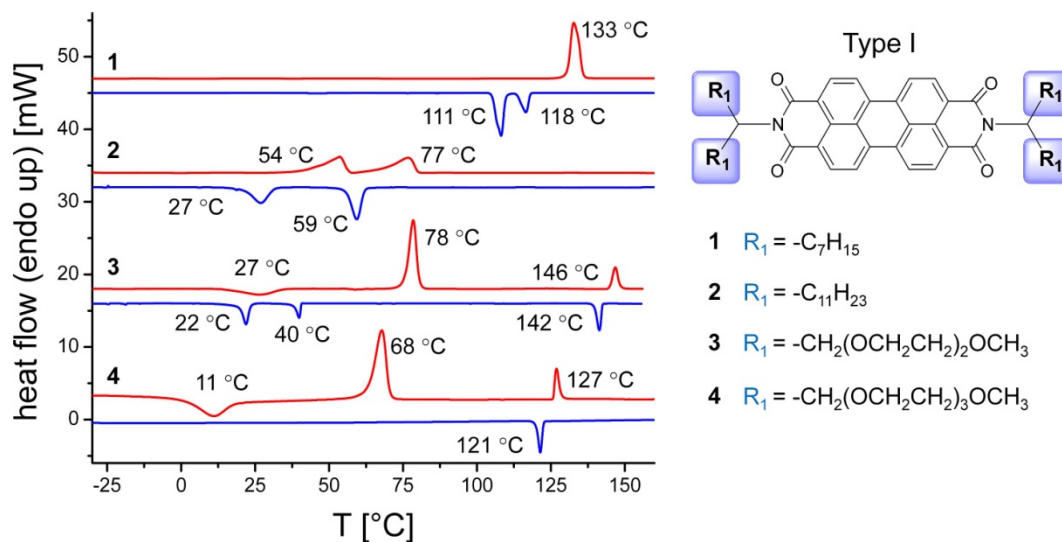


**Figure 1.** DSC thermograms of symmetrical Type I PBIs **1**, **2**, **3** and **4** showing the second heating and first cooling cycle at a heating rate of  $10 \text{ Kmin}^{-1}$  with respective transition temperatures ( $^{\circ}\text{C}$ ). Red curves represent the second heating cycle and blue curves represent the first cooling cycle.

On the other hand, a change from alkyl swallow-tail to OEG swallow-tail substituents in case of PBIs **3** and **4**, results in liquid crystalline behaviour. This can be attributed to the higher conformational freedom of the C-O bond compared to C-C bond allowing for a better space filling around the discotic mesogen. In contrast to symmetrical di-alkyl swallow-tail PBI **1**, the compounds **3** and **4** have a much broader liquid crystalline phase which is not monotropic. Additionally, the length of the OEG swallow-tail substituent influences the clearing temperature of PBIs (**3**:  $T_{iso} = 145.8 \text{ }^{\circ}\text{C}$ ; **4**:  $T_{iso} = 126.9 \text{ }^{\circ}\text{C}$ ). As expected compound **4** with longer OEG substituent exhibits a lower clearing temperature, whereas the enthalpy  $\Delta H_{Col_h \rightarrow iso}$  remains almost the same. The transition temperature from the crystalline phase to the liquid crystalline phase  $Cr \rightarrow Col_h$  is shifted only slightly from  $78.2 \text{ }^{\circ}\text{C}$  for **3** to  $67.8 \text{ }^{\circ}\text{C}$  for **4**. But here the enthalpy of the melting process to the liquid crystalline phase is with  $24.0 \text{ kJ}\cdot\text{mol}^{-1}$  for **4** much higher than  $15.8 \text{ kJ}\cdot\text{mol}^{-1}$  for **3**. In the heating cycle, the LC phase-width is  $68 \text{ }^{\circ}\text{C}$  for **3** and  $59 \text{ }^{\circ}\text{C}$  for **4**, and in the cooling cycle the LC phase-width for **3** is with  $102 \text{ }^{\circ}\text{C}$  larger, due to supercooling of crystallization. For PBI **4**, the crystallization transition upon cooling cycle could not be detected in DSC ( $10 \text{ Kmin}^{-1}$ ), but here XRD-measurements at RT showed typical multiple crystalline reflections. Also the texture observed in POM was not shearable at room temperature anymore. Transition from an isotropic liquid to columnar hexagonal mesophase ( $Col_h$ ) for both **3** and **4** was observed in POM as indicated by the formation of typical dendritic growth aggregates or fan-shaped focal conic textures upon cooling the sample from the isotropic melt under crossed polarizers (Fig. 2c, d). The straight linear defects observed in several textures are also characteristic for an

ordered columnar mesophase.<sup>18,19</sup> These textures are highly shearable in the mesophase range and no crystallization was observed upon cooling, only the viscosity of the LC-phase increases upon cooling to room temperature. For **3** an additional crystalline-crystalline transition at 22 °C can be observed upon cooling the sample in DSC. For this transition no textural changes could be observed in polarization microscopy and X-ray scattering experiments could not be performed at temperatures below room temperature, but the XRD-pattern at room temperature showed multiple reflections typical for a crystalline material. Due to the high viscosity of the mesophase the crystallization is supercooled in DSC (even at slow scanning rates) and partial recrystallization occurs for both materials upon heating the sample again. In short, a simple increase in the alkyl substituent length does not result in liquid crystalline behavior, but a change in the nature of the substituent from alkyl to OEG helps to induce liquid crystallinity in the case of symmetrically substituted swallow-tail PBI of Type I.

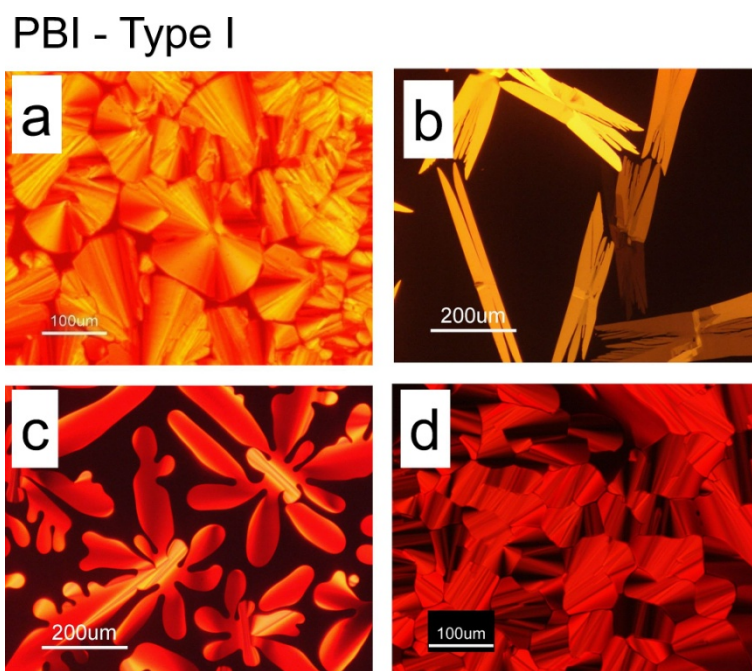


**Figure 2.** Optical microscopic images of textures of PBIs Type I (under crossed polarizers) of (a) **1** annealed in the mesophase at 118 °C showing typical focal conic texture of Col<sub>h</sub> phase. (b) Long needle-like crystals of **2** at 61.2 °C. (c) **3** in mesophase at 144 °C showing dendritic growth aggregates of Col<sub>h</sub> phase and (d) **4** at 142 °C showing fan-shaped focal conic textures. The textures were obtained upon cooling the sample from the isotropic phase and annealing at the respective temperatures slightly above phase-transition temperature.

### Thermotropic behaviour of Type II, PBIs 5-9

DSC thermograms of Type II PBIs are summarized in Figure 3. The unsymmetrical compound **5** carrying two different alkyl swallow-tail substituents remains crystalline. Also a comparison of **1**, **2** and **5** clearly shows that the LC-phase observed in **1** could not be broadened in **2** or **5**, both by

extending the length of substituents or by introducing unsymmetrical substitution. However, the unsymmetrical PBIs with one OEG swallow-tail substituent and one alkyl swallow-tail substituent (**6-9**) resulted in thermotropic liquid crystalline derivatives. Moreover, in the unsymmetrical molecules **6-9**, an increase in alkyl chain length has only a marginal influence in decreasing the clearing temperature, whereas a corresponding increase in OEG length decreases the clearing temperature considerably. Thus for instance **6** with two oxyethylene repeating units clears at 154.9 °C and **7** carrying three oxyethylene repeating units shows a clearing temperature of 108.5 °C; a difference of 46 °C. Similarly compound **8** with a shorter OEG substituent clears at 148.4 °C compared to **9** carrying a longer OEG substituent at 111.8 °C, the difference being 37 °C. Thus the clearing temperature can be tuned by appropriate substituent length. Generally the transition from Col<sub>h</sub> phase to crystalline phase is strongly supercooled here and recrystallization could be observed upon heating cycles. The crystallization processes can be observed more clearly at a heating rate of 2 Kmin<sup>-1</sup>. The effect of supercooling, for example observed in **6**, **8** or **9**, allows for freezing in the mesophase. This finding is of great relevance when these PBIs are employed in electronic devices.

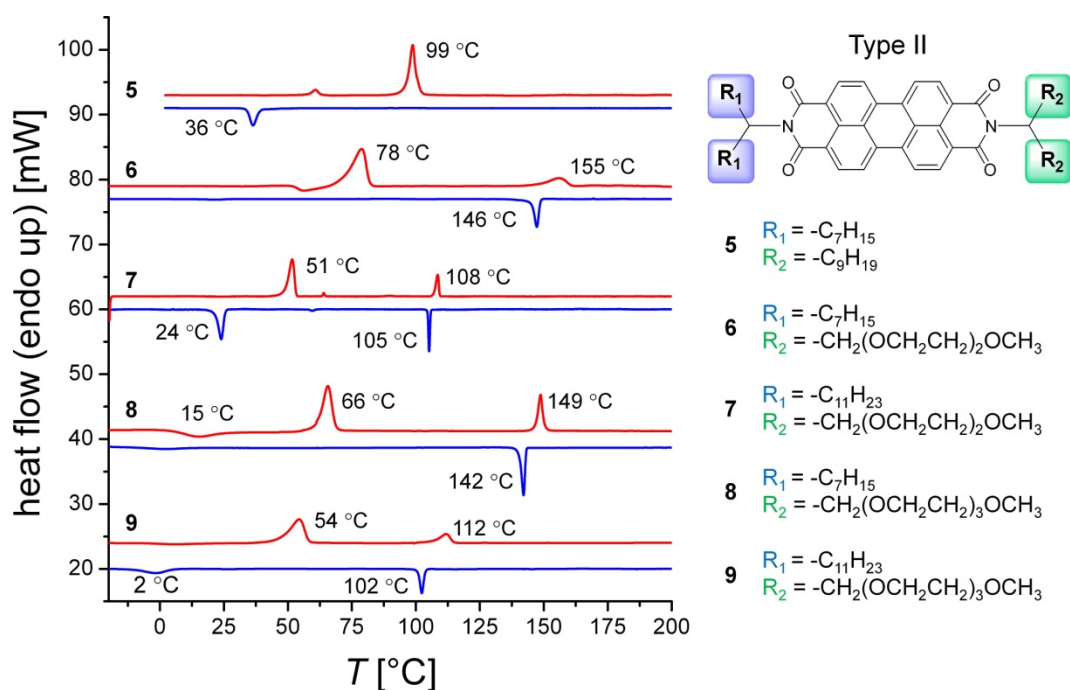


**Figure 3.** DSC thermograms of unsymmetrical Type II PBIs **5**, **6**, **8**, **9** (10 Kmin<sup>-1</sup>) and **7** (2 Kmin<sup>-1</sup>) showing the second heating and first cooling cycle with respective transition temperatures (°C). Red curves show the second heating cycle and blue curves represent the first cooling cycle.

For these PBIs **6-9** the evidence of Col<sub>h</sub> liquid crystalline behavior was further confirmed by POM (Fig. 4). The unsymmetrical Type II PBIs **6-9** carrying one OEG swallow-tail substituent show characteristic Col<sub>h</sub> textures. Figure 4a depicts the crystalline texture of PBI **5** which does not exhibit any liquid crystalline behaviour. In contrast, for PBI **6**, large snowflake-like dendritic-

growth aggregates of  $Col_h$  phase as well as ribbons with straight linear defects that are characteristic for ordered columnar mesophases can be observed at 153 °C (Fig. 4b). Figure 4c represents the texture of **7** at 108 °C showing spherulitic textures with maltese crosses, also typical for a  $Col_h$  ordering. Figure 4d shows compound **8** at 141 °C showing large spherulitic textures of  $Col_h$  phase formed upon fast cooling from isotropic melt, whereas extremely large dendritic aggregates of the  $Col_h$  phase are formed upon annealing **8** at 149 °C (Fig. 4e). Additionally domains with homeotropic alignment can be observed for **8** if a  $\lambda/4$ -plate is employed in front of the analyzer for the slowly cooled sample (Fig. 4f). This indicates an ordering parallel to the substrate surface (homeotropic alignment) at low cooling velocities. Figure 4g shows the texture of **9** annealed in the mesophase at 108 °C displaying typical dendritic aggregates of  $Col_h$  phase and Figure 4h represents the texture upon shearing the sample at the same film position, illustrating the high viscosity of these systems.

## PBI - Type II

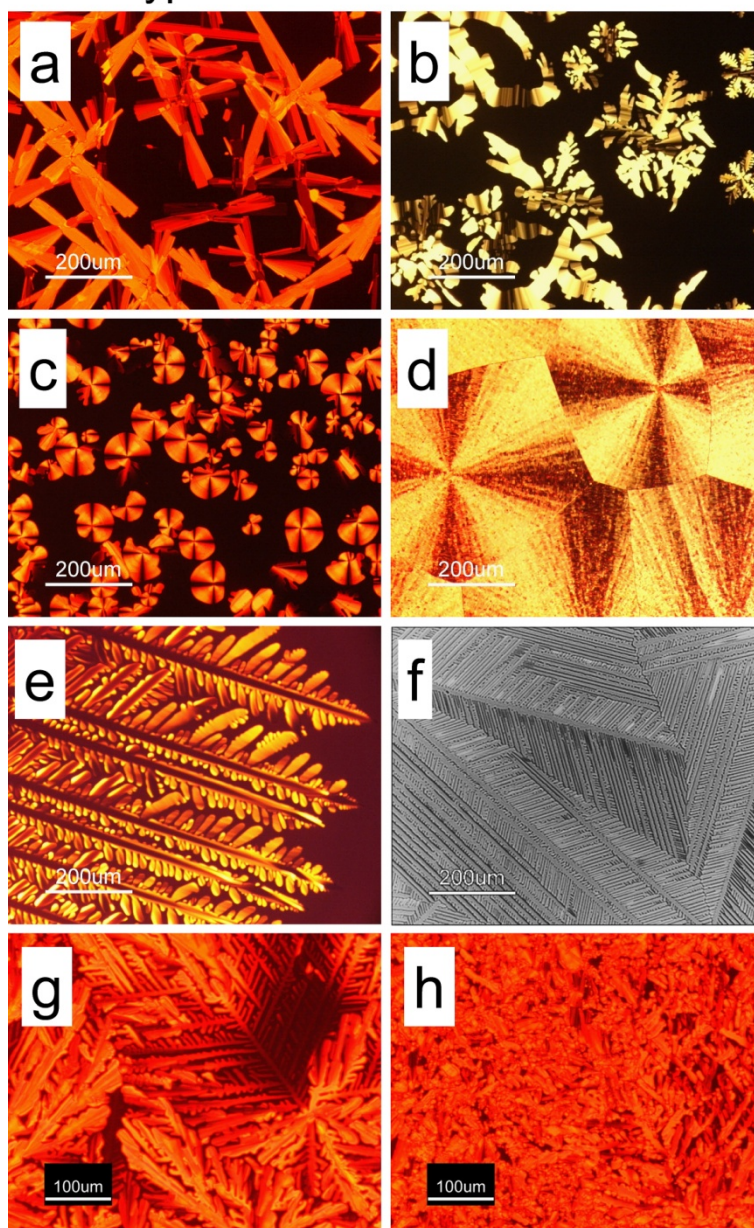


**Figure 4.** Optical microscopic images of textures of PBIs 5-9 (under crossed polarizers) of (a) crystals of **5** formed upon annealing at 63 °C. (b) Texture of **6** at 153 °C showing dendritic growth snowflake-like aggregates of  $Col_h$  phase but also ribbons with straight linear defects that are characteristic for ordered columnar mesophases. (c) **7** at 108 °C showing spherulitic texture with Maltese crosses of  $Col_h$  phase. (d) **8** at 141 °C showing large spherulitic texture of  $Col_h$  phase formed upon fast cooling from isotropic melt and (e) **8** large dendritic growth aggregates of  $Col_h$  phase formed upon annealing at 149 °C. (f) **8** annealed at 149 °C at different film region showing dendritic growth aggregates, here a  $\lambda/4$  plate is utilized to visualize partial homeotropic ordering. (g) **PBI-9** annealed in the mesophase at 108 °C showing typical dendritic-growth aggregates of the  $Col_h$  phase and (h) **9** sheared-film at same film position. The textures were obtained upon cooling the sample from the isotropic phase and annealing at the respective temperatures slightly above phase-transition temperature.

It is highly interesting to compare PBIs **5** and **6**, both bearing an identical number of side chain atoms. The only difference here lies in the flexibility of the respective substituents. For both PBIs,  $R_1$  is  $-C_7H_{15}$ , but  $R_2$  differs in flexibility. In **5** an alkyl swallow-tail substituent is used, in contrast to an OEG swallow-tail substituent in **6**. It can be observed that **5** melts from the crystalline state into the isotropic phase at 99 °C and the respective crystallization upon cooling is strongly supercooled and occurs at 36 °C (Fig. 3). Also the crystallization process of **5** upon annealing at 63 °C can be observed in POM (Fig. 4a). On the other hand PBI **6** exhibits  $Col_h$  mesophase which can be attributed to the presence of OEG-substituent. Thus, the introduction of two different alkyl swallow-tail substituents with different spatial demands does not result in liquid crystalline behavior. In contrast, in **6**, employing a combination of alkyl swallow-tail substituents with OEG swallow-tail substituents, broad liquid crystalline mesophases can be observed (77 °C mesophase window in the heating cycle). In short, the comparison of **5** and **6** clearly indicates the ability of ether substituents to suppress the crystallization tendency of the perylene bisimide moiety.

#### **Thermotropic Behaviour of Type III PBIs **10** and **11****

A reduction of the size of the *N*-substituents is of fundamental interest in designing PBI semiconductors for device applications in order to keep the content of the electronically active perylene chromophore high. To this end, one of the swallow-tail substituents was replaced with a linear one in Type III compounds. Thus unsymmetrical PBIs **10** and **11** with one swallow-tail and one linear substituent were synthesized. Both **10** and **11** are crystalline materials as can be seen from DSC-thermograms (Fig. 5) and POM textures (Fig. 6a, b). PBI **10** melts at 140 °C whereas **11** shows a melting peak at 152 °C. Both compounds recrystallize on cooling and do not exhibit any supercooling effect. The absence of any mesophase indicates that the linear substituents are spatially less demanding and may not be able to fill the space sufficiently around the columnar stacked PBI molecules.

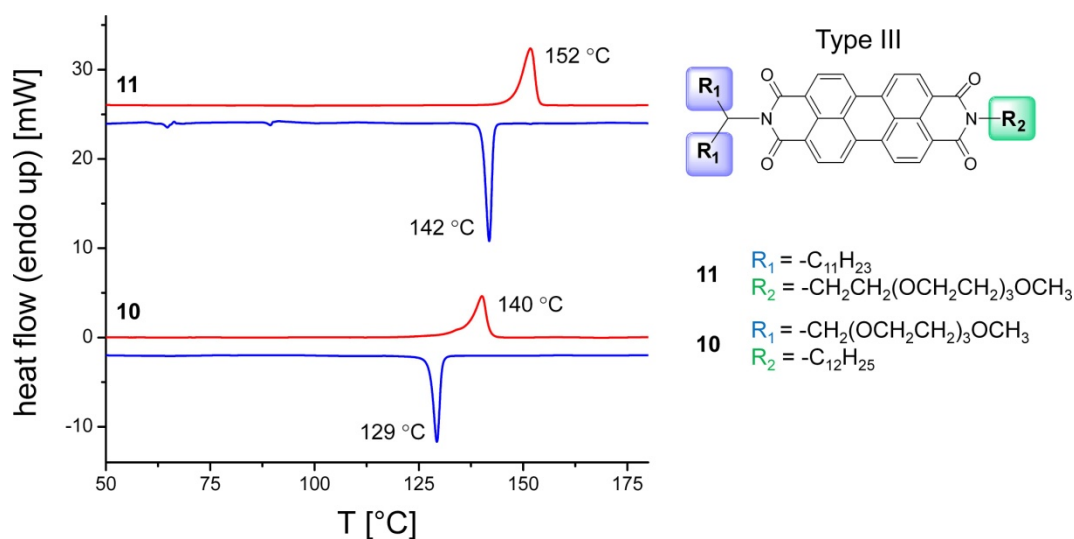


**Figure 5.** DSC thermograms of unsymmetrical Type III PBIs, **10** and **11**, showing the second heating and first cooling cycle at a heating rate of 10 Kmin<sup>-1</sup> with respective transition temperatures (°C). Red curves show the second heating cycle and blue curves represent the first cooling cycle.

### PBI - Type III

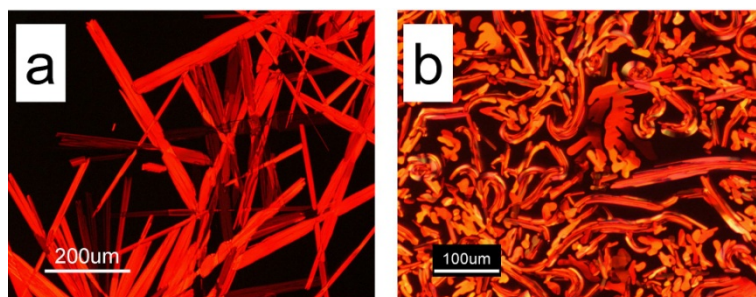


**Figure 6.** Optical microscopic images of crystalline of Type III PBIs (under crossed polarizers). (a) Very long crystals of **11** formed upon annealing at 145 °C and (b) crystals of **10** formed upon annealing at 135 °C. The textures were obtained upon cooling the sample from the isotropic phase and annealing at the respective temperatures slightly above phase-transition temperature.

### X-ray diffraction experiments on liquid crystalline PBIs

Additionally X-ray diffraction experiments were carried out to clearly elucidate the order parameters and to confirm the nature of the mesophases of the liquid crystalline PBIs **1**, **3**, **4**, **6**, **7**, **8** and **9** unequivocally. This also helps to understand the effect of the different substituents on hexagonal lattice parameters. Figure 7 presents the geometry and packing parameters for the columnar hexagonal liquid crystalline mesophase (Col<sub>h</sub>).<sup>18</sup> Packing parameters for PBIs under investigation as determined from X-ray diffraction experiments are summarized in Table 2.

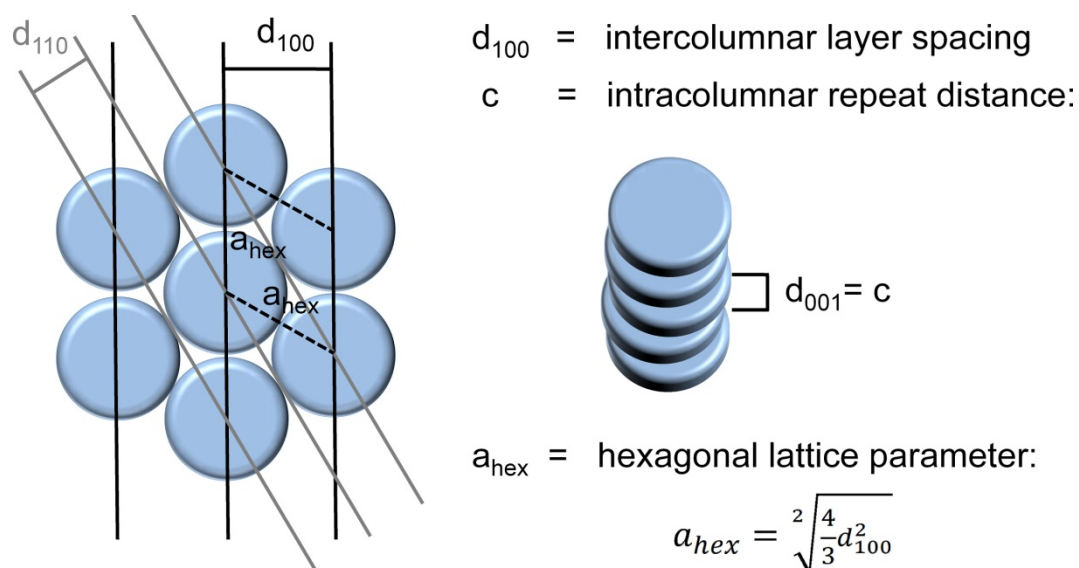


**Figure 7.** Schematic representation of discotic columnar hexagonal packing parameters in liquid crystalline mesophases. Intercolumnar layer spacing  $d_{100}$ , hexagonal lattice parameter  $a_{hex}$  and intracolumnar repeat distance  $c$  ( $d_{001}$ ) for discotic molecules. More geometric considerations result in the characteristic ratios of  $1: \frac{1}{\sqrt{3}}: \frac{1}{\sqrt{4}}: \frac{1}{\sqrt{7}}: \frac{1}{\sqrt{9}}: \frac{1}{\sqrt{12}}: \frac{1}{\sqrt{13}}$  for the  $d$  spacings of the (100), (110), (200), (210), (300), (220), and (310) reflections of a hexagonal lattice in the small-angle regime.

**Table 2.** Hexagonal lattice parameters: Intercolumnar layer spacing  $d_{100}$  [Å], hexagonal lattice parameter  $a_{hex}$  [Å] and intracolumnar repeat distance  $c$  [Å] for PBIs **1**, **3**, **4**, **6**, **7**, **8** and **9** in the liquid crystalline mesophase, as determined from temperature dependent X-ray diffraction experiments.

PBI	$R_1 / R_2$	T [°C]	Phase	$d_{100}$ [Å]	$a_{hex}$ [Å] <sup>[a]</sup>	$c$ [Å]
<b>1</b>	$R_1 = R_2 = C_7H_{15}$	120	Col <sub>h</sub>	18.02	20.81	3.51
<b>3</b>	$R_1 = R_2 = CH_2(OCH_2CH_2)_2OMe$	100	Col <sub>h</sub>	18.02	20.81	3.48
<b>4</b>	$R_1 = R_2 = CH_2(OCH_2CH_2)_3OMe$	80	Col <sub>h</sub>	19.89	22.97	3.48
<b>6</b>	$R_1 = C_7H_{15}$ $R_2 = CH_2(OCH_2CH_2)_2OMe$	120	Col <sub>h</sub>	18.39	21.23	3.48
<b>7</b>	$R_1 = C_7H_{15}$ $R_2 = CH_2(OCH_2CH_2)_3OMe$	120	Col <sub>h</sub>	19.19	22.16	3.49
<b>8</b>	$R_1 = C_{11}H_{23}$ $R_2 = CH_2(OCH_2CH_2)_2OMe$	90	Col <sub>h</sub>	19.89	22.97	3.46
<b>9</b>	$R_1 = C_{11}H_{23}$ $R_2 = CH_2(OCH_2CH_2)_3OMe$	90	Col <sub>h</sub>	20.73	23.94	3.47

[a] Hexagonal lattice parameter  $a_{hex} = \sqrt{\frac{4}{3}d_{100}^2}$

Symmetrical Type I PBIs **1**, **3** and **4** show the  $d_{100}$  and  $d_{110}$  reflections displaying a columnar hexagonal mesophase with the characteristic perylene-perylene stacking-distance of  $c = 3.4 - 3.5$  Å (from  $d_{001}$  reflection at about  $25.5^\circ$ ) in the columns (Fig. 8). Additionally, the sharp  $d_{001}$  reflexes at approximately  $25.5^\circ$  for all LC compounds are typical for a high order in the intracolumnar packing of the discotic molecules. For **1**, the  $d_{100}$  and  $d_{200}$  reflections can be observed. The diffuse halo at bigger angles ( $> 10^\circ$ ) arises from the liquid-like *N*-substituents. As expected, **4** with the larger OEG-substituent also has the biggest unit cell  $a_{\text{hex}} = 22.97$  Å. Interestingly PBI **1** carrying only alkyl substituents has the same hexagonal packing parameter  $a_{\text{hex}} = 20.81$  Å as PBI **3** with a comparatively larger OEG *N*-substituent. This fact also implies a higher conformational freedom in the packing behavior of the OEG-substituents compared to alkyl substituents.

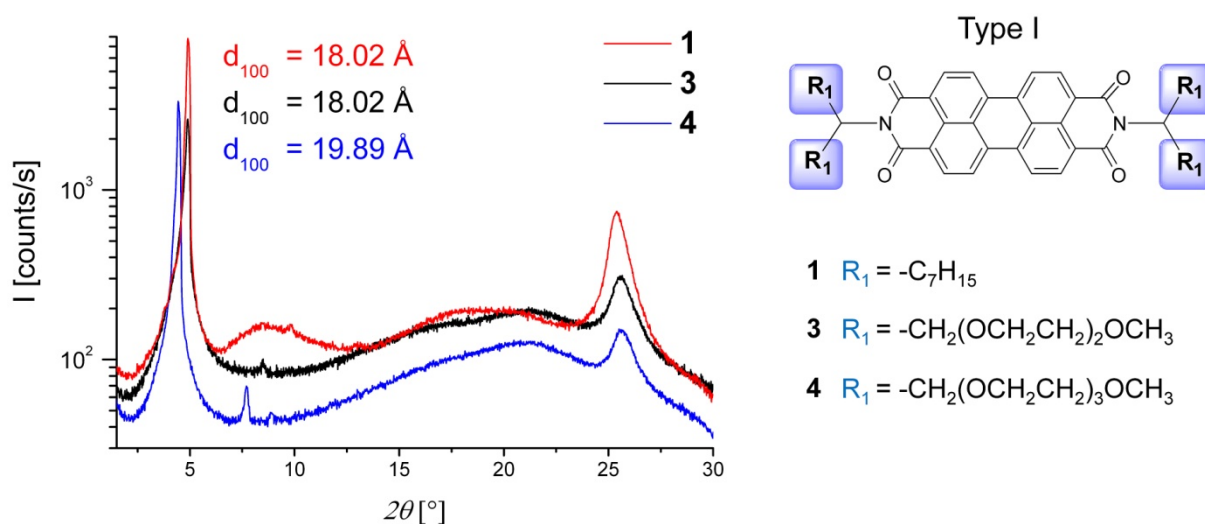


**Figure 8.** X-ray diffraction patterns of  $Col_h$  perylene bisimides **1** (at  $120^\circ\text{C}$ ), **3** (at  $100^\circ\text{C}$ ) and **4** (at  $80^\circ\text{C}$ ) measured in the  $Col_h$  mesophase.

Also for the unsymmetrically substituted Type II PBIs **6**, **7**, **8** and **9**, the diffractogram (Fig. 9) exhibits the typical liquid crystalline columnar hexagonal  $Col_h$  reflections  $d_{100}$  and  $d_{110}$ . The differences in  $d_{100}$  are about  $0.8$  Å on changing the oxyethylene repeating units from two to three in compounds **6** vs. **7** as well as **8** vs. **9**. On the other hand, a change of about  $1.5$  Å in  $d_{100}$  spacing was observed for compounds **6** vs. **8** as well as **7** vs. **9**, in which the alkyl substituent length was varied from  $R_1 = -C_7H_{15}$  to  $-C_{11}H_{23}$  respectively, maintaining the OEG length the same. Also on comparison, compound **4** carrying only OEG swallow-tail substituents exhibits a smaller  $d_{100}$  value of  $19.89$  Å than **9** with alkyl and OEG substituents with comparable length ( $d_{100} = 20.73$  Å). This shows that the ether side chains pack more tightly than alkyl substituents due to higher conformational freedom of the C-O bond in OEG.

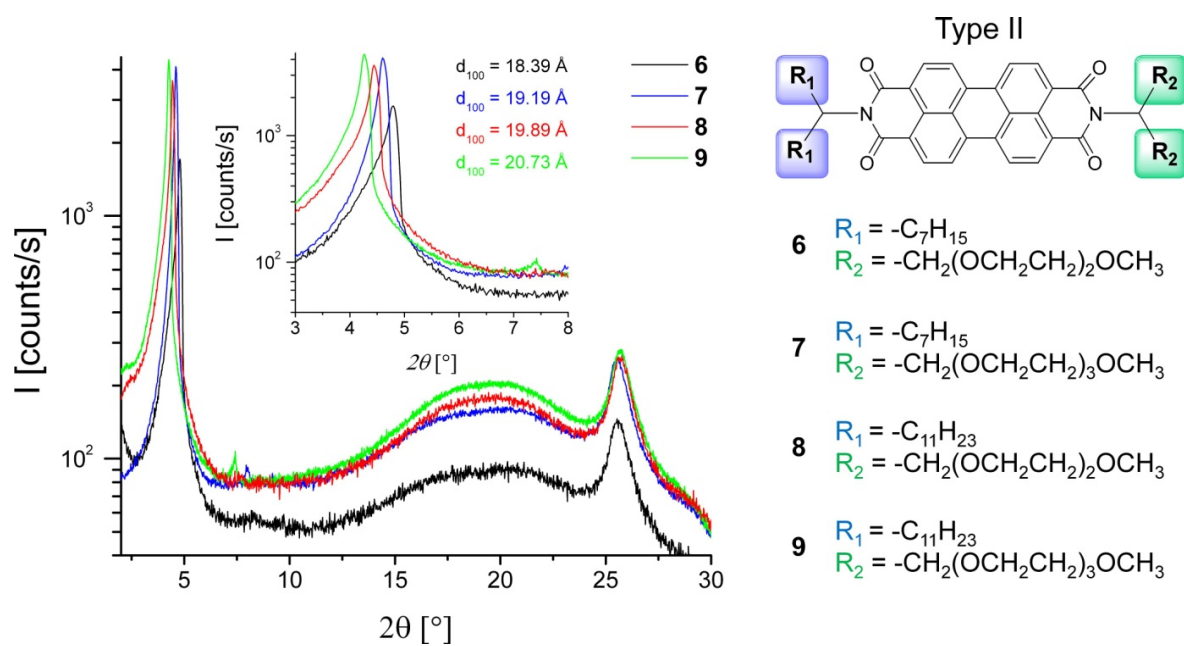


**Figure 9.** X-ray diffraction patterns of perylene bisimides **6** (at 120 °C), **7** (at 120 °C), **8** (at 90 °C) and **9** (at 90 °C) measured in the  $Col_h$  mesophase. The inset shows the  $d_{100}$  intercolumnar reflections with respective repeat distances.

The unsymmetrical Type III PBIs **10** and **11** with one linear side chain and one swallow-tail side chain show several crystalline reflections in XRD, typical for polycrystalline materials.

## CONCLUSION

Several symmetrically and unsymmetrically *N*-substituted perylene bisimides have been successfully synthesized by two different synthetic strategies. The substituents used involved swallow-tail and linear alkyl- or oligoxyethylene (OEG) substituents. The focus of investigation was directed towards designing tailor-made liquid crystalline PBIs and to elucidate a structure-property relationship with respect to thermotropic behavior in *N*-substituted derivatives of PBIs. To this end, only *N*-substitution was considered and bay substitution was avoided to keep the optical and electrical properties similar. Thermotropic behavior was examined by DSC, POM and XRD measurements in the mesophase temperature range. Several PBIs exhibiting columnar hexagonal liquid crystalline Col<sub>h</sub> behavior with broad LC temperature window were obtained by this approach. It could be shown that OEG swallow-tail substituents efficiently support Col<sub>h</sub> behavior and that both *N*-substituents have to be branched in nature. A reduction to linear *N*-substituents resulted in strongly crystalline behavior. By an unsymmetrical substitution pattern, the melting point to the liquid crystalline phase as well as clearing temperature could be controlled very efficiently. Upon cooling the LC-phase, the crystallization process of these PBIs is strongly supercooled. Thus, these novel liquid crystalline PBIs are highly promising candidates to be applied in organic electronics like field-effect transistors (OFET) or photovoltaic devices. Our current investigations towards devices deal with substrate/molecule interaction and orientation of these molecules on alignment layers deposited on device substrates. Preliminary results indicate uniaxial edge-on to the surface orientation of molecules, which is ideal for OFETs. The detailed device results will be published later.

## EXPERIMENTAL SECTION

### Materials and Methods

The starting materials, perylenetetracarboxylic acid dianhydride PTCD, pentadecane-8-one, tricosan-12-one, 1-bromononane, diethylenglycol monomethyl ether, triethylenglycol monomethyl ether, tetraethyleneglycol monomethyl ether and solvents, were purchased from Merck, Aldrich, Fluka or TCI and used without any further purification. Solvents used for precipitation and column chromatography were distilled under normal atmosphere. For the synthesis of perylene intermediates **12a,b**,<sup>35,54</sup> and **14a-c**<sup>36</sup> see Supporting Information. All swallow-tail and linear bromides<sup>43,49</sup> or amines<sup>41,42,44-48</sup> respectively were synthesized according to published procedures.

<sup>1</sup>H- and <sup>13</sup>C-NMR spectra were recorded on a Bruker AC 250 spectrometer (250 MHz). Chemical shifts are reported in ppm at room temperature using CDCl<sub>3</sub> as solvent and tetramethylsilane as internal standard unless indicated otherwise. Abbreviations used for splitting patterns are s = singlet, d = doublet, t = triplet, q = quintet, m = multiplet. Gel permeation chromatography (GPC) was performed on a Waters size exclusion chromatography system for oligomers (analytical columns: crosslinked polystyrene gel, length 2 x 60 cm, width 0.8 cm, particle size 5 μm, pore size 100 Å, eluent THF (0.5 mLmin<sup>-1</sup>, 80 bar), and polystyrene calibration). IR spectroscopy was carried out with a BioRad Digilab FTS-40 (FT-IR) in the range of 400-4000 cm<sup>-1</sup>. Mass spectroscopic data were obtained from a FINNIGAN MAT 8500 instrument. Microanalyses were carried out with a PERKIN-ELMER 2400 CHN elemental analyser. The thermal degradation of PBI derivatives was studied using a Mettler Toledo TGA/SDTA 851<sup>e</sup> with a heating rate of 10 Kmin<sup>-1</sup> under N<sub>2</sub> atmosphere. Differential scanning calorimetry (DSC) was carried out with a Perkin Elmer Diamond DSC with a heating rate of 10 Kmin<sup>-1</sup> unless otherwise indicated under N<sub>2</sub>-atmosphere. The instrument was calibrated with indium standards before measurements. Phase transitions were also examined by a polarization optical microscope (POM) Nikon Diaphot 300 with a Mettler FP 90 temperature-controlled hot stage. X-ray diffraction measurements were performed on a Huber Guinier Difraktometer 6000 equipped with a Huber quartz monochromator 611 with Cu-K<sub>α1</sub>: 1.54051 Å. For cyclic voltammetry (CV) experiments, a conventional three-electrode assembly using a Ag/AgNO<sub>3</sub> reference electrode was used. CH<sub>2</sub>Cl<sub>2</sub> containing 0.1 M Bu<sub>4</sub>NPF<sub>6</sub> was used as solvent. All measurements were carried out under N<sub>2</sub>-atmosphere at a scan rate of 0.05 Vs<sup>-1</sup> at 25 °C and all redox potentials were calibrated to ferrocene/ferrocenium couple (Fc/Fc<sup>+</sup>).

**General Procedure for the Preparation of symmetrical *N,N'*-di(1-alkyl swallow-tail)-perylene-3,4,9,10-tetracarboxylic bisimides 1 and 2:**<sup>35,54</sup>

A mixture of perylene-3,4,9,10-tetracarboxylic dianhydride PTCD A (1.0 mmol), Zn(OAc)<sub>2</sub> (0.75 mmol), imidazole (4.0 g) and the respective alkyl swallow-tail amine (3.0 mmol) was vigorously stirred at 160 °C for 2 h. After cooling to r.t. the mixture was dissolved in minimum amount of THF and precipitated in 300 mL 2N HCl/MeOH 2:1 v/v. The precipitate was collected by filtration, washed with H<sub>2</sub>O followed by MeOH and dried at 80 °C in vacuum. The crude product was further purified by column chromatography.

***N,N'*-di(1-octylheptyl)-perylene-3,4,9,10-tetracarboxylic bisimide 1:**

Perylene-3,4,9,10-tetracarboxylic dianhydride (1.96 g, 5.0 mmol) and 8-octylheptylamine (3.41 g, 15.0 mmol) were allowed to react according to the above general procedure. The crude product was further purified by silica flash-column chromatography with n-hexane/CHCl<sub>3</sub> 2:1 v/v. The final product was freeze-dried from benzene and was obtained as red solid (2.68 g, 66.1 %). M.p. 135.5 °C. Calcd. for C<sub>54</sub>H<sub>70</sub>N<sub>2</sub>O<sub>4</sub>: C 79.96, H 8.70, N 3.45. Found: C 79.84, H 8.59, N 3.32. EI-MS (70 eV): *m/z* 811.0 [M<sup>+</sup>, 70.78 %]. IR (ATR):  $\nu$  = 2952 m, 2922 m, 2853 m, 1697 s, 1654 s, 1593 s, 1578 m, 1505 w, 1460 m, 1433 m, 1404 m, 1335 s, 1251 m, 1207 m, 1172 m, 1123 w, 1108 w, 962 w, 850 w, 809 m, 795 w, 745 m, 723 cm<sup>-1</sup> m. <sup>1</sup>H-NMR (250 MHz, CDCl<sub>3</sub>, 298K):  $\delta$  = 0.82 (t, *J* = 6.8 Hz, 12H, 4CH<sub>3</sub>), 1.12-1.41 (m, 40H, 20CH<sub>2</sub>), 1.77-1.96 (m, 4H, 2 $\alpha$ CH<sub>2</sub>), 2.15-2.36 (m, 4H, 2 $\alpha$ CH<sub>2</sub>), 5.10-5.27 (m, 2H, N-CH), 8.52-8.76 (m, 8H, 8ArH) ppm. <sup>13</sup>C-NMR (62.5 MHz, CDCl<sub>3</sub>, 298K):  $\delta$  = 14.40 (4C, CH<sub>3</sub>), 22.95, 27.32, 29.56, 29.85, 32.14, 32.71 (24C, CH<sub>2</sub>), 55.11 (2C, N-CH), 123.35, 123.54, 124.28, 131.46, 132.23, 126.77, 129.93, 134.83 (20C, C<sub>Ar</sub>), 163.90, 164.99 (4C, CONR) ppm.

***N,N'*-di(1-dodecylundecyl)-perylene-3,4,9,10-tetracarboxylic bisimide 2:**

Perylene-3,4,9,10-tetracarboxylic dianhydride (3.92 g, 10 mmol) and 12-dodecylundecylamine (10.19 g, 30.0 mmol) were allowed to react according to the general procedure. The crude product was further purified by silica flash-column chromatography with CHCl<sub>3</sub>. The final product was freeze-dried from benzene and was obtained as orange solid (9.76 g, 94.3 %). M.p. 76.8 °C. Calcd. for C<sub>70</sub>H<sub>102</sub>N<sub>2</sub>O<sub>4</sub>: C 81.19, H 9.93, N 2.71. Found C 80.93, H 9.56, N 2.47. EI-MS (70 eV): *m/z* 1033.8 [M<sup>+</sup>, 76.14 %]. IR (ATR):  $\nu$  = 2952 m, 2919 s, 2849 s, 1694 s, 1650 s, 1592 s, 1577 m, 1507 w, 1466 m, 1434 w, 1405 m, 1335 s, 1273 w, 1252 s, 1211 w, 1194 w, 1175 w, 1156 w, 1125 w, 1100 w, 959 w, 866 w, 856 w, 844 w, 813 s, 796 w, 773 w, 750 s, 721 m cm<sup>-1</sup>. <sup>1</sup>H-NMR (250 MHz, CDCl<sub>3</sub>, 298K):  $\delta$  = 0.83 (t, *J* = 6.8 Hz, 12H, 4CH<sub>3</sub>), 1.01-1.44 (m, 72H, 36CH<sub>2</sub>), 1.76-1.96 (m, 4H, 2 $\alpha$ CH<sub>2</sub>), 2.15-2.34 (m, 4H, 2 $\alpha$ CH<sub>2</sub>), 5.09-5.26 (m, 2H, N-CH), 8.52-8.76 (m, 8H, 8ArH) ppm. <sup>13</sup>C-NMR (62.5 MHz, CDCl<sub>3</sub>, 298K):  $\delta$  = 14.43 (4C, CH<sub>3</sub>), 23.00, 27.30, 29.66,

29.88, 29.92, 29.94, 29.95, 32.24, 32.70 (36C, CH<sub>2</sub>), 55.11 (2C, N-CH), 123.32, 131.45, 132.21, 123.54, 124.30, 126.76, 129.92, 134.80 (20C, C<sub>Ar</sub>), 163.90, 164.97 (4C, CONR) ppm.

**General Procedure for the Preparation of symmetrical *N,N'*-di(1-OEG swallow-tail)-perylene-3,4,9,10-tetracarboxylic bisimides 3 and 4:**<sup>[24]</sup>

A mixture of perylene-3,4,9,10-tetracarboxylic dianhydride PTCDA (10.0 mmol), Zn(OAc)<sub>2</sub> (7.5 mmol) in dry pyridine (75.0 mL) and the respective OEG swallow-tail amine (27.0 mmol) was stirred at 140 °C for 48 h. The resulting burgundy colored mixture was cooled, diluted with methylene chloride, and filtered through celite to remove excess dianhydride. The filtrate was dried over MgSO<sub>4</sub> and concentrated under reduced pressure. The crude product was further purified by flash column chromatography.

***N,N'*-di(2-(1,3-bis(2-(2-(2-methoxy)ethoxy)ethoxy)propyl))-perylene-3,4,9,10-tetracarboxylic bisimide 3:**

Perylene-3,4,9,10-tetracarboxylic dianhydride (5.12 g, 13.03 mmol) and 1,3-bis(2-(2-methoxyethoxy)ethoxy) propane-2-amine (10.34 g, 35.2 mmol) were allowed to react according to the general procedure. The crude product was further purified by silica flash-column chromatography with CHCl<sub>3</sub> and then CHCl<sub>3</sub>/MeOH 98:2 v/v. The final product was freeze-dried from benzene and was obtained as red solid (10.7 g, 81.6 %). M.p. 145.8 °C. Calcd. for C<sub>50</sub>H<sub>62</sub>N<sub>2</sub>O<sub>16</sub>: C 63.41, H 6.60, N 2.96. Found C 63.19, H 6.63, N 2.85. EI-MS (70 eV): *m/z* 946.7 [M<sup>+</sup>, 10.70 %]. IR (ATR):  $\nu$  = 2984 w, 2920 m, 2870 m, 2825 w, 1695 s, 1653 s, 1593 s, 1575 m, 1508 w, 1459 w, 1435 w, 1359 m, 1341 s, 1305 w, 1284 w, 1253 m, 1196 w, 1182 w, 1092 s, 1052 m, 1026 m, 962 m, 947 m, 850 m, 810 s, 796 m, 745 s, 711 w cm<sup>-1</sup>. <sup>1</sup>H-NMR (250 MHz, CDCl<sub>3</sub>, 298K):  $\delta$  = 3.27 (s, 12H, 4OCH<sub>3</sub>-OEG), 3.38-3.45 (m, 8H, 4OCH<sub>2</sub>-OEG), 3.52-3.78 (m, 24H, 12OCH<sub>2</sub>-OEG) 3.98 (dd, *J* = 10.6 Hz, *J* = 5.9 Hz, 4H, 2 $\alpha$ OCH<sub>2</sub>-OEG), 4.19 (dd, *J* = 10.6 Hz, *J* = 7.8 Hz, 4H, 2 $\alpha$ OCH<sub>2</sub>-OPEG), 5.63-5.79 (m, 2H, 2N-CH-OEG), 8.46-8.72 (m, 8H, 8ArH in perylene ring) ppm. <sup>13</sup>C-NMR (62.5 MHz, CDCl<sub>3</sub>, 298K):  $\delta$  = 52.51 (2C, N-CH), 59.28 (4C, OCH<sub>3</sub>), 69.66, 70.70, 70.80, 70.85, 72.17 (10C, OCH<sub>2</sub>), 123.20, 123.63, 126.31, 129.57, 131.64, 134.50 (20C, C<sub>Ar</sub>), 164.03 (4C, CONR) ppm.

***N,N'*-di(2-(1,3-bis(2-(2-(2-(2-methoxy)ethoxy)ethoxy)ethoxy)propyl))-perylene-3,4,9,10-tetracarboxylic bisimide 4:**

Perylene-3,4,9,10-tetracarboxylic dianhydride (785 mg, 2.0 mmol) and 1,3-bis(2-(2-(2-methoxyethoxy)ethoxy)ethoxy)propane-2-amine (2.07 g, 5.4 mmol) were allowed to react according to the general procedure. The crude product was further purified by silica flash-column

chromatography with  $\text{CHCl}_3$  and then  $\text{CHCl}_3/\text{MeOH}$  98:2 v/v. The final product was freeze-dried from benzene and was obtained as red solid (1.79 g, 79.6 %). M.p. 126.9 °C. Calcd. for  $\text{C}_{58}\text{H}_{78}\text{N}_2\text{O}_{20}$ : C 62.02, H 7.00, N 2.49. Found: C 61.58, H 6.69, N 2.28. IR (ATR):  $\nu = 2976$  w, 2912 w, 2868 m, 2821 w, 1694 s, 1653 s, 1593 m, 1575 m, 1448 w, 1435 w, 1404 m, 1355 m, 1343 s, 1307 w, 1250 m, 1197 w, 1181 w, 1135 m, 1098 s, 1052 m, 1026 m, 967, m, 875 w, 858 m, 809 s, 797 w, 745 s, 711 w  $\text{cm}^{-1}$ .  $^1\text{H-NMR}$  (250 MHz,  $\text{CDCl}_3$ , 298K):  $\delta$  (ppm) = 3.32 (s, 12H, 4 $\text{OCH}_3$ -OEG), 3.42-3.78 (m, 48H, 12 $\text{OCH}_2$ -PEG), 3.97 (dd,  $J = 10.6$  Hz,  $J = 5.8$  Hz, 4H, 2 $\alpha\text{OCH}_2$ -OEG), 4.20 (dd,  $J = 10.6$  Hz,  $J = 7.8$  Hz, 4H, 2 $\alpha\text{OCH}_2$ -OEG), 5.64-5.76 (m, 2H, 2N-CH-OEG), 8.41-8.60 (m, 8H, 8ArH).  $^{13}\text{C-NMR}$  (62.5 MHz,  $\text{CDCl}_3$ , 298K):  $\delta = 52.46$  (2C, N-CH), 59.32 (4C,  $\text{OCH}_3$ ), 69.66, 70.67, 70.79, 70.82, 70.87, 72.21 (28C,  $\text{OCH}_2$ ), 123.35, 123.74, 126.56, 129.77, 131.79, 134.74 (20C,  $\text{C}_{\text{Ar}}$ ), 164.13 (4C, CONR).

**General Procedure for the Preparation of unsymmetrical *N*-(1-alkyl swallow-tail)-*N'*-(1-OEG swallow-tail)-perylene-3,4,9,10-tetracarboxylic bisimides 6, 7, 8 and 9 via condensation reaction:**

A mixture of the respective *N*-(1-alkyl swallow-tail)-perylene-3,4,9,10-tetracarboxylic-3,4-anhydride-9,10-imide (1.0 mmol),  $\text{Zn}(\text{OAc})_2$  (1.5 mmol) in dry DMAc (6.0 mL) and the respective amine (1.8 mmol) was stirred in a microwave pressure reactor for 20 Min at 160 °C and 200 Watt. After cooling to r.t. the mixture was dissolved in minimum amount of THF and precipitated in 300 mL 2N HCl/MeOH 2:1 v/v. After standing over night, the precipitate was collected by filtration, washed with  $\text{H}_2\text{O}$ , then MeOH and dried at 60 °C in vacuum. The crude product was further purified by column chromatography on silica flash-gel (see respective compound for details).

***N*-(1-octylheptyl)-*N'*-(2-(1,3-bis(2-(2-methoxy)ethoxy)ethoxy)propyl))-perylene-3,4,9,10-tetracarboxylic bisimide 6:**

*N*-(1-octylheptyl)-perylene-3,4,9,10-tetracarboxylic-3,4-anhydride-9,10-imide **12a** (602 mg, 1 mmol) and 1,3-bis(2-(2-methoxyethoxy)ethoxy) propane-2-amine (532 mg, 1.8 mmol) were allowed to react according to the general procedure. The crude product was further purified by silica flash-column chromatography with  $\text{CHCl}_3/\text{AcOH}$  10:1 v/v to elute impurities and then  $\text{CHCl}_3/\text{MeOH}$  95:5 v/v to elute **6**. The final product was freeze-dried from benzene and was obtained as red solid (840 mg, 95.6 %). M.p. 154.4 °C. Calcd. for  $\text{C}_{52}\text{H}_{66}\text{N}_2\text{O}_{10}$ : C 71.05, H 7.57, N 3.19. Found C 70.83, H 7.03, N 3.13. EI-MS (70 eV):  $m/z$  878.7 [ $\text{M}^+$ , 22.89 %]. IR (ATR):  $\nu = 2952$  w, 2923 m, 2854 m, 1694 s, 1653 s, 1593 m, 1576 m, 1455 m, 1434 m, 1404 m, 1335 s, 1249 m, 1197 w, 1178 w, 1123 m, 1102 m, 1078 m, 1042 m, 1018 m, 963 w, 850 m, 808 s, 797 m, 745 s, 724 w  $\text{cm}^{-1}$ .  $^1\text{H-NMR}$  (250 MHz,  $\text{CDCl}_3$ , 298K):  $\delta = 0.82$  (t,  $J = 6.8$  Hz, 6H, 2 $\text{CH}_3$ ), 1.10-1.45 (m, 20H, 10 $\text{CH}_2$ ), 1.78-1.96 (m, 2H,  $\alpha\text{CH}_2$ ), 2.15-2.35 (m, 2H,  $\alpha\text{CH}_2$ ), 3.27 (s, 6H, 2 $\text{OCH}_3$ -PEG), 3.38-

3.45 (m, 4H, 2OCH<sub>2</sub>-PEG), 3.51-3.80 (m, 12H, 6OCH<sub>2</sub>-PEG), 3.97 (dd,  $J = 10.5$  Hz,  $J = 5.8$  Hz, 2H,  $\alpha$ OCH<sub>2</sub>-OEG), 4.19 (dd,  $J = 10.5$  Hz,  $J = 7.8$  Hz, 2H,  $\alpha$ OCH<sub>2</sub>-OEG), 5.10-5.27 (m, 1H, N-CH), 5.63-5.79 (m, 1H, N-CH-OEG), 8.44-8.75 (m, 8H, 8ArH) ppm. <sup>13</sup>C-NMR (62.5 MHz, CDCl<sub>3</sub>, 298K):  $\delta = 14.39$  (2C, CH<sub>3</sub>), 22.94, 27.34, 29.56, 29.85, 32.13, 32.70 (12C, CH<sub>2</sub>), 52.50 (1C, N-CH-OEG), 55.11 (1C, N-CH), 59.29 (2C, OCH<sub>3</sub>-OEG), 69.64, 70.71, 70.81, 70.86, 72.18 (10C, OCH<sub>2</sub>-OEG), 123.12, 123.31, 123.63, 124.26, 126.48, 126.55, 129.73, 129.76, 131.39, 131.63, 132.16, 134.53, 134.70 (20C, C<sub>Ar</sub>), 163.76 (C, CONR), 164.06 (2C, CONR-OEG), 164.86 (C, CONR) ppm.

***N*-(1-octylheptyl)-*N'*-(2-(1,3-bis(2-(2-(2-methoxy)ethoxy)ethoxy)ethoxy)propyl))-perylene-3,4,9,10-tetracarboxylic bisimide 7:**

*N*-(1-octylheptyl)-perylene-3,4,9,10-tetracarboxylic-3,4-anhydride-9,10-imide (1.2 g, 2.0 mmol) and 1,3-bis(2-(2-(2-methoxyethoxy)ethoxy)ethoxy) propane-2-amine **19d** (1.38 g, 3.6 mmol) were allowed to react according to the general procedure. The crude product was further purified by silica flash-column chromatography with CHCl<sub>3</sub>/AcOH 99:1 to 9:1 v/v to elute impurities and then CHCl<sub>3</sub>/MeOH 95:5 v/v to elute **7**. The final product was freeze-dried from benzene and was obtained as red solid (1.52 g, 78.6 %). M.p. 148.7 °C. Calcd. for C<sub>56</sub>H<sub>74</sub>N<sub>2</sub>O<sub>12</sub>: C 69.54, H 7.71, N 2.90. Found C 69.33, H 7.81, N 2.77. EI-MS (70 eV):  $m/z$  966.4 [M<sup>+</sup>, 20.18 %]. IR (ATR):  $\nu = 2956$  w, 2923 m, 2855 m, 2813 w, 1694 s, 1653 s, 1593 s, 1576 m, 1506 w, 1455 w, 1435 w, 1404 m, 1337 s, 1302 m, 1250 m, 1197 w, 1178 w, 1139 m, 1102 s, 1078 m, 1034 m, 964 w, 851 m, 809 s, 797 w, 746 s, 724 w cm<sup>-1</sup>. <sup>1</sup>H-NMR (250 MHz, CDCl<sub>3</sub>, 298K):  $\delta = 0.81$  (t,  $J = 6.8$  Hz, 6H, 2CH<sub>3</sub>), 1.07-1.46 (m, 20H, 10CH<sub>2</sub>), 1.77-1.95 (m, 2H,  $\alpha$ CH<sub>2</sub>), 2.16-2.34 (m, 2H,  $\alpha$ CH<sub>2</sub>), 3.31 (s, 6H, 2OCH<sub>3</sub>-OEG), 3.44-3.77 (m, 24H, 12OCH<sub>2</sub>-OEG), 3.96 (dd,  $J = 10.6$  Hz,  $J = 5.8$  Hz, 2H,  $\alpha$ OCH<sub>2</sub>-OEG), 4.20 (dd,  $J = 10.6$  Hz,  $J = 7.8$  Hz, 2H,  $\alpha$ OCH<sub>2</sub>-OEG), 5.12-5.25 (m, 1H, N-CH), 5.64-5.76 (m, 1H, N-CH-OEG), 8.39-8.72 (m, 8H, 8ArH) ppm. <sup>13</sup>C-NMR (62.5 MHz, CDCl<sub>3</sub>, 298K):  $\delta = 14.41$  (2C, CH<sub>3</sub>), 22.94, 27.31, 29.56, 29.85, 32.12, 32.67 (12C, CH<sub>2</sub>), 52.35 (1C, N-CH-OEG), 55.09 (1C, N-CH), 59.33 (2C, OCH<sub>3</sub>-OEG), 69.60, 70.64, 70.78, 70.80, 70.84, 72.18 (14C, OCH<sub>2</sub>-OEG), 123.20, 123.37, 123.62, 124.24, 126.53, 126.59, 129.77, 131.42, 132.20, 134.59, 134.78 (20C, C<sub>Ar</sub>), 163.83 (C, CONR), 164.09 (2C, CONR-OEG), 164.92 (C, CONR) ppm.

***N*-(1-dodecylundecyl)-*N'*-(2-(1,3-bis(2-(2-(2-methoxy)ethoxy)ethoxy)propyl))-perylene-3,4,9,10-tetracarboxylic bisimide 8:**

*N*-(1-dodecylundecyl)-perylene-3,4,9,10-tetracarboxylic-3,4-anhydride-9,10-imide **12b** (714 mg, 1 mmol) and 1,3-bis(2-(2-methoxyethoxy)ethoxy) propane-2-amine (532 mg, 1.8 mmol) were allowed to react according to the general procedure. The crude product was further purified by silica flash-column chromatography with CHCl<sub>3</sub>/AcOH 10:1 v/v to elute impurities and then CHCl<sub>3</sub>/MeOH 95:5 v/v to elute **8**. The final product was freeze-dried from benzene and was obtained as red solid (620 mg, 62.1 %). M.p. 107.7 °C. Calcd. for C<sub>60</sub>H<sub>82</sub>N<sub>2</sub>O<sub>10</sub>: C 72.70, H 8.34,

N 2.83. Found C 72.37, H 8.34, N 2.83. EI-MS (70 eV):  $m/z$  990.1 [ $M^+$ , 25.66 %]. IR (ATR):  $\nu = 2952$  w, 2921 m, 2852 m, 2817 w, 1694 s, 1653 s, 1593 s, 1576 m, 1456 w, 1434 w, 1404 m, 1338 s, 1250 m, 1197 w, 1176 w, 1107 s, 1082 m, 1018 m, 963 w, 849 m, 809 s, 795 w, 745 s, 720 w  $\text{cm}^{-1}$ .  $^1\text{H-NMR}$  (250 MHz,  $\text{CDCl}_3$ , 298K):  $\delta = 0.83$  (t,  $J = 6.8$  Hz, 6H, 2 $\text{CH}_3$ ), 1.07-1.42 (m, 36H, 18 $\text{CH}_2$ ), 1.80-1.95 (m, 2H,  $\alpha\text{CH}_2$ ), 2.18-2.33 (m, 2H,  $\alpha\text{CH}_2$ ), 3.27 (s, 6H, 2 $\text{OCH}_3$ -OEG), 3.39-3.44 (m, 4H, 2 $\text{OCH}_2$ -OEG), 3.52-3.78 (m, 12H, 6 $\text{OCH}_2$ -OEG), 3.97 (dd,  $J = 10.6$  Hz,  $J = 5.8$  Hz, 2H,  $\alpha\text{OCH}_2$ -OEG), 4.20 (dd,  $J = 10.6$  Hz,  $J = 7.8$  Hz, 2H,  $\alpha\text{OCH}_2$ -OEG), 5.12-5.25 (m, 1H, N-CH), 5.65-5.77 (m, 1H, N-CH-OEG), 8.42-8.70 (m, 8H, 8ArH) ppm.  $^{13}\text{C-NMR}$  (62.5 MHz,  $\text{CDCl}_3$ , 298K):  $\delta = 14.41$  (2C,  $\text{CH}_3$ ), 22.97, 27.33, 29.64, 29.89, 29.91, 29.94, 32.21, 32.69 (20C,  $\text{CH}_2$ ), 52.50 (1C, N-CH-OEG), 55.11 (1C, N-CH), 59.28 (2C,  $\text{OCH}_3$ -OEG), 69.65, 70.71, 70.80, 70.85, 72.18 (10C,  $\text{OCH}_2$ -OEG), 123.08, 123.29, 123.59, 124.25, 126.42, 126.50, 129.68, 129.72, 131.36, 131.60, 132.14, 134.48, 134.65 (20C,  $\text{C}_{Ar}$ ), 163.77 (C, CONR), 164.04 (2C, CONR-OEG), 164.86 (C, CONR) ppm.

***N*-(1-dodecylundecyl)-*N'*-(2-(1,3-bis(2-(2-(2-methoxy)ethoxy)ethoxy)ethoxy)propyl))-  
perylene-3,4,9,10-tetracarboxylic bisimide 9:**

*N*-(1-dodecylundecyl)-perylene-3,4,9,10-tetracarboxylic-3,4-anhydride-9,10-imide **12b** (1.0 g, 1.4 mmol) and 1,3-bis(2-(2-(2-methoxyethoxy)ethoxy)ethoxy) propane-2-amine (970 mg, 2.5 mmol) were allowed to react according to the general procedure. The crude product was further purified by silica flash-column chromatography with  $\text{CHCl}_3/\text{AcOH}$  99:1 to 9:1 v/v to elute impurities and then with  $\text{CHCl}_3/\text{MeOH}$  95:5 v/v to elute **9**. The final product was freeze-dried from benzene and was obtained as red solid (652 mg, 43.1 %). M.p. 111.2 °C. Calcd. for  $\text{C}_{64}\text{H}_{90}\text{N}_2\text{O}_{12}$ : C 71.21, H 8.40, N 2.60. Found: C 70.87, H 8.67, N 2.41. EI-MS (70 eV):  $m/z$  1080.3 [ $M^+$ , 34.38 %]. IR (ATR):  $\nu = 2952$  w, 2921 m, 2852 m, 2813 w, 1694 s, 1654 s, 1593 s, 1576 m, 1507 w, 1456 m, 1435 m, 1404 m, 1337 s, 1251 m, 1197 w, 1180 w, 1139 m, 1104 s, 1078 m, 1030m, 963 w, 849 m, 809 s, 797 w, 746 s, 722 w  $\text{cm}^{-1}$ .  $^1\text{H-NMR}$  (250 MHz,  $\text{CDCl}_3$ , 298K):  $\delta = 0.82$  (t,  $J = 6.8$  Hz, 6H, 2 $\text{CH}_3$ ), 1.06-1.43 (m, 36H, 18 $\text{CH}_2$ ), 1.78-1.94 (m, 2H,  $\alpha\text{CH}_2$ ), 2.16-2.34 (m, 2H,  $\alpha\text{CH}_2$ ), 3.31 (s, 6H, 2 $\text{OCH}_3$ -OEG), 3.40-3.78 (m, 24H, 12 $\text{OCH}_2$ -OEG), 3.96 (dd,  $J = 10.6$  Hz,  $J = 5.8$  Hz, 2H,  $\alpha\text{OCH}_2$ -OEG), 4.20 (dd,  $J = 10.6$  Hz,  $J = 7.8$  Hz, 2H,  $\alpha\text{OCH}_2$ -OEG), 5.12-5.25 (m, 1H, N-CH), 5.64-5.76 (m, 1H, N-CH-OEG), 8.36-8.78 (m, 8H, 8ArH) ppm.  $^{13}\text{C-NMR}$  (62.5 MHz,  $\text{CDCl}_3$ , 298K):  $\delta = 14.44$  (2C,  $\text{CH}_3$ ), 22.99, 27.30, 29.65, 29.88, 29.92, 29.94, 32.21, 32.66 (20C,  $\text{CH}_2$ ), 52.35 (1C, N-CH-OEG), 55.08 (1C, N-CH), 59.33 (2C,  $\text{OCH}_3$ -OEG), 69.60, 70.64, 70.78, 70.80, 70.84, 72.18 (14C,  $\text{OCH}_2$ -OEG), 123.20, 123.36, 123.58, 124.24, 126.53, 126.59, 129.77, 131.44, 132.18, 134.59, 134.79 (20C,  $\text{C}_{Ar}$ ), 163.84 (C, CONR), 164.11 (2C, CONR-OEG), 164.91 (C, CONR) ppm.

**General Procedure for the Preparation of unsymmetrical Perylene-3,4,9,10-tetracarboxylic bisimides 5, 10 and 11 via nucleophilic substitution:**

**Method A:** A mixture of the respective *N*-(1-swallow-tail)-perylene-3,4,9,10-tetracarboxylic-3,4-anhydride-9,10-imide (1.0 mmol), K<sub>2</sub>CO<sub>3</sub> (1.8 mmol), KI (0.2 mmol) and the respective bromide (1.8 mmol) in 20 mL absolute DMF was stirred at 80 °C for 3-7 d. The conversion was monitored via TLC or GPC. Purification procedures are described for each compound separately.

**Method B:** To a suspension of the respective *N*-(1-swallow-tail)-perylene-3,4,9,10-tetracarboxylic-3,4-anhydride-9,10-imide (1.0 mmol) in dry DMF (30 mL) was added NaH (1.2 mmol), as 60 % suspension in mineral oil, at 0 °C. The mixture was stirred and allowed to reach RT, then the respective bromide (2.5 mmol) was added and heated to 80 °C. After 48 h, the reaction was cooled to room temperature and quenched by addition of saturated NH<sub>4</sub>Cl solution (2.5 mL). Purification procedures are described in the corresponding compound section.

***N*-(1-decylonyl)-*N'*-(1-octylheptyl)-perylene-3,4,9,10-tetracarboxylic bisimide 5:**

*N*-(1-octylheptyl)-perylene-3,4,9,10-tetracarboxylic bisimide **14a** (901 mg, 1.5 mmol) and 10-bromononadecane (938 mg, 2.7 mmol) were allowed to react according to the general procedure Method A for 7 d. After cooling to r.t., the product was precipitated in 300 mL 2N HCl/MeOH 2:1 v/v. After standing over night, the precipitate was collected by filtration, washed with H<sub>2</sub>O, then MeOH and dried at 60 °C in vacuum. The crude product was further purified by column chromatography on silica flash-gel (petrolether/CHCl<sub>3</sub> 1:1 to 1:4 v/v). The final product was freeze-dried from benzene and was obtained as red solid (762 mg, 58.6 %). M.p. 98.8 °C. Calcd. for C<sub>58</sub>H<sub>78</sub>N<sub>2</sub>O<sub>4</sub>: C 80.33, H 9.07 N 3.23. Found C 79.98, H 10.27, N 3.34. EI-MS (70 eV): *m/z* 866.6 ([M<sup>+</sup>], 81.27 %). IR (ATR):  $\nu$  = 2956 w, 2922 m, 2853 m, 1695 s, 1651 s, 1593 s, 1578 m, 1460 w, 1434 w, 1405 m, 1335 s, 1251 m, 1209 w, 1172 m, 1124 w, 1108 w, 850 w, 809 m, 795 m, 746 m, 722 w cm<sup>-1</sup>. <sup>1</sup>H-NMR (250 MHz, CDCl<sub>3</sub>, 298K):  $\delta$  = 0.82 (t, *J* = 6.2 Hz, 12H, 4CH<sub>3</sub>), 1.10-1.42 (m, 48H, 24CH<sub>2</sub>), 1.76-1.95 (m, 4H, 2 $\alpha$ CH<sub>2</sub>), 2.14-2.35 (m, 4H, 2 $\alpha$ CH<sub>2</sub>), 5.10-5.26 (m, 2H, N-CH), 8.53-8.76 (m, 8H, 8ArH) ppm. <sup>13</sup>C-NMR (62.5 MHz, CDCl<sub>3</sub>, 298K):  $\delta$  = 14.45, 14.48 (4C, CH<sub>3</sub>), 23.00, 23.03, 27.36, 29.61, 29.65, 29.93, 32.18, 32.24, 32.74 (28C, CH<sub>2</sub>), 55.14 (2C, N-CH), 123.36, 123.57, 124.28, 131.47, 132.21, 126.78, 129.95, 134.83 (20C, C<sub>Ar</sub>), 163.95, 165.03 (4C, CONR) ppm.

***N*-(2-(1,3-bis(2-(2-(2-(2-methoxy)ethoxy)ethoxy)ethoxy)propyl))-*N'*-(1-dodecyl)-perylene-3,4,9,10-tetracarboxylic bisimide 10:**

*N*-(2-(1,3-bis(2-(2-(2-(2-methoxy)ethoxy)ethoxy)ethoxy)propyl))-perylene-3,4,9,10-tetracarboxylic bisimide **14c** (946 mg, 1.25 mmol) and 12-bromododecane (561 mg, 2.25 mmol) were allowed to react according to the general procedure Method A for 3 d. After cooling to r.t.

the mixture was poured into saturated NaCl solution and was extracted with  $\text{CHCl}_3$ . After drying over  $\text{MgSO}_4$  and removal of solvent in vacuo, the crude product was further purified by column chromatography on silica flash-gel ( $\text{CHCl}_3/\text{MeOH}$  98:2 v/v). The final product was freeze-dried from benzene to afford **10** as dark red solid (547 mg, 47.3 %). M.p. 140.1 °C. Calcd. for  $\text{C}_{53}\text{H}_{68}\text{N}_2\text{O}_{12}$ : C 68.81, H 7.41, N 3.01. Found: C 68.99, H 7.35, N 3.03. EI-MS (70 eV):  $m/z$  924.0 ( $[\text{M}^+]$ , 32.38 %). IR (ATR):  $\nu = 2960$  w, 2922 m, 2854 m, 2821 w, 1693 s, 1651 s, 1593s 1577 m, 1507 w, 1460 w, 1438 m, 1403 m, 1355m, 1343 s, 1249 m, 1198 w, 1180 w, 1104 s, 1030 m, 857 m, 809 s, 794 w, 745 s, 722 w  $\text{cm}^{-1}$ .  $^1\text{H-NMR}$  (250 MHz,  $\text{CDCl}_3$ , 298K):  $\delta = 0.87$  (s, 3H,  $\text{CH}_3$ ), 1.12-1.53 (m, 18H, 9 $\text{CH}_2$ ), 1.67-1.84 (m, 2H,  $\beta\text{-CH}_2$ ), 3.31 (s, 6H, 2 $\text{OCH}_3$ ), 3.44-3.78 (m, 24H, 12 $\text{OCH}_2$ ), 3.94-4.02 (dd,  $J = 10.5$  Hz,  $J = 5.8$  Hz, 2H, OEG- $\alpha$ - $\text{OCH}_2$ ), 4.14-4.25 (m, 4H, OEG- $\alpha$ - $\text{OCH}_2$ , N- $\text{CH}_2$ ), 5.64-5.75 (m, 1H, N-CH-OEG), 8.41 (dd,  $J = 8.2$  Hz,  $J = 4.4$  Hz, 4H, 4 $\text{H}_{\text{Ar}}$ ), 8.54 (dd,  $J = 14.4$  Hz,  $J = 8.0$  Hz, 4H, 4 $\text{H}_{\text{Ar}}$ ) ppm.  $^{13}\text{C-NMR}$  (62.5 MHz,  $\text{CDCl}_3$ , 298K):  $\delta = 14.45$  (1C,  $\text{CH}_3$ ), 23.02, 27.52, 28.46, 29.68, 29.73, 29.92, 29.97, 29.99 (9C,  $\text{CH}_2$ ), 32.25 (1C,  $\beta\text{-CH}_2$ ), 41.05 (1C, N- $\text{CH}_2$ ), 52.48 (1C, N-CH-OEG), 59.32 (2C,  $\text{OCH}_3$ -OEG), 69.66, 70.68, 70.83, 70.87, 72.21 (14C,  $\text{OCH}_2$ -OEG), 123.16, 123.22, 123.48, 123.70, 126.03, 126.45, 129.39, 129.63, 131.49, 134.51, 134.57 (20C,  $\text{C}_{\text{Ar}}$ ), 163.50, 164.00 (4C, CONR) ppm.

***N*-(1-dodecylundecyl)-*N'*-(1-(2-(2-(2-(2-methoxy)ethoxy)ethoxy)ethoxy)ethyl)-perylene-3,4,9,10-tetracarboxylic bisimide 11:**

*N*-(1-dodecylundecyl)-perylene-3,4,9,10-tetracarboxylic bisimide **14b** (901 mg, 1.5 mmol) and 1-Bromo-tetraethyleneglycol monomethyl ether (881 mg, 3.25 mmol) were allowed to react according to the general procedure Method B for 48 h. After cooling to r.t., the product was precipitated in 300 mL 2N HCl/MeOH 3:1 v/v. After standing over night, the precipitate was collected by filtration, washed with  $\text{H}_2\text{O}$ , then MeOH and dried at 60 °C in vacuum. The crude product was further purified by column chromatography on silica flash-gel (THF/hexane 1:1 v/v). The final product was freeze-dried from benzene and was obtained as red solid (631 mg, 53.7 %). M.p. 151.8 °C. Calcd. for  $\text{C}_{56}\text{H}_{74}\text{N}_2\text{O}_8$ : C 74.47, H 8.26, N 3.10. Found: C 74.10, H 8.90, N 3.13. EI-MS (70 eV):  $m/z$  902.3 ( $[\text{M}^+]$ , 87.5 %). IR (ATR):  $\nu = 2956$  w, 2921 m, 2852 m, 1693 s, 1645 s, 1594 s, 1577 m, 1506 w, 1437 m, 1403 m, 1343 s, 1249 m, 1197 w, 1178 m, 1107 m, 1060 m, 1060 m, 1040 w, 857 m, 809 s, 794 m, 745 s, 720 w  $\text{cm}^{-1}$ .  $^1\text{H-NMR}$  (250 MHz,  $\text{CDCl}_3$ , 298K):  $\delta = 0.84$  (t,  $J = 6.7$  Hz, 6H, 2 $\text{CH}_3$ ), 1.07-1.43 (m, 36H, 18 $\text{CH}_2$ ), 1.78-1.97 (m, 2H,  $\alpha\text{CH}_2$ ), 2.15-2.35 (m, 2H,  $\alpha\text{CH}_2$ ), 3.34 (s, 3H,  $\text{OCH}_3$ ), 3.47-3.54 (m, 2H,  $\text{OCH}_2$ ), 3.54-3.67 (m, 8H,  $\text{OCH}_2$ ), 3.69-3.76 (m, 2H,  $\text{OCH}_2$ ), 3.86 (t,  $J = 5.9$  Hz, 2H,  $\text{OCH}_2$ ), 4.47 (t,  $J = 5.9$  Hz, 2H, N- $\text{CH}_2$ ), 5.10-5.26 (m, 1H, N-CH), 8.52-8.74 (m, 8H, 8 $\text{ArH}$ ) ppm.  $^{13}\text{C-NMR}$  (62.5 MHz,  $\text{CDCl}_3$ , 298K):  $\delta = 14.48$  (2C,  $\text{CH}_3$ ), 23.04, 27.41, 29.71, 29.96, 30.00, 32.28, 32.74 (20C,  $\text{CH}_2$ ), 39.61 (1C, N- $\text{CH}_2$ ), 55.22 (1C, N-CH), 59.39 (1C,  $\text{OCH}_3$ ), 68.25, 70.44, 70.86, 70.94, 71.03, 72.28 (7C,  $\text{OCH}_2$ ), 123.07, 123.24, 131.41, 126.36, 129.44, 129.69, 134.31, 134.63 (20C,  $\text{C}_{\text{Ar}}$ ), 163.47 (4C, CONR) ppm.

**Supporting Information available.**

This information is available free of charge via the Internet at <http://pubs.acs.org/>.

**BIBLIOGRAPHY**

- (1) Würthner, F. *Chem. Commun.* **2004**, 1564-1579.
- (2) Langhals, H. *Helv. Chim. Acta* **2005**, *88*, 1309-1343.
- (3) Struijk, C. W.; Sieval, A. B.; Dakhorst, J. E. J.; van Dijk, M.; Kimkes, P.; Koehorst, R. B. M.; Donker, H.; Schaafsma, T. J.; Picken, S. J.; van de Craats, A. M.; Warman, J. M.; Zuilhof, H.; Sudholter, E. J. R. *J. Am. Chem. Soc.* **2000**, *122*, 11057-11066.
- (4) Horowitz, G.; Kouki, F.; Spearman, P.; Fichou, D.; Nogues, C.; Pan, X.; Garnier, F. *Adv. Mater.* **1996**, *8*, 242-5.
- (5) Dimitrakopoulos, C. D.; Malenfant, P. R. L. *Adv. Mater.* **2002**, *14*, 99-117.
- (6) Jancy, B.; Asha, S. K. *J. Phys. Chem. B* **2006**, *110*, 20937-20947.
- (7) Geissler, G.; Remy, H.; (Farbwerke Hoechst A.-G.). Application: DE, 1962, p 2 pp.
- (8) Schmidt-Mende, L.; Fechtenkötter, A.; Müllen, K.; Moons, E.; Friend, R. H.; MacKenzie, J. D. *Science* **2001**, *293*, 1119-22.
- (9) Yakimov, A.; Forrest, S. R. *Appl. Phys. Lett.* **2002**, *80*, 1667-1669.
- (10) Lindner, S. M.; Huettner, S.; Chiche, A.; Thelakkat, M.; Krausch, G. *Angew. Chem. Int. Ed.* **2006**, *45*, 3364-3368.
- (11) Sommer, M.; Lindner, S. M.; Thelakkat, M. *Adv. Funct. Mater.* **2007**, *17*, 1493-1500.
- (12) Löhmannsröben, H. G.; Langhals, H. *Appl. Phys. B* **1989**, *48*, 449-452.
- (13) Liu, S.-G.; Sui, G.; Cormier, R. A.; Leblanc, R. M.; Gregg, B. A. *The Journal of Physical Chemistry B* **2002**, *106*, 1307-1315.
- (14) Simpson, C. D.; Wu, J.; Watson, M. D.; Muellen, K. *J. Mater. Chem.* **2004**, *14*, 494-504.
- (15) An, Z.; Yu, J.; Jones, S. C.; Barlow, S.; Yoo, S.; Domercq, B.; Prins, P.; Siebbeles, L. D. A.; Kippelen, B.; Marder, S. R. *Adv. Mater.* **2005**, *17*, 2580-2583.
- (16) Kato, T.; Mizoshita, N.; Kishimoto, K. *Angew. Chem. Int. Ed.* **2006**, *45*, 38-68.
- (17) Hoeben, F. J. M.; Jonkheijm, P.; Meijer, E. W.; Schenning, A. P. H. J. *Chem. Rev.* **2005**, *105*, 1491-1546.
- (18) Laschat, S.; Baro, A.; Steinke, N.; Giesselmann, F.; Haegele, C.; Scalia, G.; Judele, R.; Kapatsina, E.; Sauer, S.; Schreivogel, A.; Tosoni, M. *Angew. Chem. Int. Ed.* **2007**, *46*, 4832-4887.
- (19) Destrade, C.; Foucher, P.; Gasparoux, H.; Nguyen, H. T.; Levelut, A. M.; Malthete, J. *Mol. Cryst. Liq. Cryst.* **1984**, *106*, 121-46.
- (20) Kopitzke, J.; Wendorff, J. H. *Chem. Unserer Zeit* **2000**, *34*, 4-16.
- (21) Nelson, J. *Science* **2001**, *293*, 1059-1060.

- (22) Sergeev, S.; Pisula, W.; Geerts, Y. H. *Chem. Soc. Rev.* **2007**, *36*, 1902-1929.
- (23) Chesterfield, R. J.; McKeen, J. C.; Newman, C. R.; Ewbank, P. C.; da Silva Filho, D. A.; Bredas, J.-L.; Miller, L. L.; Mann, K. R.; Frisbie, C. D. *The Journal of Physical Chemistry B* **2004**, *108*, 19281-19292.
- (24) Cormier, R. A.; Gregg, B. A. *Chemistry of Materials* **1998**, *10*, 1309-1319.
- (25) Cormier, R. A.; Gregg, B. A. *The Journal of Physical Chemistry B* **1997**, *101*, 11004-11006.
- (26) Würthner, F.; Thalacker, C.; Diele, S.; Tschierske, C. *Chem. Eur. J.* **2001**, *7*, 2245-2253.
- (27) Chen, Z.; Baumeister, U.; Tschierske, C.; Würthner, F. *Chem. Eur. J.* **2007**, *13*, 450-465.
- (28) Jancy, B.; Asha, S. K. *Chemistry of Materials* **2008**, *20*, 169-181.
- (29) Hansen, M. R.; Schnitzler, T.; Pisula, W.; Graf, R.; Müllen, K.; Spiess, Hans W. *Angewandte Chemie International Edition* **2009**, *48*, 4621-4624.
- (30) Clarkson, G. J.; Cook, A.; McKeown, N. B.; Treacher, K. E.; Ali-Adib, Z. *Macromolecules* **1996**, *29*, 913-917.
- (31) Ali-Adib, Z.; Clarkson, G. J.; McKeown, N. B.; Treacher, K. E.; Gleeson, H. F.; Stennett, A. S. *J. Mater. Chem.* **1998**, *8*, 2371-2378.
- (32) Langhals, H.; Ismael, R.; Yürük, O. *Tetrahedron* **2000**, *56*, 5435-5441.
- (33) Langhals, H.; Demmig, S.; Potrawa, T. *J. Prakt. Chem.* **1991**, *333*, 733-48.
- (34) Langhals, H.; Demmig, S.; Huber, H. *Spectrochim. Acta A* **1988**, *44A*, 1189-93.
- (35) Kaiser, H.; Lindner, J.; Langhals, H. *Chem. Ber.* **1991**, *124*, 529-35.
- (36) Langhals, H.; Saulich, S. *Chem. Eur. J.* **2002**, *8*, 5630-5643.
- (37) Nagao, Y.; Misono, T. *Dyes Pigm.* **1984**, *5*, 171-88.
- (38) Nagao, Y.; Misono, T. *Bull. Chem. Soc. Jpn.* **1981**, *54*, 1191-4.
- (39) Tröster, H. *Dyes Pigm.* **1983**, *4*, 171-7.
- (40) Lindner, S. M.; Thelakkat, M. *Macromol. Chem. Phys.* **2006**, *207*, 2084-2092.
- (41) Borch, R. F.; Bernstein, M. D.; Durst, H. D. *Journal of the American Chemical Society* **1971**, *93*, 2897-2904.
- (42) Holman, M. W.; Liu, R.; Adams, D. M. *Journal of the American Chemical Society* **2003**, *125*, 12649-12654.
- (43) Zakeeruddin, S. M.; Nazeeruddin, M. K.; Humphry-Baker, R.; Pechy, P.; Quagliotto, P.; Barolo, C.; Viscardi, G.; Graetzel, M. *Langmuir* **2002**, *18*, 952-954.
- (44) Kratzat, K.; Finkelmann, H. *Liq. Cryst.* **1993**, *13*, 691-9.
- (45) Vacus, J.; Simon, J. *Adv. Mater.* **1995**, *7*, 797-800.

- (46) Gürek, A. G.; Ahsen, V.; Heinemann, F.; Zugenmaier, P. *Mol. Cryst. Liq. Cryst. Sci.* **2000**, *338*, 75-97.
- (47) Gürek, A. G.; Durmus, M.; Ahsen, V. *New J. Chem.* **2004**, *28*, 693-699.
- (48) Nemoto, H.; Cai, J.; Iwamoto, S.; Yamamoto, Y. *Journal of Medicinal Chemistry* **1995**, *38*, 1673-1678.
- (49) Biron, E.; Otis, F.; Meillon, J.-C.; Robitaille, M.; Lamothe, J.; Van Hove, P.; Cormier, M.-E.; Voyer, N. *Bioorg. Med. Chem.* **2004**, *12*, 1279-1290.
- (50) Pommerehne, J.; Vestweber, H.; Guss, W.; Mahrt, R. F.; Bässler, H.; Porsch, M.; Daub, J. *Advanced Materials* **1995**, *7*, 551-554.
- (51) Pisula, W.; Kastler, M.; Wasserfallen, D.; Robertson, J. W. F.; Nolde, F.; Kohl, C.; Muellen, K. *Angew. Chem. Int. Ed.* **2006**, *45*, 819-823.
- (52) Marcon, V.; Kirkpatrick, J.; Pisula, W.; Andrienko, D. *Phys. Stat. Sol. (b)* **2008**, *245*, 820-824.
- (53) Hansen, M. R.; Graf, R.; Sekharan, S.; Sebastiani, D. *Journal of the American Chemical Society* **2009**, *131*, 5251-5256.
- (54) Wescott, L. D.; Mattern, D. L. *The Journal of Organic Chemistry* **2003**, *68*, 10058-10066.

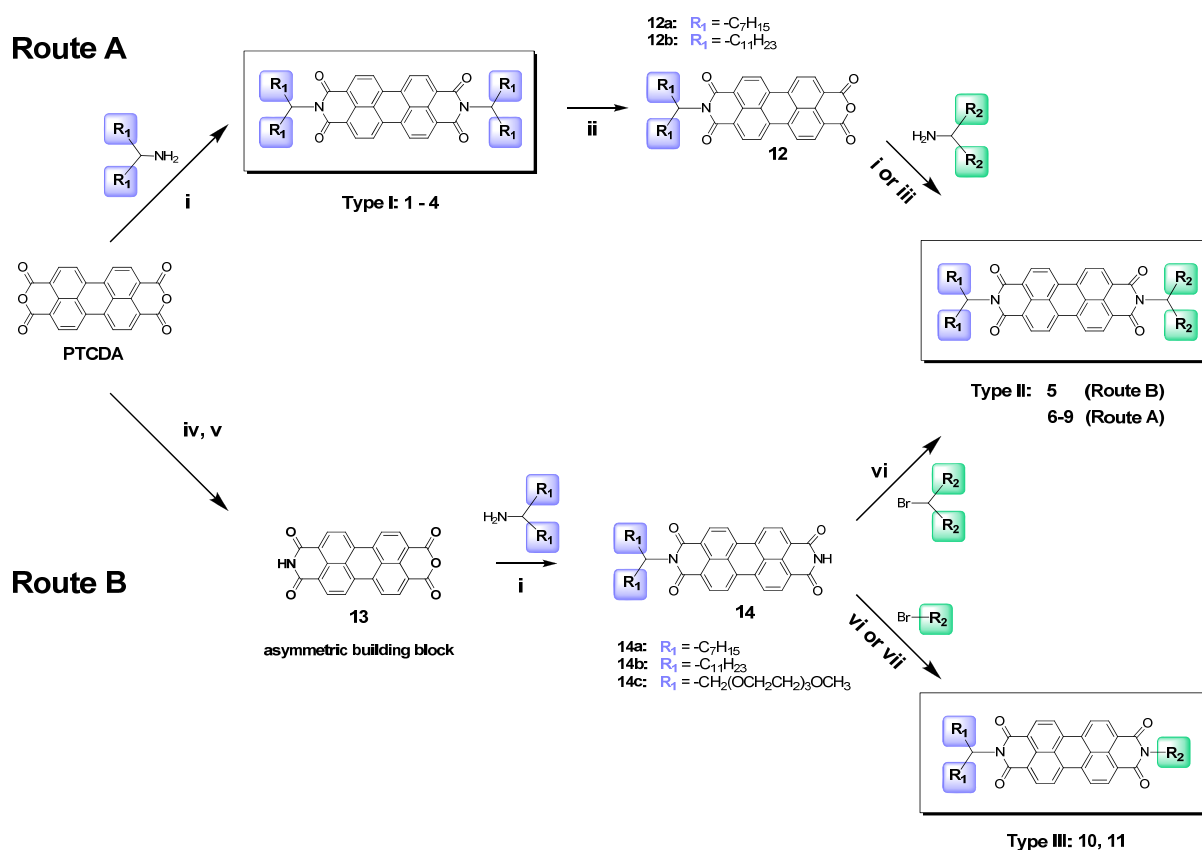
## **SUPPORTING INFORMATION**

### **Table of Contents**

- 1. General Information**
- 2. Synthesis and Characterization of Perylene-Intermediates**
  - 2.1 *General Procedure for the Preparation of N-(1-alkyl swallow-tail)-perylene-3,4,9,10-tetracarboxylic-3,4-anhydride-9,10-imides **12a** and **12b***
  - 2.2 *General Procedure for the Preparation of N-(1-swallow-tail)-perylene-3,4,9,10-tetracarboxylic bisimides **14a, b** and **c***
- 3. Literature**

## 1. General Information

The starting materials, perylenetetracarboxylic acid dianhydride PTCDA, pentadecane-8-one, tricosan-12-one, tetraethyleneglycol monomethyl ether and solvents, were purchased from Merck, Aldrich, Fluka or TCI and used without any further purification. Solvents used for precipitation and column chromatography were distilled under normal atmosphere. Compound **13**<sup>1</sup> and all swallow-tail amines<sup>2-8</sup> were synthesized according to published procedures. <sup>1</sup>H-NMR spectra were recorded on a Bruker AC 250 spectrometer (250 MHz). Chemical shifts are reported in ppm at room temperature using CDCl<sub>3</sub> as solvent and tetramethylsilane as internal standard unless indicated otherwise. Abbreviations used for splitting patterns are s = singlet, d = dublett, t = triplet, qui = quintet, m = multiplet.



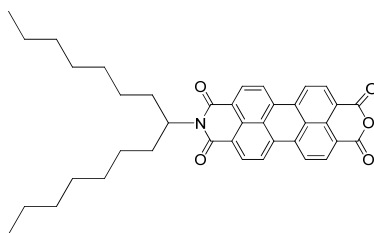
**Scheme 1.** Main synthetic pathways for unsymmetrical N-substitution of perylene bisimides. i) imidazole, Zn(OAc)<sub>2</sub>, 2-4 h, 160 °C; ii) KOH, t-BuOH, 90°C 1-1.5 h; iii) DMAc, Zn(OAc)<sub>2</sub>, 20 Min, 160 °C, 200 Watt; iv) 1. KOH, 2. AcOH; v) NH<sub>4</sub>OH, K<sub>2</sub>CO<sub>3</sub>; vi) DMF, K<sub>2</sub>CO<sub>3</sub>, KI, 80 °C, 3-5 d; vii) DMF, NaH, 80 °C, 48 h.

## 2. Synthesis and Characterization of Perylene-Intermediates

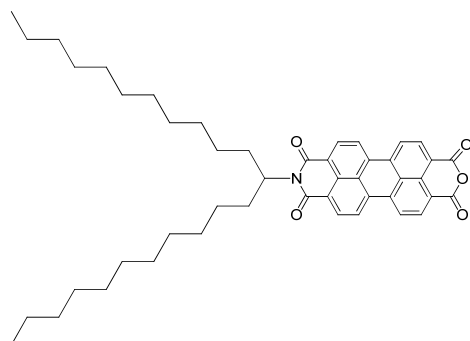
### 2.1 General Procedure for the Preparation of *N*-(1-alkyl swallow-tail)-perylene-3,4,9,10-tetracarboxylic-3,4-anhydride-9,10-imides **12a** and **12b**:<sup>9,10</sup>

To a mixture of the respective *N,N'*-di(1-alkyl-swallowtail)-perylene-3,4,9,10-tetracarboxylic bisimide (1.0 equiv.) and *t*-BuOH (25 mL per mmol PBI) was added 85% KOH powder (5.0 equiv.). The resulting mixture was refluxed for 90 °C and the conversion was monitored via TLC (CHCl<sub>3</sub>/AcOH 10:1 v/v). After complete disappearance of the bisimide (1 – 1.5 h), the mixture was poured slowly with stirring into AcOH (25 mL per mmol PBI) and stirred for 2 h. Then 2N HCl (10 mL per mmol PBI) was added and stirring was continued for additional 30 min. The resulting precipitate was collected by filtration, washed with water until the washings were neutral and dried at 80 °C in vacuum. The crude product was further purified by column chromatography on silica gel with CHCl<sub>3</sub> to remove bisimide and then with CHCl<sub>3</sub>/AcOH 10:1 v/v to elute the product.

#### Preparation of *N*-(1-octylheptyl)-perylene-3,4,9,10-tetracarboxylic-3,4-anhydride-9,10-imide **12a**:



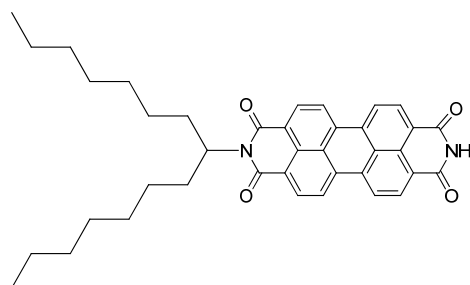
*N,N'*-di(1-octylheptyl)-perylene-3,4,9,10-tetracarboxylic bisimide **1** (16.22 g, 20.0 mmol) was allowed to react according to the general procedure. The final product was freeze-dried from benzene and was obtained as red solid (7.27 g, 60.4 %). <sup>1</sup>H-NMR (250 MHz, CDCl<sub>3</sub>, 298K):  $\delta$  = 0.82 (t, *J* = 6.8 Hz, 6H, 2CH<sub>3</sub>), 1.11-1.42 (m, 20H, 10CH<sub>2</sub>), 1.77-1.96 (m, 2H,  $\alpha$ CH<sub>2</sub>), 2.14-2.34 (m, 2H,  $\alpha$ CH<sub>2</sub>), 5.11-5.25 (m, 1H, N-CH), 8.62-8.80 (m, 8H, 8ArH) ppm.

**Preparation of *N*-(1-dodecylundecyl)-perylene-3,4,9,10-tetracarboxylic-3,4-anhydride-9,10-imide **12b**:**

*N,N'*-di(1-dodecylundecyl)-perylene-3,4,9,10-tetracarboxylic bisimide **2** (6.22 g, 6.0 mmol) was allowed to react according to the general procedure. The final product was freeze-dried from benzene and was obtained as red solid (3.06 g, 71.4 %).  $^1\text{H-NMR}$  (250 MHz,  $\text{CDCl}_3$ , 298K):  $\delta$  = 0.84 (t,  $J$  = 6.8 Hz, 6H, 2 $\text{CH}_3$ ), 1.10-1.38 (m, 36H, 18 $\text{CH}_2$ ), 1.76-1.96 (m, 2H,  $\alpha\text{CH}_2$ ), 2.14-2.34 (m, 2H,  $\alpha\text{CH}_2$ ), 5.09-5.26 (m, 1H, N-CH), 8.57-8.82 (m, 8H, 8ArH) ppm.

**2.2 General Procedure for the Preparation of *N*-(1-swallow-tail)-perylene-3,4,9,10-tetracarboxylic bisimides **14a**, **b** and **c**:<sup>11</sup>**

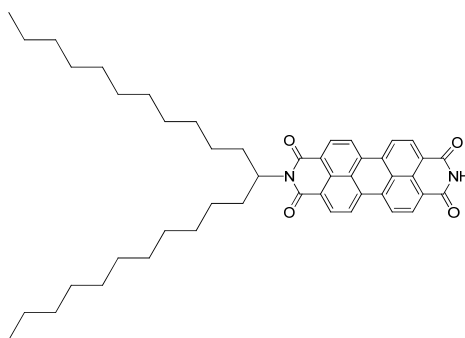
A mixture of perylene-3,4,9,10-tetracarboxylic-3,4-anhydride-9,10-imide **13** (1.0 mmol), imidazole (3.0 g per mmol **13**) and the respective swallow-tail amine (1.6 mmol) was stirred at 160 °C for 4 h. After cooling to r.t. the mixture was dissolved in minimum amount THF and precipitated in 2N HCl/MeOH 3:1 v/v. The precipitate was collected by filtration, washed with  $\text{H}_2\text{O}$  and MeOH and dried at 80 °C in vacuum. The crude product was further purified by column chromatography on silica flash-gel.

**Preparation of *N*-(1-octylheptyl)-perylene-3,4,9,10-tetracarboxylic bisimide **14a**:**

Perylene-3,4,9,10-tetracarboxylic-3,4-anhydride-9,10-imide **13** (11.74 g, 30.0 mmol) and 8-heptyloctylamine (10.92 g, 48 mmol) were allowed to react according to the general procedure.

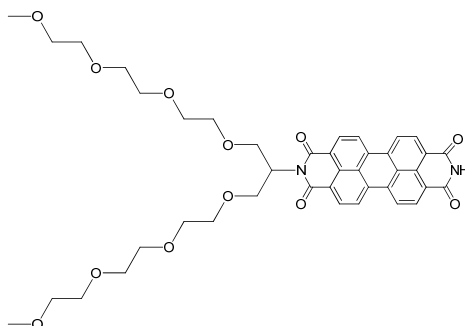
The crude product was further purified by column chromatography on silica gel ( $\text{CHCl}_3$  to remove traces of bisimide and then  $\text{CHCl}_3/\text{AcOH}$  10:1 v/v to elute product). The final product was freeze-dried from benzene and was obtained as red solid (10.49 g, 58.2 %).  $^1\text{H-NMR}$  (250 MHz,  $\text{CDCl}_3$ , 298K):  $\delta$  = 0.82 (t,  $J$  = 6.6 Hz, 6H,  $2\text{CH}_3$ ), 1.08-1.44 (m, 20H,  $10\text{CH}_2$ ), 1.77-1.96 (m, 2H,  $\alpha\text{CH}_2$ ), 2.13-2.37 (m, 2H,  $\alpha\text{CH}_2$ ), 5.10-5.25 (m, 1H, N-CH), 8.53 (br. s, 1H, NH), 8.59-8.75 (m, 8H, ArH).

#### Preparation of *N*-(1-dodecylundecyl)-perylene-3,4,9,10-tetracarboxylic bisimide **14b**:



Perylene-3,4,9,10-tetracarboxylic-3,4-anhydride-9,10-imide **13** (7.83 g, 20.0 mmol) and 12-dodecylundecylamine (10.87 g, 32 mmol) were allowed to react according to the general procedure. The crude product was further purified by column chromatography on silica gel ( $\text{CHCl}_3$  to remove traces of bisimide and then  $\text{CHCl}_3/\text{AcOH}$  10:1 v/v to elute product). The final product was freeze-dried from benzene and was obtained as red solid (9.10 g, 63.8 %).  $^1\text{H-NMR}$  (250 MHz,  $\text{CDCl}_3$ , 298K):  $\delta$  = 0.83 (t,  $J$  = 6.6 Hz, 6H,  $2\text{CH}_3$ ), 1.05-1.45 (m, 36H,  $18\text{CH}_2$ ), 1.78-2.02 (m, 2H,  $\alpha\text{CH}_2$ ), 2.12-2.38 (m, 2H,  $\alpha\text{CH}_2$ ), 5.09-5.26 (m, 1H, N-CH), 8.39-8.69 (m, 8H, ArH), 8.98 (br. s, 1H, NH).

#### Preparation of *N*-(2-(1,3-bis(2-(2-(2-methoxy)ethoxy)ethoxy)ethoxy)propyl))-perylene-3,4,9,10-tetracarboxylic bisimide **14c**:



Perylene-3,4,9,10-tetracarboxylic-3,4-anhydride-9,10-imide **13** (6.14 g, 16 mmol) and 1,3-bis(2-(2-(2-methoxyethoxy)ethoxy)ethoxy)propane-2-amine (3.91 g, 10 mmol) were allowed to react according to the general procedure. The crude product was further purified by column

chromatography on silica flash-gel with CHCl<sub>3</sub>/MeOH 95:5 v/v as eluent to afford **14c** as red solid (4.02 g, 53.1 %). <sup>1</sup>H-NMR (250 MHz, CDCl<sub>3</sub>, 298K):  $\delta$  = 3.31 (s, 3H, OCH<sub>3</sub>), 3.45-3.92 (m, 24H, 12OCH<sub>2</sub>), 4.00 (dd,  $J$  = 10.9 Hz,  $J$  = 5.4 Hz, 4H,  $\alpha$ CH<sub>2</sub>-OEG), 4.39 (dd,  $J$  = 10.9 Hz,  $J$  = 8.1 Hz, 4H,  $\alpha$ CH<sub>2</sub>-OEG), 5.72-5.83 (m, 1H, N-CH-OEG), 8.13 (br. s, 6H, ArH), 8.44 (d,  $J$  = 7.8 Hz, 2H, ArH), 9.84 (br. s, 1H, NH).

### 3. **BIBLIOGRAPHY**

- (1) Tröster, H. *Dyes Pigm.* **1983**, *4*, 171-7.
- (2) Holman, M. W.; Liu, R.; Adams, D. M. *Journal of the American Chemical Society* **2003**, *125*, 12649-12654.
- (3) Borch, R. F.; Bernstein, M. D.; Durst, H. D. *Journal of the American Chemical Society* **1971**, *93*, 2897-2904.
- (4) Vacus, J.; Simon, J. *Adv. Mater.* **1995**, *7*, 797-800.
- (5) Nemoto, H.; Cai, J.; Iwamoto, S.; Yamamoto, Y. *Journal of Medicinal Chemistry* **1995**, *38*, 1673-1678.
- (6) Kratzat, K.; Finkelmann, H. *Liq. Cryst.* **1993**, *13*, 691-9.
- (7) Gürek, A. G.; Durmus, M.; Ahsen, V. *New J. Chem.* **2004**, *28*, 693-699.
- (8) Gürek, A. G.; Ahsen, V.; Heinemann, F.; Zugenmaier, P. *Mol. Cryst. Liq. Cryst. Sci.* **2000**, *338*, 75-97.
- (9) Wescott, L. D.; Mattern, D. L. *The Journal of Organic Chemistry* **2003**, *68*, 10058-10066.
- (10) Kaiser, H.; Lindner, J.; Langhals, H. *Chem. Ber.* **1991**, *124*, 529-35.
- (11) Langhals, H.; Saulich, S. *Chem. Eur. J.* **2002**, *8*, 5630-5643.

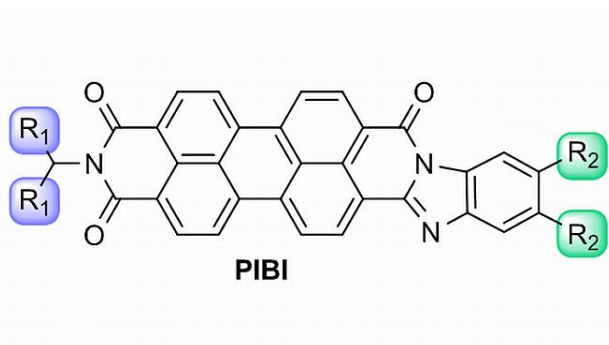
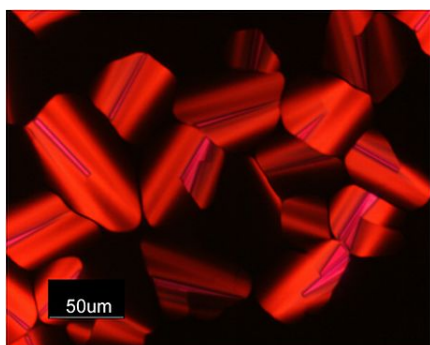
This information is available free of charge via the Internet at <http://pubs.acs.org/>.



#### 4. SYNTHESIS AND STRUCTURE ELUCIDATION OF DISCOTIC LIQUID CRYSTALLINE PERYLENE IMIDE BENZIMIDAZOLE

André Wicklein,<sup>a</sup> Peter Kohn,<sup>b</sup> Lilit Ghazaryan,<sup>b</sup> Thomas Thurn-Albrecht<sup>\*b</sup> and Mukundan Thelakkat<sup>\*a</sup>

- [a] Universität Bayreuth, Makromolekulare Chemie I – Applied Functional Polymers, Universitätsstr. 30, 95440 Bayreuth, Germany. Fax: +49 921 553206; Tel: +49 921 553108; E-mail: mukundan.thelakkat@uni-bayreuth.de
- [b] Martin-Luther-Universität Halle-Wittenberg, Institut für Physik, 06099 Halle (Saale), Germany. Fax: +49 345 5527351; Tel: +49 345 5525340; E-mail: thomas.thurn-albrecht@physik.uni-halle.de



Published in *Chemical Communications*, **2010**, 46, 2328-2330.

**We report the synthesis of a soluble perylene imide benzimidazole (PIBI) and its structural, thermotropic, optical and electrochemical characterization with emphasis on discotic liquid crystalline properties.**

Discotic molecules consisting of an aromatic core and flexible side-chains have proven to be very promising, solution processible materials for organic semiconductor applications like light emitting diodes<sup>1</sup>, field effect transistors<sup>2</sup> or photovoltaic devices<sup>3</sup>. The self-assembly of these molecules into columnar superstructures<sup>4-6</sup> with uniaxial conducting properties along the  $\pi$ - $\pi$  stacking axis provides the high charge carrier mobility which is necessary in molecular electronics<sup>7-9</sup>. However, most of the discotic semiconductor materials are good hole transport materials (p-type), and only a limited number of good electron transport materials (n-type) has been reported.<sup>10-12</sup> Discotic mesogens derived from perylene bisimides<sup>13, 14</sup> (PBI) and related molecules have gained importance in view of their favorable absorption properties and of their high electron affinity making them highly attractive as n-type semiconductors. Very recently we reported a series of highly soluble discotic liquid crystalline PBIs carrying swallow-tail substituents.<sup>15</sup> On the other hand, it is interesting to note that perylene bisbenzimidazoles, which are excellent electron transport<sup>16</sup> and charge generation materials<sup>17</sup> with an advantage of extended absorption, are highly insoluble and therefore have limited access for solution processing. Recently an intermediate class between bisimide and bisbenzimidazole - perylene imide benzimidazole (PIBI) - has been reported.<sup>18</sup> Taking these facts into account, we decided to design new soluble discotic molecules based on the PIBI structure.

Here, we describe the synthesis of an asymmetric perylene imide benzimidazole **PIBI** (Fig. 1c) with an imidazole unit at 3,4 positions and an imide moiety at 9,10 positions of the perylene core. We attached an alkyl swallow-tail substituent at the imide nitrogen atom and two long alkyl chains at the benzimidazole unit in order to guarantee sufficient solubility of the mesogen. This molecule self-assembles into columnar structures and has an extended absorption range as compared to conventional perylene bisimides.

The synthesis of **PIBI** is carried out by partial hydrolysis of symmetrically *N*-substituted perylene bisimide **PBI-1** with potassium hydroxide in *tert*-butyl alcohol allowing access to imide-anhydride **1** (Scheme 1). The benzimidazole moiety was subsequently introduced by condensation of 1,2-diaminophenyl **2** (see ESI<sup>+</sup>) with anhydride **1** in molten imidazole using zinc acetate to afford highly soluble **PIBI** with a 68 % yield. A perylene bisimide **PBI-2** (Fig. 1c) (for synthetic details see ESI<sup>+</sup>), carrying one swallow-tail substituent as in **PIBI** and with an unsymmetrical substitution pattern was synthesized for the purpose of comparison of optical and electronic properties of the PBI and PIBI derivatives.

The UV-vis absorption and fluorescence spectra of **PIBI** and **PBI-2** are shown in Fig. 1a. Compared to perylene bisimides, the introduction of the fused benzimidazole unit on the perylene core significantly extends the absorption of **PIBI** to longer wavelengths up to 650 nm, with a bathochromic shift in the absorption maximum to 556 nm. At 556 nm, **PIBI** exhibits a very

high molar extinction coefficient;  $\epsilon = 4.8 \cdot 10^4 \text{ L} \cdot \text{mol}^{-1} \cdot \text{cm}^{-1}$ . Thus the additional absorption range of 100 nm can be used for efficient light-harvesting in the visible range in photovoltaic devices. As expected the fluorescence maximum is also red-shifted and compared to **PBI-2**, **PIBI** exhibits a higher Stokes-shift.

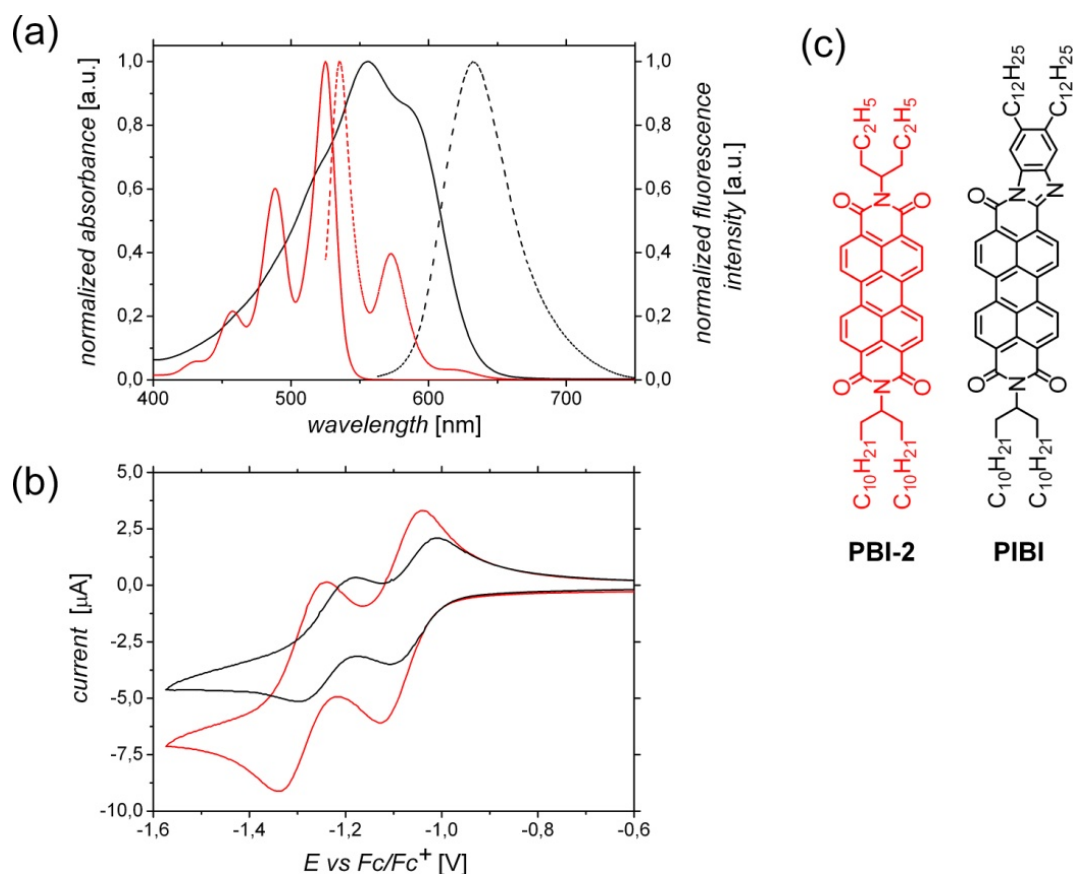
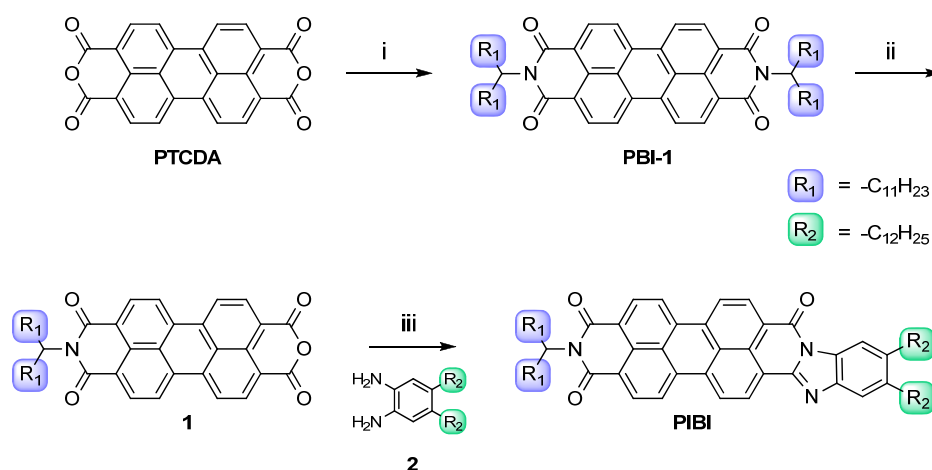


**Fig. 1** (a) Normalized UV-vis absorption spectra of **PIBI** (black bold) and **PBI-2** (red bold) in  $\text{CHCl}_3$  ( $10^{-5} \text{ M}$ ). Corresponding fluorescence spectra of **PIBI** (black dashed) and **PBI-2** (red dashed). (b) Cyclic voltammograms of **PIBI** (black) and **PBI-2** (red), showing the first and second reduction peaks. (c) Molecular structures of perylene imide benzimidazole **PIBI** and reference perylene bisimide **PBI-2**.



**Scheme 1** Synthesis of asymmetric perylene imide benzimidazole **PIBI**. Reagents and conditions: (i) 1-undecyl-dodecylamine,  $\text{Zn}(\text{OAc})_2$ , imidazole, 140 °C, 2 h; (ii)  $\text{KOH}$ ,  $\text{tert-BuOH}$ , 90 °C, 1 h; (iii) **2**, imidazole, 180 °C, 18 h.

In order to elucidate the electronic energy levels which determine the energy and electron transfer processes, and the reversibility of redox processes, cyclic voltammetry (CV) measurements were performed. Both **PIBI** and **PBI-2** exhibit two reversible reduction peaks (Fig. 1b). However, oxidation peaks were not observed in the measurement window up to +1 V vs.  $\text{Ag}/\text{AgNO}_3$ . In order to calculate the LUMO levels, the first reduction potentials were calibrated with respect to ferrocene–ferrocenium couple  $\text{Fc}/\text{Fc}^+$ , which has a quasi-calculated HOMO-energy level of 4.8 eV.<sup>19</sup> Thus, LUMO values of 3.74 and 3.71 eV were determined for **PIBI** and **PBI-2** respectively. The HOMO levels were estimated from the optical band gap and the respective LUMO values. The respective optical band gaps, 1.95 and 2.29 eV, were determined from the absorption edges (550 and 650 nm) of absorption spectra of diluted solutions. Thus, **PIBI** exhibits a HOMO value of 5.69 eV, whereas **PBI-2** has a HOMO of 6.00 eV. The extension of the  $\pi$ -conjugation system between the perylene core and the benzimidazole unit, accounts for the narrowing of the HOMO–LUMO gap for the **PIBI** dye. Moreover, the lowering of band-gap in **PIBI** is mainly caused by a shift in HOMO-value.

**PIBI** is highly thermally stable as shown by the high decomposition temperature (> 340 °C) in thermo-gravimetric analysis (TGA; see ESI<sup>†</sup>). Thermotropic behaviour of **PIBI** was investigated by a combination of differential scanning calorimetry (DSC) and polarization optical microscopy (POM). Additionally temperature-dependent small and wide angle X-ray scattering (SAXS and WAXS) experiments were performed to determine the structure on a microscopic level.

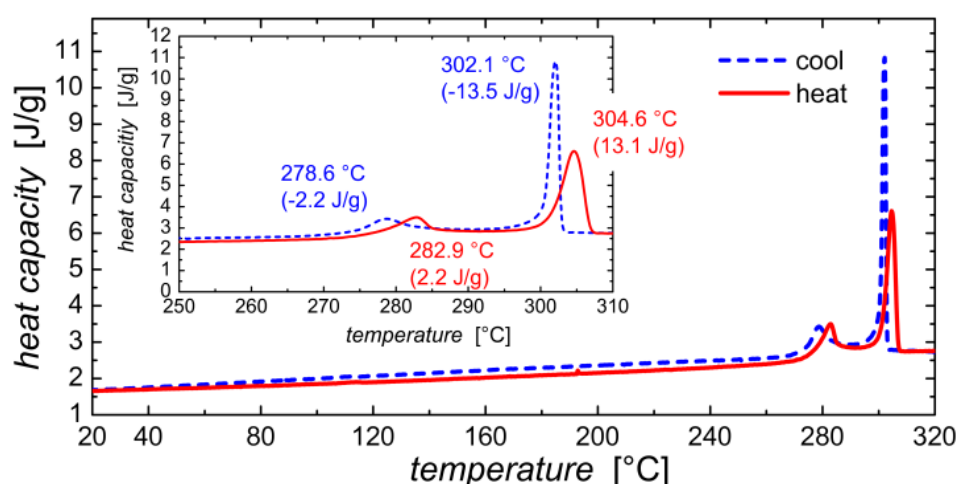


**Fig. 2** DSC thermograms of **PIBI** at a rate of  $10 \text{ Kmin}^{-1}$  showing the second heating and first cooling cycle. An enlarged view of the traces around the transitions is shown in the inset with the respective peak temperatures and the transition enthalpies ( $M = 1122.7 \text{ g/mol}$ ).

The DSC heating and cooling curves in Fig. 2 show two reversible transitions. In the heating cycle these are at  $282.9 \text{ }^\circ\text{C}$  ( $2.45 \text{ kJ mol}^{-1}$ ) and  $304.6 \text{ }^\circ\text{C}$  ( $14.68 \text{ kJ mol}^{-1}$ ). POM-experiments upon cooling from the isotropic melt (Fig. 3), gave evidence for a columnar hexagonal ( $\text{Col}_h$ ) ordering in the temperature range between  $302$  to  $280 \text{ }^\circ\text{C}$ . Here typical dendritic growth aggregates (Fig. 3a) or mosaic textures with straight linear defects (Fig. 3b) were observed. For the second phase transition at  $280 \text{ }^\circ\text{C}$ , only small textural changes are observed in POM (see ESI<sup>+</sup>). As comparison, the reference compound **PBI-2** is a crystalline material (see ESI<sup>+</sup> for DSC and POM).

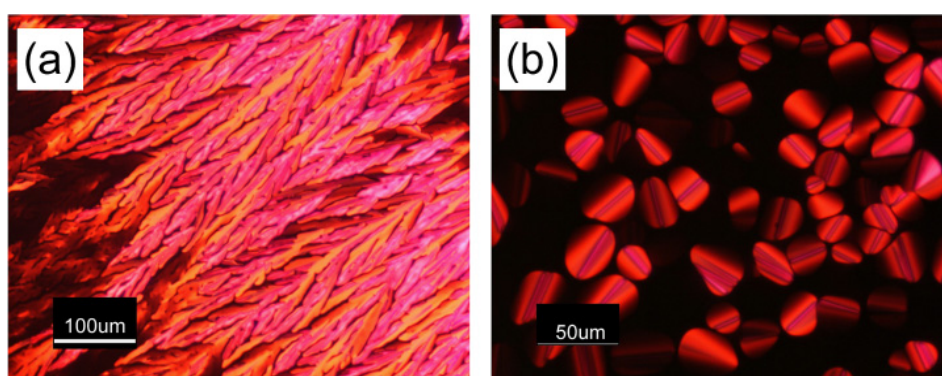


**Fig. 3** Optical microscopic images at  $302 \text{ }^\circ\text{C}$  (under crossed polarizers) of **PIBI**: (a) dendritic texture upon fast cooling and (b) mosaic texture with straight linear defects on slow cooling from isotropic melt.

To elucidate the exact mesophase structures in the observed phases below and above  $280 \text{ }^\circ\text{C}$ , temperature-dependent X-ray scattering experiments at  $20$ ,  $100$ ,  $200$ ,  $270$  and  $290 \text{ }^\circ\text{C}$  were performed. The 2-D lattice of the columnar structure can be deduced from the SAXS curves in

Fig. 4a. For example at 20 °C (red triangles), a hexagonal lattice with  $a_1 = a_2 = 3.49$  nm can be deduced (cf. Fig. 4b). The Bragg reflections are expected at positions indicated by the bars in Fig. 4a, having the typical ratios of the  $q$ -values of 1:√3:√4:√7:√9. We found reasonable agreement with the observed peaks,\* though peak 5 is somewhat broadened or split which indicates a small deviation from hexagonal symmetry. Additionally for the curves below 280 °C, a normal, positive thermal expansion coefficient was observed, *i.e.* the lattice expanded with increasing temperature as indicated by the shift of the first Bragg reflection to smaller  $q$ -values (see Fig. 4c). However, at 290 °C, the first order Bragg reflection of the hexagonal lattice was at a larger  $q$ -value. Such a behaviour is *e.g.* known for the transition from a columnar ordered (but non-crystalline) to a columnar disordered phase.<sup>20-22</sup> Concomitantly, the higher order reflections were absent at 290 °C. However, the widths of the first-order peak in both phases are comparable. Therefore, we conclude that the higher order peaks at 290 °C are weakened by a Debye-Waller factor caused by positional fluctuations of the cores perpendicular to the column axis and bending of the cylinders. This scenario is in line with a columnar disordered (Col<sub>hd</sub>) packing of the molecules above 280 °C. To confirm the ordered and disordered stacking of the discotic mesogens, we performed WAXS measurements as shown in Fig. 4d. In the ordered phase below 280 °C (orange circles, Fig. 4d), the cores were regularly stacked as can be concluded from the narrow peak at  $q = 18.07$  nm<sup>-1</sup>, corresponding to a stacking distance of  $d_{\pi\pi} = 0.35$  nm. The much broader peak for the curve at 295 °C (blue triangles, Fig. 4d) confirmed the disordered nature of the columnar phase. The peak position corresponded to a distance of  $d_{\pi\pi} = 0.36$  nm. In the isotropic phase (315 °C) the reflection was absent. Moreover, an additional peak is observed at a higher  $q$ -value (arrow in Fig. 4d) in the phase below 280 °C. Such reflections are indicative for a 3D lattice as they correspond to mixed ( $hkl$ )-reflections with  $h$  or  $k$  and  $l$  non-zero. They generally occur in crystalline phases or columnar plastic phases.<sup>22, 23</sup> However, it is to be noted that the enthalpy for the first transition at 280 °C (Col<sub>ho</sub> → Col<sub>hd</sub>) is smaller compared to the enthalpy of the second transition at 302 °C (Col<sub>hd</sub> → iso). In general, for substances with a sequence of phases crystalline → columnar → isotropic transition, the magnitude of the enthalpies is reversed.<sup>6, 24</sup> These facts suggest that the Col<sub>ho</sub> phase is a plastic phase (Col<sub>hp</sub>)<sup>22</sup>. The small changes of the textures observed in POM upon this transition also support this assumption.

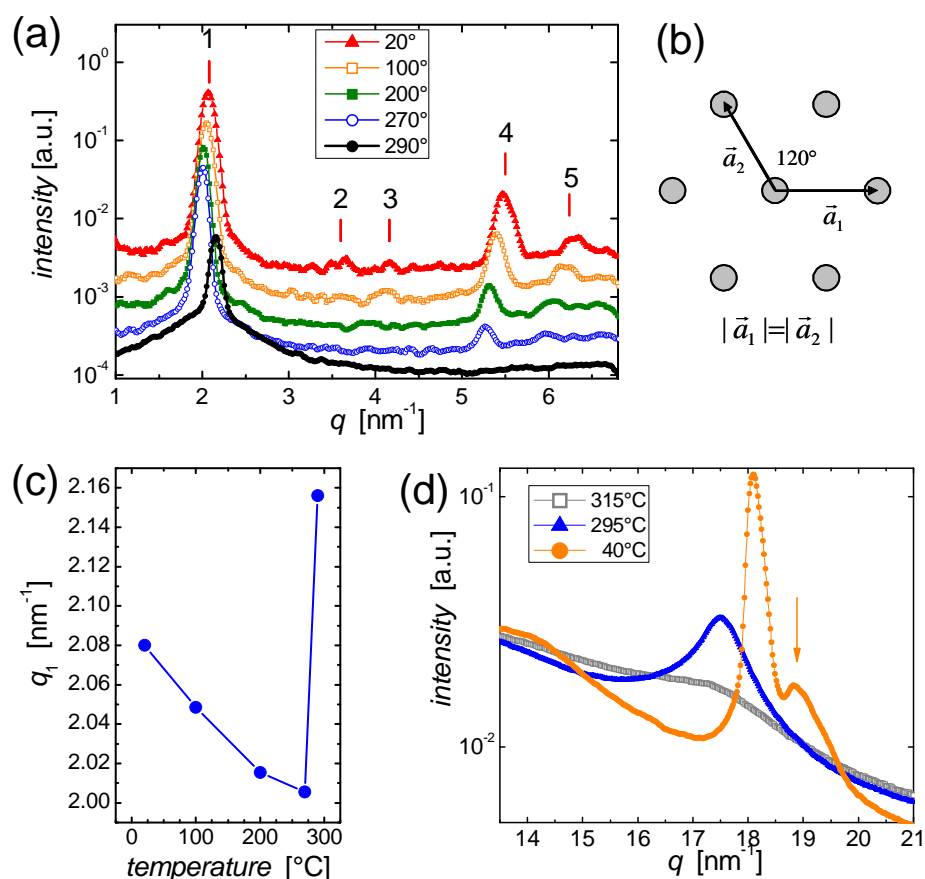


**Fig. 4** (a) Temperature dependent SAXS curves (curves are offset for clarity). (b) Scheme defining primitive lattice vectors for a two dimensional hexagonal lattice. Based on density arguments<sup>25</sup> the unit cell contains two **PIBI** molecules. (c) Temperature dependence of the  $q$ -value of the first order Bragg peak. (d) WAXS curves with the  $q$ -range corresponding to the intracolumnar stacking at three different temperatures in the phases observed by DSC.

In summary, we synthesized and performed the structural, thermotropic and optical characterization of a new discotic mesogen perylene imide benzimidazole. **PIBI** self-organizes into a hexagonal columnar liquid crystalline phase ( $\text{Col}_{\text{hd}}$ ) at high temperatures and transforms into a columnar plastic phase ( $\text{Col}_{\text{hp}}$ ) at lower temperatures. This behaviour should allow for an orientation of the material in the high temperature phase and for a transfer of the orientation during cooling to a highly ordered plastic phase at room temperature. Due to extended  $\pi$ -conjugation system compared to PBIs, the absorption of well soluble **PIBI** is significantly extended to longer wavelengths up to 650 nm. All of these properties make n-type semiconducting **PIBI** a promising candidate for applications in organic electronics.

We acknowledge the DFG (SPP1355) for financial support and the ESRF for provision of synchrotron radiation facilities and we would like to thank M. Sztucki and Dr. Narayanan for assistance in using beamline ID2.

**†Electronic Supplementary Information (ESI) available:**

Experimental details for the synthesis of PIBI, PBI-2 and additional characterization data.  
See DOI: 10.1039/b921476c

## NOTES AND REFERENCES

\*Positions  $q$  [ $\text{nm}^{-1}$ ]: ( $hk0$ )-indices of the reflections 1-5 at  $20^\circ\text{C}$ : 1:  $q_1 = 2.08$ : (010)/(100)/(1 $\bar{1}$ 0); 2:  $q_2 = 3.61$ : (110)/(2 $\bar{1}$ 0)/(1 $\bar{2}$ 0); 3:  $q_3 = 4.16$ : (200)/(020)/(2 $\bar{2}$ 0); 4:  $q_4 = 5.48$ : (120)/(210)/(1 $\bar{3}$ 0)/(3 $\bar{1}$ 0)/(2 $\bar{3}$ 0)/(3 $\bar{2}$ 0); 5:  $q_5 = 6.31$ : (300)/(030)/(3 $\bar{3}$ 0).

1. G. Lüsse and J. H. Wendorff, *Polym. Adv. Technol.*, 1998, **9**, 443-460.
2. H. E. Katz, A. J. Lovinger, J. Johnson, C. Kloc, T. Slegrist, W. Li, Y. Y. Lin and A. Dodabalapur, *Nature*, 2000, **404**, 478-481.
3. L. Schmidt-Mende, A. Fechtenkötter, K. Müllen, E. Moons, R. H. Friend and J. D. MacKenzie, *Science*, 2001, **293**, 1119-1122.
4. S. Laschat, A. Baro, N. Steinke, F. Giesselmann, C. Haegele, G. Scalia, R. Judele, E. Kapatsina, S. Sauer, A. Schreivogel and M. Tosoni, *Angew. Chem. Int. Ed.*, 2007, **46**, 4832-4887.
5. S. Kumar, *Chem. Soc. Rev.*, 2006, **35**, 83-109.
6. C. Destrade, P. Foucher, H. Gasparoux, N. H. Tinh, A. M. Levelut and J. Malthete, *Mol. Cryst. Liq. Cryst.*, 1984, **106**, 121-146.
7. P. Wojciech, Z. Matthias, C. Ji Young, M. Klaus and Z. Rudolf, *Macromol. Rapid Commun.*, 2009, **30**, 1179-1202.
8. S. Sergeev, W. Pisula and Y. H. Geerts, *Chem. Soc. Rev.*, 2007, **36**, 1902-1929.
9. D. Adam, P. Schuhmacher, J. Simmerer, L. Haussling, K. Siemensmeyer, K. H. Etzba, H. Ringsdorf and D. Haarer, *Nature*, 1994, **371**, 141-143.
10. Y.-D. Zhang, K. G. Jespersen, M. Kempe, J. A. Kornfield, S. Barlow, B. Kippelen and S. R. Marder, *Langmuir*, 2003, **19**, 6534-6536.
11. R. J. Chesterfield, J. C. McKeen, C. R. Newman, P. C. Ewbank, D. A. da Silva Filho, J.-L. Bredas, L. L. Miller, K. R. Mann and C. D. Frisbie, *J. Phys. Chem. B*, 2004, **108**, 19281-19292.
12. M. J. Sienkowska, J. M. Farrar, F. Zhang, S. Kusuma, P. A. Heiney and P. Kaszynski, *J. Mater. Chem.*, 2007, **17**, 1399-1411.
13. F. Würthner, *Chem. Commun.*, 2004, 1564-1579.
14. H. Langhals, *Helv. Chim. Acta*, 2005, **88**, 1309-1343.
15. A. Wicklein, A. Lang, M. Muth and M. Thelakkat, *J. Am. Chem. Soc.*, 2009, **131**, 14442-14453.
16. C. W. Tang, *Appl. Phys. Lett.*, 1986, **48**, 183-185.
17. Z. D. Popovic, A. Hor and R. O. Loutfy, *Chem. Phys.*, 1988, **127**, 451-457.

18. J. Y. Do, B. G. Kim, J. Y. Kwon, W. S. Shin, S.-H. Jin and Y.-I. Kim, *Macromol. Symp.*, 2007, **249-250**, 461-465.
19. J. Pommerehne, H. Vestweber, W. Guss, R. F. Mahrt, H. Bässler, M. Porsch and J. Daub, *Adv. Mater.*, 1995, **7**, 551-554.
20. E. Fontes, P. A. Heiney and W. H. De Jeu, *Phys. Rev. Lett.*, 1988, **61**, 1202-1205.
21. C. K. Lai, C.-H. Tsai and Y.-S. Pang, *J. Mater. Chem.*, 1998, **8**, 1355-1360.
22. S. K. Prasad, D. S. S. Rao, S. Chandrasekhar and S. Kumar, *Mol. Cryst. Liq. Cryst.*, 2003, **396**, 121-139.
23. B. Glösen, W. Heitz, A. Kettner and J. H. Wendorff, *Liq. Cryst.*, 1996, **20**, 627-633.
24. D. M. Collard and C. P. Lillya, *J. Am. Chem. Soc.*, 2002, **113**, 8577-8583.
25. S. Ito, M. Wehmeier, J. D. Brand, C. Kübel, R. Epsch, J. P. Rabe and K. Müllen, *Chem.-Eur. J.*, 2000, **6**, 4327-4342.

## **SUPPORTING INFORMATION**

### **Table of Contents**

#### **1. General Information**

1.1 *Characterization Methods*

1.2 *Materials*

#### **2. Synthesis and characterization of PIBI and PBI-2**

2.1 *Preparation of N,N'-di(1-dodecylundecyl)-perylene-3,4,9,10-tetracarboxylic bisimide PBI-1*

2.2 *Preparation of N-(1-dodecylundecyl)-perylene-3,4,9,10-tetracarboxylic-3,4-anhydride-9,10-imide 1*

2.3 *Preparation of N-(1-dodecylundecyl)-perylene-3,4-(4,5-didocecy-1,2-benzimidazole)-9,10-dicarboxylic imide PIBI*

2.4 *Preparation of N-(1-dodecylundecyl)-N'-(1-butylpropyl)-perylene-3,4,9,10-tetracarboxylic bisimide PBI-2*

#### **3. Additional Figures**

#### **4. References**

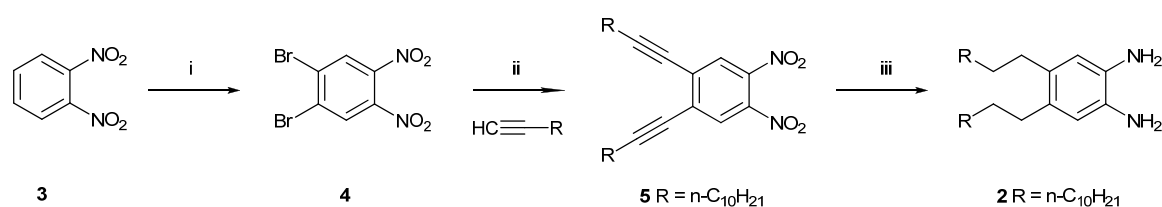
## 1. General Information

### 1.1 Characterization Methods

$^1\text{H}$ - and  $^{13}\text{C}$ -NMR spectra were recorded on a Bruker AC 300 spectrometer (300 MHz and 75 MHz, respectively). Chemical shifts are reported in ppm at room temperature using  $\text{CDCl}_3$  as solvent and tetramethylsilane as internal standard unless indicated otherwise. Abbreviations used for splitting patterns are s = singlet, d = doublet, t = triplet, q = quintet, m = multiplet. FTIR-spectra were recorded with a BIO-RAD Digilab FTS-40 (FTIR) in the range of 400-4000  $\text{cm}^{-1}$ . Oligomeric size exclusion chromatography (Oligo-SEC) measurements were performed utilizing a Waters 515-HPLC pump with stabilized THF as eluent at a flow rate of 0.5 ml/min. 20  $\mu\text{l}$  of a solution with a concentration of approx. 1 mg/ml were injected into a column setup, which consists of a guard column (Varian; 5 x 0.8 cm; mesopore gel; particle size 3  $\mu\text{m}$ ) and two separation columns (Varian; 30 x 0.8 cm; mesopore gel; particle size 3  $\mu\text{m}$ ). The compounds were monitored with a Waters 486 tuneable UV detector at 254 nm and a Waters 410 differential RI detector. Oligo-SEC was used to determine the purity of synthesized perylene bisimides. MALDI-TOF-MS spectra were obtained on a Bruker Daltonic Reflex TOF in the power reflection mode with a DCTB matrix and silver trifluoromethanesulfonate. Mass spectroscopic (MS) data were obtained from a FINNIGAN MAT 8500 instrument. UV/Vis spectra were recorded with a Perkin Elmer Lambda 900 spectrophotometer. The thermal degradation was studied using a Mettler Toledo TGA/SDTA 851<sup>e</sup> with a heating rate of 10  $\text{Kmin}^{-1}$  under  $\text{N}_2$  atmosphere. Differential scanning calorimetry (DSC) was carried out with a Perkin Elmer differential scanning calorimeter (DSC7) with heating and cooling rates of 10  $\text{K/min}$ . Phase transitions were also examined by a polarization optical microscope (POM) Nikon Diaphot 300 with a Mettler FP 90 temperature-controlled hot stage. X-ray diffraction measurements were performed on a Huber Guinier Diffraktometer 6000 equipped with a Huber quartz monochromator 611 with  $\text{Cu-K}_{\alpha 1}$ : 1.54051  $\text{\AA}$ . For cyclic voltammetry (CV) experiments, a conventional three-electrode assembly using a  $\text{Ag/AgNO}_3$  reference electrode was used.  $\text{CH}_2\text{Cl}_2$  containing 0.1 M  $\text{Bu}_4\text{NPF}_6$  was used as solvent. All measurements were carried out under  $\text{N}_2$ -atmosphere at a scan rate of 0.05  $\text{Vs}^{-1}$  at 25  $^\circ\text{C}$  and all redox potentials were calibrated to ferrocene/ferrocenium couple ( $\text{Fc/Fc}^+$ ). Temperature dependent scattering experiments in the small angle range were done in a pinhole geometry in vacuum with a setup consisting of a Rigaku rotating Cu anode, an x-ray optics device (Osram MaxFlux) and a 2D detector (Siemens High-Star). The optics focused the beam and served as a monochromator for  $\text{Cu-K}_{\alpha}$  radiation. Silverbehenate was used for the detector calibration. The sample was kept in an aluminium foil, that was put on a Linkam hotstage. After 5 minutes for temperature equilibration the intensities were recorded for 10 min. Wide angle x-ray scattering (WAXS) experiments were done at the ID2 beamline of the European Synchrotron Radiation Facility (ESRF) in Grenoble. The energy of the photons was 12.540 keV. Aluminium discs with holes with 0.8 mm diameter served as sample holders which were mounted on a Linkam hotstage flooded with nitrogen to avoid degradation. Exposure time per pattern was 0.3 seconds. *P*-bromo benzoic acid (PBBA) was used to calibrate the detector.

## 1.2 Materials

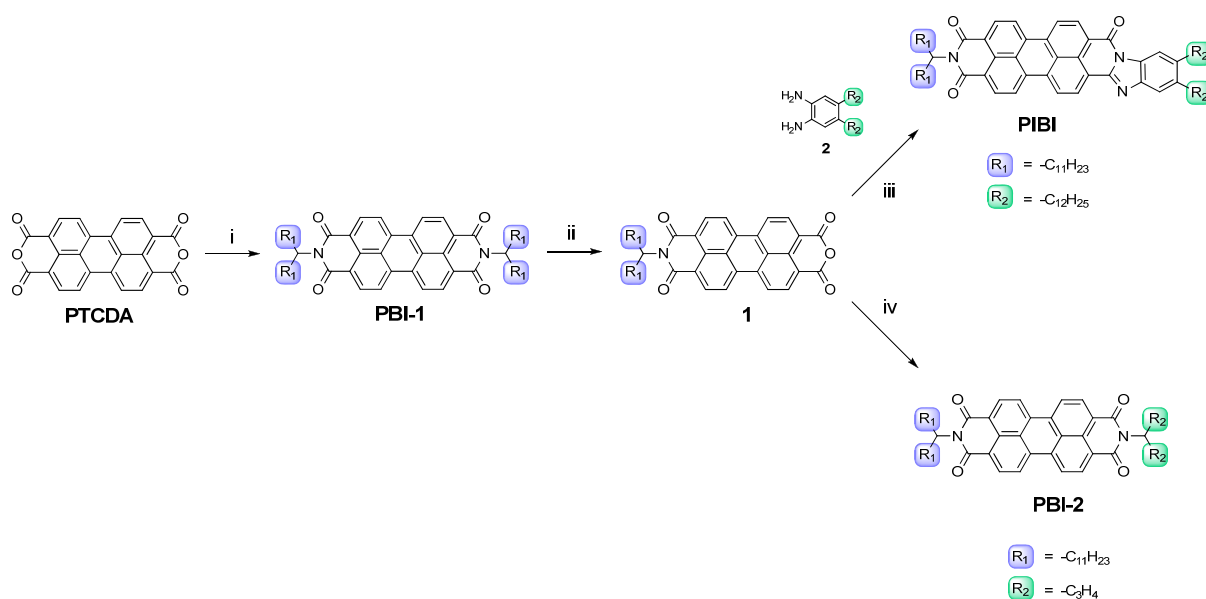
The starting materials, perylenetetracarboxylic acid dianhydride **PTCDA**, 4-heptanone, 12-tricosanone, 1,2-dinitrobenzene and solvents, were purchased from Aldrich, Fluka or TCI and used without any further purification. Solvents used for precipitation and column chromatography were distilled under normal atmosphere. Alkyl swallow-tail amines were synthesized by reductive amination of the corresponding ketones with ammonia and  $\text{NaBH}_3\text{CN}$  according to published procedures.<sup>1,2</sup> Synthesis of 4,5-dialkyl-substituted 1,2-phenylenediamine **2** was adapted from the work of Pu and coworkers.<sup>3,4</sup> Dibromination of 1,2-dinitrobenzene **3** with bromine in the presence of  $\text{Ag}_2\text{SO}_4$  and sulfuric acid gave 1,2-dibromo-4,5-dinitrobenzene **4**.<sup>5</sup> Sonogashira cross-coupling of 1,2-dibromo-4,5-dinitrobenzene with 1-dodecyne in the presence of  $\text{Pd}(\text{PPh}_3)_4/\text{CuI}$  gave **5**.<sup>6,7</sup> Catalytic hydrogenation of **5** with  $\text{Pd}(10\%)/\text{C}$  und hydrogen atmosphere gave the desired *ortho*-diamine **2** (Scheme 1).



**Scheme S1.** Preparation of alkylated aryl ortho-diamine **2**. i)  $\text{Br}_2$ ,  $\text{Ag}_2\text{SO}_4$ ,  $\text{H}_2\text{SO}_4$ ,  $155\text{ }^\circ\text{C}$ , 30 min; ii)  $\text{Pd}(\text{PPh}_3)_4$ ,  $\text{CuI}$ ,  $\text{Et}_3\text{N}$ ,  $\text{THF}$ , r.t., 4d; iii)  $\text{H}_2$ ,  $\text{Pd}(10\%)/\text{C}$ ,  $\text{MeOH}$ , r.t., 4h.

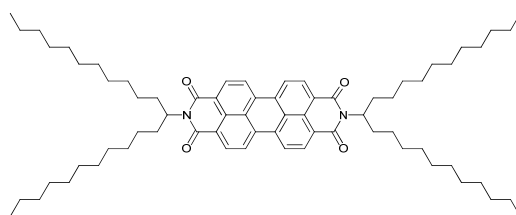
## 2. Synthesis and Characterization of PIBI and PBI-2

An overview of the respective synthetic strategy for the synthesis of asymmetric perylene imide benzimidazole **PIBI** and reference substance perylene bisimide **PBI-2** is presented in scheme 2.



**Scheme S2.** Synthesis of asymmetric perylene imide benzimidazole **PIBI** and reference perylene bisimide **PBI-2**. i) 1-undecylundecylamine,  $Zn(OAc)_2$ , imidazole, 140 °C, 2 h; ii) KOH, tert-BuOH, 90 °C, 1 h; iii) **2**, imidazole, 180 °C, 18 h; iv) 4-heptylamine,  $Zn(OAc)_2$ , imidazole, 140 °C, 3 h.

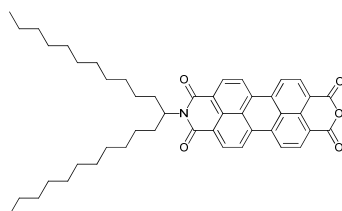
### 2.1 Preparation of N,N'-di(1-dodecylundecyl)-perylene-3,4,9,10-tetracarboxylic bisimide **PBI-1**.<sup>8,9</sup>



A mixture of perylene-3,4,9,10-tetracarboxylic dianhydride PTCDA (3.92 g, 10 mmol),  $Zn(OAc)_2$  (1.38 g, 7.5 mmol), imidazole (40 g) and 12-dodecylundecylamine (10.19 g, 30.0 mmol) was vigorously stirred at 160 °C for 2 h. After cooling to r.t. the mixture was dissolved in minimum amount of THF and precipitated in 2000 mL 2N HCl/MeOH 2:1 v/v. The orange precipitate was collected by filtration, washed with  $H_2O$  followed by MeOH, dried at 80 °C in vacuum and further purified by silica flash-column chromatography with  $CHCl_3$ . The final product was freeze-dried from benzene and was obtained as orange solid (9.76 g, 94.3 %). M.p. 76.8 °C. EI-MS (70 eV):  $m/z$

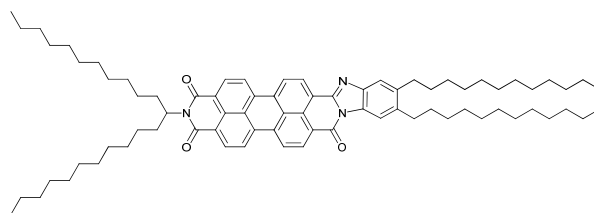
1033.8 [ $M^+$ , 76.14 %]. IR (ATR):  $\nu = 2952$  m, 2919 s, 2849 s, 1694 s, 1650 s, 1592 s, 1577 m, 1507 w, 1466 m, 1434 w, 1405 m, 1335 s, 1273 w, 1252 s, 1211 w, 1194 w, 1175 w, 1156 w, 1125 w, 1100 w, 959 w, 866 w, 856 w, 844 w, 813 s, 796 w, 773 w, 750 s, 721 m  $\text{cm}^{-1}$ .  $^1\text{H-NMR}$  (300 MHz,  $\text{CDCl}_3$ , 298K):  $\delta = 0.83$  (t,  $J = 6.8$  Hz, 12H, 4CH<sub>3</sub>), 1.01-1.44 (m, 72H, 36CH<sub>2</sub>), 1.76-1.96 (m, 4H, 2 $\alpha$ CH<sub>2</sub>), 2.15-2.34 (m, 4H, 2 $\alpha$ CH<sub>2</sub>), 5.09-5.26 (m, 2H, N-CH), 8.52-8.76 (m, 8H, 8ArH) ppm.  $^{13}\text{C-NMR}$  (75 MHz,  $\text{CDCl}_3$ , 298K):  $\delta = 14.43$  (4C, CH<sub>3</sub>), 23.00, 27.30, 29.66, 29.88, 29.92, 29.94, 29.95, 32.24, 32.70 (36C, CH<sub>2</sub>), 55.11 (2C, N-CH), 123.32, 131.45, 132.21, 123.54, 124.30, 126.76, 129.92, 134.80 (20C, C<sub>Ar</sub>), 163.90, 164.97 (4C, CONR) ppm.

## 2.2 Preparation of N-(1-dodecylundecyl)-perylene-3,4,9,10-tetracarboxylic-3,4-anhydride-9,10-imide **1**:<sup>8,9</sup>



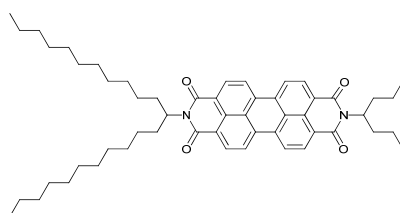
To a mixture of *N,N'*-di(1-dodecylundecyl)-perylene-3,4,9,10-tetracarboxylic bisimide **PBI-1** (6.22 g, 6.0 mmol) and *t*-BuOH (150 mL) was added 85% KOH powder (1.98 g, 30.0 mmol). The resulting mixture was refluxed for 90 °C and the conversion was monitored via TLC ( $\text{CHCl}_3/\text{AcOH}$  10:1 v/v). After complete disappearance of the bisimide (1 – 1.5 h), the mixture was poured slowly with stirring into AcOH (150 mL) and stirred for 2 h. Then 2N HCl (60 mL) was added and stirring was continued for additional 30 min. The resulting precipitate was collected by filtration, washed with water until the washings were neutral and dried at 80 °C in vacuum. The crude product was further purified by column chromatography on silica gel with  $\text{CHCl}_3$  to remove bisimide and then with  $\text{CHCl}_3/\text{AcOH}$  10:1 v/v to elute **1**. Compound **1** was freeze-dried from benzene and was obtained as red solid (3.06 g, 71.4 %).  $^1\text{H-NMR}$  (300 MHz,  $\text{CDCl}_3$ , 298K):  $\delta = 0.84$  (t,  $J = 6.8$  Hz, 6H, 2CH<sub>3</sub>), 1.10-1.38 (m, 36H, 18CH<sub>2</sub>), 1.76-1.96 (m, 2H,  $\alpha$ CH<sub>2</sub>), 2.14-2.34 (m, 2H,  $\alpha$ CH<sub>2</sub>), 5.09-5.26 (m, 1H, N-CH), 8.57-8.82 (m, 8H, 8ArH) ppm.

### 2.3 Preparation of N-(1-dodecylundecyl)-perylene-3,4-(4,5-didoceyl-1,2-benzimidazole)-9,10-dicarboxylic imide PIBI:



A mixture of *N*-(1-dodecylundecyl)-3,4,9,10-perylenecarboxylic-3,4-anhydride-9,10-imide **1** (360 mg, 0.5 mmol) and 1,2-diamino-4,5-dodecylbenzene **2** (400 mg, 1.8 mmol) in imidazole (3.75 g, 55 mmol) was stirred for 18 h at 180 °C under argon atmosphere. After cooling to r.t. the mixture was dissolved in minimum amount of THF and precipitated in 300 mL 1.5 N HCl/MeOH 2:1 v/v. After standing over night, the precipitate was collected by filtration, washed with H<sub>2</sub>O, then EtOH and dried at 60 °C in vacuum. The crude product was further purified by column chromatography on silica flash-gel with THF/*n*-hexane as eluent. The final product was freeze-dried from benzene and was obtained as dark purple solid (384 mg, 68 %). M.p. 304.6 °C. EI-MS (MALDI-TOF MS): *m/z* 1122.03. IR (ATR):  $\nu = 2956$  w, 2921 s, 2852 s, 1692 s, 1655 s, 1593 m, 1575 w, 1545 w, 1504 w, 1455 m, 1422 w, 1396 m, 1354 s, 1342 s, 1314 m, 1246 m, 1207 w, 1164 w, 1121 w, 973 w, 881 w, 846 m, 823 w, 806 s, 740 s, 720 m cm<sup>-1</sup>. <sup>1</sup>H-NMR (300 MHz, CDCl<sub>3</sub>, 298K):  $\delta = 0.84$  (t, *J* = 6.7 Hz, 6H, 2CH<sub>3</sub>), 0.88 (t, *J* = 6.3 Hz, 6H, 2CH<sub>3</sub>), 1.08-1.50 (m, 72H, 36CH<sub>2</sub>), 1.57-1.73 (m, 4H, 2CH<sub>2</sub>), 1.80-1.99 (m, 2H,  $\alpha$ CH<sub>2</sub>), 2.16-2.36 (m, 2H,  $\alpha$ CH<sub>2</sub>), 2.58-2.74 (m, 4H, 2CH<sub>2</sub>), 5.12-5.28 (m, 1H, N-CH), 7.51 (s, 1H, ArH), 8.14 (s, 1H, ArH), 8.45-8.76 (m, 8H, 8ArH). <sup>13</sup>C-NMR (75 MHz, CDCl<sub>3</sub>, 298K):  $\delta = 14.45$  (2C, CH<sub>3</sub>), 14.49 (2C, CH<sub>3</sub>), 23.02, 23.07, 27.49, 29.70, 29.76, 30.01, 30.03, 30.06, 30.10, 30.12, 30.32, 31.12, 31.52, 32.27, 32.31, 32.80, 33.20, 33.67, (42C, CH<sub>2</sub>), 55.09 (1C, N-CH), 115.30, 119.59, 121.72, 122.62, 123.11, 123.18, 123.68, 123.81, 126.07, 126.82, 126.90, 127.91, 129.65, 130.04, 131.47, 132.15, 134.21, 134.67, 135.55, 139.43, 139.98, 142.40, 147.58, 159.35 (30 C, C<sub>Ar</sub>) ppm.

### 2.4 Preparation of N-(1-dodecylundecyl)-N'-(1-butylpropyl)-perylene-3,4,9,10-tetracarboxylic bisimide PBI-2:



A mixture of *N*-(1-dodecylundecyl)-perylene-3,4,9,10-tetracarboxylic-3,4-anhydride-9,10-imide **1** (930 mg, 1.3 mmol), Zn(OAc)<sub>2</sub> (356 mg, 1.95 mmol) and 4-heptylamine (300 mg, 2.6 mmol) in dry DMAc (15.0 mL) was stirred in a microwave pressure reactor for 20 Min at 150 °C and

250 Watt. After cooling to r.t. the mixture was dissolved in minimum amount of THF and precipitated in 300 mL 2N HCl/MeOH 2:1 v/v. After standing over night, the precipitate was collected by filtration, washed with H<sub>2</sub>O, then MeOH and dried at 60 °C in vacuum. The crude product was further purified by column chromatography on silica flash-gel with CHCl<sub>3</sub>/petrolether 4:1 v/v. **PBI-2** was freeze-dried from benzene and was obtained as red solid (635 mg, 60.2 %). M.p. 164.6 °C. EI-MS (70 eV): *m/z* 811.2 [M<sup>+</sup>, 58.1 %]. IR (ATR):  $\nu$  = 2956 w, 2922 s, 2853 m, 1696 s, 1650 s, 1594 s, 1577 m, 1506 w, 1465 w, 1444 w, 1495 m, 1336 s, 1250 m, 1209 w, 1191 w, 1175 w, 1123 w, 1096 w, 964 w, 849 w, 809 s, 795 w, 746 s cm<sup>-1</sup>. <sup>1</sup>H-NMR (300 MHz, CDCl<sub>3</sub>, 298K):  $\delta$  = 0.83 (t, *J* = 6.8 Hz, 6H, 2CH<sub>3</sub>), 0.93 (t, *J* = 7.4 Hz, 6H, 2CH<sub>3</sub>), 1.09-1.42 (m, 20H, 10CH<sub>2</sub>), 1.74-1.94 (m, 4H, 2 $\alpha$ CH<sub>2</sub>), 2.15-2.37 (m, 4H, 2 $\alpha$ CH<sub>2</sub>), 5.10-5.32 (m, 2H, N-CH), 8.54-8.76 (m, 8H, 8ArH) ppm. <sup>13</sup>C-NMR (75 MHz, CDCl<sub>3</sub>, 298K):  $\delta$  = 14.41, 14.48 (4C, CH<sub>3</sub>), 20.54, 23.04, 27.35, 29.71, 29.93, 29.97, 29.98, 32.28, 32.74. 34.88 (24C, CH<sub>2</sub>), 54.57, 55.14 (2C, N-CH), 123.34, 131.44, 132.22, 126.73, 129.92, 134.80 (20C, C<sub>Ar</sub>), 163.86, 164.90 (4C, CONR) ppm.

### 3. Additional Figures

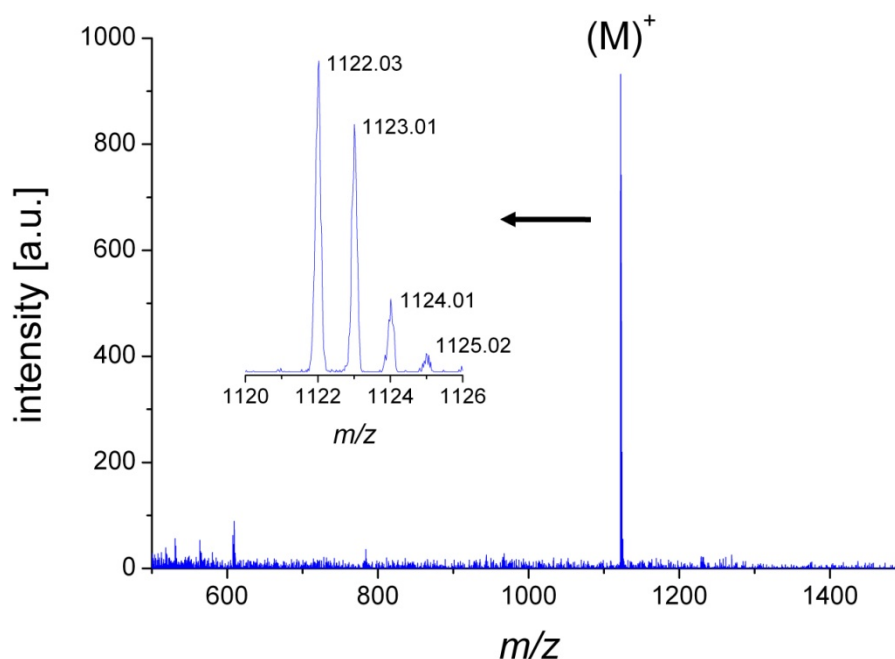


**Figure S1.** MALDI-TOF MS spectra of **PBI**.

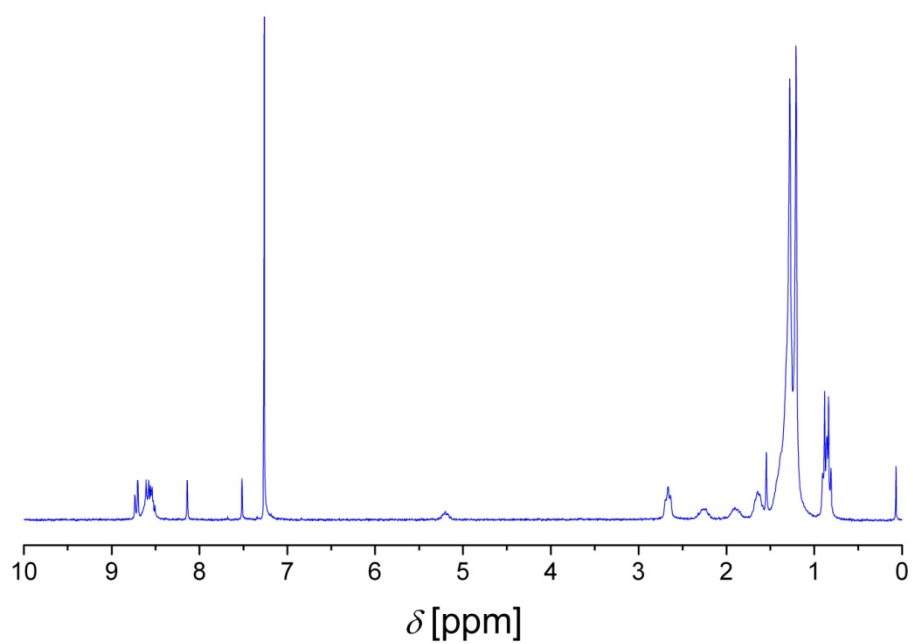


**Figure S2.**  $^1\text{H-NMR}$  (300 MHz,  $\text{CDCl}_3$ , 298K) of **PIBI**.

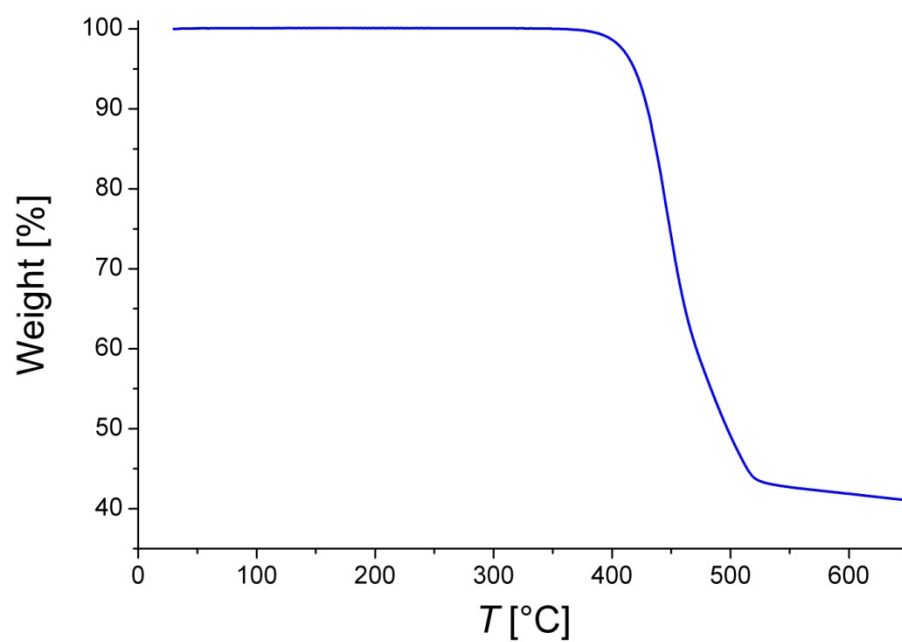


**Figure S3.** TGA curve of **PIBI**. The onset of **PIBI** decomposition is at  $T_{\text{dec}} = 341$  °C.

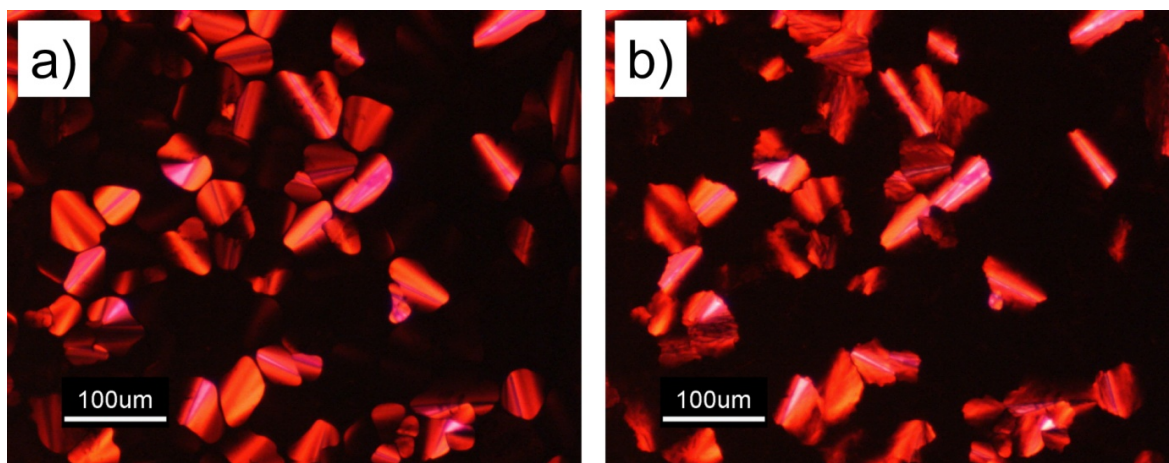


**Figure S4.** Optical microscopic images (under crossed polarizers) of PIBI formed upon cooling from the isotropic melt at 2.5 K/min cooling rate: (a) mosaic texture with straight linear defects of hexagonal columnar mesophase ( $Col_h$ ) at 300 °C (b) transition to hexagonal columnar plastic phase ( $Col_{hp}$ ) at 275 °C.

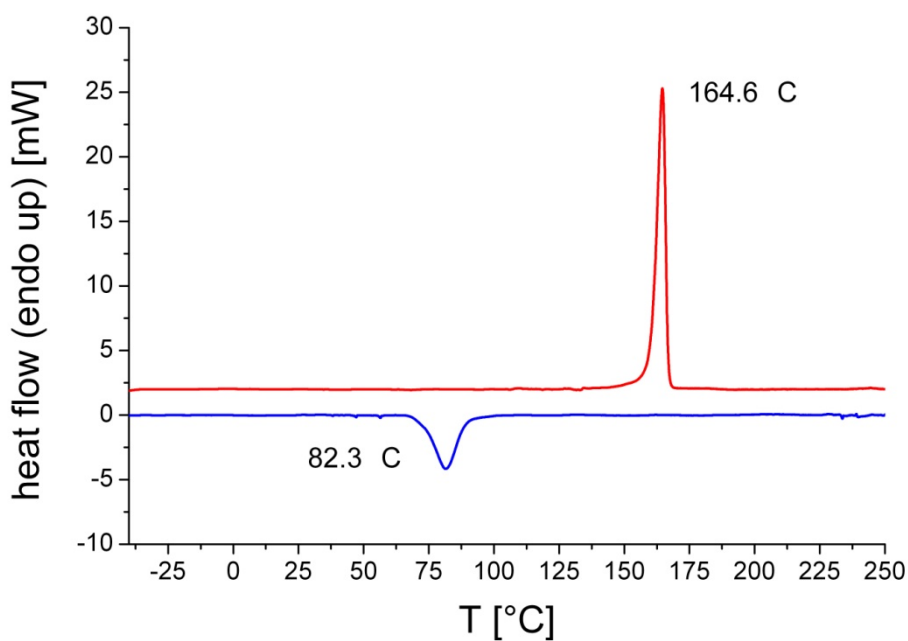


**Figure S5.** DSC thermograms of reference **PBI-2** (scanning rate 10 Kmin<sup>-1</sup>) showing the second heating (red curve) and first cooling cycle (blue curve) with respective phase transition temperatures.

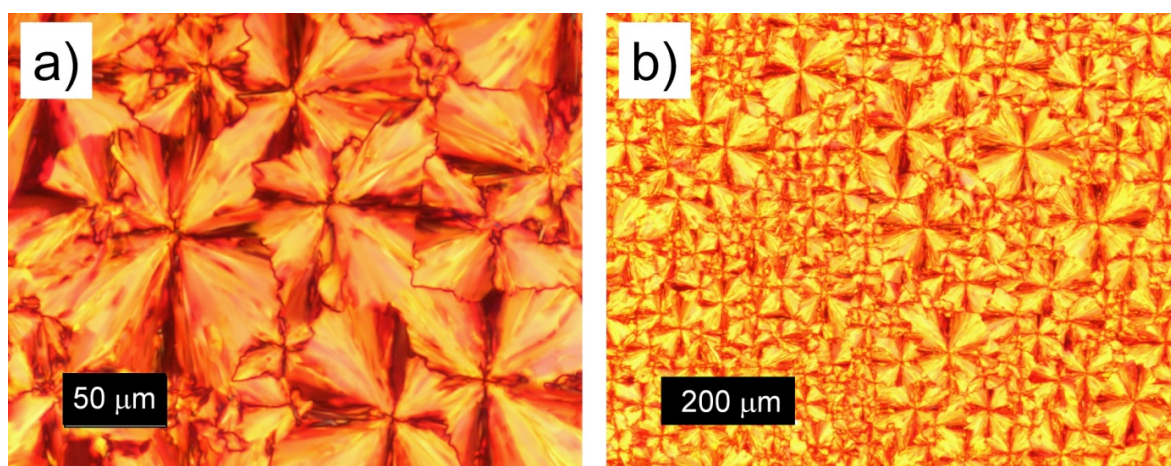


**Figure S6.** Optical microscopic images (under crossed polarizers) of **PBI-2** formed upon cooling from isotropic melt (a) and (b) spherulitic crystallites formed at 80 °C.

### 3. **BIBLIOGRAPHY**

1. R. F. Borch, M. D. Bernstein and H. D. Durst, *J. Am. Chem. Soc.*, 1971, **93**, 2897-2904.
2. M. W. Holman, R. Liu and D. M. Adams, *J. Am. Chem. Soc.*, 2003, **125**, 12649-12654.
3. F. Zhang, S. Bai, G. P. A. Yap, V. Tarwade and J. M. Fox, *J. Am. Chem. Soc.*, 2005, **127**, 10590-10599.
4. H.-C. Zhang, W.-S. Huang and L. Pu, *J. Org. Chem.*, 2001, **66**, 481-487.
5. L. Ma, Q.-S. Hu, D. Vitharana, C. Wu, C. M. S. Kwan and L. Pu, *Macromolecules*, 1997, **30**, 204-218.
6. K. Sonogashira, Y. Tohda and N. Hagihara, *Tetrahedron Lett.*, 1975, **16**, 4467-4470.
7. Y. Tohda, K. Sonogashira and N. Hagihara, *Synthesis*, 1977, 777-778.
8. H. Kaiser, J. Lindner and H. Langhals, *Chem. Ber.*, 1991, **124**, 529-535.
9. L. D. Wescott and D. L. Mattern, *J. Org. Chem.*, 2003, **68**, 10058-10066.

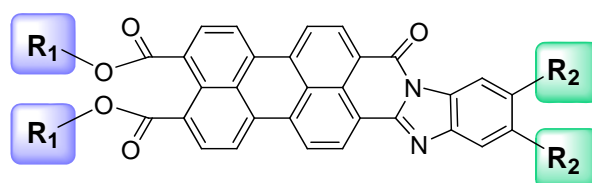
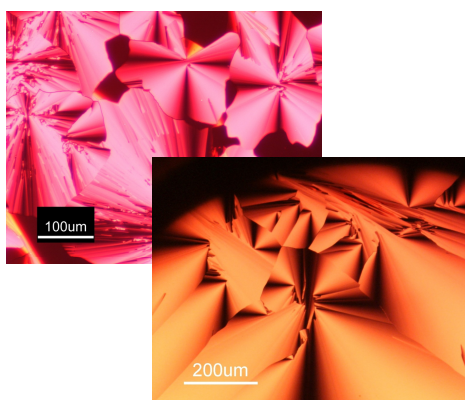


## 5. ROOM TEMPERATURE LIQUID CRYSTALLINE PERYLENE DIESTER BENZIMIDAZOLES WITH EXTENDED ABSORPTION

André Wicklein, Andreas Lang, Mathis Muth and Mukundan Thelakkat\*

Department of Macromolecular Chemistry I, Applied Functional Polymers, Universität Bayreuth,  
Universitätsstr. 30, 95440 Bayreuth, Germany.

Fax: +49-921-55-3206; E-mail: [mukundan.thelakkat@uni-bayreuth.de](mailto:mukundan.thelakkat@uni-bayreuth.de)



Submitted.

**ABSTRACT**

The synthesis and thermotropic properties of novel asymmetrically substituted discotic molecules, perylene diester benzimidazoles (**PDBIs**), are presented. **PDBIs** were designed with an imidazole unit at 3,4 positions and a bisester moiety at 9,10 positions of the perylene tetracarboxylic acid core. By attaching linear or branched aliphatic substituents at the ester moiety and two alkyl or alkoxy substituents at the benzimidazole unit, sufficient solubility and the flexibility to obtain mesophases was guaranteed. Thermotropic behaviour, which is strongly influenced by the nature of the respective substituents at the diester and benzimidazole moiety, was investigated using differential scanning calorimetry (DSC), polarization optical microscopy (POM) and X-ray diffraction measurements (XRD). All **PDBIs** under investigation self-organize into liquid crystalline columnar hexagonal phases ( $Col_h$ ), among them **PDBI-3** even at room temperature. Also the formation of a room temperature columnar plastic phase ( $Col_{hp}$ ) and the formation of a lamellar phase was observed. Due to extension of the  $\pi$ -conjugation system, the absorption of these well soluble discogens is significantly extended to longer wavelengths in the visible regime up to 680 nm.

**Keywords:** discotic liquid crystals / n-type semiconductor / organic electronics / perylene diester / benzimidazole

## INTRODUCTION

Self-organizing organic semiconductor molecules like discotic liquid crystals (LCs)<sup>1-3</sup> have found increased interest as solution processable materials for organic semiconductor applications in areas like light emitting diodes,<sup>4</sup> field effect transistors<sup>5</sup> or photovoltaic devices.<sup>6</sup> The uniaxial conducting properties along the  $\pi$ - $\pi$  stacking axis in self-assembled columnar superstructures of disc-like molecules, consisting of a rigid aromatic core with flexible side-chains attached at the periphery of the mesogen, provide the high charge carrier mobility within the bulk phase which is decisive in organic electronics.<sup>7-9</sup> In such materials charge carrier mobilities up to 0.1 - 1.3  $\text{cm}^2 \cdot \text{V}^{-1} \cdot \text{s}^{-1}$  in their liquid crystalline mesophases have been measured.<sup>8,10-12</sup> Liquid crystalline organization also increases the local order without creating too many grain boundaries on the macroscopic level as in the case of crystalline materials. It is also desirable to have room temperature LC materials, so that devices can be processed from isotropic melt at high temperatures and the LC order can be maintained at room temperature. However, most discotic semiconductor materials are good hole transporting materials (p-type), while the number of suitable electron transporting materials (n-type) is still very limited.<sup>13-15</sup> In this context discotic mesogens derived from perylene bisimides<sup>16,17</sup> (**PBI**) and related molecules are a promising class of dyes. This is in view of their high electron affinity making them highly attractive as n-type semiconductors and their favourable absorption properties in the visible wavelength regime. Unfortunately, high solubility of **PBIs** is often gained at the expense of planarity and loss of strong  $\pi$ - $\pi$  interactions, by incorporating substituents at the bay position, which results in twisting of the perylene core. However strong  $\pi$ - $\pi$  interactions are required for intermolecular order and efficient charge carrier transport. Very recently we reported on a series of highly soluble discotic liquid crystalline **PBIs** carrying swallow-tail *N*-substituents<sup>18</sup>

Another class of liquid crystalline perylene dyes are tetraalkyl esters of perylene tetracarboxylic acid (**PTE**).<sup>19</sup> But **PTEs** absorb only in the blue region and are less electron deficient compared to **PBIs**.<sup>20</sup> Therefore it is of fundamental interest to improve the electron deficiency and extend the absorption to longer wavelength region in this class of materials. One elegant way to achieve this is to introduce a fused benzimidazole moiety to the perylene core. It was recently demonstrated for bisimides to get a new class of n-type semiconductors.<sup>21</sup> Taking these facts into account, we decided to design new soluble asymmetric molecules based on a perylene diester benzimidazole (**PDBI**) structure in which liquid crystalline organization along with an extended absorption in the red region of visible spectrum was realized. The electron affinity could also be maintained close to that of **PBI**.<sup>18</sup> A substitution at the bay positions of the perylene core was avoided in all cases in order to maintain planarity and to promote strong  $\pi$ - $\pi$  interactions.

## RESULTS AND DISCUSSION

### Synthesis

Herein, we describe the synthesis of asymmetrically substituted perylene diester benzimidazoles **PDBIs 1-3** (Fig. 1) and their structural, thermotropic, optical and electrochemical properties. **PDBIs** were designed with an imidazole unit at 3,4 positions and a bisester moiety at 9,10 positions of the perylene tetracarboxylic acid core. We attached linear or branched aliphatic substituents at the ester moiety and two alkyl or alkoxy chains at the benzimidazole unit in order to guarantee sufficient solubility and flexibility to obtain mesophases. All these molecules self-assemble into discotic columnar structures also at low temperatures and have an extended absorption range up to 680 nm.

The synthesis of **PDBIs** is carried out by partial hydrolysis of symmetrically substituted perylene tetraesters **PTEs** with  $p\text{TosOH}\cdot\text{H}_2\text{O}$  allowing access to diester-anhydrides **1a, b** (Fig. 1).<sup>22</sup> The benzimidazole moiety was subsequently introduced by condensation of 1,2-diaminophenyls **2a, b** with the respective anhydride **1a, b** in DMAc using zinc acetate under microwave irradiation conditions to afford highly soluble **PDBIs 1-3** in good yields (> 60 %). All three compounds were fully characterized by means of  $^1\text{H}$ -,  $^{13}\text{C}$ -NMR spectroscopy, IR, GPC, MS and Microanalyses after thorough purification by column chromatography (for details see Experimental Section). The details of synthesis of perylene tetraesters, diester anhydrides and aromatic *ortho*-diamines are given in ES1†.

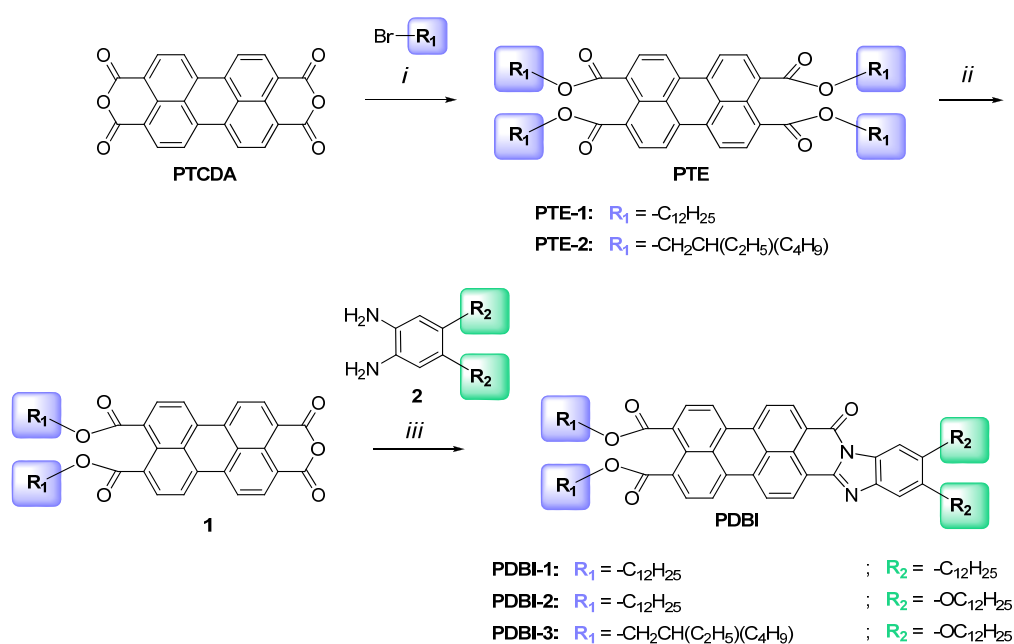


**Figure 1.** Synthesis of asymmetric perylene diester benzimidazoles **PDBIs 1-3** i) 1.  $\text{KOH}$ ,  $\text{H}_2\text{O}$ . 2.  $\text{HCl}$ , pH 8-9. 3.  $\text{R}_1\text{-Br}$ , Aliquat 336,  $\text{KI}$ ,  $100^\circ\text{C}$  ii)  $p\text{TosOH}\cdot\text{H}_2\text{O}$ ,  $n$ -dodecane/toluene (5:1),  $95^\circ\text{C}$ . iii) **2**,  $\text{Zn}(\text{OAc})_2$ , DMAc, 300 Watt,  $160^\circ\text{C}$ , 20 Min.

### Optical and electronic properties

The UV-vis absorption spectra of **PDBIs 1-3** and **PTE-1** in  $\text{CHCl}_3$  solution are presented in Figure 2. Both tetraesters **PTE-1** and **PTE-2** exhibit similar absorption spectra as perylene bisimide with characteristic vibronic bands, but with a blue shift of 54 nm ( $\lambda_{\text{max}} = 471$  nm). The incorporation of the fused benzimidazole unit significantly extends the absorption of **PDBIs 1-3** to longer wavelengths, up to 680 nm. This is almost 100 nm red-shifted compared to perylene bisimides (**PBIs**). The alkoxy substituted **PDBIs 2** and **3** exhibit a better absorption range than **PDBI-1** carrying only alkyl substituents. All derivatives possess high molar extinction coefficients ( $\epsilon$ ) in the visible range; for instance **PDBI-2**  $\epsilon = 3.32 \cdot 10^4 \text{ L} \cdot \text{mol}^{-1} \cdot \text{cm}^{-1}$  at  $\lambda_{\text{max}} = 554$  nm. Thus the extended absorption range of these dyes can be used for efficient light-harvesting in photovoltaic devices. **PDBI-2** and **3** absorb in the same wavelength regime but have different fine structures, for instance absorption maxima are located at 554 nm for **PDBI-2** and at 516 nm for **PDBI-3**. As expected the fluorescence maxima are also red-shifted and compared to **PDBI-1**, **PDBI-3** exhibits a higher Stokes-shift (see ESI<sup>†</sup>). For **PDBI-2** no fluorescence could be observed in solution.

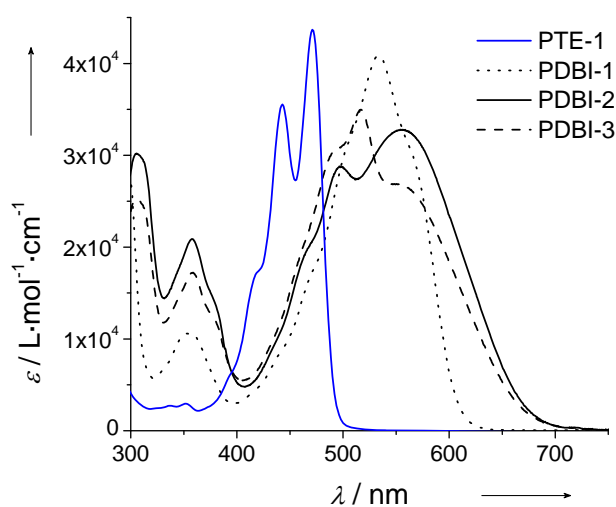


**Figure 2.** UV-vis absorption spectra of **PTE-1** and **PDBIs 1-3** measured in  $1.0 \cdot 10^{-5} \text{ M CHCl}_3$  solution. All **PDBIs** exhibit high molar extinction coefficient values in the whole range from 450 to 600 nm.

Further the electrochemical stability and reversibility of redox processes were studied using cyclic voltammetry (CV). All the compounds exhibit two reversible reduction peaks. Figure 3a shows the cyclic voltammograms of **PDBIs 1-3** and Figure 3b shows the HOMO- and LUMO-energy levels with corresponding bandgaps. In order to calculate the LUMO levels, the first reduction potentials were calibrated with respect to ferrocene–ferrocenium couple  $\text{Fc}/\text{Fc}^+$ , which has a quasi-calculated HOMO-energy level of 4.8 eV.<sup>23</sup> The HOMO levels were estimated from the optical band gap and the respective LUMO values. The respective optical band gaps, were determined from the absorption edges of absorption spectra of diluted  $\text{CHCl}_3$  solutions. The

extension of the  $\pi$ -conjugation system between the perylene core and the benzimidazole unit generally accounts for a narrowing of the HOMO–LUMO gap of the **PDBI** dyes. Moreover, the lowering of band-gap in **PDBIs** is mainly caused by a positive shift in HOMO-value rather than a negative shift in LUMO values. For **PDBIs 2** and **3**, the band-gap could further be decreased by 0.2 eV by introduction of electron-donating alkoxy substituents at the benzimidazole moiety. This is highly desired if energy loss during charge transfer from donor molecules to **PDBI** is to be minimized and can also contribute to high open-circuit voltages in photovoltaic devices using **PDBIs** as acceptors.

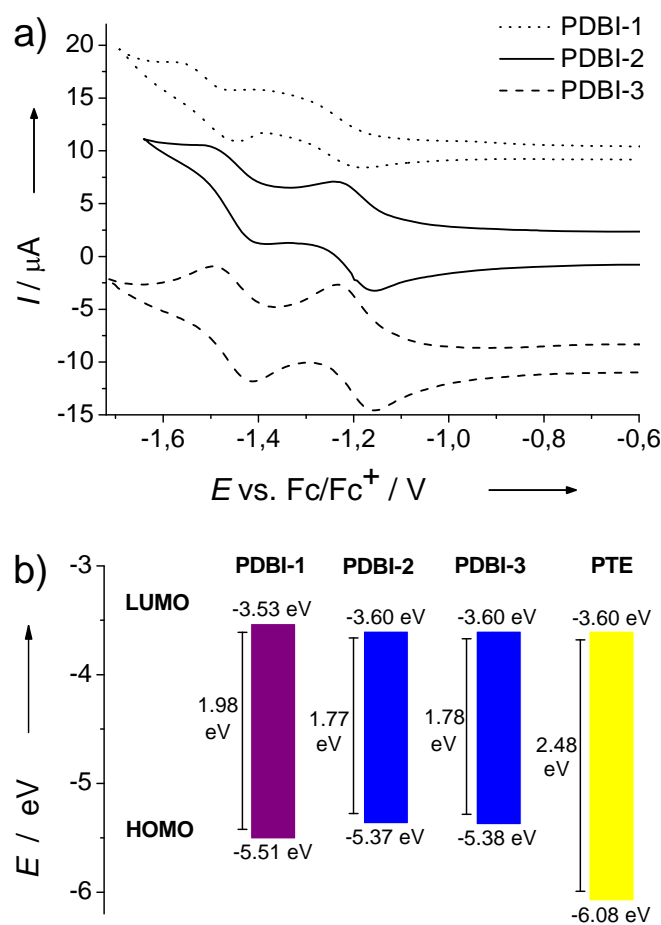


**Figure 3.** (a) Cyclic voltammograms of **PDBIs 1-3**, showing the first and second reduction peaks. The measurements were conducted in  $\text{CH}_2\text{Cl}_2$  containing 0.1 M  $\text{Bu}_4\text{NPF}_6$  with respect to ferrocene–ferrocenium couple ( $\text{Fc}/\text{Fc}^+$ ) at a scan rate of  $50 \text{ mVs}^{-1}$ . (b) Energy band level diagram showing HOMO- and LUMO-energy levels with corresponding bandgaps of perylene tetraester **PTE-1**<sup>24</sup> and perylene diester benzimidazoles **PDBIs 1-3**.

### Thermotropic properties

**PDBIs** are highly thermally stable as shown by the high onset decomposition temperatures ( $T_{on}$  between 303 and 319 °C) in thermogravimetric analysis (TGA; see ESI<sup>†</sup>). Thermotropic behaviour of **PDBIs** was analyzed by a combination of differential scanning calorimetry (DSC) and polarization optical microscopy (POM). Additionally temperature dependent small and wide angle X-ray scattering (SAXS and WAXS) experiments were performed to unequivocally determine the structure of the mesophases on the molecular level. All of the derivatives under investigation exhibit thermotropic liquid crystalline mesophases; two of them maintaining their liquid crystalline behavior even at room temperature. DSC thermograms of all **PDBIs** are summarized in Figure 4a and phase transition temperatures with corresponding transitions enthalpies are presented in Table 1.

**Table 1.** Summary of the thermal behaviour, phase transition temperatures with corresponding transitions enthalpies and phases<sup>[a]</sup> of investigated **PDBIs 1-3**.

<b>PDBI</b>	phase transitions <sup>[b]</sup> (T [°C] / $\Delta H$ [kJmol <sup>-1</sup> ])
<b>1</b>	Cr <sub>L</sub> (120 / 49.4) → Col <sub>h</sub> (172 / 3.9) → I I (168 / -2.4) → Col <sub>h</sub> (89 / -51.9) → Cr <sub>L</sub>
<b>2</b>	Cr (-16 / 18.8) → Col <sub>hp</sub> (165 / 2.1) → Col <sub>hd</sub> (235 / 4.5) → I I (232 / -4.6) → Col <sub>hd</sub> (160 / -2.6) → Col <sub>hp</sub> (-23 / -17.4) → Cr
<b>3</b>	Col <sub>h</sub> (183 / 1.2) → I I (168 / -1.9) → Col <sub>h</sub>

[a] Cr = crystalline phase; Cr<sub>L</sub> = crystalline lamellar phase; Col<sub>h</sub> = columnar hexagonal mesophase; Col<sub>hd</sub> = disordered columnar hexagonal mesophase; Col<sub>hp</sub> = columnar plastic phase; I = isotropic phase. [b] Obtained from DSC measurements at a heating rate of 10 Kmin<sup>-1</sup> under nitrogen atmosphere.

The DSC heating curve of **PDBI-1** shows two reversible transitions at 120 °C (49.4 kJ/mol) and 172 °C (3.9 kJ/mol). The corresponding transitions on cooling are observed at 168 °C and 89 °C (Fig. 4a). POM experiments upon cooling from the isotropic melt (Fig. 4b) gave evidence for a columnar hexagonal (Col<sub>h</sub>) ordering in the high temperature phase (ca. 120 – 172 °C). As can be seen, large focal conic textures were observed.

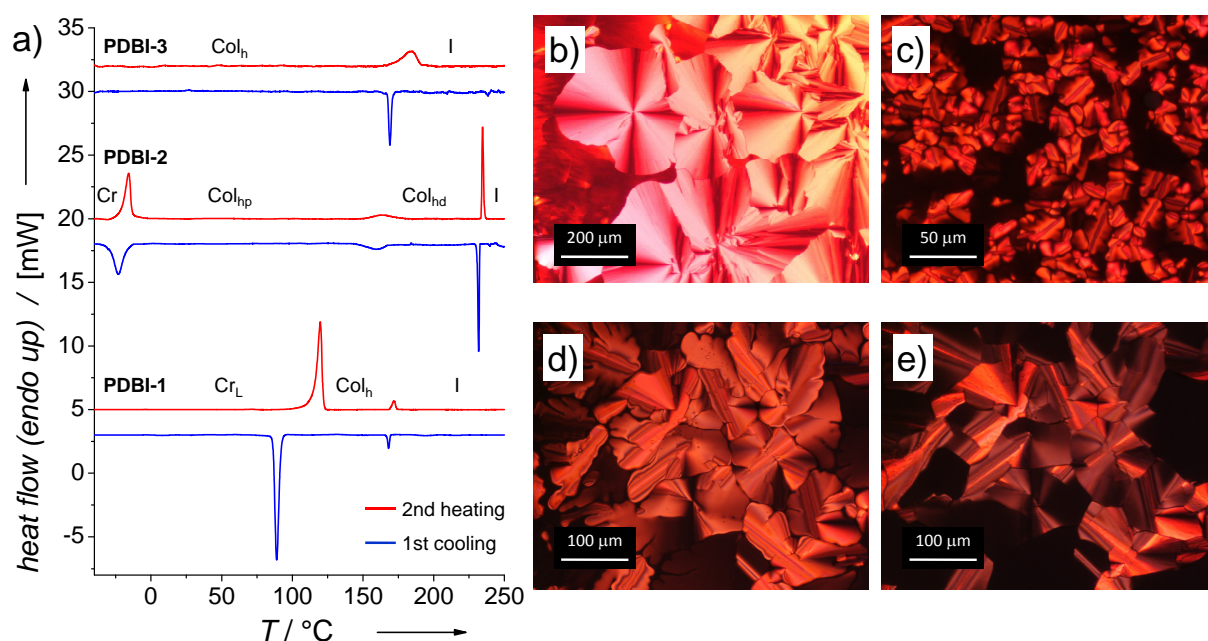


**Figure 4.** (a) DSC thermograms of **PDBIs 1-3** (scan rate  $10 \text{ Kmin}^{-1}$ ) showing the second heating (red curves) and first cooling cycle (blue curve). (b-e) Optical microscopic images of textures of **PDBIs 1-3** (under crossed polarizers). (b) Focal conic texture of  $\text{Col}_h$  phase of **PDBI-1** at  $169 \text{ }^\circ\text{C}$ . (c) Mosaic texture of  $\text{Col}_h$  phase of **PDBI-3** at  $175 \text{ }^\circ\text{C}$ . (d) Mixture of mosaic and pseudo focal conic textures representing the  $\text{Col}_h$ -phase of **PDBI-2** at  $220 \text{ }^\circ\text{C}$  and (e) same film region showing the  $\text{Col}_{hp}$  phase of **PDBI-2** at  $130 \text{ }^\circ\text{C}$ .

Also X-ray diffraction experiments are in accordance with a columnar hexagonal ordering of the mesogens. The diffractogram of **PDBI-1** in the mesophase is shown in red and at room temperature in blue colour (Fig. 5a). At  $140 \text{ }^\circ\text{C}$ , we observed a 2D hexagonal lattice with  $a_{hex} = 32.9 \text{ \AA}$  which is in reasonable agreement with the (100), (110) and (210) Bragg reflections with the typical ratios of the  $d$ -values of  $1:\sqrt{3}:\sqrt{7}$  (For details see ESI<sup>†</sup>). The relatively broad reflection at  $25.3^\circ$  in the wide angle regime depicts a moderate intracolumnar long-range order with a  $\pi$ - $\pi$  stacking distance of  $d_{\pi\pi} = 3.52 \text{ \AA}$ . Upon further cooling to  $95 \text{ }^\circ\text{C}$ , **PDBI-1** forms spherulites under crossed polarizers (see ESI<sup>†</sup>). This texture remains the same on cooling down to room temperature. X-ray diffraction experiments at RT show (001) and its corresponding higher-order reflections, up to (006) as shown in Fig. 5a (blue curve). This corresponds to one dimensional translational order<sup>25,26</sup> with a layer distance of  $41.6 \text{ \AA}$ . The  $d$ -spacings estimated from the position of Bragg reflections are exactly in the ratios  $1 : 1/2 : 1/3 : 1/4$ , etc. Thus **PDBI-1** exhibits a lamellar ordering below  $95 \text{ }^\circ\text{C}$ . Nevertheless the mixed reflexes in the wide-angle regime could not yet be assigned.

**PDBI-2** carrying alkoxy substituents at the benzimidazole moiety depicts a quite different thermotropic behaviour. Here three reversible transitions can be observed in DSC measurements, at  $-16 \text{ }^\circ\text{C}$  ( $18.8 \text{ kJ/mol}$ ),  $165 \text{ }^\circ\text{C}$  ( $2.1 \text{ kJ/mol}$ ) and  $235 \text{ }^\circ\text{C}$  ( $4.5 \text{ kJ/mol}$ ) during heating. From POM and XRD the transitions can be assigned as  $\text{Cr} \rightarrow \text{Col}_{hp} \rightarrow \text{Col}_{hd}$ . Thus compared to **PDBI-1**, **PDBI-2** exhibits additionally a transition from a highly ordered liquid crystalline columnar plastic phase

(Col<sub>hp</sub>)<sup>27</sup> to a columnar hexagonal disordered phase (Col<sub>hd</sub>) at 165 °C. The fact that the enthalpy for the Col<sub>hp</sub> → Col<sub>hd</sub> transition is small compared to the enthalpy of the Col<sub>hd</sub> → I transition at 235 °C supports the existence of a Col<sub>hp</sub> phase between -16 °C and 165 °C.<sup>3,28</sup> This is in line with the loss of shear ability of the texture in POM when the sample is cooled under 165 °C. In the Col<sub>hd</sub> phase **PDBI-2** features a mixture of mosaic and pseudo focal conic textures under crossed polarizers (Fig. 4d) and only negligible textural changes are observable for the transition at 165 °C to the plastic phase (Fig. 4e). XRD measurements in the Col<sub>hp</sub> phase (cf. Fig. 5b blue curve) indicates that the cores of the mesogen are regularly stacked as can be deduced from the relatively sharp reflection peak at 24.5 °. This corresponds to a stacking distance of  $d_{\pi\pi} = 3.50 \text{ \AA}$ . The absence of any peaks in the wide angle regime between 165 °C and 235 °C is characteristic for a disordered nature of the columns in the Col<sub>hd</sub> phase (red curve). For both phases the Bragg reflections in the small-angle regime correspond to a 2D hexagonal lattice (see ESI†). **PDBI-3** with two branched alkyl chains at the ester groups possess only one reversible phase transition at 183 °C in DSC upon heating. Here mosaic textures can be observed at 175 °C in POM (Fig. 4c), indicating a Col<sub>h</sub> phase. Further characteristic dendritic textures are given in ESI†. It is also worthy to note that **PDBI-3** shows a partial homeotropic alignment of the columns as observed in POM micrographs employing a  $\lambda/4$  plate (see ESI†).

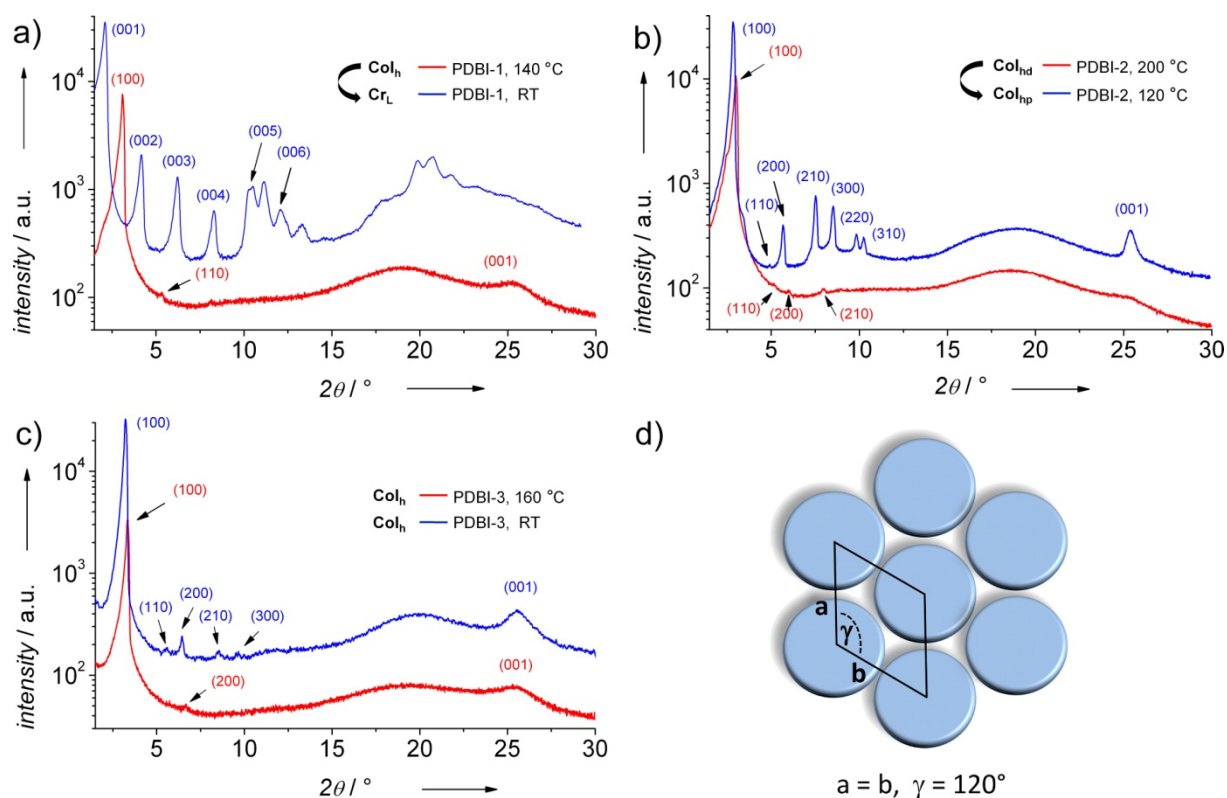


**Figure 5.** X-ray diffraction patterns of (a) **PDBI-1** in  $Col_h$  phase (140 °C) and crystalline lamellar  $Cr_L$  phase (RT). (b) **PDBI-2** in  $Col_{hd}$  phase (200 °C) and  $Col_{hp}$  phase (120 °C). (c) **PDBI-3** in  $Col_h$  phase at 160 °C and RT. (d) Schematic representation of 2D discotic columnar hexagonal packing.

Here X-ray diffraction gave evidence for the existence of a liquid crystalline columnar hexagonal lattice in the whole temperature range below the transition to the isotropic phase. Fig. 5c depicts the diffractograms at 160 °C and at RT. It is obvious that the intracolumnar ordering (see 001 reflection) increases with lowering of temperature. The fact that **PDBIs 2** and **3** are liquid crystalline even at RT is highly interesting for applications requiring high order in molecular arrangement. 2D lattice parameters and  $\pi$ - $\pi$  stacking distances  $d_{\pi\pi}$  of all **PDBIs** are summarized in Table 2.

**Table 2.** X-ray diffraction data of liquid crystalline mesophases of **PDBIs 1-3**. 2D Lattice parameters and  $\pi$ - $\pi$  stacking distance  $d_{\pi\pi}$  as determined from temperature dependent X-ray diffraction experiments.

PDBI	T [°C]	lattice parameters <sup>[a]</sup> [Å]	$d_{\pi\pi}$ <sup>[b]</sup> [Å]	phase <sup>[c]</sup>
<b>PDBI-1</b>	120	$a_{\text{hex}} = 32.9$	3.52	Col <sub>h</sub>
	RT	$d_{\text{L}} = 41.6$	-	Cr <sub>L</sub>
<b>PDBI-2</b>	200	$a_{\text{hex}} = 34.0$	-	Col <sub>hd</sub>
	120	$a_{\text{hex}} = 35.9$	3.50	Col <sub>hp</sub>
<b>PDBI-3</b>	160	$a_{\text{hex}} = 30.6$	3.49	Col <sub>h</sub>
	RT	$a_{\text{hex}} = 31.8$	3.49	Col <sub>h</sub>

[a] Hexagonal lattice parameter  $a_{\text{hex}} = \sqrt{\frac{4}{3}a_{100}^2}$ . [b] From (001) reflex.

[c] Col<sub>ho</sub> = ordered columnar hexagonal; Col<sub>hd</sub> = disordered columnar hexagonal; Col<sub>hp</sub> = columnar plastic; Cr<sub>L</sub> = crystalline lamellar phase.

## Conclusion

In summary, we synthesized three discotic molecules belonging to a novel class of semiconductors, perylene diester benzimidazoles. All these molecules exhibit extended absorption up to 680 nm. Even compared to perylene bisimides, these materials thus exhibit longer wavelength absorption with 130 nm red-shift due to further extension of  $\pi$ -conjugation via the benzimidazole group. The decrease in band gap energy was essentially achieved by a shift of the HOMO value. All **PDBIs** self-organize into liquid crystalline columnar hexagonal phases (Col<sub>h</sub>) at higher temperatures below 250 °C; **PDBIs 2** and **3** even at room temperature. Also the existence of a columnar plastic phase (Col<sub>hp</sub>) for **PDBI-2** and a lamellar ordering for **PDBI-1** was observed at room temperature. This self-assembling behaviour should allow for an orientation of **PDBIs 2** and **3** in the high temperature liquid crystalline phase and for a transfer of the orientation during cooling to a highly ordered phase at room temperature. All of these properties make n-type semiconducting **PDBIs** promising candidates for applications in organic electronics.

## EXPERIMENTAL SECTION

### Materials and Methods

$^1\text{H}$ - and  $^{13}\text{C}$ -NMR spectra were recorded on a Bruker AC 300 spectrometer (300 MHz and 75 MHz, respectively). Chemical shifts are reported in ppm at room temperature using  $\text{CDCl}_3$  as solvent and tetramethylsilane as internal standard unless indicated otherwise. Abbreviations used for splitting patterns are s = singlet, d = doublet, t = triplet, q = quartet, m = multiplet. FTIR-spectra were recorded with a Perkin Elmer Spectrum 100 (FTIR) in the range of 400-4000  $\text{cm}^{-1}$ . Oligomeric size exclusion chromatography (Oligo-SEC) was used to determine the purity of synthesized perylene bisimides. Oligo-SEC measurements were performed utilizing a Waters 515-HPLC pump with stabilized THF as eluent at a flow rate of 0.5 ml/min. 20  $\mu\text{l}$  of a solution with a concentration of approx. 1 mg/ml were injected into a column setup, which consists of a guard column (Varian; 5 x 0.8 cm; mesopore gel; particle size 3  $\mu\text{m}$ ) and two separation columns (Varian; 30 x 0.8 cm; mesopore gel; particle size 3  $\mu\text{m}$ ). The compounds were monitored with a Waters 486 tunable UV detector at 254 nm and a Waters 410 differential RI detector. Mass spectroscopic (MS) data were obtained from a FINNIGAN MAT 8500 instrument. UV-vis spectra were recorded with a Perkin Elmer Lambda 900 spectrophotometer. Photoluminescence spectra were acquired on a Shimadzu RF 5301 PC spectrofluorophotometer. The thermal degradation was studied using a Mettler Toledo TGA/SDTA 851e with a heating rate of 10  $\text{Kmin}^{-1}$  under  $\text{N}_2$  atmosphere. Differential scanning calorimetry (DSC) was carried out with a Perkin Elmer differential scanning calorimeter (Diamond) with heating and cooling rates of 10 K/min under  $\text{N}_2$  atmosphere. The instrument was calibrated with indium standards before measurements. Phase transitions were also examined by a polarization optical microscope (POM) Nikon Diaphot 300 with a Mettler FP 90 temperature-controlled hot stage. X-ray diffraction measurements were performed on a Huber Guinier Difraktometer 6000 equipped with a Huber quartz monochromator 611 with  $\text{Cu-K}\alpha_1$ : 1.54051  $\text{\AA}$ . For cyclic voltammetry (CV) experiments, a conventional three-electrode assembly using a  $\text{Ag}/\text{AgNO}_3$  reference electrode was used.  $\text{CH}_2\text{Cl}_2$  containing 0.1 M  $\text{Bu}_4\text{NPF}_6$  was used as solvent. All measurements were carried out under  $\text{N}_2$ -atmosphere at a scan rate of 0.05  $\text{Vs}^{-1}$  at 25  $^\circ\text{C}$  and all redox potentials were calibrated to ferrocene/ferrocenium couple ( $\text{Fc}/\text{Fc}^+$ ).

### Materials

The starting materials, perylenetetracarboxylic acid dianhydride PTCDA, 1-bromododecane, 3-(bromomethyl)heptane, Aliquat 336, Catechol, dibenzo-18-crown-6, hydrazine monohydrate, palladium on carbon (10% Pd), *p*-toluenesulfonic acid monohydrate, zinc acetate and solvents were purchased from Aldrich, Fluka, Acros or TCI and used without any further purification. Solvents used for precipitation and column chromatography were distilled under normal atmosphere. DMAc (anhydrous with crown cap, 99.5 %) and *ortho*-dichlorobenzene (anhydrous with crown cap, 99.0 %) were purchased from Fluka and Aldrich.

**General Procedure for the Preparation of perylene diester benzimidazoles PDBI 1 to 3:**

A mixture of the respective diester anhydride **1a, b** (0.3 mmol) and zinc acetate (0.5 mmol) were dissolved in dry DMAc (6 mL) in a microwave pressure tube and the respective *ortho*-diamine **2a, b** (0.4 mmol) was added. The condensation was carried out under microwave irradiation conditions for 25 minutes at 160 °C and 300 W. The violet crude product was precipitated in methanol (300 mL) and filtered. The residue was washed with H<sub>2</sub>O (2 x 30 mL) and methanol (3 x 30 mL) and dried over night at 60 °C in vacuo. The crude product was purified via column chromatography.

**Synthesis of Bisdodecyl-perylene-3,4-(4,5-bisdodecyl-1,2-benzimidazole)-9,10-dicarboxylate PDBI-1:**

**1a** (0.22 g, 0.3 mmol) and diamine **2a** (0.20 g, 0.4 mmol) were allowed to react according to the general procedure. The crude product was purified via column chromatography (silica flashgel, eluent CHCl<sub>3</sub>:acetone 20:1 v/v). Yield: 0.27 g (80 %) as violet solid. Calcd. for C<sub>78</sub>H<sub>110</sub>N<sub>2</sub>O<sub>5</sub>: C 80.06, H 9.59, N 2.42. Found: C 80.58, H 9.66, N 2.16. EI-MS (70 eV): *m/z* 1155 ([M<sup>+</sup>], 8%). IR (ATR):  $\nu = 2915$  (s), 2848 (s), 1714 (s), 1690 (s), 1596 (m), 1468 (s), 1358 (s), 1171 (s), 743 (s) cm<sup>-1</sup>. <sup>1</sup>H-NMR (300 MHz, CDCl<sub>3</sub>, 298K)  $\delta = 8.74$ -8.65 (m, 2H, H<sub>Ar</sub>), 8.48-8.36 (m, 4H, H<sub>Ar</sub>), 8.28-8.24 (m, 1H, H<sub>Ar</sub>), 8.12-8.06 (m, 2H, H<sub>Ar</sub>), 7.61-7.57 (m, 1H, H<sub>Ar</sub>), 4.36 (t, <sup>3</sup>J = 6.9 Hz, 4H, O-CH<sub>2</sub>), 2.80-2.69 (m, 4H, benzimidazol-CH<sub>2</sub>), 1.90-1.78 (m, 4H, OCH<sub>2</sub>-CH<sub>2</sub>), 1.76-1.62 (m, 4H, benzimidazole-CH<sub>2</sub>-CH<sub>2</sub>), 1.53-1.15 (m, 72H, CH<sub>2</sub>), 0.95-0.84 (m, 12H, CH<sub>3</sub>) ppm. <sup>13</sup>C-NMR (62.5 MHz, CDCl<sub>3</sub>, 298K)  $\delta = 168.3$  (2C, O-C=O), 159.4 (1C, N-C=O), 147.6 (1C, N-C=N), 142.1, 139.4, 139.0, 135.9, 132.5, 132.3, 131.8, 131.0, 130.3, 130.0, 129.8, 129.0, 128.6, 127.4, 126.6, 126.1, 122.4, 121.8, 120.3, 119.2, 115.1 (26C, C<sub>Ar</sub>), 65.8 (2C, O-CH<sub>2</sub>), 32.8, 32.0, 31.3, 30.9, 30.0, 29.8, 29.7, 29.6, 29.4, 28.7, 26.1, 22.7 (42C, CH<sub>2</sub>), 14.1 (4C, CH<sub>3</sub>) ppm.

**Synthesis of Bisdodecyl-perylene-3,4-(4,5-bisdodecyloxy-1,2-benzimidazole)-9,10-dicarboxylate PDBI-2:**

**1a** (0.30 g, 0.4 mmol) and diamine **2b** (0.29 g, 0.6 mmol) were allowed to react according to the general procedure. The crude product was purified via column chromatography (silica flashgel, eluent CHCl<sub>3</sub>:acetone 20:1 v/v). Freeze-drying from benzene gave the violet product **PDBI-2**. Yield: 0.28 g (59 %) as violet solid. Calcd. for C<sub>78</sub>H<sub>110</sub>N<sub>2</sub>O<sub>7</sub>: C 78.88, H 9.33, N 2.36. Found: C 78.75, H 9.32, N 2.30. EI-MS (70 eV): *m/z* 1187 ([M<sup>+</sup>], 5%). IR (ATR):  $\nu = 2917$  (s), 2849 (s), 1720 (s), 1677 (s), 1592 (m), 1465 (s), 1364 (m), 1293 (s), 1170 (s), 746 (s) cm<sup>-1</sup>. <sup>1</sup>H-NMR (300 MHz, CDCl<sub>3</sub>, 298K)  $\delta = 8.69$  (d, <sup>3</sup>J = 8.12 Hz, 2H, H<sub>Ar</sub>), 8.50-8.38 (m, 4H, H<sub>Ar</sub>), 8.13-8.05 (m, 3H, H<sub>Ar</sub>), 7.34 (s, 1H, H<sub>Ar</sub>), 4.36 (t, <sup>3</sup>J = 6.8 Hz, 4H, O-CH<sub>2</sub>), 4.22-4.09 (m, 4H, benzimidazole-OCH<sub>2</sub>), 2.01-1.89 (m, 4H, OCH<sub>2</sub>-CH<sub>2</sub>), 1.89-1.78 (m, 4H, benzimidazole-CH<sub>2</sub>-CH<sub>2</sub>), 1.52-1.14 (m, 72H, CH<sub>2</sub>), 0.97-0.82 (m,

12H, CH<sub>3</sub>) ppm. <sup>13</sup>C-NMR (62.5 MHz, CDCl<sub>3</sub>, 298K)  $\delta$  = 168.3 (2C, O-C=O), 159.5 (1C, N-C=O), 148.8 (1C, N-C=N), 147.0, 139.4, 137.8, 136.3, 132.5, 132.2, 131.9, 131.3, 131.0, 130.4, 130.2, 129.2, 128.7, 127.4, 126.4, 126.1, 125.6, 122.4, 121.8, 120.6, (26C, C<sub>Ar</sub>), 69.7, 69.5 (2C, benzimidazole-O-CH<sub>2</sub>), 65.8 (2C, O-CH<sub>2</sub>), 31.9, 31.3, 29.8, 29.7, 29.6, 29.5, 29.4, 29.3, 28.6, 26.1, 22.7 (40C, CH<sub>2</sub>), 14.1 (4C, CH<sub>3</sub>) ppm.

**Synthesis of Bis(2-ethylhexyl)-perylene-3,4-(4,5-bisdodecyloxy-1,2-benzimidazole)-9,10-dicarboxylate PDBI-3:**

**1b** (0.50 g, 0.8 mmol) and diamine **2b** (0.80 g, 1.7 mmol) were allowed to react according to the general procedure. Then, CHCl<sub>3</sub> (100 mL) was added to the mixture and the violet crude product was washed with water (2x100 mL). The organic layer was dried over Na<sub>2</sub>SO<sub>4</sub> and the solvent was evaporated under reduced pressure. The crude product was purified via column chromatography (silica flashgel, eluent CHCl<sub>3</sub>:MeOH 95:5 v/v). Freeze-drying from benzene gave the violet product **PDBI-3**. Yield: 0.55 g (65 %) as violet solid. Calcd. for C<sub>70</sub>H<sub>94</sub>N<sub>2</sub>O<sub>7</sub>: C 78.17, H 8.81, N 2.60. Found: C 77.26, H 8.93, N 2.46. EI-MS (70 eV): *m/z* 1074 ([M<sup>+</sup>], 29%). IR (ATR):  $\nu$  = 2922 (s), 2853 (s), 1710 (s), 1687 (s), 1592 (m), 1455 (s), 1364 (w), 1290 (s), 1169 (s), 745 (m) cm<sup>-1</sup>. <sup>1</sup>H-NMR (300 MHz, CDCl<sub>3</sub>, 298K)  $\delta$  = 8.76-8.64 (m, 2H, H<sub>Ar</sub>), 8.54-8.41 (m, 4H, H<sub>Ar</sub>), 8.15-8.07 (m, 3H, H<sub>Ar</sub>), 7.36 (s, 1H, H<sub>Ar</sub>), 4.37-4.26 (m, 4H, O-CH<sub>2</sub>), 4.23-4.10 (m, 4H, benzimidazole-O-CH<sub>2</sub>), 2.00-1.88 (m, 2H, OCH<sub>2</sub>-CH), 1.87-1.77 (m, 4H, benzimidazole-CH<sub>2</sub>-CH<sub>2</sub>), 1.61-1.23 (m, 52H, CH<sub>2</sub>), 1.05-0.86 (m, 18H, CH<sub>3</sub>) ppm. <sup>13</sup>C-NMR (62.5 MHz, CDCl<sub>3</sub>, 298K)  $\delta$  = 168.4 (2C, O-C=O), 159.9 (1C, N-C=O), 148.8 (1C, N-C=N), 147.1, 137.9, 136.4, 132.4, 132.3, 131.9, 131.3, 131.1, 130.2, 129.9, 129.2, 128.8, 127.4, 126.4, 126.1, 125.7, 122.6, 121.8, 120.6, 103.7, 100.1 (26C, C<sub>Ar</sub>), 69.7, 69.5 (2C, benzimidazole-O-CH<sub>2</sub>), 68.0 (2C, O-CH<sub>2</sub>), 38.8 (2C, O-CH<sub>2</sub>-CH), 32.0, 30.5, 29.8, 29.7, 29.6, 29.5, 29.4, 29.3, 29.0, 26.1, 23.9, 23.0, 22.7 (28C, CH<sub>2</sub>), 14.1, 11.0 (6C, CH<sub>3</sub>) ppm.

Financial Support from SPP 1355 (DFG) is kindly acknowledged

**Supporting Information available.**

Synthesis and characterization of perylene tetraesters, perylene diester anhydrides and aromatic *ortho*-diamines. Additional data of X-ray diffraction experiments.

## **BIBLIOGRAPHY**

- (1) Laschat, S.; Baro, A.; Steinke, N.; Giesselmann, F.; Haegele, C.; Scalia, G.; Judele, R.; Kapatsina, E.; Sauer, S.; Schreivogel, A.; Tosoni, M. *Angew. Chem. Int. Ed.* **2007**, *46*, 4832-4887.
- (2) Kumar, S. *Chem. Soc. Rev.* **2006**, *35*, 83-109.
- (3) Destrade, C.; Foucher, P.; Gasparoux, H.; Tinh, N. H.; Levelut, A. M.; Malthete, J. *Mol. Cryst. Liq. Cryst.* **1984**, *106*, 121-146.
- (4) Lüssem, G.; Wendorff, J. H. *Polym. Adv. Technol.* **1998**, *9*, 443-460.
- (5) Katz, H. E.; Lovinger, A. J.; Johnson, J.; Kloc, C.; Slegrist, T.; Li, W.; Lin, Y. Y.; Dodabalapur, A. *Nature* **2000**, *404*, 478-481.
- (6) Schmidt-Mende, L.; Fechtenkötter, A.; Müllen, K.; Moons, E.; Friend, R. H.; MacKenzie, J. D. *Science* **2001**, *293*, 1119-22.
- (7) Wojciech, P.; Matthias, Z.; Ji Young, C.; Klaus, M.; Rudolf, Z. *Macromol. Rapid Commun.* **2009**, *30*, 1179-1202.
- (8) Sergeev, S.; Pisula, W.; Geerts, Y. H. *Chem. Soc. Rev.* **2007**, *36*, 1902-1929.
- (9) Adam, D.; Schuhmacher, P.; Simmerer, J.; Haussling, L.; Siemensmeyer, K.; Etzbacher, K. H.; Ringsdorf, H.; Haarer, D. *Nature* **1994**, *371*, 141-143.
- (10) Warman, J. M.; de Haas, M. P.; Dicker, G.; Grozema, F. C.; Piris, J.; Debije, M. G. *Chem. Mater.* **2004**, *16*, 4600-4609.
- (11) Jones, B. A.; Ahrens, M. J.; Yoon, M.-H.; Facchetti, A.; Marks, T. J.; Wasielewski, M. R. *Angew. Chem. Int. Ed.* **2004**, *43*, 6363-6366.
- (12) Gsänger, M.; Oh, J. H.; Könemann, M.; Höffken, H. W.; Krause, A.-M.; Bao, Z.; Würthner, F. *Angew. Chem. Int. Ed.* **2009**, *9999*, NA.
- (13) Zhang, Y.-D.; Jespersen, K. G.; Kempe, M.; Kornfield, J. A.; Barlow, S.; Kippelen, B.; Marder, S. R. *Langmuir* **2003**, *19*, 6534-6536.
- (14) Chesterfield, R. J.; McKeen, J. C.; Newman, C. R.; Ewbank, P. C.; da Silva Filho, D. A.; Bredas, J.-L.; Miller, L. L.; Mann, K. R.; Frisbie, C. D. *J. Phys. Chem. B* **2004**, *108*, 19281-19292.
- (15) Sienkowska, M. J.; Farrar, J. M.; Zhang, F.; Kusuma, S.; Heiney, P. A.; Kaszynski, P. *J. Mater. Chem.* **2007**, *17*, 1399-1411.
- (16) Langhals, H. *Helv. Chim. Acta* **2005**, *88*, 1309-1343.
- (17) Würthner, F. *Chem. Commun.* **2004**, 1564-1579.
- (18) Wicklein, A.; Lang, A.; Muth, M.; Thelakkat, M. *J. Am. Chem. Soc.* **2009**, *131*, 14442-14453.
- (19) Benning, S.; Kitzerow, H.-S.; Bock, H.; Achard, M.-F. *Liq. Cryst.* **2000**, *27*, 901 - 906.

- (20) Oukachmih, M.; Destruel, P.; Seguy, I.; Ablart, G.; Jolinat, P.; Archambeau, S.; Mabilia, M.; Fouet, S.; Bock, H. *Sol. Energy Mater. Sol. Cells* **2005**, *85*, 535-543.
- (21) Wicklein, A.; Kohn, P.; Ghazaryan, L.; Thurn-Albrecht, T.; Thelakkat, M. *Chem. Commun.* **2010**, DOI: 10.1039/b921476c.
- (22) Xue, C.; Sun, R.; Annab, R.; Abadi, D.; Jin, S. *Tetrahedron Lett.* **2009**, *50*, 853-856.
- (23) Pommerehne, J.; Vestweber, H.; Guss, W.; Mahrt, R. F.; Bäessler, H.; Porsch, M.; Daub, J. *Adv. Mater.* **1995**, *7*, 551-554.
- (24) Mo, X.; Chen, H.-Z.; Wang, Y.; Shi, M.-M.; Wang, M. *J. Phys. Chem. B* **2005**, *109*, 7659-7663.
- (25) Ohta, K.; Muroki, H.; Takagi, A.; Hatada, K.-I.; Ema, H.; Yamamoto, I.; Matsuzaki, K. *Mol. Cryst. Liq. Cryst.* **1986**, *140*, 131 - 152.
- (26) Sakashita, H.; Nishitani, A.; Sumiya, Y.; Terauchi, H.; Ohta, K.; Yamamoto, I. *Mol. Cryst. Liq. Cryst.* **1988**, *163*, 211 - 219.
- (27) Prasad, S. K.; Rao, D. S. S.; Chandrasekhar, S.; Kumar, S. *Mol. Cryst. Liq. Cryst.* **2003**, *396*, 121-139.
- (28) Collard, D. M.; Lillya, C. P. *J. Am. Chem. Soc.* **2002**, *113*, 8577-8583.

***SUPPORTING INFORMATION***

**Table of Contents**

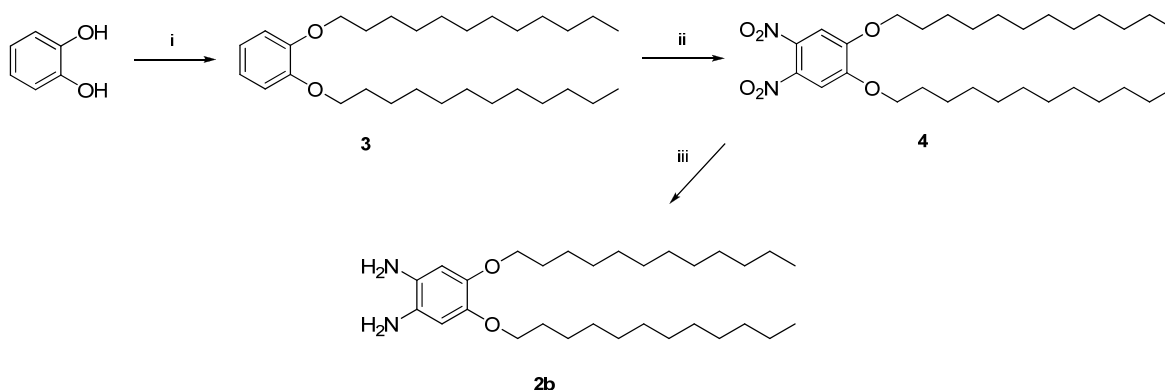
- 1. General Information**
- 2. Synthesis and Characterization of Intermediates**
- 3. Literature**
- 4. Additional Figures**

## 1. General Information

The starting materials, perylenetetracarboxylic acid dianhydride PTCDA, 1-bromododecane, 3-(bromomethyl)heptane, Aliquat 336, Catechol, dibenzo-18-crown-6, hydrazine monohydrate, palladium on carbon (10% Pd), *p*-toluenesulfonic acid monohydrate, zinc acetate and solvents were purchased from Aldrich, Fluka, Acros or TCI and used without any further purification. Solvents used for precipitation and column chromatography were distilled under normal atmosphere. DMAc (anhydrous with crown cap, 99.5 %) and *ortho*-dichlorobenzene (anhydrous with crown cap, 99.0 %) were purchased from Fluka and Aldrich.

$^1\text{H}$ - and  $^{13}\text{C}$ -NMR spectra were recorded on a Bruker AC 300 spectrometer (300 MHz and 75 MHz, respectively). Chemical shifts are reported in ppm at room temperature using  $\text{CDCl}_3$  as solvent and tetramethylsilane as internal standard unless indicated otherwise. Abbreviations used for splitting patterns are s = singlet, d = doublet, t = triplet, q = quintet, m = multiplet. FTIR-spectra were recorded with a Perkin Elmer Spectrum 100 (FTIR) in the range of 400-4000  $\text{cm}^{-1}$ . Mass spectroscopic (MS) data were obtained from a FINNIGAN MAT 8500 instrument.

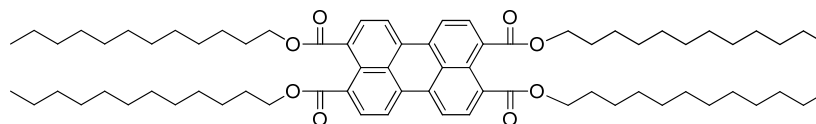
Synthesis of 4,5-dialkyl-substituted 1,2-phenylenediamine **2a** was adapted from the work of Pu and coworkers.<sup>1,2</sup> Synthesis of 4,5-bis(dodecyloxy)benzene-1,2-diamine **2b** was carried out with catechol as starting material. The alkylation of catechol with 1-bromododecane and dibenzo-18-crown-6 as phase transfer catalyst was adapted by the work of Howard and coworkers<sup>3</sup> and gave 1,2-bis(dodecyloxy)benzene **3**. Reaction with sulphonic acid at room temperature gave 1,2-bis(dodecyloxy)-4,5-dinitrobenzene **4**, which was described by Grolik et al.<sup>4</sup> Catalytic hydrogenation of **4** with Pd (10 %)/C and hydrazine monohydrate gave the desired *ortho*-diamine **2b** (Scheme 1).<sup>3</sup>



**Scheme S1.** Preparation of bisalkoxy *ortho*-diamine **2b**. i)  $\text{Br}-(\text{CH}_2)_{11}\text{CH}_3$ , dibenzo-18-crown-6,  $\text{K}_2\text{CO}_3$ , 2-butanone, 85 °C; ii)  $\text{HNO}_3$ ,  $\text{H}_2\text{SO}_4$ , DCM, r.t.; iii) hydrazine monohydrate, Pd (10 %)/C, ethanol, 85 °C.

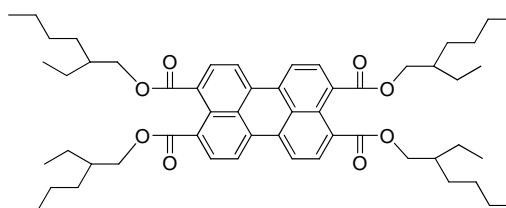
## 2. Synthesis and Characterization of Intermediates

### Synthesis of Tetradodecyl-perylene-3,4,9,10-tetracarboxylat PTE-1:<sup>5</sup>



**PTCDA** (7.84 g, 20.0 mmol), **KOH** (6.00 g, 106.0 mmol) and 100 mL deionized water were added into a 250 mL beaker and stirred at 70 °C for 30 minutes. The solution was filtered to a 250 mL round-bottomed flask. After adjustment of pH value to 8-9 with 1 M HCl solution, **ALIQUAT 336** (2.70 g, 6.0 mmol) and **KI** (0.50 g, 4.0 mmol) were added. The mixture was stirred vigorously for 10 minutes followed by addition of 1-bromododecane (39.90 g, 160.0 mmol). The solution was refluxed with vigorous stirring for 2 hours. Subsequently, the yellow product was extracted with  $\text{CHCl}_3$ . The organic phase was washed three times with 15 % NaCl aqueous solution and concentrated under reduced pressure. The product was precipitated dropwise in methanol (500 mL). The solid was collected by suction filtration and dried in vacuum at 60 °C over night. Yield: 13.19 g (60 %) as yellow solid. EI-MS (70 eV):  $m/z$  1101 ( $[\text{M}^+]$ , 100 %). IR (ATR):  $\nu = 2918$  (s), 2850 (m), 1731 (s), 1718 (s), 1592 (m) 1278 (s), 1170 (s), 746 (m)  $\text{cm}^{-1}$ .  $^1\text{H-NMR}$  (300 MHz,  $\text{CDCl}_3$ , 298K)  $\delta = 8.16$  (d,  $^3J = 8.9$  Hz, 4H,  $\text{H}_{\text{Ar}}$ ), 7.97 (d,  $^3J = 7.7$  Hz, 4H,  $\text{H}_{\text{Ar}}$ ), 4.38-4.30 (m, 8H, O- $\text{CH}_2$ ), 1.90-1.76 (m, 8H, O $\text{CH}_2$ - $\text{CH}_2$ ), 1.52-1.20 (m, 72H,  $\text{CH}_2$ ), 0.94-0.84 (m, 12H,  $\text{CH}_3$ ) ppm.

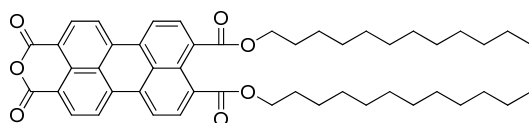
### Synthesis of Tetra(2-ethylhexyl)-perylene-3,4,9,10-tetracarboxylate PTE-2:<sup>5</sup>



**PTCDA** (10.00 g, 25.0 mmol), **KOH** (7.60 g, 135.0 mmol) and 150 mL deionized water were added into a 250 mL beaker and stirred at 70 °C for 30 minutes. The solution was filtered to a 500 mL round-bottomed flask. After adjustment of pH value to 8-9 with 1 M HCl solution, **ALIQUAT 336** (4.00 g, 9.0 mmol) and **KI** (2.28 g, 14.0 mmol) were added. The mixture was stirred vigorously for 10 minutes followed by addition of 3-(bromomethyl)heptane (25.0 g, 129.0 mmol). The solution was refluxed with vigorous stirring, more 3-(bromomethyl)heptane (15.00 g, 77.0 mmol) was added after 16 h and the solution was refluxed with vigorous stirring for additional 10 hours. Subsequently, the yellow product was extracted with  $\text{CHCl}_3$ . The  $\text{CHCl}_3$  phase was washed three times with 15 % NaCl aqueous solution and concentrated under reduced pressure. The product was precipitated dropwise into methanol (500 mL). The solid was collected

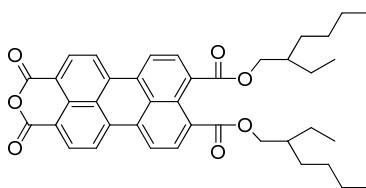
by suction filtration and dried in vacuum at 60 °C over night. Yield: 9.24 g (41 %) as orange viscous solid. EI-MS (70 eV):  $m/z$  876 ( $[M^+]$ , 100 %). IR (ATR):  $\nu = 2929$  (m), 2859 (m), 1709 (s), 1590 (w), 1267 (s), 1159 (s), 746 (s)  $\text{cm}^{-1}$ .  $^1\text{H-NMR}$  (300 MHz,  $\text{CDCl}_3$ , 298K)  $\delta = 8.29$  (d,  $^3J = 8.9$  Hz, 4H,  $\text{H}_{\text{Ar}}$ ), 8.03 (d,  $^3J = 7.7$  Hz, 4H,  $\text{H}_{\text{Ar}}$ ), 4.35-4.22 (m, 8H, O- $\text{CH}_2$ ), 1.87-1.74 (m, 4H, O $\text{CH}_2$ -CH), 1.55-1.28 (m, 32H,  $\text{CH}_2$ ), 1.03-0.89 (m, 24H,  $\text{CH}_3$ ) ppm.

#### Synthesis of Bisdodecyl-perylene-3,4,9,10-tetracarboxyl-monoanhydride 1a:<sup>5</sup>



A round-bottomed flask was charged with perylene tetraester **PTE-1** (6.00 g, 5.4 mmol), 1.5 mL toluene and 7.3 mL *n*-dodecane and heated to 95 °C. After complete dissolution of the yellow powder, *p*-toluenesulfonic acid monohydrate (1.04 g, 5.4 mmol) was added and the solution was stirred at 95 °C for 5 hours. The dark red mixture was dissolved in hot THF (25 mL) and precipitated dropwise in methanol (800 mL). The red solid was collected by suction filtration and was dried in vacuum at 60 °C over night. Yield: 3.56 g (88 %) as red solid. EI-MS (70 eV):  $m/z$  745 ( $[M^+]$ , 100%). IR (ATR):  $\nu = 2920$  (s), 2851 (m), 1762 (s), 1730 (s), 1708 (s), 1593 (s), 1284 (s), 1150 (s), 751 (m)  $\text{cm}^{-1}$ .  $^1\text{H-NMR}$  (300 MHz,  $\text{CDCl}_3$ , 298K)  $\delta = 8.65$  (d,  $^3J = 8.2$  Hz, 2H,  $\text{H}_{\text{Ar}}$ ), 8.51 (d,  $^3J = 8.1$  Hz, 4H,  $\text{H}_{\text{Ar}}$ ), 8.14 (d,  $^3J = 7.9$  Hz, 2H,  $\text{H}_{\text{Ar}}$ ), 4.36 (t,  $^3J = 6.9$  Hz, 4H, O- $\text{CH}_2$ ), 1.88-1.77 (m, 4H, O $\text{CH}_2$ - $\text{CH}_2$ ), 1.53-1.21 (m, 36H,  $\text{CH}_2$ ), 0.94-0.84 (m, 6H,  $\text{CH}_3$ ) ppm.

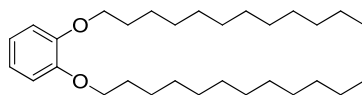
#### Synthesis of Bis(2-ethylhexyl)-perylene-3,4,9,10-tetracarboxyl-monoanhydride 1b:<sup>5</sup>



A round-bottomed flask was charged with perylene tetraester **PTE-2** (5.00 g, 5.7 mmol) and 12.5 mL *n*-dodecane and heated to 95 °C. After **PTE-2** was dissolved completely, *p*-toluenesulfonic acid monohydrate (1.08 g, 5.7 mmol) was added and the solution was stirred at 95 °C for 4 hours. Then the dark red mixture was dissolved in hot THF (25 mL) and the product was precipitated dropwise in methanol (800 mL). The red solid was collected by suction filtration and dried in vacuum at 60 °C over night. Yield: 3.34g (92 %) as red solid. EI-MS (70 eV):  $m/z$  634 ( $[M^+]$  73 %). IR (ATR):  $\nu = 2928$  (s), 2859 (m), 1768 (s), 1738 (m), 1706 (s), 1592 (s), 1262 (s), 1148 (s), 748 (m)  $\text{cm}^{-1}$ .  $^1\text{H-NMR}$  (300 MHz,  $\text{CDCl}_3$ , 298K)  $\delta = 8.66$ -8.58 (m, 2H,  $\text{H}_{\text{Ar}}$ ), 8.53-8.40 (m, 4H,  $\text{H}_{\text{Ar}}$ ), 8.14-8.05

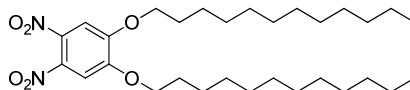
(m, 2H, H<sub>Ar</sub>), 4.38-4.24 (m, 4H, O-CH<sub>2</sub>), 1.88-1.75 (m, 2H, OCH<sub>2</sub>-CH), 1.60-1.26 (m, 16H, CH<sub>2</sub>), 1.08-0.86 (m, 12H, CH<sub>3</sub>) ppm.

### Synthesis of 1,2-bis(dodecyloxy) benzene **3**:<sup>3</sup>

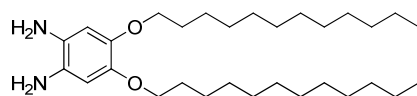


Catechol (1.99 g, 18.0 mmol), anhydrous K<sub>2</sub>CO<sub>3</sub> (10.00 g, 72.4 mmol), 1-bromododecane (9.92 g, 39.8 mmol) and dibenzo-18-crown-6 (0.30 g, 0.8 mmol) in 2-butanone (100 mL) were heated for 16 h under reflux and argon atmosphere. The mixture was filtered hot and the solvent evaporated at reduced pressure. Recrystallization from methanol afforded **3** as a white solid, which was collected by suction filtration and then dried in vacuum at 60 °C over night. Yield: 5.38 g (67 %) as white solid. EI-MS (70 eV): *m/z* 446 ([M<sup>+</sup>], 100%). IR (ATR):  $\nu$  = 2916 (s), 2848 (s), 1594 (m), 1466 (m), 1256 (s), 1121 (s), 731 (s) cm<sup>-1</sup>. <sup>1</sup>H-NMR (300 MHz, CDCl<sub>3</sub>, 298K)  $\delta$  = 6.90 (s, 4H, H<sub>Ar</sub>), 4.01 (t, <sup>3</sup>*J* = 6.6 Hz, 4H, O-CH<sub>2</sub>), 1.88-1.77 (m, 4H, OCH<sub>2</sub>-CH<sub>2</sub>), 1.54-1.43 (m, 4H, CH<sub>3</sub>-CH<sub>2</sub>), 1.42-1.22 (m, 32H, CH<sub>2</sub>), 0.95-0.86 (m, 6H, CH<sub>3</sub>) ppm.

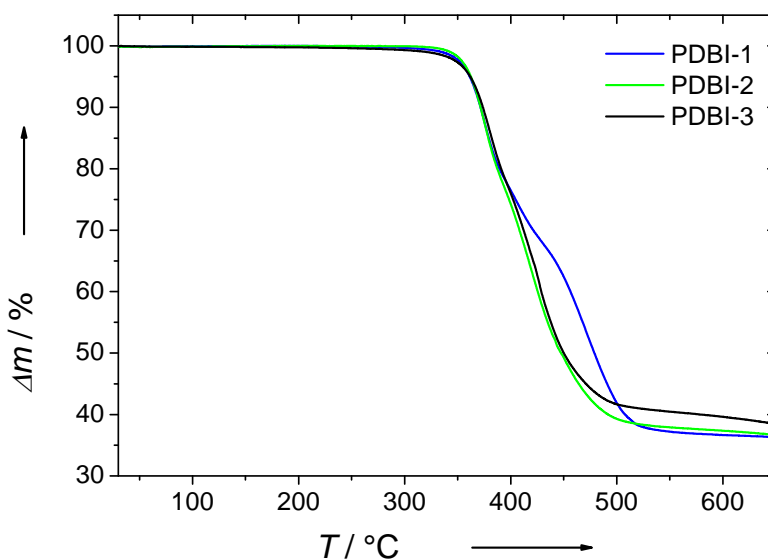
### Synthesis of 1,2-bis(dodecyloxy)-4,5-dinitrobenzene **4**:<sup>4</sup>



A solution of **3** (3.32 g, 7.4 mmol) in dichloromethane (40 mL) was added dropwise to vigorously stirred concentrated HNO<sub>3</sub> (16 mL) over a period of 30 min at 0 °C. Then concentrated H<sub>2</sub>SO<sub>4</sub> (8 mL) was added in portions and stirring was continued for 2 h at room temperature. The reaction mixture was poured onto crushed ice (150 mL) and the resultant yellow precipitate was extracted with dichloromethane (2 x 50 mL). The organic layer was washed thoroughly with saturated aqueous Na<sub>2</sub>CO<sub>3</sub>, then with H<sub>2</sub>O, and finally dried over anhydrous MgSO<sub>4</sub>. The solvent was evaporated to give a yellow product. Yield: 3.63 g (91 %) as yellow solid. EI-MS (70 eV): *m/z* 536 ([M<sup>+</sup>], 12%). IR (ATR):  $\nu$  = 2917 (s), 2849 (s), 1586 (w), 1465 (m), 1223 (s), 720 (m) cm<sup>-1</sup>. <sup>1</sup>H-NMR (300 MHz, CDCl<sub>3</sub>, 298K)  $\delta$  = 7.31 (s, 2H, H<sub>Ar</sub>), 4.11 (t, <sup>3</sup>*J* = 6.7 Hz, 4H, O-CH<sub>2</sub>), 1.94-1.82 (m, 4H, OCH<sub>2</sub>-CH<sub>2</sub>), 1.54-1.43 (m, 4H, CH<sub>3</sub>-CH<sub>2</sub>), 1.42-1.23 (m, 32H, CH<sub>2</sub>), 0.94-0.86 (m, 6H, CH<sub>3</sub>) ppm.

**Synthesis of 4,5-bis(dodecyloxy)benzene-1,2-diamine 2b:**<sup>3</sup>

Hydrazine monohydrate (4.24 g, 84.8 mmol) and palladium on charcoal (0.43 g, 10 %) were added to a suspension of the dinitroarene **4** (1.25 g, 2.3 mmol) in ethanol (175 mL). The mixture was heated for 16 h at 80 °C under argon atmosphere. The hot solution was filtered through Celite under argon atmosphere. After the solvent was evaporated under reduced pressure, the product was obtained as a white solid, which was unstable in air and used immediately upon preparation. Yield: 0.77 g (69 %) as white solid. <sup>1</sup>H-NMR (300 MHz, CDCl<sub>3</sub>, 298K)  $\delta$  = 6.40 (s, 2H, H<sub>Ar</sub>), 3.90 (t, <sup>3</sup>J = 6.8 Hz, 4H, O-CH<sub>2</sub>), 3.20 (broad s, 4H, NH<sub>2</sub>), 1.81-1.71 (m, 4H, OCH<sub>2</sub>-CH<sub>2</sub>), 1.50-1.40 (m, 4H, CH<sub>3</sub>-CH<sub>2</sub>), 1.37-1.22 (m, 32H, CH<sub>2</sub>), 0.93-0.86 (m, 6H, CH<sub>3</sub>). ppm.

**2. Additional Figures**

**Figure S1.** Thermogravimetric data of **PDBIs 1-3** measured with a heating rate of 10 Kmin<sup>-1</sup> under N<sub>2</sub> atmosphere.

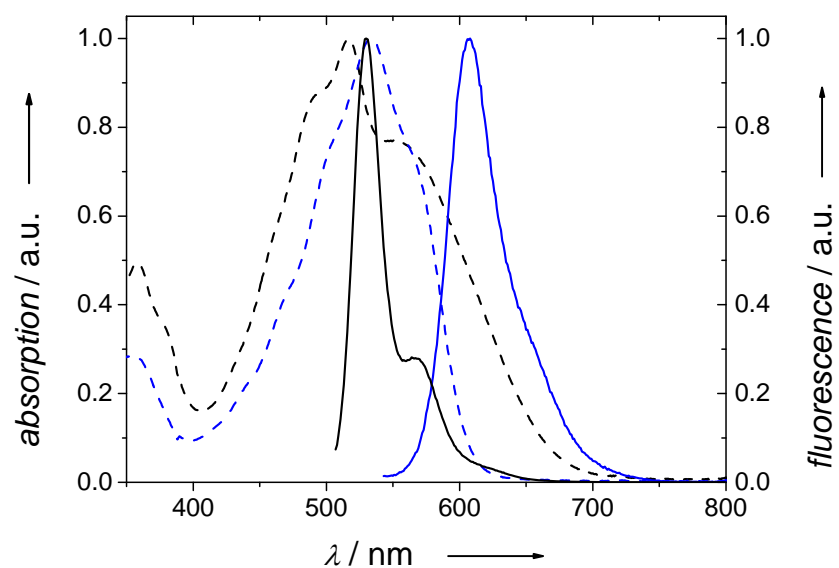


**Figure S2.** Normalized UV-vis absorption (dashed lines) and photoluminescence spectra of **PDBI-1** (blue;  $\lambda_{ex} = 533$  nm) and **PDBI-2** (black;  $\lambda_{ex} = 497$  nm).

**Table S1.** Half-wave reduction potentials<sup>[a]</sup> and LUMO<sup>[b]</sup>- and HOMO<sup>[c]</sup>-energy levels of **PDBIs 1-3, PBI** and **PTE**<sup>6</sup>.

perylene	$E_{1/2}^{-1[a]}$ [V]	$E_{1/2}^{-2[a]}$ [V]	LUMO <sup>[b]</sup> [eV]	HOMO <sup>[c]</sup> [eV]	band gap <sup>[d]</sup> [eV]
<b>PDBI-1</b>	-1.27	-1.49	-3.53	-5.51	1.98
<b>PDBI-2</b>	-1.20	-1.46	-3.60	-5.37	1.77
<b>PDBI-3</b>	-1.20	-1.46	-3.60	-5.38	1.78
<b>PBI</b> <sup>7</sup>	-1.09	-1.28	-3.71	-6.00	2.29
<b>PTE</b> <sup>6</sup>			-3.60	-6.08	2.48

[a] With respect to  $Fc/Fc^+$ , [b] set ferrocene–ferrocenium = -4.80 eV, [c] from  $E_{1/2}^{-1}$  and optical band gap, [d] determined from the absorption edges of absorption spectra of  $1 \cdot 10^{-5}$  M  $CHCl_3$  solutions.

**Table S2.** X-ray diffraction data of liquid crystalline mesophases<sup>[a]</sup> of **PDBIs 1-3**. 2D Lattice parameters, as determined from temperature dependent X-ray diffraction experiments.

<b>PDBI</b>	T [°C]	2θ <sup>[b]</sup> [°]	d <sub>obs</sub> <sup>[c]</sup> [Å]	d <sub>calc</sub> <sup>[d]</sup> [Å]	(hkl) <sup>[c]</sup>	Mesophase parameters			
<b>PDBI-1</b>	120	3.10	28.48	28.48	(100)	Col <sub>h</sub> a = 32.9 Å			
		5.34	16.54	16.44	(110)				
		8.14	10.85	10.76	(210)				
		25.3	3.52	-	(001)				
	RT	2.12	41.64	41.64	(001)	Cr <sub>L</sub> d = 41.6 Å			
		4.23	20.87	20.82	(002)				
		6.36	13.89	13.88	(003)				
		8.46	10.44	10.41	(004)				
		10.56	8.37	8.33	(005)				
		12.75	6.94	6.94	(006)				
	<b>PDBI-2</b>	200	2.99	29.47	29.47	(100)	Col <sub>hd</sub> a = 34.03 Å		
			5.17	17.07	17.01	(110)			
			6.04	14.61	14.74	(200)			
			7.98	11.07	11.14	(210)			
120		2.84	31.08	31.08	(100)	Col <sub>hp</sub> a = 35.89 Å			
		4.92	17.93	17.94	(110)				
		5.68	15.55	15.54	(200)				
		7.54	11.72	11.75	(210)				
		8.54	10.35	10.36	(300)				
		9.85	8.97	8.97	(220)				
		10.3	8.61	8.62	(310)				
		24.5	3.50	-	(001)				
		<b>PDBI-3</b>	160	3.32	26.59		26.59	(100)	Col <sub>h</sub> a = 30.6 Å
				6.66	13.26		13.30	(200)	
25.5	3.49			-	(001)				
RT	3.21		27.50	27.50	(100)	Col <sub>h</sub> a = 31.8 Å			
	5.58		15.83	15.88	(110)				
	6.44		13.71	13.75	(200)				
	8.54		10.34	10.39	(210)				
	9.65		9.16	9.17	(300)				
	25.52		3.49	-	(001)				

[a] Col<sub>h</sub> = columnar hexagonal mesophase; Col<sub>hd</sub> = disordered columnar hexagonal mesophase; Col<sub>hp</sub> = columnar plastic phase; Cr<sub>L</sub> = crystalline lamellar phase. [b] Diffraction angle, [c] observed and calculated diffraction spacings, [d] Miller indices. [e] Hexagonal lattice parameter  $a_{hex} = \sqrt{\frac{4}{3}d_{100}^2}$ .

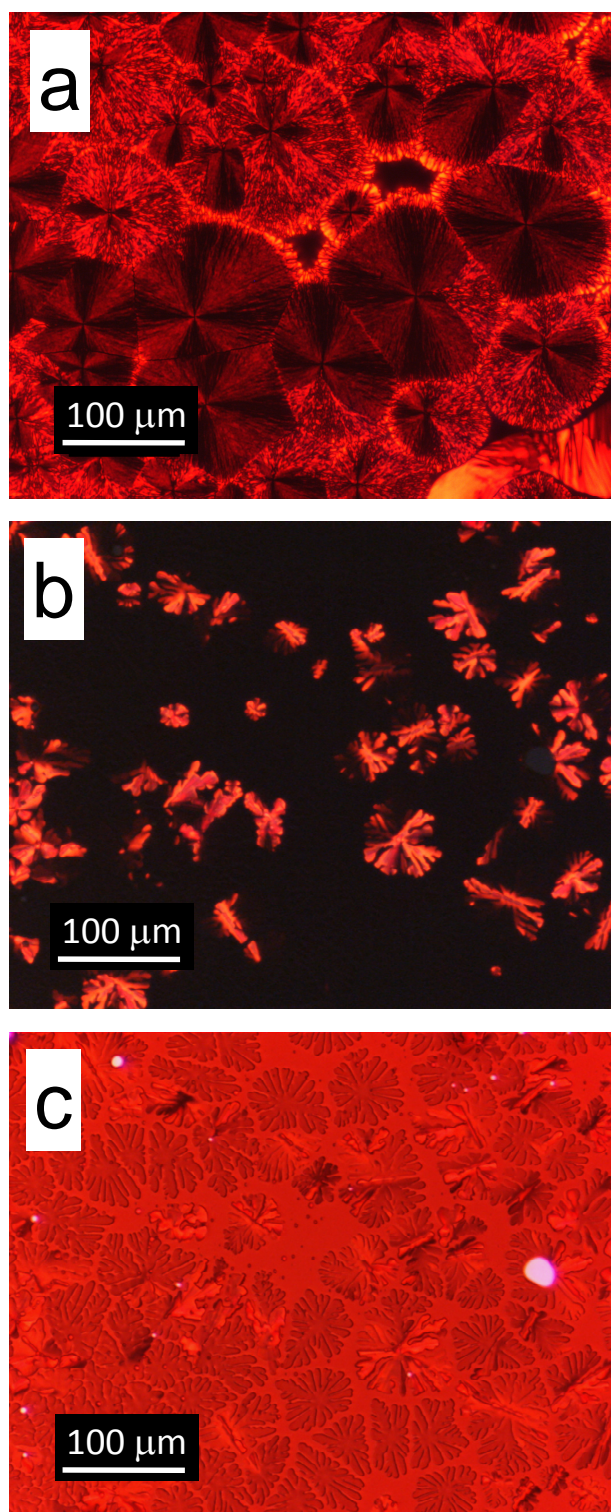


**Figure S3.** Additional optical microscopic images of textures of **PDBIs 1** and **3** (under crossed polarizers). (a) Crystalline lamellar phase ( $Cr_L$ ) of **PDBI-1** at 95 °C exhibiting a broken fanshaped texture. (b) Dendritic aggregates of  $Col_h$  phase of **PDBI-3** at 175 °C and (c) same film region, here a  $\lambda/4$  plate is utilized to visualize partial homeotropic ordering.

### 3. BIBLIOGRAPHY

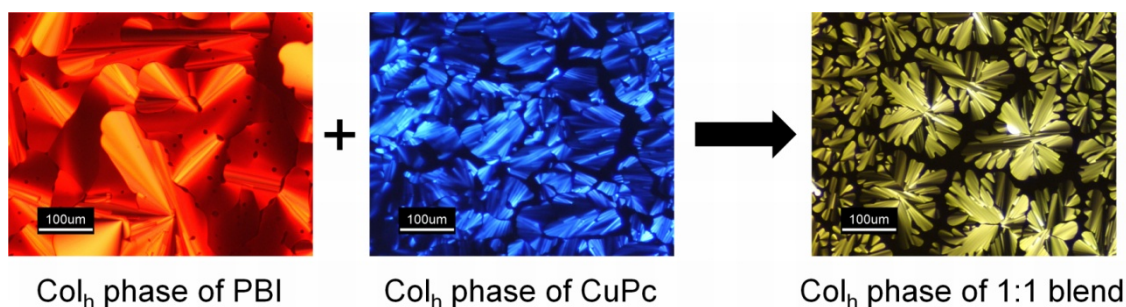
- (1) Zhang, F.; Bai, S.; Yap, G. P. A.; Tarwade, V.; Fox, J. M. *J. Am. Chem. Soc.* **2005**, *127*, 10590-10599.
- (2) Zhang, H.-C.; Huang, W.-S.; Pu, L. *J. Org. Chem.* **2001**, *66*, 481-487.
- (3) Howard, M. J.; Heirtzler, F. R.; Dias, S. I. G. *J. Org. Chem.* **2008**, *73*, 2548-2553.
- (4) Grolik, J.; Sieron, L.; Eilmes, J. *Tetrahedron Lett.* **2006**, *47*, 8209-8213.
- (5) Xue, C.; Sun, R.; Annab, R.; Abadi, D.; Jin, S. *Tetrahedron Lett.* **2009**, *50*, 853-856.
- (6) Mo, X.; Chen, H.-Z.; Wang, Y.; Shi, M.-M.; Wang, M. *J. Phys. Chem. B* **2005**, *109*, 7659-7663.
- (7) Wicklein, A.; Lang, A.; Muth, M.; Thelakkat, M. *J. Am. Chem. Soc.* **2009**, *131*, 14442-14453.

**6. SELF-ASSEMBLY OF DONOR/ACCEPTOR DISCOGENS IN  
BLENDS: A STRUCTURAL STUDY OF BINARY  
Cu-PHTHALOCYANINE – PERYLENE BISIMIDE SYSTEMS**

André Wicklein<sup>[a]</sup>, Devrim Atilla<sup>[b]</sup>, Vefa Ahsen<sup>[b]</sup> and Mukundan Thelakkat\*<sup>[a]</sup>

[a] Department of Macromolecular Chemistry I, Applied Functional Polymers, Universität Bayreuth, Universitätsstr. 30, 95440 Bayreuth, Germany, Fax: +49-921-55-3206  
E-mail: [mukundan.thelakkat@uni-bayreuth.de](mailto:mukundan.thelakkat@uni-bayreuth.de)

[b] Gebze Institute of Technology, Department of Chemistry, P.O. Box 141, 41400 Gebze, Kocaeli, Turkey



Prepared for submission.

## **ABSTRACT**

The thermotropic and structural properties of donor/acceptor blends have been studied comprehensively by a combination of differential scanning calorimetry (DSC), polarized optical microscopy (POM) and X-ray diffraction experiments (XRD). The blends under investigations consisted of chemically distinct, disk-like mesogens of similar dimensions, namely liquid crystalline copper phthalocyanines (**CuPc**) as donor and perylene bisimide (**PBI**) as acceptor material. Depending on the polarity of substituents at the periphery of the **CuPc** and **PBI** derivatives, different supramolecular organizations were obtained in binary blends. Differences in morphology arise due to distinct degrees of miscibility between the particular donor and acceptor mesogens. A mixed blend consisting of components with hydrophobic-hydrophilic interactions results in phase separation. In contrast, a substantially enhanced, mixed columnar hexagonal mesophase packing, as compared to pristine constituents was observed, when both mesogens have similar polarity. To elucidate the suitability of these systems for light-harvesting and charge-separation in photovoltaic devices, also optical properties of donor/acceptor blends in thin films have been studied by UV/Vis absorption and photoluminescence spectra.

## **INTRODUCTION**

Electron-donor and electron-acceptor molecules and their assemblies in thin films are of fundamental relevance for the development of large-area, structurally flexible, and low-temperature processable photovoltaic devices.<sup>1-3</sup> Self-assembly and self-organization processes represent powerful tools for the programmed generation of supramolecular assemblies with well-defined structures and morphologies in such systems.<sup>4-6</sup> In this context, also self-organizing organic semiconductor molecules like discotic liquid crystals (DLCs)<sup>7-9</sup> have found increased interest as solution processable materials for application in organic electronics.<sup>10,11</sup> Generally discogens consist of a rigid aromatic core with flexible side-chains attached at the periphery of the mesogen. The electronic transport properties along the  $\pi$ - $\pi$  stacking axis in self-assembled columnar superstructures with liquid-like dynamics of the discotic molecules provide the high charge carrier mobility within the bulk phase which can be decisive in organic electronics.<sup>12-14</sup> In such materials, charge carrier mobilities of up to  $1.3 \text{ cm}^2 \text{ V}^{-1}\cdot\text{s}^{-1}$ , in their liquid crystalline mesophases have been measured.<sup>12,15</sup> Liquid crystalline organization also increases the local order without creating too many grain boundaries on the macroscopic level as in the case of crystalline materials. Another crucial aspect in organic photovoltaics is the miscibility of their active components, which dramatically influences charge separation processes.<sup>16</sup> Schmidt-Mende et al. already demonstrated discotic-based solar cells with blends of hexabenzocoronenes and a crystalline perylene bisimide derivative.<sup>10</sup> Blending two discotic liquid crystalline semiconductors constitutes a novel approach to address issues of charge transport and charge separation processes. We study such interactions by employing two liquid crystalline materials, phthalocyanines and perylene bisimides, in order to control miscibility, morphology and

alignment in blends thereof. This can be tuned by utilizing the hydrophobic-hydrophilic interactions of the components. In general, both classes of materials, phthalocyanines<sup>17</sup> and PBIs<sup>18</sup> exhibit good charge carrier mobilities.

The mixing of two molecules that self-assemble into columnar superstructures is a complex process, since additional interactions between the different components complicate the description of such systems.<sup>19</sup> As illustrated in Figure 1, different supramolecular assemblies can be formed in such mixtures. For discotic-shaped molecules, that self-assemble in columnar superstructures by  $\pi$ - $\pi$  stacking interactions, the picture ranges from a macro- to meso- and even nanophase separation. In blends of discotic materials, novel stabilized or induced columnar mesophases<sup>20,21</sup> and a significantly higher level of order within the columnar stacks have been described.<sup>19</sup> Such stabilization effects have been attributed to complementary polytopic interactions (CPI) rather than charge-transfer interactions and were documented for disc-shaped molecules of different sizes.<sup>22,23</sup> Here an alternating intercolumnar ABAB ordering is suggested and blends with an exact 1:1 molar ratio have been reported. It is worthy to note that an enhanced columnar organization by CPI-interactions can also result in considerably higher charge carrier mobilities in donor/donor blends.<sup>24-26</sup> Recent studies report on miscibility between disc-like phthalocyanines and lath-like perylene bisimide mesogens.<sup>27,28</sup>

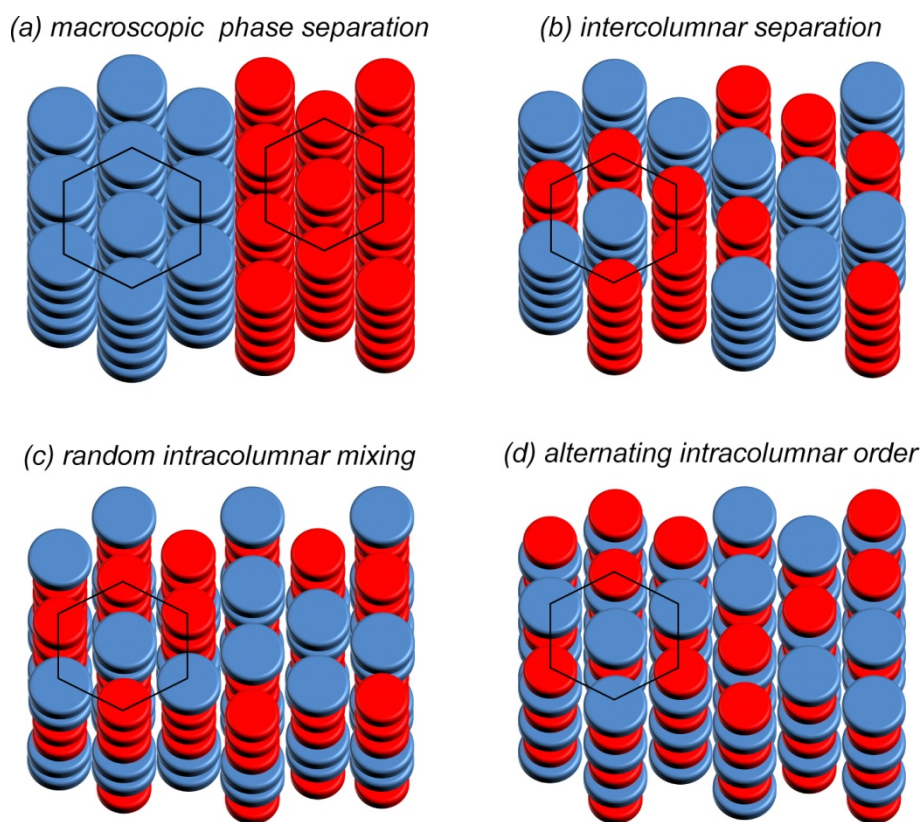
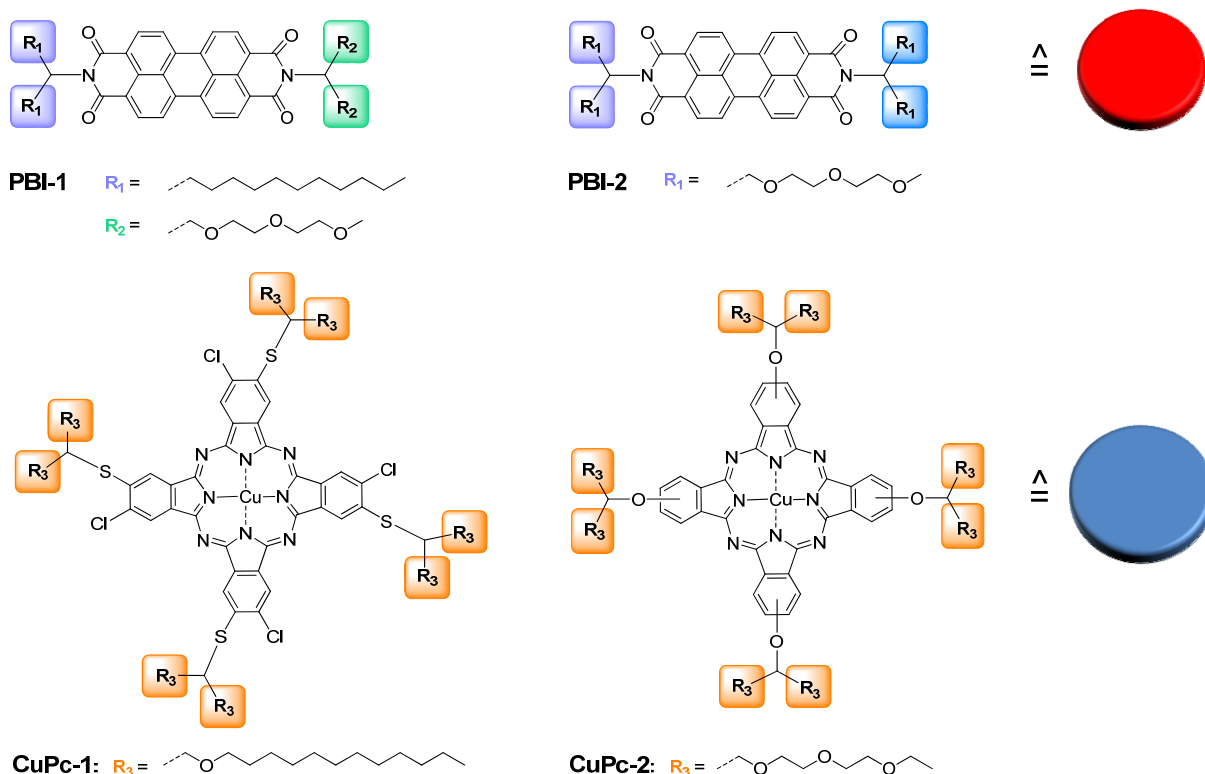


**Figure 1.** Different supramolecular organizations in a binary mixture of two discotic compounds with different molecular architectures: (a) macroscopic phase separation due to complete demixing, (b) intercolumnar separation due to partial miscibility of substituents, (c) random intracolumnar mixing, and (d) alternating intercolumnar order.

We have chosen two discotic materials which differ significantly in their electronic properties. Copper-phthalocyanines **CuPc-1** and **2** act as donor materials and perylene bisimides **PBI-1** and **2** as electron-acceptors (Scheme 1). They have been selected because both classes of materials strongly absorb in the visible wavelength region and have complementary absorption spectra. In addition, the blended molecules are compatible in size, permitting possible intracolumnar packing. All compounds under investigation bear flexible side chains at the periphery of the mesogen in order to guarantee sufficient solubility and to induce liquid crystalline mesophases. Additionally the materials exhibit distinct side-chain polarities due to either hydrophobic alkyl or hydrophilic oligooxyethylene (OEG) substituents. Thus **PBI-1** has both, branched alkyl and branched OEG substituents, whereas **PBI-2** carries only OEG side-chains. In contrast, **CuPc-1** is hydrophobic in nature, whereas **CuPc-2** is hydrophilic. Two different blends were analyzed in detail; **blend-1** is a mixture of **PBI-1** and **CuPc-1** and for **blend-2**, **PBI-2** was blended with **CuPc-2**. By choosing these blend compositions we wanted to study the effect of side-chain polarities on miscibility of the two components. Polarities are matched for the composition in **blend-2** and are less compatible for **blend-1**. As an example, we have chosen to study 1:1 (wt-%) blends of **PBI:CuPc**.



**Scheme 1.** Molecular structures of discotic liquid crystalline materials used in this study: perylene bisimides **PBI-1** and **2** and Cu-phthalocyanines **CuPc-1** and **2**.

## RESULTS AND DISCUSSION

All the pristine materials and their blends exhibit thermotropic liquid crystalline behaviour. Thermotropic behaviour of the blends and the individual components was analyzed by a combination of differential scanning calorimetry (DSC) and polarization optical microscopy (POM). Additionally temperature dependent X-ray scattering experiments were performed to unequivocally determine the structure of observed mesophases on the molecular level. DSC thermograms of the binary blends and the respective components are summarized in Figure 2 and phase transition temperatures with corresponding transitions enthalpies are presented in Table 1. Phase assignments and lattice parameters derived from XRD experiments for all materials under discussion are summarized in Table 2 and Table 3. Recent investigations have shown that **PBI-1** and **2** exhibit a columnar hexagonal mesophase ( $Col_h$ ) between 51 – 108 °C and 78 – 146 °C respectively.<sup>29</sup> At room temperature both perylene dyes are crystalline materials. On the other hand **CuPc-1** and **2** feature a columnar hexagonal ordering below 185 °C and 196 °C respectively; and both phthalocyanine derivatives are liquid crystalline, even at room temperature. In the following, the influence of hydrophobic-hydrophilic interactions of side-chains of **CuPcs** and **PBIs** on supramolecular organization in **blend-1** and **blend-2** are investigated in detail.

**Table 1.** Summary of the thermal behaviour, phase transition temperatures with corresponding transition enthalpies and phases<sup>[a]</sup> of blends and its pristine components.

material	phase transitions (T [°C] / $\Delta H$ [kJmol <sup>-1</sup> ])
<b>PBI-1</b> <sup>(a)</sup>	Cr (51 / 10.7) → $Col_h$ (108 / 3.0) → I I (105 / -2.9) → $Col_h$ (23 / -7.6) → Cr
<b>CuPc-1</b> <sup>(c)</sup>	Cr (1 / 32.9) → $Col_h$ (185 / 9.2) → I I (180 / -8.2) → $Col_h$ (-6 / -32.0) → Cr
<b>blend-1</b> <sup>(c)</sup>	Cr <sub>CuPc</sub> /Cr <sub>PBI</sub> (0 / 29.8) → $Col_{h\_CuPc}$ /Cr <sub>PBI</sub> (52 / 8.1) → $Col_{h\_CuPc}$ / $Col_{h\_PBI}$ (104 / 2.9) → $Col_{h\_CuPc}$ / $I_{PBI}$ (133 / 4.2) → $I_{CuPc}$ / $I_{PBI}$ $I_{CuPc}$ / $I_{PBI}$ (114 / -5.3) → $Col_{h\_CuPc}$ / $I_{PBI}$ (95 / -2.7) → $Col_{h\_CuPc}$ / $Col_{h\_PBI}$ (22 / -3.8) → $Col_{h\_CuPc}$ /Cr <sub>PBI</sub> (-10 / -32.6) → Cr <sub>CuPc</sub> /Cr <sub>PBI</sub>
<b>PBI-2</b> <sup>(c)</sup>	Cr <sub>1</sub> (78 / 15.2) → $Col_h$ (146 / 3.5) → I I (142 / -3.3) → $Col_h$ (40 / -1.8) → Cr <sub>2</sub> (22 / -3.7) → Cr <sub>1</sub>
<b>CuPc-2</b> <sup>(b)</sup>	$Col_h$ (196 / 1.9) → I I (191 / -2.2) → $Col_h$
<b>blend-2</b> <sup>(d)</sup>	$Col_h$ (265 / 3.7) → I I (244 / -2.7) → $Col_h$

[a] Cr = crystalline phase;  $Col_h$  = columnar hexagonal mesophase; I = isotropic phase. Obtained from DSC measurements under N<sub>2</sub>-atmosphere at a heating rate of: (a) 2 Kmin<sup>-1</sup>, (b) 5 Kmin<sup>-1</sup>, (c) 10 Kmin<sup>-1</sup> and (d) 40 Kmin<sup>-1</sup>.

DSC thermogram of **blend-1** (Fig. 2a) clearly demonstrates that all individual phase transitions of the components **PBI-1** and **CuPc-1** are still present in the blend. Only the enthalpy values are slightly influenced and the transition of **CuPc-1** from Col<sub>h</sub> → I is strongly shifted to lower temperatures from 185 °C to 133 °C. It is also interesting to note that XRD-studies of **blend-1** support changes in the Col<sub>h</sub> packing of **CuPc-1**. These findings indicate a strong phase separation between the two materials in **blend-1**.

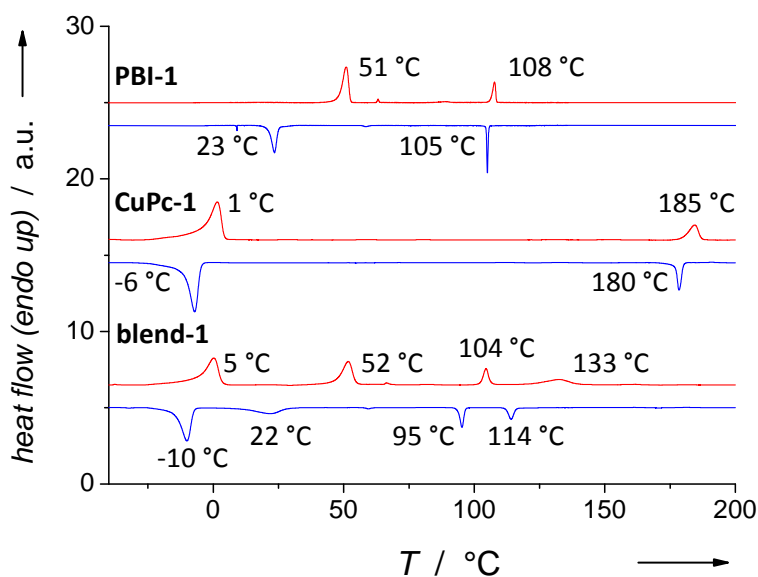


**Figure 2.** Differential Scanning Calorimetry (DSC) thermograms showing **blend-1** with thermograms of individual components respectively. Blue curves represent the first cooling and red curves the second heating cycle under N<sub>2</sub>-atmosphere. The corresponding phase transition temperatures are also presented.

Also POM observations are in accordance with the DSC results (Fig. 3). The focal conic texture of **PBI-1**, which is characteristic for its Col<sub>h</sub> ordering in the liquid crystalline phase (Fig. 3a, b) and the broken fan-shaped texture (Fig. 3c) as well as homeotropic domains with dendritic growth aggregates (Fig. 3d with λ/4-plate), typical for **CuPc-1** can be observed under crossed polarizers in **blend-1** in the relevant temperature regime in which only one component self-assembles. Thus, in **blend-1**, the transition of **CuPc-1** from the isotropic liquid to the Col<sub>h</sub>-phase can be observed at 115 °C, whereas **PBI-1** still remains in the isotropic phase at this temperature (Fig. 3e, f). The transition of **PBI-1** from I → Col<sub>h</sub> occurs at 95 °C, recognizable by the appearance of red-colored domains in the former black regions under crossed polarizers (Fig. 3g, h). Formation of characteristic textures of **PBI-1** seems to be hindered by the presence of Col<sub>h</sub>-phase of **CuPc-1**. In general a phase separation could be observed in **blend-1** during cooling down from the isotropic melt.

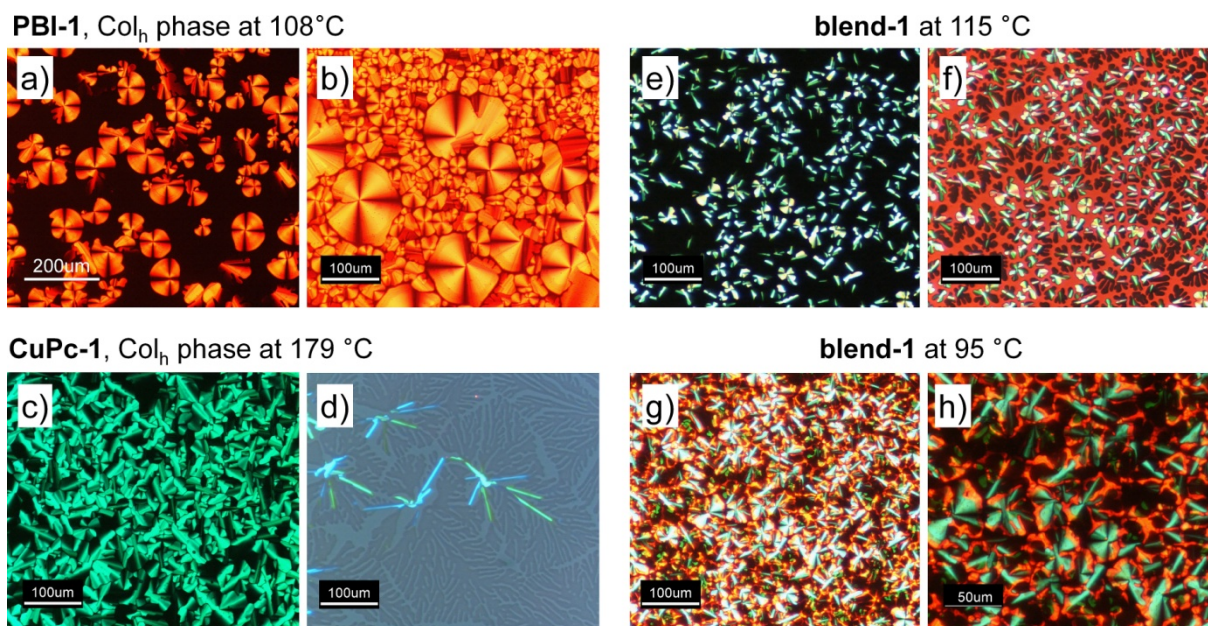


**Figure 3.** Optical microscopic images of textures of **PBI-1**, **CuPc-1** and **blend-1** (under crossed polarizers): (a-b) Focal conic texture of  $Col_h$ -phase of **PBI-1** at 108 °C. (c) Broken fan-shaped texture of  $Col_h$ -phase of **CuPc-1** at 179 °C. (d) Dendritic growth aggregates of  $Col_h$ -phase of **CuPc-1** at 179 °C, visualized by a  $\lambda/4$ -plate. (e)  $I \rightarrow Col_h$  transition of **CuPc-1** in **blend-1** at 115 °C. Black regions correspond to isotropic **PBI-1** (f) Same film position with a  $\lambda/4$ -plate. (g-h)  $I \rightarrow Col_h$  transition of **PBI-1** in **blend-1** at 95 °C.

This is further supported by X-ray diffraction experiments of the blend and its components (Fig. 4 and Table 2). At 105 °C the diffractogram of **blend-1** is an unperturbed superposition of the individual diffractograms (Fig. 4a). At this temperature XRD data are in accordance with a columnar hexagonal ordering of the mesogens of **CuPc-1**. We observed a 2D hexagonal lattice with  $a_{hex} = 34.9 \text{ \AA}$  which is in reasonable agreement with the (100), (110) and (210) Bragg reflections with the typical ratios of the d-values of  $1:1/\sqrt{3}:1/\sqrt{7}$ . A diffuse halo in the small angle regime can be observed for **PBI-1** at 105 °C. At 80 °C both materials are present in their  $Col_h$  phase and the additional reflections for the perylene component correspond to a 2D hexagonal lattice with  $a_{hex} = 23.0 \text{ \AA}$  can be detected. It is worthy to note that the hexagonal lattice for **CuPc-1** in **blend-1** is with  $a_{hex} = 33.8 \text{ \AA}$  smaller than in the discrete material at 80 °C with  $a_{hex} = 34.8 \text{ \AA}$ . Thus the diffractograms of **blend-1** consistently is represented by a superposition of its components (Fig. 4b). Moreover, at room temperature we could observe a crystalline phase for **PBI-1** and a  $Col_h$ -ordering for **CuPc-2**.

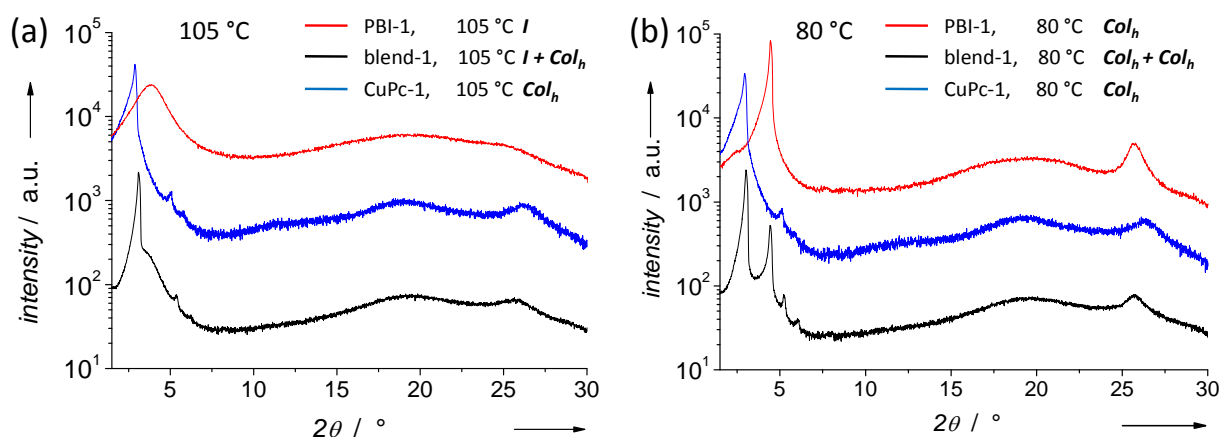


**Figure 4.** XRD diffractograms of **blend-1** and its components **PBI-1** and **CuPc-1** at 105 °C and 80 °C. For **blend-1** a superposition of the individual diffractograms of **PBI-1** and **CuPc-1** was found for all temperatures under investigations. Thus a macroscopic phase separation can be observed. (a) At 105 °C **CuPc-1** is in the  $Col_h$ -phase, whereas **PBI-1** still remains as isotropic liquid. (b) At 80 °C both materials are present in their  $Col_h$ -phase.

For **blend-2**, consisting of components both with similar side-chains of hydrophilic nature, a quite different thermotropic behavior can be seen. The components **PBI-2** and **CuPc-2**, both exhibit  $Col_h$  phases with clearing temperatures of 146 °C and 196 °C respectively. **PBI-2** crystallizes at 22 °C, whereas **CuPc-2** remains in the mesophase, even at 0 °C. In contrast to **blend-1**, only one, relatively broad reversible transition, can be observed in DSC measurements for **blend-2**; at 265 °C ( $3.7 \text{ kJmol}^{-1}$ ) during heating cycle (Fig. 5).

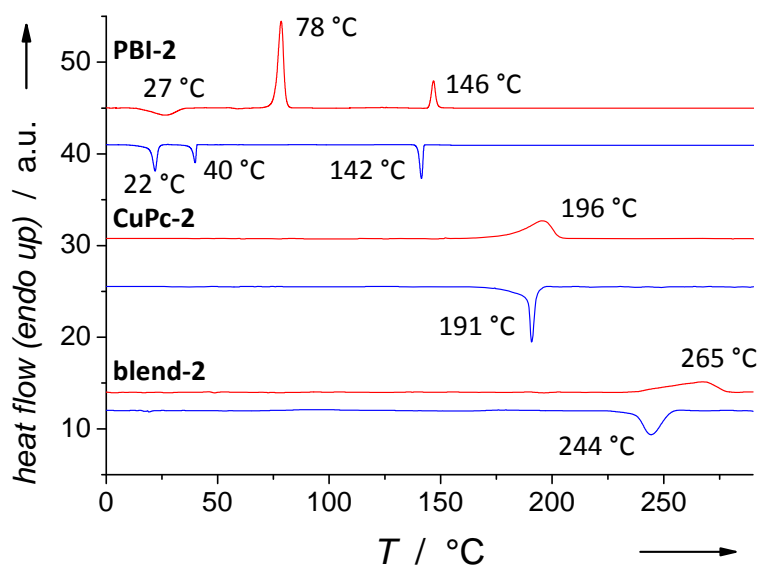
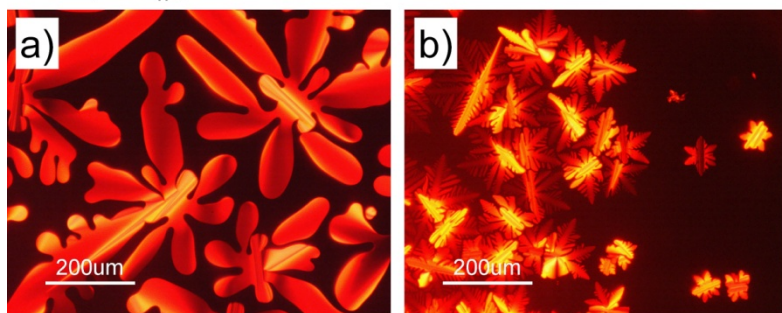


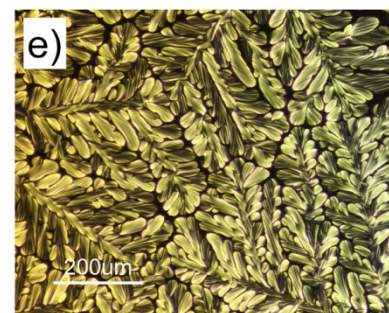
**Figure 5.** Differential Scanning Calorimetry (DSC) thermograms showing **blend-1** with thermograms of individual components respectively. Blue curves represent the first cooling and red curves the second heating cycle under  $N_2$ -atmosphere. The corresponding phase transition temperatures are also presented.

From POM and XRD experiments, this transition can be assigned as  $Col_h \rightarrow I$ . Thus **blend-2** clears at a considerably higher temperature than its discrete components. Furthermore this liquid crystalline phase exists over a broad temperature range, no crystallization was detected in the DSC cooling cycle until 0 °C. These results indicate a high miscibility of the two components and are in line with conclusions from POM experiments (Fig. 6). For **PBI-2** dendritic-growth aggregates are observed in the mesophase under crossed polarizers (Fig. 6a, b) and for **CuPc-2**, broken fan-shaped textures indicate a  $Col_h$ -ordering between 191 °C and room temperature (Fig. 6c). Again, homeotropic alignment was found for **CuPc-2** in the mesophase (Fig. 6d). For the corresponding binary **blend-2**, entirely new textures developed upon cooling from the isotropic melt at 230 °C (Fig. 6e, f). These textures feature highly branched dendritic growth structures and no crystallization takes place on cooling the sample to room temperature.

**PBI-2,  $Col_h$  phase at 144 °C**



**blend-2 at 230 °C**



**CuPc-2,  $Col_h$  phase at 191 °C**

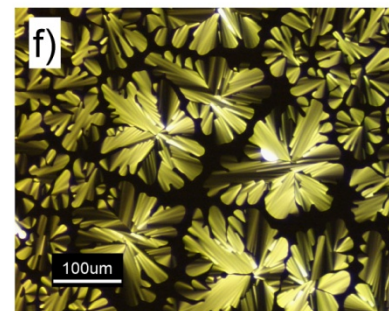
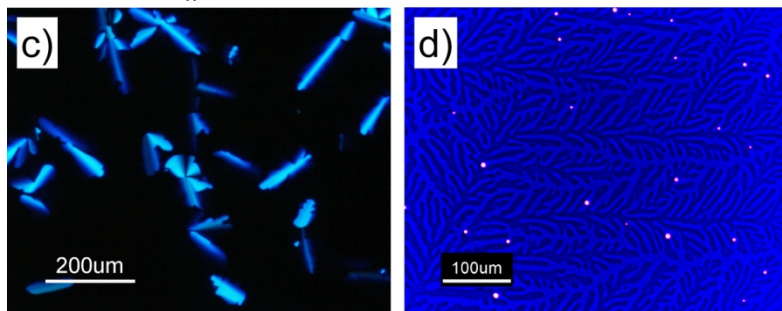


**Figure 6.** Optical microscopic images of textures of **PBI-2**, **CuPc-2** and **blend-2** (under crossed polarizers): (a-b) Dendritic textures of **PBI-2** in  $Col_h$  phase at 144 °C. (c) Broken fan-shaped texture of **CuPc-2** in  $Col_h$ -phase at 191 °C. Black regions correspond to an homeotropic alignment and (d) dendritic growth aggregates of **CuPc-2**, here a  $\lambda/4$ -plate is used to visualize partial homeotropic ordering. (e) Dendritic texture and (f) mixture of dendritic and fan-shaped texture of **blend-2** in  $Col_h$ -phase at 230 °C.

Further insight into the packing behavior of **blend-2** is provided by X-ray diffraction experiments (Fig. 7 and Table 3). **PBI-2** and **CuPc-2** possess columnar hexagonal lattices with values of  $a_{hex}$  values of 20.85 Å and 28.96 Å (at 100 °C) within their mesophases. At 240 °C, considerably above the clearing point of both components, a 2D-hexagonal lattice with  $a_{hex} = 26.0$  Å was found for **blend-2** (Tab. 2). Also the cores of the mesogens are stacked regularly at this temperature as

can be deduced from a diffuse reflection in the wide-angle regime. XRD-diffractograms at 160 °C at which **CuPc-2** exhibits a  $Col_h$ -phase and **PBI-2** is isotropic, **blend-2** remains in its  $Col_h$ -phase (Fig. 7a). The relatively sharp reflection at 25.82 ° in the wide angle regime depicts a strongly pronounced intracolumnar long-range order with a  $\pi$ - $\pi$  stacking distance of  $d_{\pi\pi} = 3.45$  Å for the cores of the mesogens in **blend-2**, compared to the relatively broad (001) reflection for **CuPc-2**. At 100 °C all three diffractograms represent a  $Col_h$ -ordering (Fig. 7b) and **blend-2** does not show the individual reflections originally present for **PBI-2** and **CuPc-2**. **Blend-2** remains in the liquid crystalline phase even at room-temperature, although **PBI-2** is crystalline at this temperature (Fig. 7c). Thus the columnar phase of **blend-2** is more ordered (extension of  $\pi$ - $\pi$  stacking over a long distance of correlation along the column axis) and the phase stability is extended by 120 °C compared to the columnar hexagonal mesophase of pure **PBI-2**. Additionally crystallization of **PBI-2** is suppressed in **blend-2** resulting in a room temperature  $Col_h$ -phase in the binary blend. The dimensions of the hexagonal unit cell of **blend-2** lies with  $a_{hex} = 24.75$  Å in between the size of its components with  $a_{hex} = 20.85$  Å for **PBI-2** and  $a_{hex} = 28.96$  Å for **CuPc-2** (values collected at 100 °C).

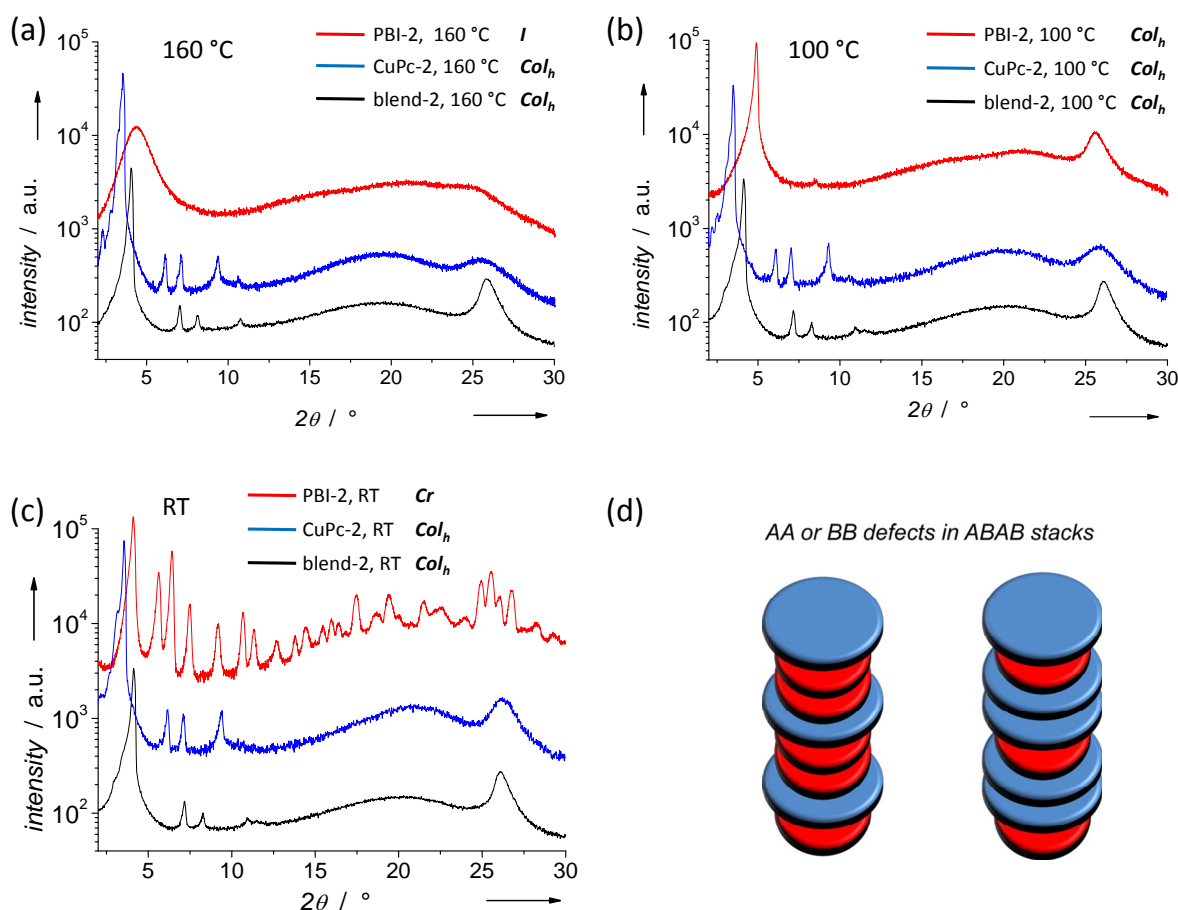


**Figure 7.** XRD diffractograms of **blend-2** and its components **PBI-2** and **CuPc-2** at 160 °C, 100 °C and room temperature. (a) At 160 °C **CuPc-2** is in the  $Col_h$ -phase, whereas **PBI-2** is an isotropic liquid. For **blend-2** a  $Col_h$ -phase with enhanced intracolumnar ordering is observed. (b) At 100 °C all diffractograms show  $Col_h$ -ordering. (c) At RT **blend-2** invariably resides in  $Col_h$ -ordering, whereas **PBI-2** features crystalline reflections. (d) AA or BB defects in ABAB stacks of discotic columns.

The fact that there is a single intracolumnar repeat distance  $d_{\pi\pi}$  and a single 2D-hexagonal lattice shows that there cannot be segregated stacks of donor and acceptor respectively. There is probably an intracolumnar mixing (Fig. 1c), which can also be described as alternating ABAB structure with AA or BB defects (Fig. 7d). As the individual components are conformable in size for both blend systems, we assume that the different degrees of miscibility observed in this study are related to the different hydrophobic-hydrophilic interactions of side chains. For **blend-1** with different side-chain polarities of the components, a phase separation was observed, whereas for **blend-2** with matched polarities a new stabilized columnar mesophase with an enhanced columnar organization was obtained.

**Table 2.** X-ray diffraction data of liquid crystalline phases of **PBI-1**, **CuPc-1** and respective mesophases of components in **blend-1**: 2D Lattice parameters  $a_{\text{hex}}$  as determined from temperature dependent X-ray diffraction experiments.

material	$T$ [°C]	$2\theta^{[a]}$ [°]	$d_{\text{obs}}^{[b]}$ [Å]	$d_{\text{calc}}^{[b]}$ [Å]	(hkl) <sup>[c]</sup>	mesophase parameters
<b>PBI-1</b>	80	4.44	19.89	-	(100)	$\text{Col}_h$ $a_{\text{hex}} = 22.97 \text{ \AA}$
		7.74	11.41	11.48	(110)	
		25.72	3.46	-	(001)	
<b>CuPc-1</b>	105	2.91	30.23	-	(100)	$\text{Col}_h$ $a_{\text{hex}} = 34.91 \text{ \AA}$
		5.06	17.45	17.45	(110)	
		5.82	15.17	15.12	(200)	
		26.16	3.41	-	(001)	
	80	2.93	30.13	-	(100)	$\text{Col}_h$ $a_{\text{hex}} = 34.79 \text{ \AA}$
		5.09	17.35	17.40	(110)	
		5.88	15.02	15.07	(200)	
		26.28	3.39	-	(001)	
<b>blend-1 (PBI-1)</b>	80	4.44	19.89	-	(100)	$\text{Col}_h$ $a_{\text{hex}} = 22.97 \text{ \AA}$
		25.75	3.46	-	(001)	
<b>blend-1 (CuPc-1)</b>	80	3.02	29.23	-	(100)	$\text{Col}_h$ $a_{\text{hex}} = 33.75 \text{ \AA}$
		5.24	16.85	16.88	(110)	
		6.06	14.57	14.61	(200)	
		25.75	3.46	.	(001)	

[a] Diffraction angle, [b] observed and calculated diffraction spacings, [c] Miller indices.

Self-Assembly of Donor/Acceptor Discogens in Blends: A Structural Study of Binary  
Cu-Phthalocyanine - Perylene Bisimide Systems

**Table 3.** X-ray diffraction data of liquid crystalline phases of **PBI-2**, **CuPc-2** and induced mesophase in **blend-2**: 2D Lattice parameters  $a_{\text{hex}}$  as determined from temperature dependent X-ray diffraction experiments.

material	$T$ [°C]	$2\theta^{[a]}$ [°]	$d_{\text{obs}}^{[b]}$ [Å]	$d_{\text{calc}}^{[b]}$ [Å]	$(hkl)^{[c]}$	mesophase parameters
<b>PBI-2</b>	100	4.89	18.06	-	(100)	$\text{Col}_h$
		8.55	10.33	10.42	(110)	$a_{\text{hex}} = 20.85 \text{ \AA}$
		25.52	3.49	-	(001)	
<b>CuPc-2</b>	160	3.52	25.08	-	(100)	$\text{Col}_h$
		6.12	14.43	14.48	(110)	$a_{\text{hex}} = 28.96 \text{ \AA}$
		7.07	12.49	12.54	(200)	
		9.34	9.46	9.48	(210)	
		10.58	8.34	8.36	(300)	
		25.46	3.50	-	(001)	
	100	3.52	25.08	-	(100)	$\text{Col}_h$
		6.12	14.43	14.50	(110)	$a_{\text{hex}} = 28.96 \text{ \AA}$
		7.06	12.51	12.54	(200)	
		9.36	9.44	9.48	(210)	
		25.98	3.43	-	(001)	
	RT	3.54	24.94	-	(100)	$\text{Col}_h$
		6.16	14.34	14.40	(110)	$a_{\text{hex}} = 28.80 \text{ \AA}$
		7.08	12.48	12.47	(200)	
		9.40	9.40	9.43	(210)	
26.24		3.39	-	(001)		
<b>blend-2</b>	240	3.92	22.52	-	(100)	$\text{Col}_h$
		6.80	12.99	13.00	(110)	$a_{\text{hex}} = 26.00 \text{ \AA}$
		7.84	11.27	11.26	(200)	
		10.36	8.53	8.51	(210)	
		25.62	3.47	-	(001)	
	160	4.06	21.75	-	(100)	$\text{Col}_h$
		7.04	12.55	12.56	(110)	$a_{\text{hex}} = 25.11 \text{ \AA}$
		8.14	10.85	10.88	(200)	
		10.74	8.23	8.22	(210)	
		25.82	3.45	-	(001)	
	100	4.12	21.43	-	(100)	$\text{Col}_h$
		7.16	12.34	12.37	(110)	$a_{\text{hex}} = 24.75 \text{ \AA}$
		8.28	10.67	10.72	(200)	
		10.92	8.10	8.10	(210)	
		26.10	3.42	-	(001)	
	RT	4.20	21.02	21.02	(100)	$\text{Col}_h$
		7.30	12.10	12.14	(110)	$a_{\text{hex}} = 24.27 \text{ \AA}$
		8.40	10.52	10.51	(200)	
11.16		7.92	7.94	(210)		
26.28		3.39	-	(001)		

[a] Diffraction angle, [b] observed and calculated diffraction spacings, [c] Miller indices.

In order to elucidate the suitability of these binary blend systems of different miscibility for light-harvesting and possible energy or charge transfer, also optical properties of donor/acceptor thin films have been studied by UV/Vis absorption and photoluminescence spectra. Thin films were prepared by spin-coating from 2.0 wt-%  $\text{CHCl}_3$  solutions. Figure 8a, b summarizes UV/Vis absorption spectra of spin-coated films of **blend-1** and **2**. Also spectra of the corresponding components in dilute  $\text{CHCl}_3$  solution and films are shown in order to identify their individual contributions to absorption behaviour. **PBI-1** and **PBI-2** show identical absorption behavior in solution, as the nodes in the HOMO and LUMO at the imide nitrogen reduce electronic coupling of the perylene bisimide core and the imide substituents to a minimum.<sup>30</sup> Both dyes exhibit the characteristic finger-print vibronic fine structure of the electronic  $S_0$ - $S_1$  transitions of isolated PBI-dyes with peaks at about 525, 489, 458 and 432 nm respectively. The solution spectrum of **CuPc-1** shows a sharp peak at 696 nm (Q-band), whereas this peak is blue-shifted for **CuPc-2** to 682 nm. Both CuPc-dyes show a Soret band at around 340 nm, originating from  $\pi \rightarrow \pi^*$  transitions.

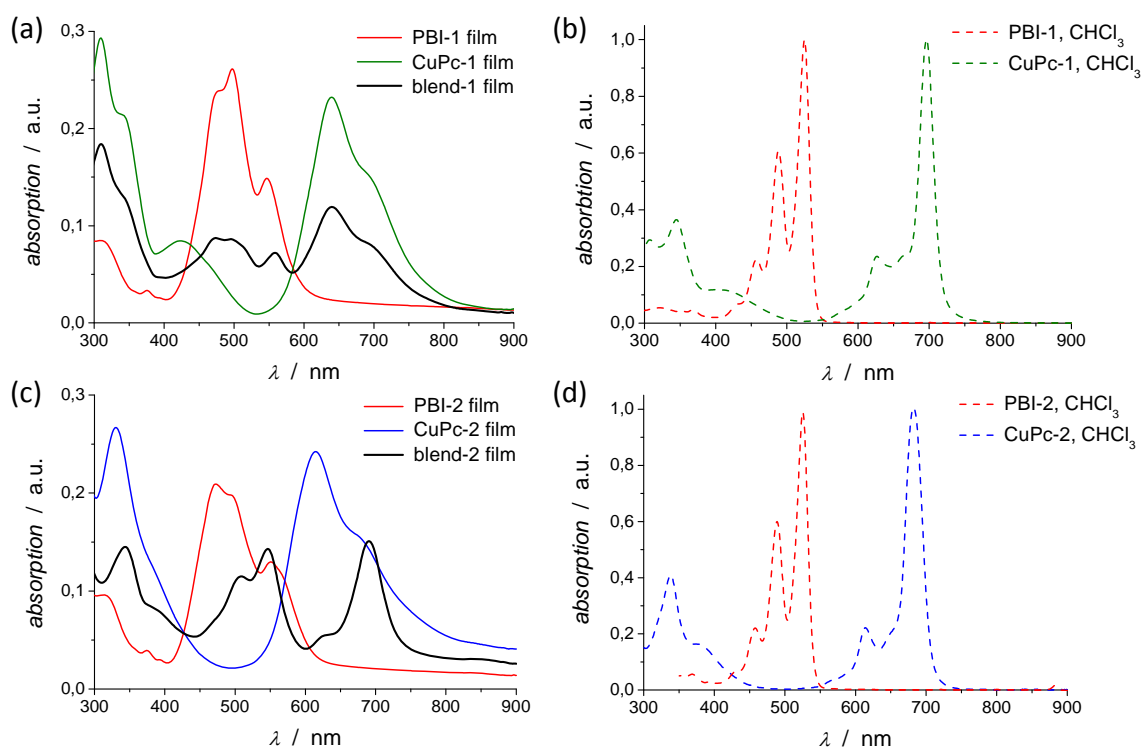


**Figure 8.** UV/Vis-absorption spectra of: (a) **Blend-1** film and corresponding components **PBI-1** and **CuPc-1** in film and as  $1 \cdot 10^{-5}$  M  $\text{CHCl}_3$  solution. (b) **Blend-2** film and corresponding components **PBI-2** and **CuPc-2** in film and as  $1 \cdot 10^{-5}$  M  $\text{CHCl}_3$  solution. Films were prepared by spin-coating from 2.0 wt-%  $\text{CHCl}_3$  solutions.

In thin films, pure **PBI-1** and **PBI-2** absorb between 400 and 600 nm with a maximum at  $\lambda_{\text{max}} = 497$  nm and 472 nm respectively. The decreased intensity of the first vibronic transition as compared to diluted solution spectra and the broadened red-shifted absorption are a typical feature of highly aggregated PBI-dyes.<sup>31</sup> Complementary, **CuPc-1** and **CuPc-2** absorb between 600

and 800 nm in thin films with an absorption maximum of the Q-band at  $\lambda_{\text{max}} = 640$  nm and 615 nm respectively. The broadening and hypsochromic shift of the Q-band, as compared to solution spectra, is indicative for aggregated phthalocyanine moieties with a cofacial arrangement in the spin-coated film.<sup>32,33</sup> For the film of **blend-1**, the absorption spectrum displays a superposition of the individual components contribution with a cofacial arrangement of **CuPc-1** and aggregated **PBI-1** (Fig. 8a). In contrast, **blend-2** system exhibits a rather different absorption behavior than its components (Fig. 8b). Here the absorption behavior of the blend is not a superposition of individual contributions as **PBI-2** and **CuPc-2** have distinct fine structures. Compared to solution spectra, **blend-2** displays an absorption spectra in thin film typical for the isolated chromophores. This finding suggests the dissolution of one component in the other and supports a high degree of miscibility between **PBI-2** and **CuPc-2**. This can lead to different packing of the mesogens in **blend-2** as in the discrete material, as observed in XRD. In both blend systems the whole wavelength regime of 400 - 800 nm can be used for efficient light harvesting in this system.

Pure perylene bisimide films exhibit intense fluorescence upon excitation at  $\lambda = 497$  nm for **PBI-1** and at  $\lambda = 546$  nm for **PBI-2** (Fig. 9). For both phthalocyanine dyes, no photoluminescence could be detected in thin films. Upon excitation of the PBI-dyes in either of the blend films, a strong fluorescence quenching by the respective copper-phthalocyanine dye was observed. This indicates efficient photoinduced charge transfer or possible energy transfer in both donor/acceptor systems.

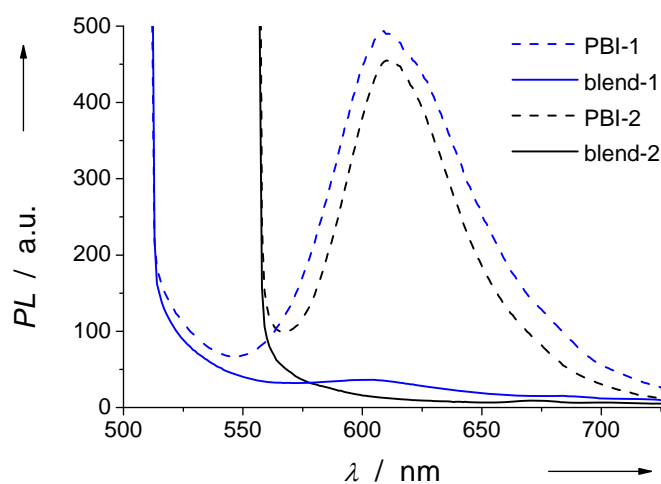


**Figure 9.** Photoluminescence spectra of thin films of perylene bisimides **PBI-1** and corresponding **blend-1** upon excitation at  $\lambda = 497$  nm and **PBI-2** with corresponding **blend-2** upon excitation at  $\lambda = 546$  nm.

## **CONCLUSION**

In conclusion, two different donor/acceptor blend systems consisting of copper-phthalocyanine and perylene bisimide dyes have been prepared. Depending on the chemical nature of side chain substituents, distinct supramolecular organizations were obtained in these binary blend systems. A phase separation was observed for **blend-1** consisting of components with opposed polarities, whereas a substantially enhanced columnar hexagonal mesophase ( $Col_h$ ) range combined with extended intracolumnar long-range order was observed for mesogens with similar polarities in **blend-2**. As all discogens are compatible in size, the difference in morphology can be attributed to the degree of miscibility between donor and acceptor. Additionally both blend systems exhibit strong absorption in the whole visible wavelength regime and have shown efficient photoinduced charge transfer upon perylene excitation in photoluminescence experiments. Further investigations are directed towards characterization of these promising blend systems in bulk heterojunction photovoltaic devices.

## **EXPERIMENTAL**

Differential scanning calorimetry (DSC) was carried out with a Perkin Elmer differential scanning calorimeter (Diamond) with heating and cooling rates between 2 to 40 K/min under  $N_2$  atmosphere. The instrument was calibrated with indium standards before measurements. Phase transitions were also examined by a polarization optical microscope (POM) Nikon Diaphot 300 with a Mettler FP 90 temperature-controlled hot stage. X-ray diffraction measurements were performed on a Huber Guinier Diffraktometer 6000 equipped with a Huber quartz monochromator 611 with  $Cu-K_{\alpha 1}$ : 1.54051 Å. UV/Vis absorption spectra were recorded with a Perkin Elmer Lambda 900 spectrophotometer. Photoluminescence spectra were acquired on a Shimadzu RF 5301 PC spectrofluorophotometer. Perylene bisimides **PBI-1** or **2** were synthesized according to published procedures.<sup>29</sup> The synthesis of copper phthalocyanines **CuPc-1** and **2** will be described elsewhere.<sup>34</sup> Blends of **CuPc-1** or **2** with **PBI-1** or **2** were prepared by simple mixing of concentrated solutions of the individual components in benzene, followed by freeze-drying. We have chosen to document this study for a **PBI:CuPc** 1:1 wt-% ratio respectively (likewise a 2.5 : 1 molar ratio in **blend-1** and a 2:1 molar ration in **blend-2**). Thin films were obtained by spin-coating from 2.0 wt-%  $CHCl_3$  solutions onto precleaned quartz substrates.

## **BIBLIOGRAPHY**

- (1) Halls, J. J. M.; Walsh, C. A.; Greenham, N. C.; Marseglia, E. A.; Friend, R. H.; Moratti, S. C.; Holmes, A. B. *Nature* **1995**, *376*, 498-500.
- (2) Gunes, S.; Neugebauer, H.; Sariciftci, N. S. *Chem. Rev.* **2007**, *107*, 1324-1338.
- (3) Coakley, K. M.; McGehee, M. D. *Chem. Mater.* **2004**, *16*, 4533-4542.
- (4) Wicklein, A.; Ghosh, S.; Sommer, M.; Würthner, F.; Thelakkat, M. *ACS Nano* **2009**, *3*, 1107-1114.
- (5) Sommer, M.; Lindner, S. M.; Thelakkat, M. *Adv. Funct. Mater.* **2007**, *17*, 1493-1500.
- (6) Lindner, S. M.; Hüttner, S.; Chiche, A.; Thelakkat, M.; Krausch, G. *Angew. Chem. Int. Ed.* **2006**, *45*, 3364-3368.
- (7) Laschat, S.; Baro, A.; Steinke, N.; Giesselmann, F.; Haegele, C.; Scalia, G.; Judele, R.; Kapatsina, E.; Sauer, S.; Schreivogel, A.; Tosoni, M. *Angew. Chem. Int. Ed.* **2007**, *46*, 4832-4887.
- (8) Kumar, S. *Chem. Soc. Rev.* **2006**, *35*, 83-109.
- (9) Destrade, C.; Foucher, P.; Gasparoux, H.; Tinh, N. H.; Levelut, A. M.; Malthete, J. *Mol. Cryst. Liq. Cryst.* **1984**, *106*, 121-146.
- (10) Schmidt-Mende, L.; Fechtenkötter, A.; Müllen, K.; Moons, E.; Friend, R. H.; MacKenzie, J. D. *Science* **2001**, *293*, 1119-1122.
- (11) O'Neill, M.; Kelly, S. M. *Adv. Mater.* **2003**, *15*, 1135-1146.
- (12) Sergeev, S.; Pisula, W.; Geerts, Y. H. *Chem. Soc. Rev.* **2007**, *36*, 1902-1929.
- (13) Pisula, W.; Zorn, M.; Chang, J. Y.; Müllen, K.; Zentel, R. *Macromol. Rapid Commun.* **2009**, *30*, 1179-1202.
- (14) Adam, D.; Schuhmacher, P.; Simmerer, J.; Haussling, L.; Siemensmeyer, K.; Etzbachi, K. H.; Ringsdorf, H.; Haarer, D. *Nature* **1994**, *371*, 141-143.
- (15) An, Z.; Yu, J.; Jones, S. C.; Barlow, S.; Yoo, S.; Domercq, B.; Prins, P.; Siebbeles, L. D. A.; Kippelen, B.; Marder, S. R. *Adv. Mater.* **2005**, *17*, 2580-2583.
- (16) Yu, G.; Gao, J.; Hummelen, J. C.; Wudl, F.; Heeger, A. J. *Science* **1995**, *270*, 1789-1791.
- (17) Warman, J. M.; de Haas, M. P.; Dicker, G.; Grozema, F. C.; Piris, J.; Debije, M. G. *Chem. Mater.* **2004**, *16*, 4600-4609.
- (18) Horowitz, G.; Kouki, F.; Spearman, P.; Fichou, D.; Nogues, C.; Pan, X.; Garnier, F. *Adv. Mater.* **1996**, *8*, 242-245.
- (19) Pisula, W.; Kastler, M.; Wasserfallen, D.; Robertson, J. W. F.; Nolde, F.; Kohl, C.; Müllen, K. *Angew. Chem. Int. Ed.* **2006**, *45*, 819-823.

- (20) Tschierske, C. *Annu. Rep. Prog. Chem., Sect. C: Phys. Chem.* **2001**, *97*, 191-267.
- (21) Ringsdorf, H.; Bengs, H.; Karthaus, O.; Wüstefeld, R.; Ebert, M.; Wendorff, J. H.; Kohne, B.; Praefcke, K. *Adv. Mater.* **1990**, *2*, 141-144.
- (22) Arikainen, E. O.; Boden, N.; Bushby, R. J.; Owen, R. L.; Vinter, J. G.; Wood, A. *Angew. Chem. Int. Ed.* **2000**, *39*, 2333-2336.
- (23) Boden, N.; Bushby, R. J.; Cooke, G.; Lozman, O. R.; Lu, Z. *J. Am. Chem. Soc.* **2001**, *123*, 7915-7916.
- (24) Wegewijs, B. R.; Siebbeles, L. D. A.; Boden, N.; Bushby, R. J.; Movaghar, B.; Lozman, O. R.; Liu, Q.; Pecchia, A.; Mason, L. A. *Phys. Rev. B: Condens. Matter* **2002**, *65*, 245112.
- (25) Pecchia, A.; Lozman, O. R.; Movaghar, B.; Boden, N.; Bushby, R. J.; Donovan, K. J.; Kreouzis, T. *Phys. Rev. B: Condens. Matter* **2002**, *65*, 104204.
- (26) Kreouzis, T.; Scott, K.; Donovan, K. J.; Boden, N.; Bushby, R. J.; Lozman, O. R.; Liu, Q. *Chem. Phys.* **2000**, *262*, 489-497.
- (27) Zucchi, G. I.; Viville, P.; Donnio, B.; Vlad, A.; Melinte, S.; Mondeshki, M.; Graf, R.; Spiess, H. W.; Geerts, Y. H.; Lazzaroni, R. *J. Phys. Chem. B* **2009**, *113*, 5448-5457.
- (28) Zucchi, G.; Donnio, B.; Geerts, Y. H. *Chem. Mater.* **2005**, *17*, 4273-4277.
- (29) Wicklein, A.; Lang, A.; Muth, M.; Thelakkat, M. *J. Am. Chem. Soc.* **2009**, *131*, 14442-14453.
- (30) Langhals, H.; Demmig, S.; Huber, H. *Spectrochim. Acta A* **1988**, *44A*, 1189-93.
- (31) Gregg, B. A. *J. Phys. Chem.* **1996**, *100*, 852-859.
- (32) McKeown, N. B. *in Phthalocyanine Materials: Synthesis, Structure and Function*; Cambridge University Press: Cambridge, 1998.
- (33) Hassan, B. M.; Li, H.; McKeown, N. B. *J. Mater. Chem.* **2000**, *10*, 39-45.
- (34) Atilla, D. **2010**, *to be published*.



## 7. SELF-ASSEMBLY OF SEMICONDUCTOR NANOWIRES FOR PHOTO-INDUCED CHARGE SEPARATION

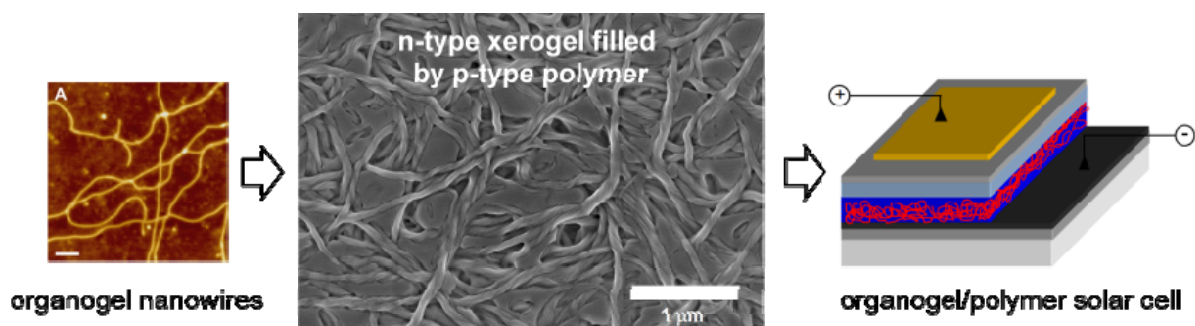
André Wicklein<sup>†</sup>, Suhrit Ghosh<sup>‡</sup>, Michael Sommer<sup>†</sup>, Frank Würthner<sup>\*\*,‡</sup> and Mukundan Thelakkat<sup>\*,†</sup>

<sup>†</sup>University of Bayreuth, Macromolecular Chemistry I – Applied Functional Polymers, Universitätsstr. 30, 95440 Bayreuth, Germany.

<sup>‡</sup>Universität Würzburg, Institut für Organische Chemie, Am Hubland, 97074 Würzburg, Germany.

\*Corresponding Author. E-mail: mukundan.thelakkat@uni-bayreuth.de. Tel: (+49) 921-55-3204.

\*\*Corresponding Author. E-mail: wuerthner@chemie.uni-wuerzburg.de. Tel: (+49) 931-888-5340.



**ABSTRACT**

We investigated an innovative concept of general validity based on an organogel/polymer system to generate donor-acceptor nanostructures suitable for charge generation and charge transport. An electron conducting (acceptor) perylene bisimide organogelator forms nanowires in suitable solvents during gelation process. This phenomenon was utilized for its self-assembly in an amorphous hole conducting (donor) polymer matrix to realize an interpenetrating donor-acceptor interface with inherent morphological stability. The self-assembly and interface generation were carried out either step-wise or in a single-step. Morphology of the donor-acceptor network in thin films obtained via both routes were studied by a combination of scanning electron microscopy and atomic force microscopy. Additionally, photoinduced charge separation and charge transport in these systems were tested in organic solar cells. Fabrication steps of multi-layer organogel/polymer photovoltaic devices were optimized with respect to morphology and surface roughness by introducing additional smoothing layers and charge injection/blocking layers. An inverted cell geometry was used here in which electrons are collected at the bottom electrode and holes at the top electrode. The simultaneous preparation of the interface exhibits almost three-fold improvement in device characteristics compared to the successive method. The device characteristics under AM1.5 spectral conditions and  $100 \text{ mW/cm}^2$  for the simultaneous preparation route are: short circuit current  $J_{sc} = 0.28 \text{ mAcm}^{-2}$ , open circuit voltage  $V_{oc} = 390 \text{ mV}$ , fill factor  $FF = 38\%$  and a power conversion efficiency  $\eta = 0.041 \%$ .

**Keywords:** Donor-Acceptor Heterojunction, Nanostructure, Self-Assembly, Organogelator, Photovoltaic Devices, Solar Cells.

## **INTRODUCTION**

Electronic devices made of organic materials, in particular photovoltaic devices, were intensively studied during the last years owing to their potential regarding cheap processing costs, their application to large areas, and their compatibility with flexible substrates.<sup>1,2</sup> In organic solar cells, charge separation of the strongly bound electron-hole pairs, so called excitons is enabled at a donor-acceptor (DA) interface or heterojunction upon illumination, where they dissociate and then drift towards the respective electrodes. For an ideal heterojunction, an interpenetrating network between an electron-acceptor and -donor material with a suitable concentration gradient in the two materials towards the respective charge collecting electrodes is the most ideal one. This led to the introduction of the bulk heterojunction concept.<sup>3-5</sup> There are different approaches to generate organic bulk heterojunctions. Blending donor and acceptor components has led to highly efficient solar cell systems, even though the desired stable bicontinuous morphology in the nanometer scale in entire bulk is still difficult to achieve.<sup>6</sup> It is desirable not only to match the domain size of the components and the exciton diffusion length, but also to obtain equilibrium nanostructures which assure morphological and device stability. Therefore, generating "nanostructured bulk heterojunctions" that guarantee an adequate percolation of charges is the ultimate goal. One of the ways to accomplish this task has already been demonstrated by some of us, in which equilibrium nanostructures have been realized using self-organization of semiconductor diblock copolymers.<sup>7,8</sup> Other concepts include so-called double cable polymers<sup>9</sup> and supramolecular p-n-heterojunctions.<sup>10-13</sup>

Organogelators in general form physical networks originating from nanostructures, extending over large area and volume.<sup>14-17</sup> The self-assembly process of gelators results in the formation of one-dimensional supramolecular fibers that are bundled up together and entangled at nodes to form a complex fibrous three-dimensional physical network. The solvent molecules are entrapped by this network that interlaces the whole system. These unique structural features are more or less maintained in the xerogel, obtained after the removal of the solvent, if sudden aggregation leading to loss of structures during drying is avoided. The fundamental question in this work is whether this supramolecular approach can be elegantly realized using an acceptor-type organogelator, which can then be embedded into a donor-type matrix or vice versa. Such a self-organized, nanostructured functional material incorporated into another functional material, without hindering the self-assembly process to a large extent, would provide a large interface area suitable for charge separation. It also provides charge percolation pathways on the nanometer scale. Perylene bisimides (PBI) are excellent electron conducting (acceptor) dyes exhibiting high charge carrier mobility.<sup>18</sup> Similarly there are a variety of hole conductor materials (donors) such as tetraphenyl benzidines<sup>19</sup>, conjugated polymers<sup>20</sup> with high charge carrier mobility. It is also worthy to note that photoinduced charge separation in general has already been reported in perylene bisimide - hole conductor polymer blend systems.<sup>21-23</sup> Organogelators have also been successfully employed in quasi-solid-state dye sensitized solar cells in order to gelate the liquid electrolyte. Here the organogelators do not have any electronic functions

suitable for charge separation and charge transport.<sup>24,25</sup> But a direct use of a semiconducting organogel as active material in donor-acceptor systems is not yet reported.

Based on this idea we describe here an innovative novel concept to create a nanostructured donor-acceptor interface by combining hydrogen bond-directed self-assembly of an n-type organogelator, perylene bisimide (PBI)<sup>26,27</sup> with a p-type polymer, poly(vinyl-dimethoxytetraphenylbenzidine) (pvDMTPD)<sup>28</sup> (Figure 1). Due to non-covalent hydrogen-bonding and  $\pi$ - $\pi$ -stacking interactions, the PBI organogelator forms well defined  $\pi$ -stacks with favorable J-type packing of the dyes.<sup>26</sup> AFM height image of semiconductor nanowires as formed by spin-coating from diluted gel solutions of PBI in methylcyclohexane onto HOPG substrate is shown in Figure 2a. These J-type PBI  $\pi$ -stacks are almost black and accordingly act as efficient light harvesting moieties over the whole visible range. To verify the utility of this approach, prototype organogel/polymer solar cells were also prepared and characterized. A detailed characterization of morphology of the donor-acceptor system using SEM and AFM was also carried out.

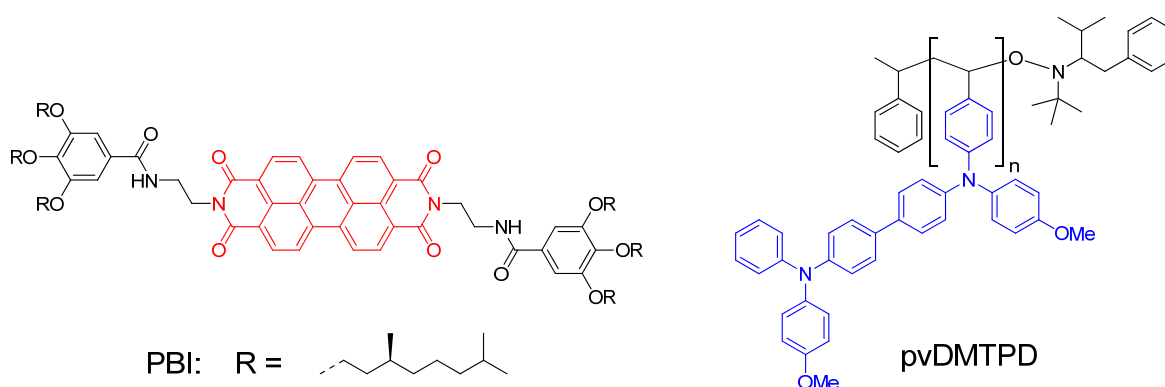


**Figure 1.** Molecular structures of perylene bisimide organogelator PBI and hole-transporting polymer Poly{N,N'-bis(4-methoxyphenyl)-N-phenyl-N'-4-vinylphenyl-[1,1'-biphenyl]-4,4'-diamin} pvDMTPD.

## RESULTS AND DISCUSSION

We prepared the gelled network by two different methods (Figure 2). Route A) Step-wise method of preparation of PBI-organogel followed by removal of solvent (leading to xerogel) and subsequent filling of pores and grooves by using pvDMTPD and route B) Single-step method of simultaneous formation of a three-dimensional physical network of PBI-organogel embedded into amorphous pvDMTPD matrix by a blend approach. The details of preparation of the xerogel, donor-acceptor interpenetrating network, its optimization to get smooth films suitable for device preparation and device characteristics are discussed below.

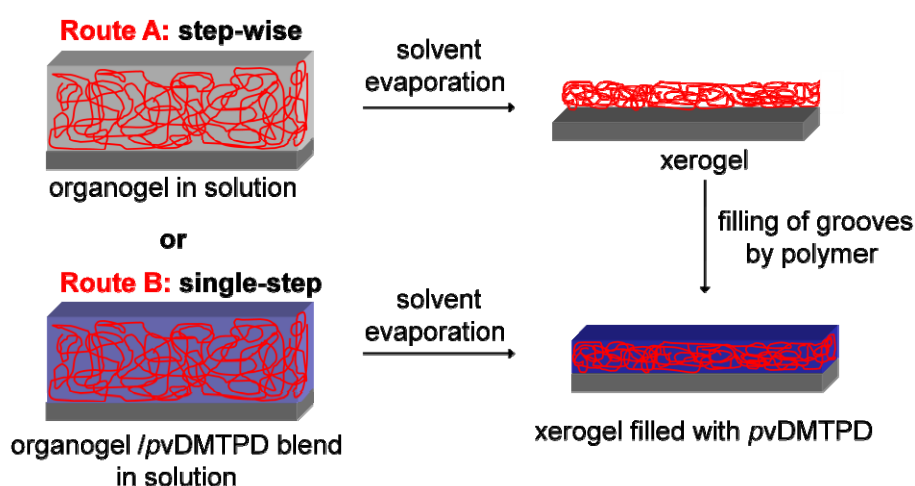
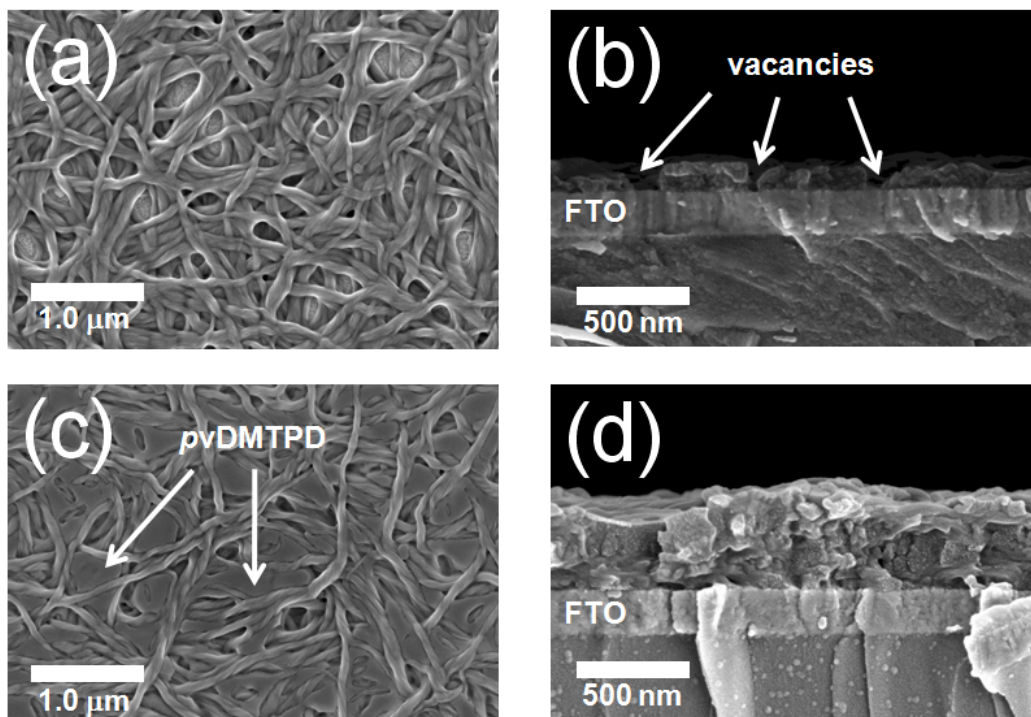


**Figure 2.** Schematic representation of organogel-polymer concept for realization of an interpenetrating organic bulk heterojunction: Route A: Formation of *n*-type xerogel with subsequent filling with *p*-type polymer. Route B: concomitant embedding of the physical network by a blend approach.

For the realization of working devices it is of extreme importance to use smooth films of high optical quality. This guarantees good contacts at organic-metal interfaces resulting in efficient charge extraction. With this in mind we tried different solvents, such as methylcyclohexane, chlorobenzene, toluene and  $\text{CHCl}_3$  for the preparation of gelled layers in devices. Since PBI is not soluble enough at room temperature, hot solutions in these solvents were used to optimize film formation. The films from hot chlorobenzene solution resulted in coarse gel structures not suitable for blend heterojunction. Only by using 2.0 wt-%  $\text{CHCl}_3$ , high optical quality films for both routes A and B were obtained. And therefore  $\text{CHCl}_3$  solutions were used for further optimization and characterization. For film preparation we used doctor-blading technique, in which different film applicator blades, such as spiral blade or quadruple blade were drawn over a concentrated solution of the material placed on a substrate. The use of spiral applicator blade delivered the desired uniform films suitable for device preparation. In route A, thin films of PBI-xerogel were prepared from hot, 2.0 wt-%  $\text{CHCl}_3$  solution onto FTO-glass (FTO: fluorine doped tin oxide) substrates. Initially a thin gel film is formed which upon solvent evaporation subsequently shrinks to develop the xerogel-structure. A striking advantage of PBI-xerogel is that the xerogel-network is almost insoluble in  $\text{CHCl}_3$  at room temperature and therefore suited for filling by pvDMTPD, by using solution processing, in a subsequent step. For route B, blends of PBI:pvDMTPD in different compositions, B1 = 3:1, B2 = 1:1 and B3 = 1:3 weight percentages respectively were prepared in  $\text{CHCl}_3$  and films of different thicknesses were prepared by doctor-blading. As shown later (solar cell discussion), the blend with 3:1 (PBI:pvDMTPD) composition delivered highest current and power conversion values. Therefore, for a comparison of film morphologies obtained via Route A and Route B, only this blend composition B1 (3:1) is taken as a typical example here. For both routes, the doctor-blading technique is essential for the formation of an extensive and continuous network in thin films. The organogel acceptor molecule builds nanostructures in solution as well as in the donor polymer blend. These structural features aggregate during drying in both routes A

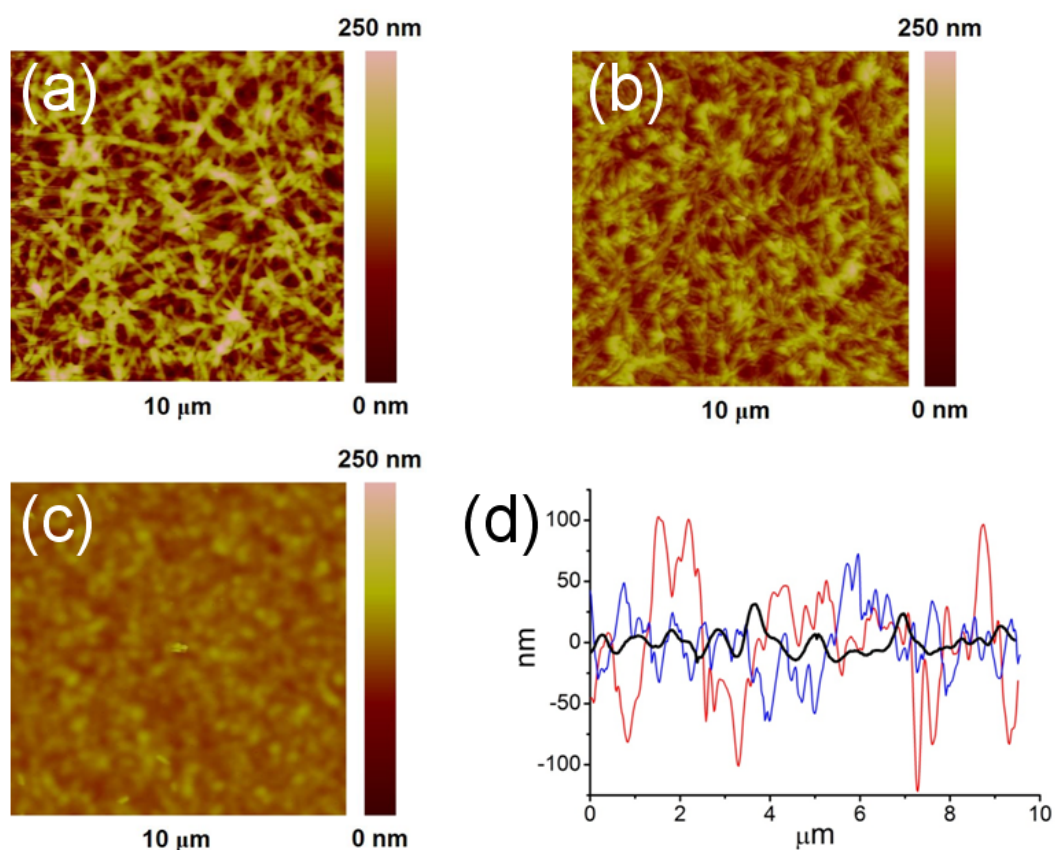
and B, but still resulting in a large area of donor-acceptor interface suitable for charge separation and charge transport.

Figure 3 shows Scanning Electron Microscopy (SEM) images of the PBI-xerogel (Figure 3a, b) and the PBI-xerogel/*p*vDMTPD (3:1) blend (Figure 3c, d). The superstructure of PBI-xerogel consists of twisted strands of about 50 nm thickness which are entangled. Thus the real morphology available for device preparation in thin films is strongly aggregated compared to the individual PBI-strands observed in dilute solutions. Even though the PBI nanofiber morphology formed in dilute solutions is metastable and can aggregate over time,<sup>29,30</sup> the drying process in route A to obtain the xerogel and the blending process in route B to fix the xerogel network in a polymer matrix allow us to freeze the partially aggregated morphology as seen in SEM of thin films. The xerogel with its nanometer sized grooves exhibits enough interstitial volume for filling with the hole-transport polymer. It can clearly be seen from Figure 3c, d that the amorphous polymer *p*vDMTPD fills very efficiently the vacancies in the xerogel in the case of the blend film obtained via route B. Nevertheless, there are still some voids observable in Figure 3c, requiring an additional overstanding hole conductor *p*vDMTPD layer to guarantee smooth contacts with top electrode (see AFM results, Figure 4). Furthermore the polymer chains hinder individual gel-strands from additional sticking or collapsing compared to the pure xerogel which forms thicker strands. This also leads to an increased interface area between electron-donor and acceptor material in route B, compared to that in route A.



**Figure 3.** SEM surface images of (a) PBI-xerogel via route A and (b) corresponding cross section. (c) Surface image of PBI-xerogel/*p*vDMTPD blend (3:1) via route B and (d) corresponding cross section. The hole-transporting polymer *p*vDMTPD acts as filler for the interstitial volume in the xerogel. Films were prepared by doctor-blading technique from hot (55 °C) 2.0 wt-% CHCl<sub>3</sub> solutions.

The topography of the films obtained by both routes was also examined by Atomic Force Microscopy (AFM) measurements. The surface of both films revealed a high roughness as seen in Figure 4a, b. The roughness of PBI-xerogel/*p*vDMTPD 3:1 blend film is less compared to pure PBI-xerogel film (Figure 4d). This is due to a partial filling of the xerogel by the amorphous polymer in blend films. Even then such rough surfaces are not suitable for evaporation of metal-electrodes on top and therefore an additional smoothing layer is necessary. Thus overstanding *p*vDMTPD layers were prepared on top in both cases before gold deposition, not only to smoothen the rough surface in all cases, but also to fill cavities in the xerogel film. To this end, *p*vDMTPD solution in chlorobenzene was doctor-bladed resulting in an overstanding hole-transporting layer of 150 nm thickness. The smoothening effect can be observed clearly in Figure 4c, in which the average roughness of the films is drastically reduced (Figure. 4d). This overstanding layer has an additional electron-blocking function in devices, which helps to avoid direct contact of electron conducting PBI and hole collecting gold electrode on the top. For device preparation an additional hole injection layer of highly conducting poly(3,4-ethylenedioxythiophene):poly(styrene sulfonate) (PEDOT:PSS) was coated on top of *p*vDMTPD layer to improve the contact between *p*vDMTPD and gold.



**Figure 4.** AFM height-images of (a) PBI-xerogel via route A, (b) PBI-xerogel/*p*vDMTPD blend (3:1) via route B, (c) corresponding PBI-xerogel/*p*vDMTPD blend (3:1) with additional overstanding *p*vDMTPD layer, scale 0-250 nm. (d) Respective topography cross sections of PBI-xerogel (red), PBI-xerogel/*p*vDMTPD blend (3:1) (blue) and PBI-xerogel/*p*vDMTPD blend (3:1) with additional overstanding *p*vDMTPD layer (black).

A fundamental question regarding light harvesting in multilayer devices is the individual contributions of each layer towards absorption. This can be studied by comparing the absorption spectra of individual layers in such a device. Figure 5 compares the absorption spectra of pure PBI-xerogel, pure *pvDMTPD*, *pvDMTPD* with PEDOT:PSS on top and a 3:1 blend of PBI/*pvDMTPD* as prepared on quartz substrates. The hole transport polymer *pvDMTPD* absorbs up to 400 nm, whereas grafted PBI absorbs mainly in the region between 400 and 650 nm. The contribution of PEDOT:PSS towards absorption in these devices is negligible as observed by the comparison of the absorption spectra of *pvDMTPD* with or without PEDOT:PSS layer. This is also the reason why PEDOT:PSS is used as a common charge injection layer for holes without any adverse effect on the transmission property of the electrode used. The absorption spectra of PBI/*pvDMTPD* 3:1 blend film is a superposition of the individual absorption spectra indicating no charge-transfer in the ground-state. Additionally, both PBI and blend spectra show the characteristic *J*-type absorption peaks of PBI nanofibers at 619 nm and at 462 nm.<sup>26</sup> Thus, in both systems efficient light harvesting in the range of 400 to 650 nm is guaranteed by the broad absorption band of the black PBI organogelator and below 400 nm by *pvDMTPD*.

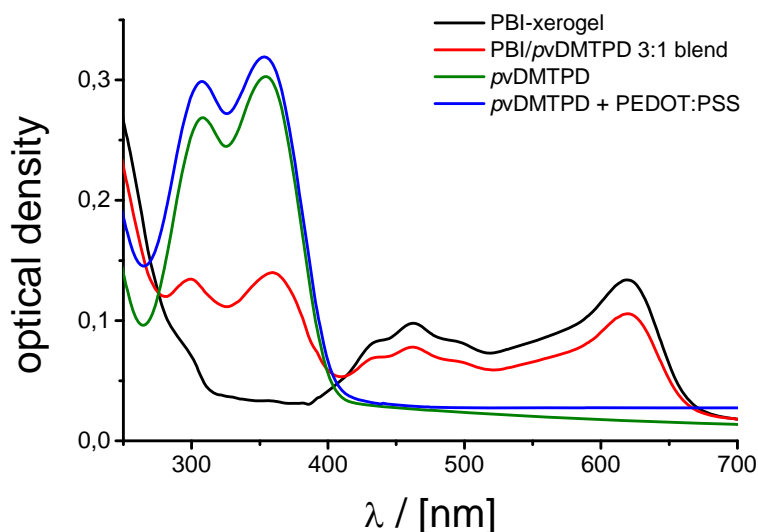


**Figure 5.** UV/Vis absorption spectra of individual layers and blend films. The films were prepared on quartz substrates by doctor-blading using the same conditions as those used in solar cell preparation. The film thicknesses correspond to the respective thicknesses in solar cell devices. *pvDMTPD* layer was prepared from 5.0 wt-% chlorobenzene solution whereas the blend B1 (3:1) as well as PBI-xerogel layers were prepared from 2.0 wt-% hot chloroform solution.

In order to elucidate the photo-induced charge-separation in organogel/polymer systems, first the influence of PBI:*pvDMTPD* composition on solar cell performance was studied. Three different PBI:*pvDMTPD* blend compositions, B1 = 3:1, B2 = 1:1 and B3 = 1:3 weight percentages respectively were prepared and integrated into solar cells using route B. Figure 6a represents schematically

the device structure and Figure 6b a typical SEM cross section for blend B1 (3:1). Here the individual layers of such a device can be observed clearly. No remarkable differences could be observed in SEM cross-sections of B1, B2 and B3.

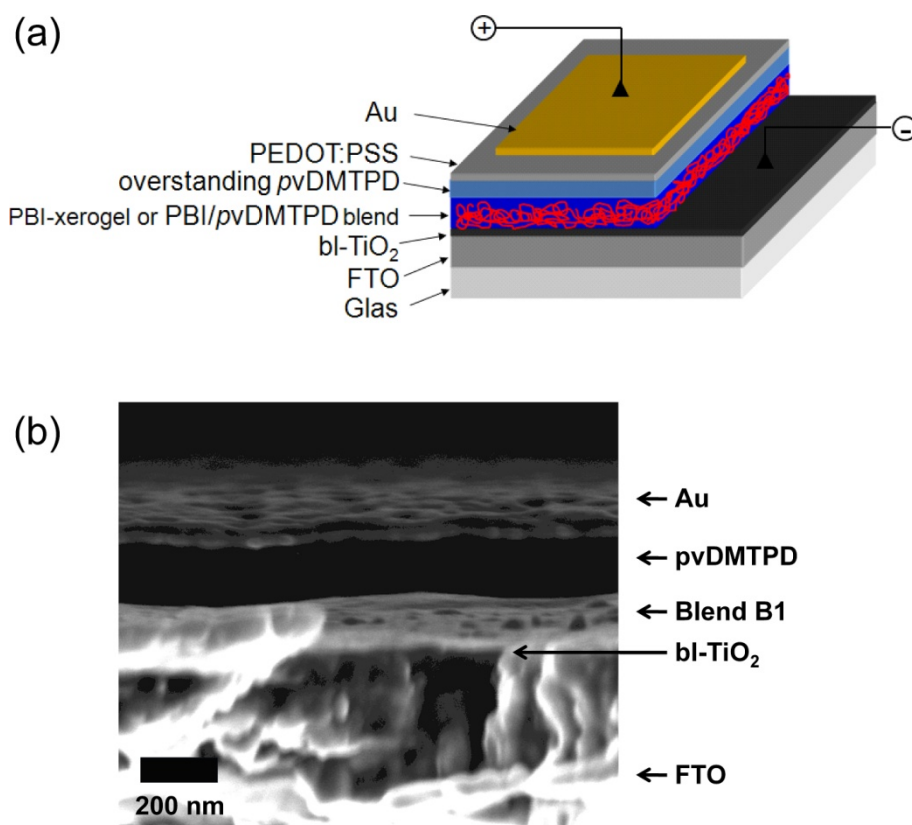


**Figure 6.** (a) General device architecture with inverted cell configuration. FTO = Fluorine doped tin oxide, PEDOT = poly(3,4-ethylenedioxythiophene), PSS = poly(styrene sulfonate). (b) SEM cross section of a typical blend device B1 prepared via route B.

With the optimized conditions of film preparation the photovoltaic devices were prepared. Due to the fact that an overstanding hole-transporting layer is essential in these devices, an inverted cell configuration with an electron collecting electrode at the bottom (FTO) and a hole-collecting electrode (Au) at the top was utilized (Figure 6a). The general device structure is FTO/bi-TiO<sub>2</sub>/PBI-xerogel:pvDMTPD blend / pvDMTPD / PEDOT:PSS/Au. Any contact between hole conducting pvDMTPD and FTO electrode leads to significant loss of current in photovoltaic devices. Hence an additional TiO<sub>2</sub> blocking layer (bi-TiO<sub>2</sub>) onto the FTO-layer is essential to avoid short-circuiting and loss of current through recombination between FTO and pvDMTPD. To ensure uniform film thickness for the bi-TiO<sub>2</sub> layer, an automated method of preparation of such a compact layer of TiO<sub>2</sub> starting from Titanium(IV)bis(acetoacetonato)-di(isopropanoxylate) (TAA) by spray pyrolysis deposition, which was developed in our laboratories, was used here.<sup>31</sup> Also an additional injection layer of PEDOT:PSS was coated on top. Gold electrodes were evaporated on

top of the active layers by vacuum deposition at  $10^{-6}$  mbar. The active area of a single device was  $0.12 \text{ cm}^2$ . These double-layer devices were characterized by means of current–voltage measurements in the dark and under illumination with a calibrated AM1.5 white-light source. All measurements and preparation steps were performed at ambient conditions without any encapsulation or protection of the devices against degradation (See Methods section for details).

In the following the results of the three different blend cells are discussed first. The overall solar cell parameters for all devices are given in Table 1. The current-voltage characteristics of the three blend solar cells are depicted in Figure 7. All devices deliver appreciable photocurrent and photovoltage, demonstrating the presence of percolation paths for photogenerated electrons and holes in organogel-polymer composite material. The B3 (1:3) blend delivers the smallest photocurrent and photovoltage, whereas the blend B1 (3:1) gives the best performance. The performance of blend B2 (1:1) lies in between B1 and B3. Thus blend B1 gives a short-circuit current density ( $J_{sc}$ ) of  $0.28 \text{ mAcm}^{-2}$ , an open-circuit voltage ( $U_{oc}$ ) of 390 mV, a fill factor (FF) of 38 % and a power conversion efficiency of 0.04 %. The highest current observed in device B1 is due to better light-harvesting in the 400 – 650 nm region, due to increased PBI-chromophore content in blend B1. A further improvement in overall light-harvesting and efficiency can be achieved by increasing the perylene content in the organogelator. For the discussion of the two different routes (A, B) of device preparation, only the best performing blend device B1 will be considered further.

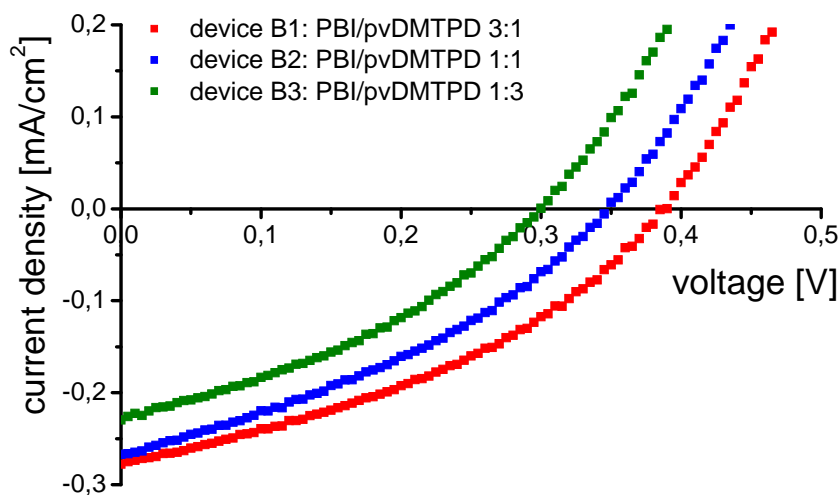


**Figure 7.** Plot of current density ( $J$ ) versus voltage ( $V$ ) under illumination with white light (AM 1.5 spectral conditions,  $100 \text{ mWcm}^{-2}$ ) for photovoltaic devices constructed from PBI-xerogel/pvDMTPD blend with an additional overstanding pvDMTPD layer. The compositions for the devices B1, B2 and B3 are 3:1, 1:1 and 1:3 (PBI:pvDMTPD wt-%) respectively.

An exact control test using non gelled PBI under the same conditions of film and device preparation as that for the gelled system in order to understand the importance of network structure towards charge-separation and charge-transport is extremely difficult to realize. This was because the used PBI gelled extremely fast in solvents suitable for film preparation, since PBI exists in non-gelated form only in hot solutions and during film preparation it suddenly forms the gel network with different degrees of agglomeration. Therefore, a control experiment with an electronically similar, highly soluble and non gelating PBI derivative, *N*-(1-nonyldecyl)-*N'*-(1-pentylhexyl)-perylene-3,4,9,10-tetracarboxylic diimide in combination with *p*vDMTPD, was performed. This control device delivered very low current, voltage and overall efficiency values ( $J_{sc} = 0.04 \text{ mAcm}^{-2}$ ,  $V_{oc} = 275 \text{ mV}$ ,  $FF = 33 \%$ ,  $\eta = 0.003 \%$ ) compared to all the three blend devices. This clearly supports the necessity of an interpenetrating donor-acceptor network as in organogel/polymer systems for efficient charge separation and charge transport. This is in full agreement with reports in the literature regarding bulk-heterojunction devices versus devices lacking interpenetrating networks.<sup>3,7</sup>

**Table 1.** Photovoltaic characteristics of different photovoltaic devices employing the organogel/polymer concept via route A and B.

cell	Blend composition PBI: <i>p</i> vDMTPD	$J_{sc}$ [mA/cm <sup>2</sup> ]	$V_{oc}$ [mV]	FF [%]	$\eta$ [%]
device B1	3 : 1	0.28	390	38	0.041
device B2	1 : 1	0.27	350	35	0.033
device B3	1 : 3	0.23	300	36	0.024
device A	-	0.18	210	41	0.015

Finally the efficacy of route A (step-wise method) was compared with that of route B (single-step method), using the best blend composition B1 (3:1). Device A (FTO/bl-TiO<sub>2</sub>/PBI-xerogel/*p*vDMTPD/PEDOT:PSS/Au) follows route A using PBI-xerogel subsequently filled up with *p*vDMTPD. The device B1 has the structure, FTO/bl-TiO<sub>2</sub>/PBI-xerogel:*p*vDMTPD blend (3:1)/*p*vDMTPD/PEDOT:PSS/Au). Figure 8a, b compares the current–voltage characteristics of devices A and B1 measured in the dark and under illumination. PBI-xerogel/*p*vDMTPD (3:1) blend device B1 works significantly better than the PBI-xerogel device A. The short circuit current  $J_{sc}$  is 0.18 mAcm<sup>-2</sup> and 0.28 mAcm<sup>-2</sup> for the device A and B1 respectively. The open circuit voltage  $V_{oc}$  increases from 210 mV for device A to 390 mV for the device B1. The fill factors are 41 % and 38 % for device A and B1 respectively. Accordingly the power conversion efficiency  $\eta$  is improved by a factor of almost three from 0.015 % for device A to 0.041 % for device B1. It is also worthy to note that all the devices prepared via route B (B1, B2 and B3) perform better than device A. On comparison of devices A and B1, both having similar optical density resulting in similar light-harvesting, the difference in performance can only be attributed to the difference in interface

area as well as morphology in the active layer. In route A the xerogel was prepared in the absence of *pvDMTPD*, whereas in route B the drying process took place in presence of matrix polymer. This can lead to better contact between gel fibers and polymer in device B1.

The generally observed low current values for these organogel/polymer devices are in accordance with the very low optical density in these devices ( $< 0.15$  in the range of 400-650 nm), which has to be improved considerably for efficient light-harvesting. A further elaborate fine-tuning of the relative thicknesses of each individual layer and device preparation conditions under inert atmosphere may also be required to improve the performance. It is noteworthy that both devices are quite stable against degradation with only a small loss in fill factor after several weeks. Both  $J_{sc}$  and  $V_{oc}$  remained constant for 8 weeks.

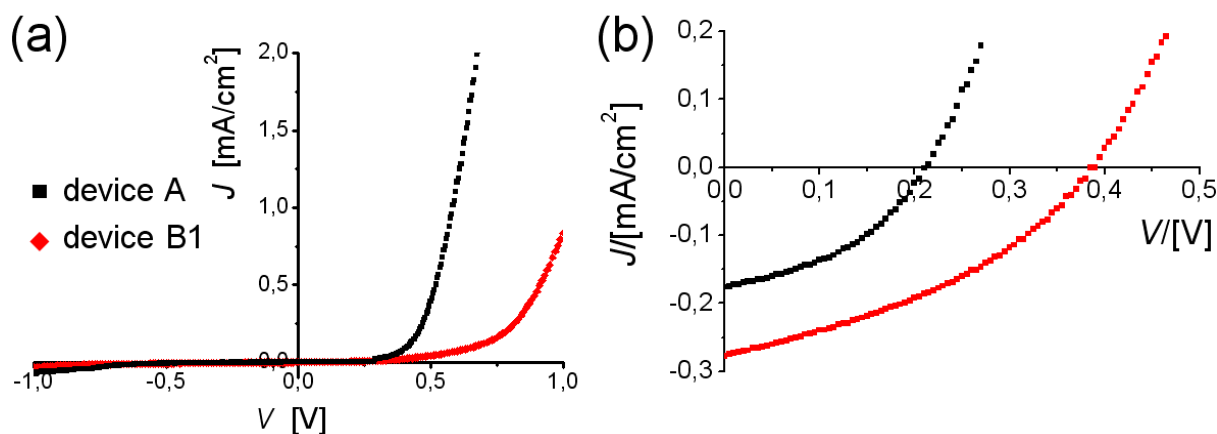


**Figure 8.** Plots of current density ( $J$ ) versus voltage ( $V$ ) for photovoltaic devices constructed from PBI-xerogel device A (black) and PBI-xerogel/*pvDMTPD* blend B1 (3:1) device B1 (red). (a) Measurements under dark and (b) under illumination with AM 1.5 spectral conditions and  $100 \text{ mWcm}^{-2}$ . The short circuit current ( $J_{sc}$ ) and the open circuit voltage ( $V_{oc}$ ) are  $0.18 \text{ mAcm}^{-2}$  and  $210 \text{ mV}$  for the device A and  $0.28 \text{ mAcm}^{-2}$  and  $390 \text{ mV}$  for the device B1, respectively. The power conversion efficiency could also be improved from  $0.015 \%$  for device A to  $0.041 \%$  for device B1.

The performance of reported blend devices prepared from conjugated p-type polymers and low molecular weight PBIs, reported up to now exhibit very low photocurrent and efficiency.<sup>21-23</sup> These state of the art blend systems suffer from crystallisation of perylene bisimides and lack of nanostructured interpenetrating networks. Even though the absolute values reported here are not comparable to the highly optimized blend systems using polythiophene and fullerene, the performance of our organogel/polymer devices can be improved by increasing the active amount of chromophore content as well as using better hole transport conjugated polymers. Future investigations will be directed towards this by developing PBI organogelators bearing smaller substituents at the imide nitrogen which increases the chromophore content resulting in higher optical densities and better charge transport properties. One important advantage of this concept is the possible morphological stability of this system guaranteed via the insoluble xerogel network

frozen into a polymer matrix, which avoids the diffusion of molecules and large scale macrophase separation.

## **CONCLUSIONS**

To conclude, we could provide an innovative and simple donor-acceptor heterojunction concept utilizing the self-assembly principle of a low molecular weight organogelator in presence of an amorphous hole conductor polymer. The organogel acceptor molecule builds nanostructures in presence of the donor polymer resulting in a large area of donor-acceptor interface suitable for charge separation and charge transport. This is a universal approach to use blends of functional gelators in combination with complementary semiconductor polymers. Also a proof-of-principle for application in organic solar cells is given. This concept has great potentials of improvement by utilizing low band-gap conjugated polymers and organogelators that combine favourable absorption properties and high charge carrier mobilities. This is a conceptual novelty in the field of nanostructured donor-acceptor bulk heterojunction.

## **METHODS**

The synthetic details of the preparation of PBI-organogelator<sup>26,27</sup> and poly(vinyl-dimethoxytetraphenylbenzidine) (*pvDMTPD*)<sup>28</sup> were reported elsewhere. Titanium(IV)bis(acetoacetonato)-di(isopropanoxylate) (TAA) and PEDOT/PSS dispersion were purchased (Aldrich) and used as received. Glass substrates (Tec 8) covered with ~ 3 mm fluorine-doped tin oxide (FTO) layer having a sheet resistance of 8  $\Omega$  per square were purchased from Hartford Glass Co. Inc., Indiana, USA. UV/Vis spectra were recorded on a Hitachi U-3000 spectrometer. Photovoltaic devices were prepared onto pre-etched and cleaned, patterned FTO substrates. The TiO<sub>2</sub> blocking layer was deposited via spray pyrolysis deposition using a TiO<sub>2</sub> precursor, TAA, diluted with ethanol to a concentration of 0.2 M. The pyrolysis was carried out at 480 °C. After the required number of spraying cycles under optimized conditions<sup>31</sup>, the substrates were annealed at 500 °C for another hour before cooling down to room temperature. The substrates were kept in an inert atmosphere for further layer preparation. The active layers were processed via doctor-blading technique using a COATMASTER 509 MC-I Film Applicator from ERICHSEN GMBH & CO KG, Germany. Films were processed at ambient conditions and the processing speed was 25 mms<sup>-1</sup> for all films. The films were dried at ambient conditions for one hour. Three types of film application blades, (a) Spiral Film Applicator blade, Model 358, (20  $\mu$ m blade gap), (b) Quadruple Film Applicator Model 360 (120  $\mu$ m blade gap) and (c) Film Applicator blade BAKER 286 (5  $\mu$ m blade gap) (ERICHSEN GMBH & CO KG) were used for optimization of the optical quality of the films. The best method for the preparation of PBI-xerogel and PBI-xerogel/*pvDMTPD* blend layers was found to be that using Spiral Film Applicator blade. All

films were prepared from 30  $\mu\text{L}$  hot ( $\sim 55\text{ }^\circ\text{C}$ ) 2.0 wt-%  $\text{CHCl}_3$  solutions resulting in 160 nm thick blend films. The additional overstanding *p*VDMTPD layer was prepared with the Film Applicator blade BAKER 286 (5  $\mu\text{m}$  blade gap) from 10  $\mu\text{L}$  5.0 wt-% chlorobenzene solution to get 140 nm smooth films. Film thicknesses were measured with a Dek Tak 3030 ST profilometer from Veeco Instruments. PEDOT:PSS dispersion, obtained from ALDRICH, was spin coated (4000 rpm, ramp 1 s, 90 s) and post-baked on a hot-stage at 80  $^\circ\text{C}$  for 10 minutes in a nitrogen atmosphere. The gold electrode (60 nm) was deposited by vacuum sublimation in a vacuum chamber of BA 510 type from Balzers (Liechtenstein) at  $10^{-6}$  mbar. The active area of the cells was 0.12  $\text{cm}^2$ . Current–voltage characteristics were measured under 100  $\text{mWcm}^{-2}$  and AM 1.5 spectral light (Oriel light source setup with 150-W xenon arc lamp and suitable AM 1.5 filters). This setup was calibrated using a reference Si cell from ISE Freiburg at the same sample position and height. Samples for SEM were prepared on FTO substrates under the same conditions as those used for solar cell preparation and sputtered with platinum (2 nm) to improve the conductivity for SEM imaging. The measurements were performed with a LEO 1530 (FE-SEM) with Schottky-field-emission cathode and in-lens detector. AFM measurements were performed with a Dimension 3100 device from Digital Instruments. Images were recorded in the tapping mode.

#### **ACKNOWLEDGMENT**

Financial Support from DFG (SPP 1355 and SFB 481) is acknowledged. Dr. S. Ghosh thanks the Alexander von Humboldt foundation for a postdoctoral fellowship.

## **BIBLIOGRAPHY**

- [1] Günes, S.; Neugebauer, H.; Sariciftci, N. S. Conjugated Polymer-Based Organic Solar Cells. *Chem. Rev.* **2007**, *107*, 1324-1338.
- [2] Hoppe, H.; Sariciftci, N. S. Polymer Solar Cells. in *Advances in Polymer Science Photoresponsive Polymers II*; Marder, S. R., Lee, K.-S. Eds.; Springer-Verlag: Heidelberg, 2008; pp 1-86.
- [3] Brabec, C. J.; Sariciftci, N. S.; Hummelen, J. C. Plastic Solar Cells. *Adv. Funct. Mater.* **2001**, *11*, 15-26.
- [4] Halls, J. J. M.; Walsh, C. A.; Greenham, N. C.; Marseglia, E. A.; Friend, R. H.; Moratti, S. C.; Holmes, A. B. Efficient Photodiodes from Interpenetrating Polymer Networks. *Nature* **1995**, *376*, 498-500.
- [5] Yang, X.; Loos, J. Toward High-Performance Solar Cells: The Importance of Morphology Control. *Macromolecules* **2007**, *40*, 1353-1362.
- [6] Ma, W.; Yang, C.; Gong, X.; Lee, K.; Heeger, A. J. Thermally Stable, Efficient Polymer Solar Cells with Nanoscale Control of the Interpenetrating Network Morphology. *Adv. Funct. Mater.* **2005**, *15*, 1617-1622.
- [7] Lindner, S. M.; Hüttner, S.; Chiche, A.; Thelakkat, M.; Krausch, G. Charge Separation at Self-Assembled Nanostructured Bulk Interface in Block Copolymers. *Angew. Chem. Int. Ed.* **2006**, *45*, 3364-3368.
- [8] Sommer, M.; Lindner, S. M.; Thelakkat, M. Microphase-Separated Donor-Acceptor Diblock Copolymers: Influence of HOMO Energy Levels and Morphology on Polymer Solar Cells. *Adv. Funct. Mater.* **2007**, *17*, 1493-1500.
- [9] Cravino, A.; Zerza, G.; Maggini, M.; Bucella, S.; Svensson, M.; Andersson, M. R.; Neugebauer, H.; Sariciftci, N. S. A Novel Polythiophene with Pendant Fullerenes: Toward Donor/Acceptor Double-Cable Polymers. *Chem. Commun.* **2000**, 2487-2488.
- [10] Würthner, F.; Chen, Z.; Hoeben, F. J. M.; Osswald, P.; You, C.-C.; Jonkheijm, P.; van Herrikhuyzen, J.; Schenning, A. P. H. J.; van der Schoot, P. P. A. M.; Meijer, E. W.; Beckers, E. H. A.; Meskers, S. C. J.; Janssen, R. A. J. Supramolecular p-n-Heterojunctions by Co-Self-Organization of Oligo(p-phenylene Vinylene) and Perylene Bisimide Dyes. *J. Am. Chem. Soc.* **2004**, *126*, 10611-10618.
- [11] McClenaghan, N. D.; Grote, Z.; Darriet, K.; Zimine, M.; Williams, R. M.; De Cola, L.; Bassani, D. M. Supramolecular Control of Oligothiophenevinylene-Fullerene Interactions: Evidence for a Ground-State EDA Complex. *Org. Lett.* **2005**, *7*, 807-810.
- [12] Sisson, A. L.; Sakai, N.; Banerji, N.; Fürstenberg, A.; Vauthey, E.; Matile, S. Zipper Assembly of Vectorial Rigid-Rod  $\pi$ -Stack Architectures with Red and Blue Naphthalenediimides:

- Toward Supramolecular Cascade n/p-Heterojunctions. *Angew. Chem. Int. Ed.* **2008**, *47*, 3727-3729.
- [13] Haryono, A.; Binder, W. H. Controlled Arrangement of Nanoparticle Arrays in Block-Copolymer Domains. *Small* **2006**, *2*, 600-611.
- [14] Terech, P.; Weiss, R. G. Low Molecular Mass Gelators of Organic Liquids and the Properties of Their Gels. *Chem. Rev.* **1997**, *97*, 3133-3159.
- [15] Hirst, A. R.; Escuder, B.; Miravet, J. F.; Smith, D. K. High-Tech Applications of Self-Assembling Supramolecular Nanostructured Gel-Phase Materials: From Regenerative Medicine to Electronic Devices. *Angew. Chem. Int. Ed.* **2008**, *47*, 8002-8018.
- [16] Puigmartí-Luis, J.; Laukhin, V.; Pérez del Pino, A.; Vidal-Gancedo, J.; Rovira, C.; Laukhina, E.; Amabilino, D. B. Supramolecular Conducting Nanowires from Organogels. *Angew. Chem. Int. Ed.* **2007**, *46*, 238-241.
- [17] Lee, D.-C.; Jang, K.; McGrath, K. K.; Uy, R.; Robins, K. A.; Hatchett, D. W. Self-Assembling Asymmetric Bisphenazines with Tunable Electronic Properties. *Chem. Mater.* **2008**, *20*, 3688-3695.
- [18] Hüttner, S.; Sommer, M.; Thelakkat, M. N-type Organic Field Effect Transistors from Perylene Bisimide Block Copolymers and Homopolymers. *Appl. Phys. Lett.* **2008**, *92*, 093302.
- [19] Thelakkat, M.; Star-Shaped, Dendrimeric and Polymeric Triarylamines as Photoconductors and Hole Transport Materials for Electro-Optical Applications. *Macromol. Mater. Eng.* **2002**, *287*, 442-461.
- [20] Semiconducting Polymers. Chemistry, Physics and Engineering; Hadziioannou, G., Malliaras, G. G., Eds.; Wiley-VCH: Weinheim, 2007.
- [21] Dittmer, J. J.; Marseglia, E. A.; Friend, R. H. Electron Trapping in Dye/Polymer Blend Photovoltaic Cells. *Adv. Mater.* **2000**, *12*, 1270-1274.
- [22] Breeze, A. J.; Salomon, A.; Ginley, D. S.; Tillmann, H.; Hörhold, H.-H.; Gregg, B. A. Polymer-Perylene Diimide Heterojunction Solar Cells. *Appl. Phys. Lett.* **2002**, *81*, 3085-3087.
- [23] Shin, W. S.; Jeong, H.-H.; Kim, M.-K.; Jin, S.-H.; Kim, M.-R.; Lee, J.-K.; Lee, J. W.; Gal, Y.-S. Effects of Functional Groups at Perylene Diimide Derivatives on Organic Photovoltaic Device Application. *J. Mater. Chem.* **2006**, *16*, 384-390.
- [24] Mohmeyer, N.; Wang, P.; Schmidt, H.-W.; Zakeeruddin, S. M.; Grätzel, M. Quasi-Solid-State Dye-Sensitized Solar Cells with 1,3:2,4-di-O-benzylidene-D-sorbitol Derivatives as Low Molecular Weight Organic Gelators. *J. Mater. Chem.* **2004**, *14*, 1905-1909.
- [25] Kubo, W.; Kitamura, T.; Hanabusa, K.; Wada, Y.; Yanagida, S. Quasi-Solid-State Dye-Sensitized Solar Cells Using Room Temperature Molten Salts and a Low Molecular Weight Gelator. *Chem. Commun.* **2002**, 374-375.

- [26] Würthner, F.; Bauer, C.; Stepanenko, V.; Yagai, S. A Black Perylene Bisimide Super Gelator with an Unexpected J-Type Absorption Band. *Adv. Mat.* **2008**, *20*, 1695-1698.
- [27] Ghosh, S.; Li, X.-Q.; Stepanenko, V.; Würthner, F. Control of H- and J-Type  $\pi$ -Stacking by Peripheral Alkyl Chains and Self-Sorting Phenomena in Perylene Bisimide Homo- and Heteroaggregates. *Chem. Eur. J.* **2008**, *14*, 11343-11357.
- [28] Lindner, S. M.; Thelakkat, M. Nanostructured n-type Organic Semiconductor in a p-type Matrix via Self-Assembly of Block Copolymers. *Macromolecules* **2004**, *37*, 8832-8835.
- [29] Moffat, J. R.; Smith, D. K. Metastable Two-Component Gel-Exploring The Gel-Crystal Interface. *Chem. Commun.* **2008**, 2248-2250.
- [30] Ballabh, A.; Adalder, T. K.; Dastidar, P. Structures and Gelation Properties of a Series of Salts Derived from an Acyclic Dicarboxylic Acid and n-Alkyl Primary Amines. *Cryst. Growth Des.* **2008**, *8*, 4144-4149.
- [31] Peng, B.; Jungmann, G.; Jäger, C.; Haarer, D.; Schmidt, H.-W.; Thelakkat, M. Systematic Investigation of the Role of Compact TiO<sub>2</sub> Layer in Solid-State, Dye-Sensitized TiO<sub>2</sub> Solar Cells. *Coord. Chem. Rev.* **2004**, *248*, 1479-1489.

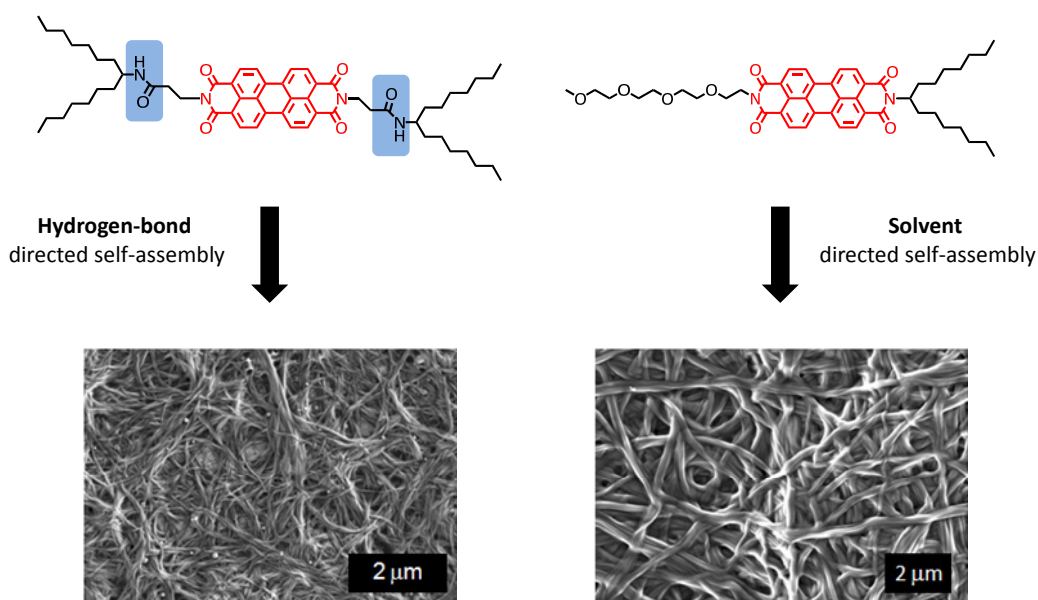


## 8. APPENDIX: SOLVENT AND HYDROGEN-BOND DIRECTED SELF-ASSEMBLY OF PERYLENE BISIMIDES

André Wicklein and Mukundan Thelakkat

Department of Macromolecular Chemistry I, Applied Functional Polymers, Universität Bayreuth,  
Universitätsstr. 30, 95440 Bayreuth, Germany, Fax: +49-921-55-3206

E-mail: [mukundan.thelakkat@uni-bayreuth.de](mailto:mukundan.thelakkat@uni-bayreuth.de)



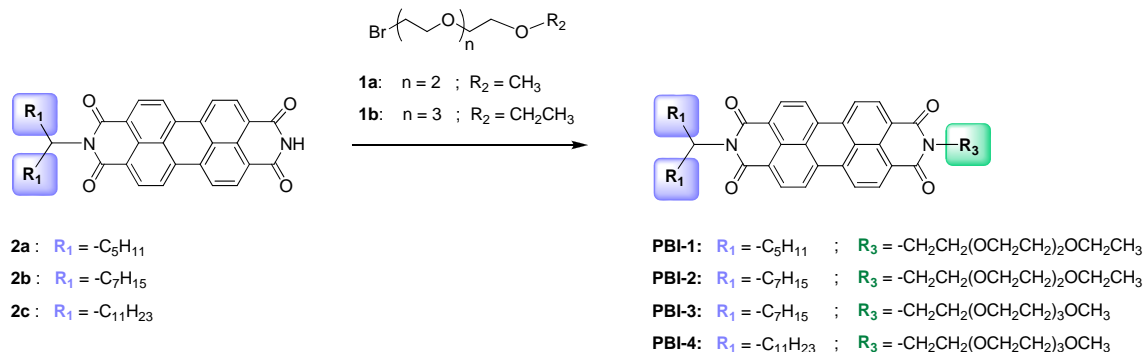
This chapter contains additional experimental data on synthesis and basic studies on self-assembly phenomena of several perylene bisimide dyes. The work presented here, is strongly related to the studies on xerogel/polymer interpenetrating networks for photovoltaic devices, presented in chapter 7.

## INTRODUCTION

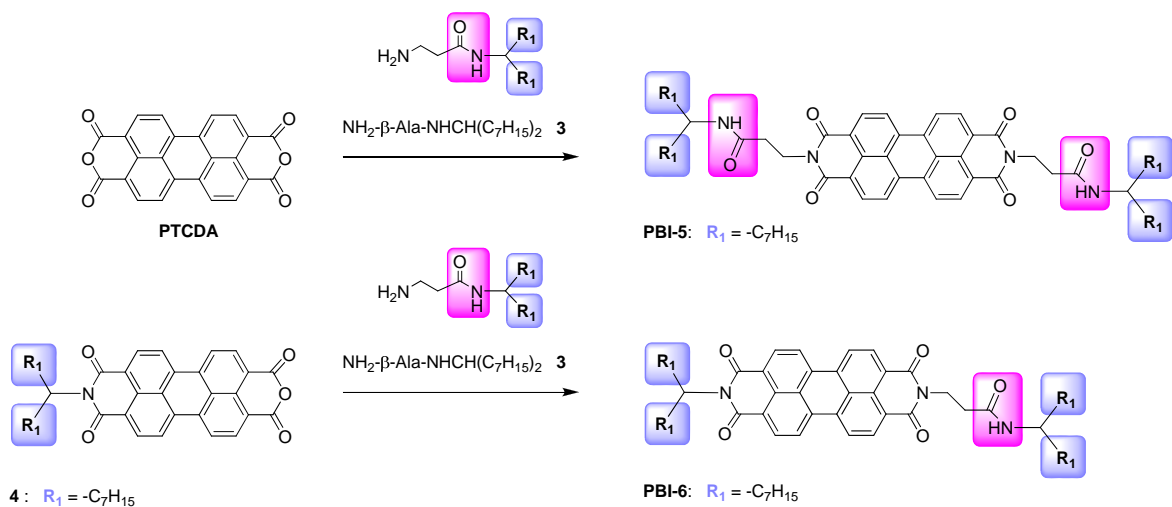
Over the past decades, supramolecular chemistry has come to the fore as an extensively studied research area owing to its tremendous impact on materials science and biology.<sup>1</sup> As an example, self-organization of lipids in the form of bilayers within the cell membrane or multiple hydrogen bonding interactions as seen in DNA base pairing are nature's essential tools for complex life. Molecular self-assembly is described as the spontaneous association of molecules under equilibrium conditions into stable, structurally well-defined aggregates joined by noncovalent bonds.<sup>2</sup> Various noncovalent interactions such as hydrogen bonding, metal-ion-to-ligand coordination, electrostatic interactions,  $\pi$ - $\pi$  stacking, dipole-dipole interactions, hydrophobic interactions, and so forth, have been identified so far to enable the construction of various well-defined supramolecular architectures from specifically designed small molecule building blocks under a programmed manner.<sup>3</sup> Furthermore, the self-assembly processes of  $\pi$ -conjugated organic molecules in solution became of fundamental relevance in designing bottom-up electronic and optoelectronic devices in recent years, and the concept of supramolecular electronics was established.<sup>4-6</sup> The controlled formation of self-organized nano-architectures over all length scales in organic electronic devices is crucial as they determine the electronic and optical properties of the materials. It is also an enormous challenge to achieve these requirements. In this context, perylene bisimide (PBI) dyes have received a great deal of attention due to their outstanding optical and electronic properties that are appreciably favorable for their application as functional material in organic electronics.<sup>7,8</sup> A combination of their outstanding  $\pi$ - $\pi$  stacking propensity with other noncovalent interactions enables the creation of diverse hierarchically organized functional soft-materials such as organogels,<sup>9,10</sup> liquid crystals<sup>11-13</sup> or discrete nanofibers.<sup>14-17</sup> Recently it was shown, that amphiphilic substituted PBIs with an alkyl swallow-tail side-chain and a hydrophilic oligoethyleneglycol (OEG) side-chain as *N*-substituents can self-assemble into well-defined 1D like nanobelts or nanofibers.<sup>14,15</sup> Depending on the polarity of the solvents used for the self-assembly process, the nanostructural morphology formed could be controlled as a result of the amphiphilic substitution pattern of the PBIs. On the other hand, Würthner et al. report on PBI based organogelators with an amide functionality between the chromophore core and the solubilizing 3,4,5-trialkoxy-gallic acid side group.<sup>9,10</sup> As demonstrated in chapter 7, such dyes could be used to generate donor-acceptor heterojunctions in a supramolecular approach by the self-assembly process of a PBI dye in presence of a suitable donor material.<sup>18</sup>

The fundamental question in this chapter is whether we can provide novel semiconducting perylene bisimide dyes that self-organize into morphological stable nano- and mesostructures and additionally bear minimum sized side-chain substituents at the imide nitrogen. On the one hand, these *N*-substituents are of primary relevance for the self-organization process, but in order to increase the chromophore content resulting in higher optical densities and better charge transport properties a compromise between active chromophore content and structure imposing side-chains has to be accepted. Here, we focus on two different self-assembly principles: solvent-assisted self-assembly of **PBIs 1-4** (Typ I, Scheme 1) and hydrogen bond-directed self-assembly of **PBIs 5 and 6** (Typ II, Scheme 1).

**Typ I:** unsymmetrically N-substituted PBIs with different side chain hydrophilicities



**Typ II:** PBIs with intermolecular H-Bonding capability



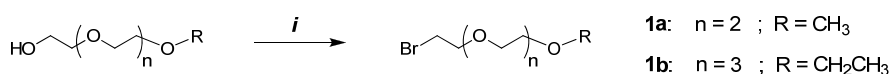
**Scheme 1.** Synthesis of perylene bisimides used for solvent-directed self-assembly studies (**Typ I**, **PBIs 1-4**) and hydrogen-bond directed self assembly (**Typ II**, **PBI-5 and 6**).

## RESULTS AND DISCUSSION

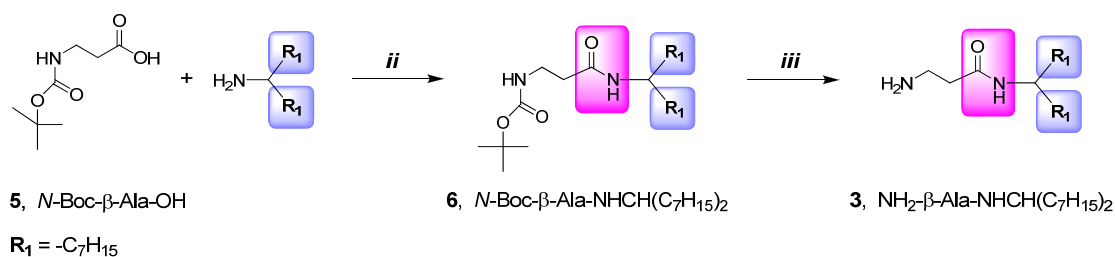
In general **PBIs 1 to 6** were synthesized according to the general reaction scheme 1. The details of the synthetic routes are described in chapter 3.<sup>12</sup> Synthesis and structural characterization of compound **PBI-4** is also discussed in chapter 3. Linear oligooxyethylene bromides **1a, b** were obtained by bromination of the respective alcohols according to literature procedure (Scheme 2).<sup>19</sup> Synthesis of amide bond containing side chain amine  $\text{NH}_2-\beta\text{-Ala}-\text{NHCH}(\text{C}_7\text{H}_{15})_2$  **3** was realized by amidization of *N*-Boc protected  $\beta$ -alanine **5** with DCC (Scheme 2).<sup>20</sup> After cleavage of the Boc protecting group with TFA, the free amine **3** was liberated by treatment with NaOH in MeOH in 80 % yield. For the synthesis of **PBIs 1 to 4**, the respective *N*-(1-alkyl swallow-tail)-perylene bisimides **2a, b, c** were reacted with the respective oligooxyethylene bromide **1a, b** via nucleophilic substitution at the imide nitrogen (Scheme 1). Symmetrical **PBI-5** was obtained by reaction of **PTCDA** with  $\text{NH}_2-\beta\text{-Ala}-\text{NHCH}(\text{C}_7\text{H}_{15})_2$  **3** in a mixture of imidazole/chlorobenzene and

Zn(OAc)<sub>2</sub> as imidization catalyst (Scheme 1). As **PBI-5** is almost insoluble in common organic solvents, purification was carried out by multiple soxhlet extractions. Structural characterization of **PBI-5** was performed via <sup>1</sup>H-NMR spectroscopy in *o*-DCB-d<sub>4</sub> at 120 °C. Asymmetric substituted **PBI-6** was synthesized by reacting mono-imide mono-anhydride **4** with the respective amine (Scheme 1). Thus *N*-(1-heptyloctyl)-perylene-3,4,9,10-tetracarboxylic-3,4-anhydride-9,10-imide **4**<sup>12</sup> was allowed to react with NH<sub>2</sub>-β-Ala-NHCH(C<sub>7</sub>H<sub>15</sub>)<sub>2</sub> **3** under microwave irradiation conditions at 140 °C to yield **PBI-6** with 82 %.

Synthesis of oligooxyethylene bromides **1a, b**



Synthesis of NH<sub>2</sub>-β-Ala-NHCH(C<sub>7</sub>H<sub>15</sub>)<sub>2</sub> **3**



**Scheme 2.** Synthesis of oligooxyethylene bromides **1a, b** and NH<sub>2</sub>-β-Ala-NHCH(C<sub>7</sub>H<sub>15</sub>)<sub>2</sub> **3**. i) PPh<sub>3</sub>, Br<sub>2</sub>, AcCN. ii) DCC, *N*-HOSu, CH<sub>2</sub>Cl<sub>2</sub>/1,4-dioxane 2:1 v/v. H<sub>2</sub>N-CH(C<sub>7</sub>H<sub>15</sub>)<sub>2</sub>. iii) 1. CH<sub>2</sub>Cl<sub>2</sub>/TFA 3:1 v/v, 2. NaOH, MeOH.

### Perlyene bisimides for solvent-assisted self-assembly, Typ I

Perylene bisimides **PBIs 1 to 4** are highly crystalline materials. Thermotropic behaviour was analyzed by a combination of differential scanning calorimetry (DSC) and polarization optical microscopy (POM). Phase transition temperatures with corresponding transition enthalpies are summarized in Table 1 and DSC thermograms of the compounds are presented in Figure 1. As can be seen from the DSC thermograms, all the **PBIs 1-4** exhibit only one reversible phase transition corresponding to the Cr → I transition respectively (Fig. 1). Depending on the size of the side chains at the imide position, the melting point can be tuned in a range between 219 °C for **PBI-1** (with shorter *N*-substituents) and 152 °C for **PBI-4**, carrying larger *N*-substituents. Concomitantly the phase transition enthalpy  $\Delta H_{Cr \rightarrow I}$  also decreases from **PBI-1** to **PBI-4**.

**Table 1.** Summary of the thermal behaviour, phase transition temperatures with corresponding transition enthalpies and phases<sup>[a]</sup> of **PBIs 1-4**.

PBI	phase transitions and enthalpies <sup>[b]</sup> (T [°C] / ΔH [kJmol <sup>-1</sup> ])	
	2. heating cycle	1. cooling cycle
<b>PBI-1</b>	Cr (218.9 / 23.7) → I	I (208.1 / -23.6) → Cr
<b>PBI-2</b>	Cr (188.1 / 17.0) → I	I (179.6 / -16.7) → Cr
<b>PBI-3</b>	Cr (167.9 / 15.0) → I	I (158.0 / -14.1) → Cr
<b>PBI-4</b>	Cr (151.8 / 13.7) → I	I (142.0 / -13.4) → Cr

[a] Cr = crystalline phase; I = isotropic phase. [b] Obtained from DSC measurements at a heating rate of 10 Kmin<sup>-1</sup> under N<sub>2</sub>-atmosphere.

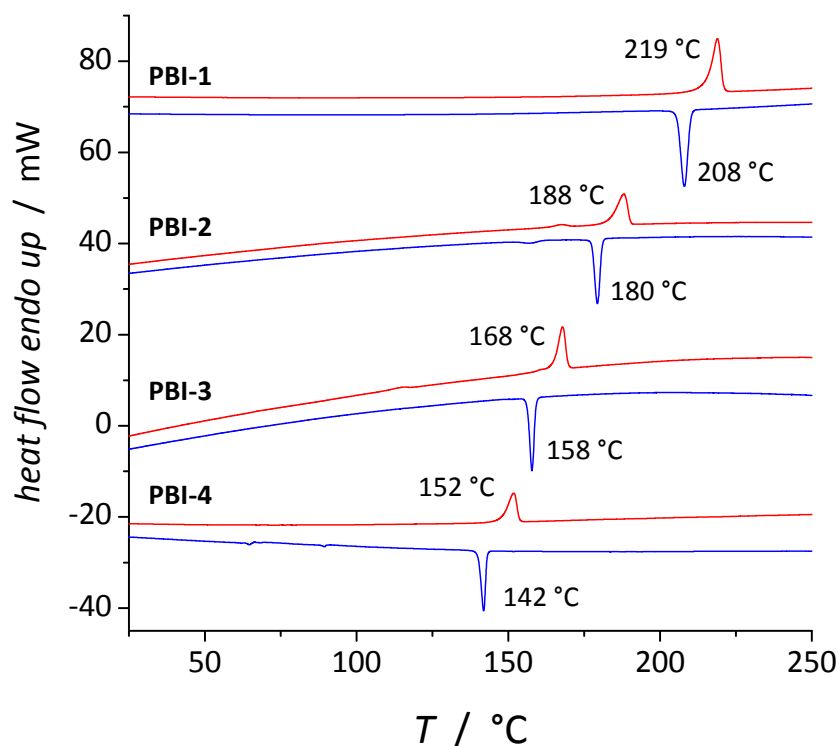


**Figure 1.** Differential Scanning Calorimetry (DSC) thermograms of **PBI-1** to **4**. Blue curves represent the first cooling and red curves the second heating cycle under N<sub>2</sub>-atmosphere. The corresponding phase transition temperatures are also presented.

Also POM observations are in accordance with the DSC results (Fig. 2). All PBI derivatives form long needle-like crystals growing from a central seed, when cooled down from the isotropic melt. For **PBI-1**, especially long crystals can be obtained upon annealing the sample at 209 °C, whereas for **PBI-4** with larger substituents a comparatively irregular crystal growth is observed.

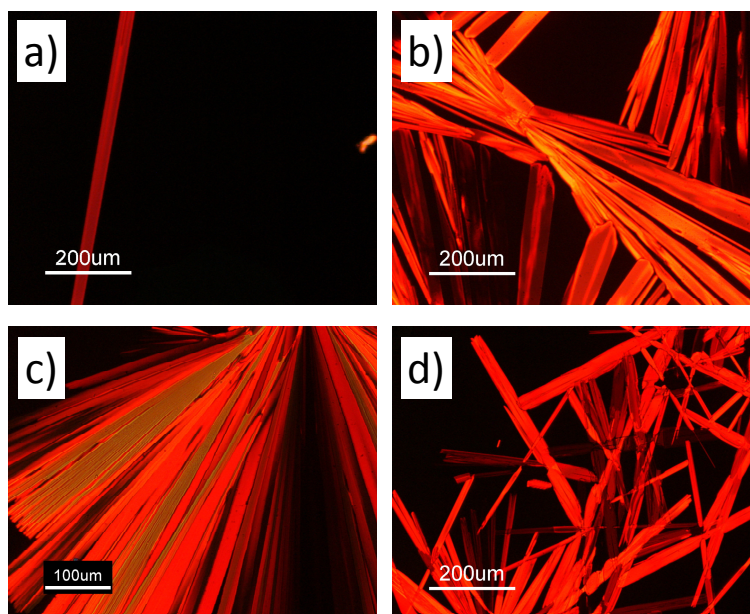


**Figure 2.** Optical microscopic images of textures of **PBI-1** to **4** (under crossed polarizers). All derivatives form long needle-like crystals growing from a central seed, when cooled from the isotropic melt. (a) **PBI-1** annealed at 209 °C, (b) **PBI-2** annealed at 181 °C, (c) **PBI-3** annealed at 159 °C and (d) **PBI-4** annealed at 145 °C.

We conducted the self-assembly studies of **PBIs 1-4** through a solvent exchange processing, where the molecules are transferred from a “good” solvent (e.g. EtOH) into a “poor” solvent (e.g. H<sub>2</sub>O, see Experimental Section).<sup>14</sup> Upon the intended decrease of solubility, the molecules start the self-assembly process. The introduction of linear OEG side chains at the imide position results in increased solubility of these **PBIs** in hydrophilic solvents such as short-chain alcohols. Upon addition of water to alcohol solutions of these compounds, the increase in solvent polarity will force solvophobic association between the alkyl swallow-tail side chains. Thus self-assembly processes are feasible in a similar manner as for other amphiphilic building blocks. The hydrophobic interdigitation between the alkyl swallow-tail chains brings the molecules in such vicinity where the  $\pi$ - $\pi$  stacking interactions control the self-organization process. The intermolecular  $\pi$ - $\pi$  stacking is likely facilitated by the stretching-out conformation of the OEG substituents, which is preferential in hydrophilic solvents. As demonstrated by the SEM surface images presented in Figure 3, different assembly levels, particulate aggregates, very short fibers and long nanofibers, were formed for **PBIs 1-4** by the solvent exchange process. As the preparation conditions were the same for all derivatives, this has to be due to particular differences in the hydrophilic/hydrophobic balance of OEG/alkyl-substituent combination. For **PBIs 1** and **2**, carrying a rather short OEG substituent, very short fibers and particulate aggregates were observed (Fig. 3a, b). Also the self-assembly process was quite fast, recognizable by the formation of a precipitate after 30 minutes. Thus the molecular aggregation is too fast here, leading to the formation of more seeding particles leaving no molecules available for the later stage growth of longer fibers. The picture changes completely for **PBI-3** with a longer OEG substituent, here an ultralong fibrillar structure was formed (Fig. 3c, d) by a slow 1D crystal

growing process (> 24 h). Such a slow crystallization process allows for more organized molecular stacking and extended growth along the fibril long axis with fiber thicknesses down to ~100 nm. Upon the drying process during sample preparation for SEM, these fibers strongly entangle and aggregate to form thicker fibers. A change of solvent ratio to EtOH/H<sub>2</sub>O 2:1 v/v or an increase of alkyl swallow-tail length, leads to the formation of more coarse nanofibers of **PBI-3** (Fig. 3e) or **PBI-4** (Fig. 3f) respectively. This is due to a decrease of solvent hydrophilicity in the case of **PBI-3** or an increase of side-chain hydrophobicity for **PBI-4**. Thus an optimal balance of hydrophilic/hydrophobic substituents in combination with an optimized solvent polarity is essential for the formation of an extended nanofibrillar self-assembly process of amphiphilic **PBIs**.

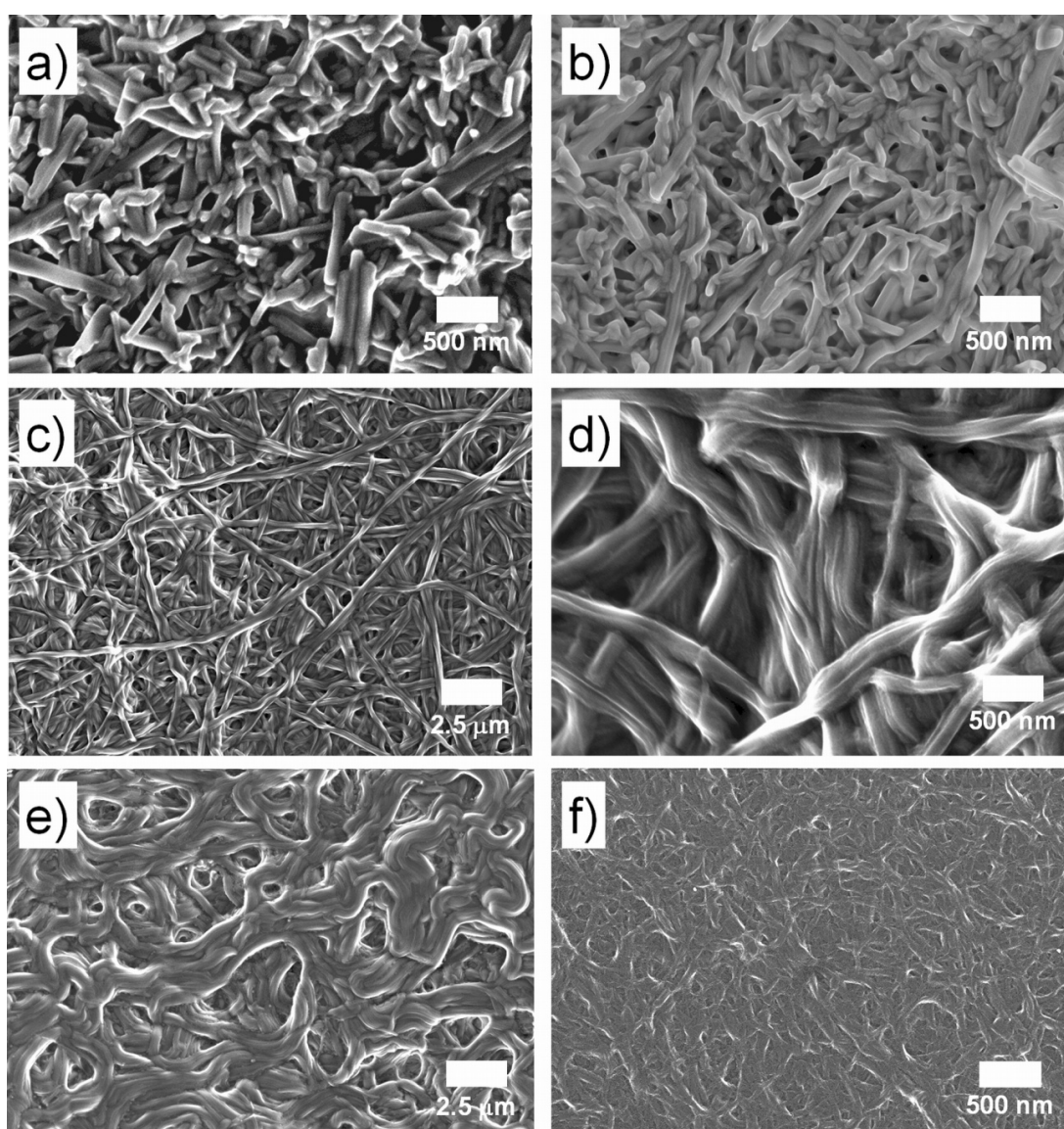


**Figure 3.** SEM surface images of **PBI** aggregates and nanofibers prepared by dropcasting of nanofiber suspension on ITO. The suspensions were prepared as 0.25 wt-% EtOH/H<sub>2</sub>O 1:1 v/v solutions, unless indicated otherwise. (a) Particulate aggregates and some very short fibers of **PBI-1**. (b) Particulate aggregates and some very short fibers of **PBI-2**. (c) Nanofibers of **PBI-3**. (d) Nanofibers of **PBI-3**. (e) Nanofibers of **PBI-3** from 0.33 wt-% EtOH/H<sub>2</sub>O 2:1 v/v solution. (f) Nanofibers of **PBI-4**.

We have chosen **PBI-3** nanofibers for further characterization by X-ray diffraction experiments. Both XRD-diffractograms of **PBI-3** crystals formed upon slow cooling from the melt and **PBI-3** nanofibers prepared from the solvent-exchange process show multiple reflections, typical for a crystalline organization of the material (Fig. 4). It can clearly be seen, that the extended 1D self-assembly for the nanofibers is likely dominated by strong  $\pi$ - $\pi$  interactions between the PBI chromophores, as indicated by the sharp reflections in the wide-angle regime between  $25.42^\circ$  and  $26.78^\circ$  corresponding to the typical  $\pi$ - $\pi$  stacking distance of 3.33-3.50 Å. Additionally the  $\pi$ - $\pi$  stacking in the nanofibers is strongly pronounced as compared to crystalline **PBI-3** prepared from the melt. For other amphiphilic **PBIs** with other substitution patterns, for instance, a combination of a swallow-tail alkyl with an OEG swallow-tail substituent or a linear alkyl substituent and an OEG swallow-tail substituent, as introduced in chapter 3, no self-assembly could be observed under the previously described conditions.

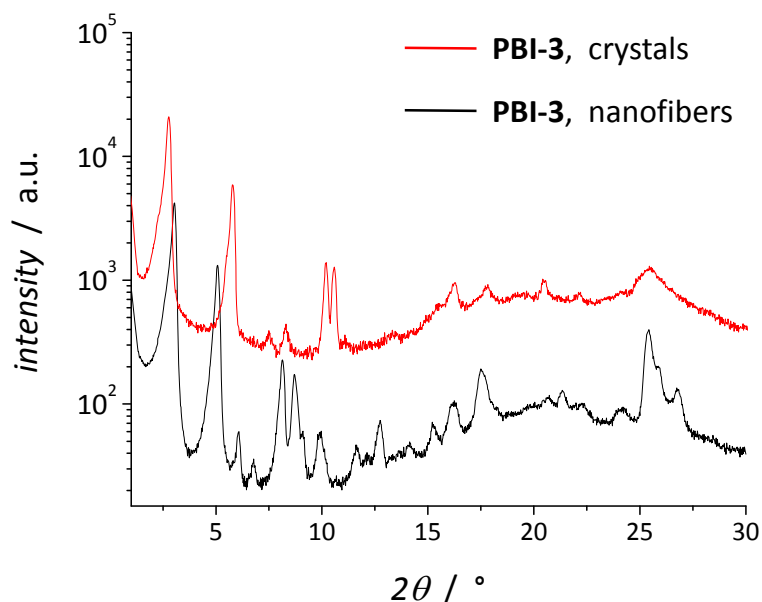


**Figure 4.** XRD diffractograms measured at room temperature of **PBI-3** crystals (red) and **PBI-3** nanofibers formed in 0.25 wt-% EtOH/H<sub>2</sub>O 1:1 v/v solutions (black).

It could be shown here, that amphiphilic PBIs, as **PBI-3** can form interdigitated nanofibrillar structures by solvent-assisted self-assembly. This nanostructured network has a high degree of  $\pi$ - $\pi$  stacking of the chromophores and thus provides charge transport pathways. These amphiphilic derivatives have high chromophore content in the range of 50 %. Nevertheless, for device applications, the self-assembly process has to be conducted at considerably higher concentrations and in presence of suitable donor materials to form an interpenetrating network between both materials. Current investigations are directed towards the investigation of suitable thin film preparation techniques compatible with the slow self-assembly via solvent exchange processing to obtain smooth films of a donor-acceptor network.

**Perylene bisimides for hydrogen-bond directed self-assembly, Typ II**

Symmetrical **PBI-5** was designed with an amide group between the perylene chromophore and a solubilizing alkyl swallow-tail and is thus capable of developing superstructures by intermolecular hydrogen bonding. In contrast we reduced the number of amide bonds to one in unsymmetrical **PBI-6** in order to study the influence of asymmetry on self-organization of these dyes. The self-assembly of symmetrical **PBI-5** was carried out firstly in 0.1 wt-% PhCl/MeOH 95:5 v/v solution. The addition of MeOH was essential to homogeneously dissolve **PBI-5** in hot solution. Figure 5a presents photographs of the self-assembly process of **PBI-5** at different stages. The molecules are molecularly dissolved in hot solution and upon cooling the self-assembly process begins, recognizable by the color change to deep red after 30 minutes. After 12 h a subtle precipitate of **PBI-5** was formed. SEM surface images of a drop-casted and dried sample of this precipitate (Fig. 6a, b) show the formation of long belt-like aggregates with a width between 100 to 350 nm. A completely different self-assembly behaviour was found, when **PBI-5** was doctor bladed from a 1.0 wt-% PhCl/MeOH 95:5 v/v solution onto ITO surface. Here very thin nanowires with a width of ~40 nm can be observed for a dried film in SEM (Fig. 6c, d). These fibrous nanostructures observed for the doctor-bladed film of **PBI-5** with a high chromophore content are very promising for an application in photovoltaic devices. The difference in nanostructure can be explained by the fast drying process of the hot solution upon doctor-blading and thus a fast self-assembly directed by H-bonding. Additionally, the gelation ability of **PBI-5** can be observed at higher concentrations in high-boiling aromatic solvents: for instance **PBI-5** completely dissolves at 140 °C as 2.0 wt-% *o*-DCB solution. The typical “stable-to-inversion test” for gels succeeds after 12 h in *o*-DCB (Fig. 5b). The formed gel is stable over several days.

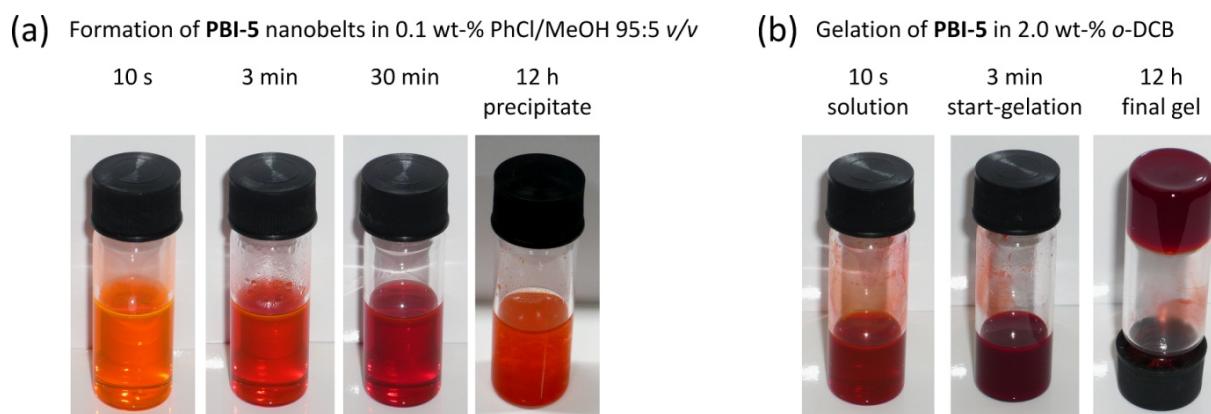


**Figure 5.** (a) Time dependent formation of **PBI-5** nanobelts in 0.1 wt-% PhCl/MeOH 95: 5 v/v solution after 10s, 3 min, 10 min and 12 h. (b) Time dependent gelation process of **PBI-5** in 2.0 wt-% *o*-DCB.

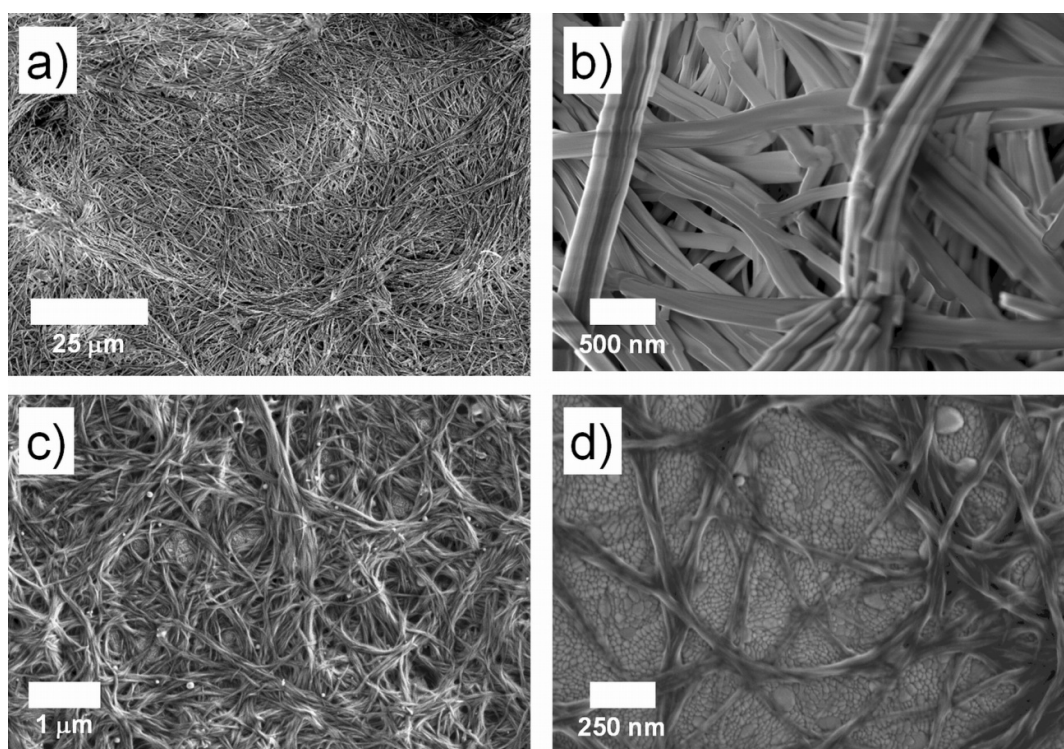


**Figure 6.** SEM surface images of (a, b) nanobelts of **PBI-5** formed in 0.1 wt-% PhCl/MeOH 95:5 v/v solution, (c, d) nanowires of **PBI-5** formed upon doctor-blading a 1.0 wt-% PhCl/MeOH 95:5 v/v solution on ITO. All the structures do not contain any solvent.

It can clearly be seen from the X-ray diffractogram depicted in Figure 7, that the belt-like aggregates of **PBI-5** have a high degree of  $\pi$ - $\pi$  stacking between the perylene moieties. Furthermore, this amide group containing **PBI-5** has an increased chromophore content of 41 % as compared to 26 % for the PBI organogelator used in the organogel/polymer system presented in chapter 7.

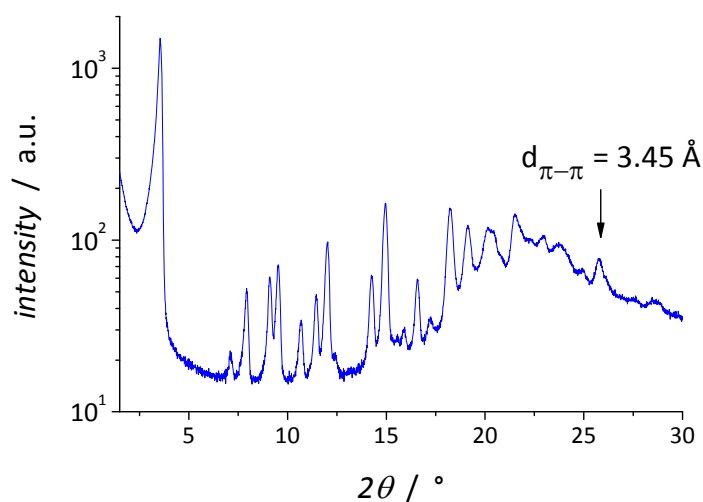


**Figure 7.** XRD diffractogram of **PBI-5** nanofibers formed in 0.1 wt-% PhCl/MeOH 95:5 v/v.

The self-assembly of unsymmetrical **PBI-6** was carried out from 1.0 wt-%  $\text{CHCl}_3/\text{MeOH}$  1:1 v/v solution. Upon drop-casting on ITO surface, flat particulate aggregates with diameters of  $\sim 2.5 \mu\text{m}$  can be observed after the drying process (Fig. 8). In contrast to the fibrous morphology of symmetrical **PBI-5**, the curved morphology observed here, is due to the asymmetry of **PBI-6** with only one amide bond containing *N*-substituent.

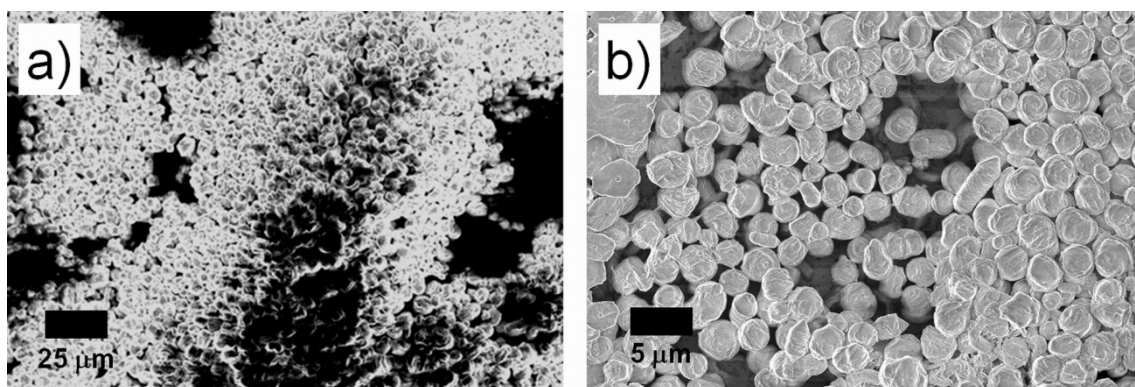


**Figure 8.** SEM surface images of particulate aggregates of **PBI-6** formed upon drop-casting a 1.0 wt-%  $\text{CHCl}_3/\text{MeOH}$  1:1 v/v solution on ITO at different magnifications. All the structures do not contain any solvent.

**EXPERIMENTAL**

The starting materials, perylenetetracarboxylic acid dianhydride **PTCDA**,  $\text{Zn}(\text{OAc})_2$ , triethyleneglycol monomethyl ether, tetraethyleneglycol monomethyl ether, *N*-Boc- $\beta$ -Ala-OH **5**, *N*-Hydroxysuccinimide HOSu, Dicyclohexylcarbodiimide DCC and solvents, were purchased from Merck, Aldrich, Fluka or TCI and used without any further purification. Solvents used for precipitation and column chromatography were distilled under normal atmosphere. Perylene intermediates **2a**, **b**, **c**<sup>12,21</sup> and **4**<sup>12,22,23</sup> were synthesized according to published procedures. Linear 1-bromo-oligoethyleneglycol ethers **1a**, **b** were synthesized according to published procedures.<sup>19</sup>

<sup>1</sup>H- and <sup>13</sup>C-NMR spectra were recorded on a Bruker AC 300 spectrometer (300 MHz and 75 MHz, respectively). Chemical shifts are reported in ppm at room temperature using  $\text{CDCl}_3$  as solvent and tetramethylsilane as internal standard unless indicated otherwise. Abbreviations used for splitting patterns are s = singlet, d = dublett, t = triplet, qui = quintet, m = multiplet. Oligomeric size exclusion chromatography (Oligo-SEC) was used to determine the purity of synthesized perylene bisimides. Oligo-SEC measurements were performed utilizing a Waters 515-HPLC pump with stabilized THF as eluent at a flow rate of 0.5 ml/min. 20  $\mu\text{l}$  of a solution with a concentration of approx. 1 mg/ml were injected into a column setup, which consists of a guard column (Varian; 5 x 0.8 cm; mesopore gel; particle size 3  $\mu\text{m}$ ) and two separation columns (Varian; 30 x 0.8 cm; mesopore gel; particle size 3  $\mu\text{m}$ ). The compounds were monitored with a Waters 486 tunable UV detector at 254 nm and a Waters 410 differential RI detector. Mass spectroscopic (MS) data were obtained from a FINNIGAN MAT 8500 instrument. The thermal degradation was studied using a Mettler Toledo TGA/SDTA 851e with a heating rate of 10  $\text{Kmin}^{-1}$  under  $\text{N}_2$  atmosphere. Differential scanning calorimetry (DSC) was carried out with a Perkin Elmer differential scanning calorimeter (Diamond) with heating and cooling rates of 10 K/min under  $\text{N}_2$  atmosphere. The instrument was calibrated with indium standards before measurements. Phase transitions were also examined by a polarization optical microscope (POM) Nikon Diaphot 300 with a Mettler FP 90 temperature-controlled hot stage. X-ray diffraction measurements were performed on a Huber Guinier Diffraktometer 6000 equipped with a Huber quartz monochromator 611 with  $\text{Cu-K}\alpha_1$ : 1.54051 Å. Self-assembly of **PBIs 1-4** was performed through a solvent exchange processing, in which the molecules were transferred from a “good” solvent (here: ethanol) into a “poor” solvent (here:  $\text{H}_2\text{O}$ ) where the molecules have limited solubility and thus self-assemble into nanostructures via molecular stacking.<sup>14</sup> Such a self-assembly approach takes the advantage of the strong intermolecular  $\pi$ - $\pi$  interactions, which is enhanced in a solvent where the solvophobic interactions are maximized. Briefly, 1 mg of the respective **PBI** derivative was dissolved in 2 mL of hot ethanol (60 °C), followed by addition of 2 mL water via syringe, resulting in ~ 0.25 wt-% EtOH/ $\text{H}_2\text{O}$  1:1 v/v solutions. Samples for SEM were prepared by dropping one drop of the respective solutions on top of ITO substrates or on double sided adhesive carbon discs and sputtered with platinum (2 nm) to improve the conductivity for SEM imaging. The measurements were performed with a LEO 1530 (FE-SEM) with Schottky-field-emission cathode and in-lens detector.

**General Procedure for the Preparation of 1-Bromo-oligoethyleneglycol Ethers 1a, b:**<sup>19</sup>

Triphenylphosphine (24 mmol) was suspended in dry acetonitrile (30 mL) under argon atmosphere at 0 °C. Bromine (24 mmol) was added through a dropping funnel during 45 minutes. The respective oligoethyleneglycol ether (24 mmol) was dissolved in dry acetonitrile (5.0 mL) and added dropwise. The reaction mixture was stirred for 48 h at room temperature. The white precipitate was eliminated by filtration and the solvent was evaporated under reduced pressure. The resulting pasty orange-colored residue was further purified by column chromatography on silica gel with cyclohexane/ethylacetate 1:1 v/v as eluent.

**1-Bromo-triethyleneglycol Monoethyl Ether 1a:** Triethyleneglycol monomethyl ether (10.0 g, 56.1 mmol) was allowed to react according to the general procedure. **1a** was obtained as colorless oil (10.58 g, 78.2 %). <sup>1</sup>H-NMR (300 MHz, CDCl<sub>3</sub>, 298K):  $\delta$  = 1.20 (t, <sup>3</sup>J = 7.0 Hz, 3H, CH<sub>3</sub>), 3.46 (t, <sup>3</sup>J = 6.4 Hz, 2H, Br-CH<sub>2</sub>), 3.52 (q, <sup>3</sup>J = 7.0 Hz, 2H, OCH<sub>2</sub>), 3.55-3.69 (m, 8H, OCH<sub>2</sub>), 3.80 (t, <sup>3</sup>J = 6.4 Hz, 2H, OCH<sub>2</sub>) ppm.

**1-Bromo-tetraethyleneglycol Monomethyl Ether 1b:** Tetraethyleneglycol monomethyl ether (5.0 g, 24 mmol) was allowed to react according to the general procedure. **1b** was obtained as colorless oil (4.03 g, 61.9 %). <sup>1</sup>H-NMR (300 MHz, CDCl<sub>3</sub>, 298K):  $\delta$  = 3.37 (s, 3H, OCH<sub>3</sub>), 3.46 (t, <sup>3</sup>J = 6.3 Hz, 2H, Br-CH<sub>2</sub>), 3.51-3.69 (m, 12H, 6OCH<sub>2</sub>), 3.80 (t, <sup>3</sup>J = 6.3 Hz, 2H, OCH<sub>2</sub>).

**N-Boc-protected 3-amino-N-(1-heptyloctyl)propanamide N-Boc- $\beta$ -Ala-NHCH(C<sub>7</sub>H<sub>15</sub>)<sub>2</sub> 6:**<sup>20</sup>

A solution of *N*-Boc- $\beta$ -Ala-OH **5** (3.78 g, 20.0 mmol) and *N*-Hydroxysuccinimide HOSu (2.30 g, 20.0 mmol) in 200 mL of CH<sub>2</sub>Cl<sub>2</sub>/1,4-dioxane 2:1 v/v was cooled in an ice-water bath. Dicyclohexylcarbodiimide DCC (4.54 g, 22.0 mmol) was added and the mixture was stirred at room temperature for 1h. Then 8-Heptyloctylamine (6.82 g, 30.0 mmol) was added to the resulting solution. After 6 h of stirring at room temperature, the precipitate was removed by filtration and washed with ethylacetate. The organic layers were combined and washed sequentially with 10% aqueous citric acid and saturated aqueous NaHCO<sub>3</sub>. The organic layer was dried over MgSO<sub>4</sub> and concentrated in vacuo. The residue was taken up in 250 mL hot hexane/CH<sub>2</sub>Cl<sub>2</sub>/ethylacetate 4:5:1 v/v, filtrated to remove impurities and stored at 0 °C to crystallize colorless *N*-Boc- $\beta$ -Ala-NHCH(C<sub>7</sub>H<sub>15</sub>)<sub>2</sub> **6** (5.68 g, 71.3 %). <sup>1</sup>H-NMR (300 MHz, CDCl<sub>3</sub>, 298K):  $\delta$  = 0.87 (t, <sup>3</sup>J = 6.6 Hz, 6H, 2CH<sub>3</sub>), 1.14-1.36 (m, 24H, 12CH<sub>2</sub>), 1.42 (s, 9H, <sup>t</sup>Bu), 2.38 (t, <sup>3</sup>J = 6.0 Hz, 2H, COCH<sub>2</sub>), 3.39 (dt, <sup>3</sup>J = 6.0 Hz, <sup>3</sup>J = 6.0 Hz, 2H, COCH<sub>2</sub>), 3.80-3.98 (m, 1H, CONH-CH), 5.09-5.22 (m, 1H, O<sub>2</sub>C-NH), 5.32 (d, 1H, OC-NH) ppm.

**3-amino-N-(1-heptyloctyl)propanamide NH<sub>2</sub>- $\beta$ -Ala-NHCH(C<sub>7</sub>H<sub>15</sub>)<sub>2</sub> 3:** A solution of *N*-Boc- $\beta$ -Ala-NHCH(C<sub>7</sub>H<sub>15</sub>)<sub>2</sub> **6** (1.99 g, 5.0 mmol) in cool TFA (7.0 mL) was stirred at room temperature for 20 minutes. After dilution with ethyl acetate (15.0 mL), TFA was removed by streaming N<sub>2</sub>. After removal of TFA and removal of solvent, the ammonium salt was dried in vacuo and was obtained

as colorless solid, which was taken up in MeOH (40 mL) and treated with powdered NaOH (1.80 g, 45 mmol). After stirring at 45 °C for 30 minutes, the solution was diluted with H<sub>2</sub>O (60 mL) and extracted with ethyl acetate (3 x 100 mL). The combined organic layers were washed with brine (until pH = 7), dried over Mg<sub>2</sub>SO<sub>4</sub>. After removal of solvent in vacuo, H<sub>2</sub>N-β-Ala-NHCH(C<sub>7</sub>H<sub>15</sub>)<sub>2</sub> **3** was obtained as colorless solid (746 mg, 80.5 %). <sup>1</sup>H-NMR (300 MHz, CDCl<sub>3</sub>, 298K): δ = 0.87 (t, <sup>3</sup>J = 6.6 Hz, 6H, 2CH<sub>3</sub>), 1.14-1.53 (m, 24H, 12CH<sub>2</sub>), 2.13 (s, 2H, NH<sub>2</sub>), 2.33 (t, <sup>3</sup>J = 5.9 Hz, 2H, COCH<sub>2</sub>), 3.02 (t, <sup>3</sup>J = 5.9 Hz, 2H, N-CH<sub>2</sub>), 3.79-3.99 (m, 1H, N-CH), 6.43 (d, <sup>3</sup>J = 8.9 Hz, 1H, CONH) ppm.

**General Procedure for the Preparation of unsymmetrical Perylene-3,4,9,10-tetracarboxylic Bisimides PBI-1 to 4 via nucleophilic substitution:**<sup>12</sup>

To a suspension of the respective *N*-(1-swallow-tail)-perylene-3,4,9,10-tetracarboxylic-3,4-anhydride-9,10-imide **2** (1.0 mmol) in dry DMF (30 mL) was added NaH (1.2 mmol), as 60 % suspension in mineral oil, at 0 °C. The mixture was stirred and allowed to reach r.t., then the respective bromide **1a, b** (2.5 mmol) was added and the solution was heated to 80 °C. After 48 h, the reaction was cooled to room temperature and quenched by addition of saturated NH<sub>4</sub>Cl solution (2.5 mL). Purification procedures of the respective derivatives are described in the corresponding compound section.

***N*-(1-hexylpentyl)-*N'*-(2-(2-(2-(2-ethoxyl)ethoxyl)ethoxyl)ethyl)-perylene-3,4,9,10-**

**tetracarboxylic Bisimide PBI-1:** *N*-(1-hexylpentyl)-perylene-3,4,9,10-tetracarboxylic bisimide **2a** (871 mg, 1.6 mmol) and 1-Bromo-triethylglycol monomethyl ether **1a** (965 mg, 4.0 mmol) were allowed to react according to the general procedure for 48 h. After cooling to r.t., the product was precipitated in 300 mL H<sub>2</sub>O/MeOH 3:1 v/v. After standing over night, the precipitate was collected by filtration, washed with H<sub>2</sub>O, then MeOH and dried at 60 °C in vacuum. The crude product was further purified by column chromatography on silica flash-gel (cyclohexane/ethylacetate 1:1 v/v). The final product was freeze-dried from benzene and was obtained as red solid (750 mg, 66.5 %). M.p. 218.9 °C. Calcd. for C<sub>43</sub>H<sub>48</sub>N<sub>2</sub>O<sub>7</sub>: C 73.27, H 6.86, N 3.97. Found: C 72.98, H 6.71, N 3.79. EI-MS (70 eV): *m/z* 704.7 ([M<sup>+</sup>], 100 %). HR-EI MS: *m/z* calcd. 704.34615 for C<sub>43</sub>H<sub>48</sub>N<sub>2</sub>O<sub>7</sub>. Found 704.34765. <sup>1</sup>H-NMR (300 MHz, CDCl<sub>3</sub>, 298K): δ = 0.84 (t, <sup>3</sup>J = 6.5 Hz, 6H, 2CH<sub>3</sub>), 1.15 (t, <sup>3</sup>J = 7.0 Hz, 3H, CH<sub>3</sub>), 1.20-1.42 (m, 12H, 6CH<sub>2</sub>), 1.79-1.97 (m, 2H, αCH<sub>2</sub>), 2.15-2.35 (m, 2H, αCH<sub>2</sub>), 3.46 (q, <sup>3</sup>J = 7.0 Hz, 2H, OCH<sub>2</sub>), 3.48-3.55 (m, 2H, OCH<sub>2</sub>), 3.56-3.68 (m, 4H, OCH<sub>2</sub>), 3.70-3.77 (m, 2H, OCH<sub>2</sub>), 3.86 (t, <sup>3</sup>J = 5.9 Hz, 2H, OCH<sub>2</sub>), 4.46 (t, <sup>3</sup>J = 5.9 Hz, 2H, N-CH<sub>2</sub>), 5.11-5.26 (m, 1H, N-CH), 8.41-8.75 (m, 8H, 8ArH) ppm. <sup>13</sup>C-NMR (75 MHz, CDCl<sub>3</sub>, 298K): δ = 14.46 (2C, CH<sub>3</sub>), 15.51 (1C, CH<sub>3</sub>), 22.97, 27.07, 32.17, 32.71 (8C, CH<sub>2</sub>), 39.60 (1C, N-CH<sub>2</sub>), 55.21 (1C, N-CH), 66.96, 68.24, 70.16, 70.47, 71.03 (6C, OCH<sub>2</sub>), 123.07, 123.23, 126.36, 129.44, 129.69, 131.41, 134.31, 134.63 (20C, C<sub>Ar</sub>), 163.47 (4C, CONR) ppm.

***N*-(1-heptyloctyl)-*N'*-(2-(2-(2-(2-ethoxy)ethoxy)ethoxy)ethyl)-perylene-3,4,9,10-tetracarboxylic Bisimide PBI-2:** *N*-(1-heptyloctyl)-perylene-3,4,9,10-tetracarboxylic bisimide **2b** (961 mg, 1.6 mmol) and 1-Bromo-triethylenglycol monomethyl ether **1a** (965 mg, 4.0 mmol) were allowed to react according to the general procedure for 48 h. After cooling to r.t., the product was precipitated in 300 mL H<sub>2</sub>O/MeOH 3:1 v/v. After standing over night, the precipitate was collected by filtration, washed with H<sub>2</sub>O, then MeOH and dried at 60 °C in vacuum. The crude product was further purified by column chromatography on silica flash-gel (cyclohexane/ethylacetate 1:1 to 1:3 v/v). The final product was freeze-dried from benzene and was obtained as red solid (783 mg, 64.3 %). M.p. 188.1 °C. Calcd. for C<sub>47</sub>H<sub>56</sub>N<sub>2</sub>O<sub>7</sub>: C 74.18, H 7.42, N 3.68. Found: C 73.57, H 7.34, N 3.46. EI-MS (70 eV): *m/z* 760.8 ([M<sup>+</sup>], 93.4 %). HR-EI MS: *m/z* calcd. 760.40875 for C<sub>47</sub>H<sub>56</sub>N<sub>2</sub>O<sub>7</sub>. Found 760.40810. <sup>1</sup>H-NMR (300 MHz, CDCl<sub>3</sub>, 298K): δ = 0.82 (t, <sup>3</sup>J = 6.7 Hz, 6H, 2CH<sub>3</sub>), 1.15 (t, <sup>3</sup>J = 7.0 Hz, 3H, CH<sub>3</sub>), 1.16-1.39 (m, 20H, 10CH<sub>2</sub>), 1.78-1.96 (m, 2H, αCH<sub>2</sub>), 2.14-2.34 (m, 2H, αCH<sub>2</sub>), 3.46 (q, <sup>3</sup>J = 7.0 Hz, 2H, OCH<sub>2</sub>), 3.48-3.54 (m, 2H, OCH<sub>2</sub>), 3.56-3.68 (m, 4H, OCH<sub>2</sub>), 3.70-3.77 (m, 2H, OCH<sub>2</sub>), 3.86 (t, <sup>3</sup>J = 5.9 Hz, 2H, OCH<sub>2</sub>), 4.46 (t, <sup>3</sup>J = 5.9 Hz, 2H, N-CH<sub>2</sub>), 5.11-5.26 (m, 1H, N-CH), 8.46-8.72 (m, 8H, 8ArH) ppm. <sup>13</sup>C-NMR (75 MHz, CDCl<sub>3</sub>, 298K): δ = 14.40 (2C, CH<sub>3</sub>), 15.45 (1C, CH<sub>3</sub>), 22.95, 27.36, 29.57, 29.87, 32.15, 32.71 (12C, CH<sub>2</sub>), 39.59 (1C, N-CH<sub>2</sub>), 55.17 (1C, N-CH), 66.92, 68.22, 70.11, 70.45, 70.97 (6C, OCH<sub>2</sub>), 123.09, 123.25, 126.39, 126.44, 129.48, 129.70, 131.47, 134.35, 134.71 (20C, C<sub>Ar</sub>), 163.51 (4C, CONR) ppm.

***N*-(1-heptyloctyl)-*N'*-(1-(2-(2-(2-(2-methoxy)ethoxy)ethoxy)ethoxy)ethyl)-perylene-3,4,9,10-tetracarboxylic Bisimide PBI-3:** *N*-(1-heptyloctyl)-perylene-3,4,9,10-tetracarboxylic bisimide **2a** (901 mg, 1.5 mmol) and 1-Bromo-tetraethyleneglycol monomethyl ether **1b** (1018 mg, 3.75 mmol) were allowed to react according to the general procedure for 48 h. After cooling to r.t., the product was precipitated in 300 mL H<sub>2</sub>O/MeOH 3:1 v/v. After standing over night, the precipitate was collected by filtration, washed with H<sub>2</sub>O, then MeOH and dried at 60 °C in vacuum. The crude product was further purified by column chromatography on silica flash-gel (cyclohexane/ethylacetate 1:1 to 1:3 v/v). The final product was freeze-dried from benzene and was obtained as red solid (701 mg, 59.1 %). M.p. 167.9 °C. Calcd. for C<sub>48</sub>H<sub>58</sub>N<sub>2</sub>O<sub>8</sub>: C 72.89, H 7.39, N 3.54. Found: C 71.87, H 8.19, N 3.48. EI-MS (70 eV): *m/z* 790.9 ([M<sup>+</sup>], 71.4 %). HR-EI MS: *m/z* calcd. 790.41932 for C<sub>47</sub>H<sub>56</sub>N<sub>2</sub>O<sub>7</sub>. Found 790.42150. <sup>1</sup>H-NMR (300 MHz, CDCl<sub>3</sub>, 298K): δ = 0.82 (t, <sup>3</sup>J = 6.7 Hz, 6H, 2CH<sub>3</sub>), 1.12-1.42 (m, 20H, 10CH<sub>2</sub>), 1.78-1.96 (m, 2H, αCH<sub>2</sub>), 2.15-2.34 (m, 2H, αCH<sub>2</sub>), 3.34 (s, 3H, OCH<sub>3</sub>), 3.48-3.54 (m, 2H, OCH<sub>2</sub>), 3.54-3.67 (m, 8H, OCH<sub>2</sub>), 3.69-3.76 (m, 2H, OCH<sub>2</sub>), 3.86 (t, <sup>3</sup>J = 5.9 Hz, 2H, OCH<sub>2</sub>), 4.46 (t, <sup>3</sup>J = 5.9 Hz, 2H, N-CH<sub>2</sub>), 5.09-5.27 (m, 1H, N-CH), 8.50-8.72 (m, 8H, 8ArH) ppm. <sup>13</sup>C-NMR (75 MHz, CDCl<sub>3</sub>, 298K): δ = 14.46 (2C, CH<sub>3</sub>), 23.00, 27.41, 29.63, 29.93, 32.20, 32.75 (12C, CH<sub>2</sub>), 39.61 (1C, N-CH<sub>2</sub>), 55.22 (1C, N-CH), 59.39 (1C, OCH<sub>3</sub>), 68.25, 70.44, 70.86, 70.94, 71.02, 72.28 (7C, CH<sub>2</sub>), 123.13, 126.42, 126.46, 129.50, 129.73, 131.50, 134.37, 134.73 (20C, C<sub>Ar</sub>), 163.53 (4C, CONR) ppm.

***N*-(1-undecyldodecyl)-*N'*-(1-(2-(2-(2-(2-methoxy)ethoxy)ethoxy)ethoxy)ethyl)-perylene-3,4,9,10-tetracarboxylic Bisimide PBI-4:** *N*-(1-undecyldodecyl)-perylene-3,4,9,10-tetracarboxylic bisimide **2c** (901 mg, 1.5 mmol) and 1-Bromo-tetraethyleneglycol monomethyl ether **1b** (1018 mg, 3.75 mmol) were allowed to react according to the general procedure for 48 h. After cooling to

r.t., the product was precipitated in 300 mL 2N HCl/MeOH 3:1 v/v. After standing over night, the precipitate was collected by filtration, washed with H<sub>2</sub>O, then MeOH and dried at 60 °C in vacuum. The crude product was further purified by column chromatography on silica flash-gel (THF/hexane 1:1 v/v). The final product was freeze-dried from benzene and was obtained as red solid (631 mg, 53.7 %). M.p. 151.8 °C. Calcd. for C<sub>56</sub>H<sub>74</sub>N<sub>2</sub>O<sub>8</sub>: C 74.47, H 8.26, N 3.10. Found: C 74.10, H 8.90, N 3.13. EI-MS (70 eV): *m/z* 902.3 ([M<sup>+</sup>], 87.5 %). HR-EI MS: *m/z* calcd. 902.54452 for C<sub>56</sub>H<sub>74</sub>N<sub>2</sub>O<sub>8</sub>. Found 902.54590. <sup>1</sup>H-NMR (300 MHz, CDCl<sub>3</sub>, 298K): δ = 0.84 (t, *J* = 6.7 Hz, 6H, 2CH<sub>3</sub>), 1.07-1.43 (m, 36H, 18CH<sub>2</sub>), 1.78-1.97 (m, 2H, αCH<sub>2</sub>), 2.15-2.35 (m, 2H, αCH<sub>2</sub>), 3.34 (s, 3H, OCH<sub>3</sub>), 3.47-3.54 (m, 2H, OCH<sub>2</sub>), 3.54-3.67 (m, 8H, OCH<sub>2</sub>), 3.69-3.76 (m, 2H, OCH<sub>2</sub>), 3.86 (t, *J* = 5.9 Hz, 2H, OCH<sub>2</sub>), 4.47 (t, *J* = 5.9 Hz, 2H, N-CH<sub>2</sub>), 5.10-5.26 (m, 1H, N-CH), 8.52-8.74 (m, 8H, 8ArH) ppm. <sup>13</sup>C-NMR (75 MHz, CDCl<sub>3</sub>, 298K): δ = 14.48 (2C, CH<sub>3</sub>), 23.04, 27.41, 29.71, 29.96, 30.00, 32.28, 32.74 (20C, CH<sub>2</sub>), 39.61 (1C, N-CH<sub>2</sub>), 55.22 (1C, N-CH), 59.39 (1C, OCH<sub>3</sub>), 68.25, 70.44, 70.86, 70.94, 71.03, 72.28 (7C, OCH<sub>2</sub>), 123.07, 123.24, 131.41, 126.36, 129.44, 129.69, 134.31, 134.63 (20C, C<sub>Ar</sub>), 163.47 (4C, CONR) ppm.

***N,N*'-Di(1-(1-heptyloctyl)propanamide)-perylene-3,4,9,10-tetracarboxylic Bisimide PBI-5:**

A mixture of perylene-3,4,9,10-tetracarboxylic dianhydride **PTCDA** (196 mg, 0.5 mmol), Zn(OAc)<sub>2</sub> (194 mg, 1.05 mmol), imidazole (5.0 g) *o*-DCB (1.2 mL) and H<sub>2</sub>N-β-Ala-NH-CH(C<sub>7</sub>H<sub>15</sub>)<sub>2</sub> **3** (478 mg, 1.6 mmol) was vigorously stirred at 140 °C for 24 h. After cooling to r.t. the mixture was dissolved in 2 L hot CHCl<sub>3</sub> and filtered over a P3 glass-frit. After cooling and standing over night, the formed precipitate was filtered and soxhlet extracted with MeOH, followed by THF and then chlorobenzene. The precipitate of the chlorobenzene fraction was recrystallized from a chlorobenzene/MeOH 95:5 v/v solution (85 mg, 19.0 %). M.p. > T<sub>dec</sub>. <sup>1</sup>H-NMR (300 MHz, *o*-DCB-d<sub>4</sub>, 393K): δ = 1.04-1.28 (m, 12H, 4CH<sub>3</sub>), 1.41-1.97 (m, 48H, 24CH<sub>2</sub>), 3.01-3.22 (m, 4H, COCH<sub>2</sub>), 4.24-4.41 (m, 2H, N-CH), 4.71-4.92 (m, 4H, N-CH<sub>2</sub>), 6.18-6.36 (m, 2H, NH), 8.13-8.33 (m, 4H, 4H<sub>Ar</sub>), 8.42-8.62 (m, 4H, 4H<sub>Ar</sub>) ppm.

***N*-(1-heptyloctyl)-*N*'-(1-(1-heptyloctyl)propanamide)-perylene-3,4,9,10-tetracarboxylic**

**Bisimide PBI-6:** A mixture of *N*-(1-heptyloctyl)-perylene-3,4,9,10-tetracarboxylic-3,4-anhydride-9,10-imide **4**<sup>12</sup> (241 mg, 0.4 mmol), Zn(OAc)<sub>2</sub> (185 mg, 0.84 mmol) in dry DMAc (3.0 mL) and H<sub>2</sub>N-β-Ala-NH-CH(C<sub>7</sub>H<sub>15</sub>)<sub>2</sub> **3** (215 mg, 0.72 mmol) was stirred in a microwave pressure reactor for 30 Min at 140 °C and 250 Watt. After cooling to r.t. the mixture was dissolved in minimum amount of THF and precipitated in 120 mL H<sub>2</sub>O/MeOH 2:1 v/v. After standing over night, the precipitate was collected by filtration, washed with H<sub>2</sub>O, then MeOH and dried at 60 °C in vacuum. The crude product was further purified by column chromatography on silica flash-gel (CHCl<sub>3</sub>/MeOH 95:5 v/v). The final product was freeze-dried from benzene and was obtained as red solid (290 mg, 82.2 %). M.p. 183.4 °C. <sup>1</sup>H-NMR (300 MHz, CDCl<sub>3</sub>, 298K): δ = 0.79 (t, *J* = 6.9 Hz, 6H, 2CH<sub>3</sub>), 0.83 (t, *J* = 6.3 Hz, 6H, 2CH<sub>3</sub>), 1.08-1.50 (m, 44H, 22CH<sub>2</sub>), 1.77-1.97 (m, 2H, αCH<sub>2</sub>), 2.14-2.34 (m, 2H, αCH<sub>2</sub>), 2.76 (t, *J* = 7.1 Hz, 2H, COCH<sub>2</sub>), 3.81-3.99 (m, 1H, CONH-CH), 4.52 (t, *J* = 7.1 Hz, 2H, N-CH<sub>2</sub>), 5.10-5.25 (m, 1H, N-CH), 5.73 (d, *J* = 9.0 Hz, 1H, NH), 8.40-8.72 (m, 8H, 8H<sub>Ar</sub>) ppm.

**BIBLIOGRAPHY**

- (1) Lehn, J.-M. *PNAS* **2002**, *99*, 4763-4768.
- (2) Whitesides, G. M.; Mathias, J. P.; Seto, C. T. *Science* **1991**, *254*, 1312-1319.
- (3) Steed, J. W.; Atwood, J. L. *Supramolecular Chemistry*; 2 ed.; Wiley VCH: Weinheim, 2009.
- (4) Hoeben, F. J. M.; Jonkheijm, P.; Meijer, E. W.; Schenning, A. P. H. J. *Chem. Rev.* **2005**, *105*, 1491-1546.
- (5) Meijer, E. W.; Schenning, A. P. H. J. *Nature* **2002**, *419*, 353-354.
- (6) Simpson, C. D.; Wu, J.; Watson, M. D.; Müllen, K. *J. Mater. Chem.* **2004**, *14*, 494-504.
- (7) Langhals, H. *Helv. Chim. Acta* **2005**, *88*, 1309-1343.
- (8) Würthner, F. *Chem. Commun.* **2004**, 1564-1579.
- (9) Ghosh, S.; Li, X.-Q.; Stepanenko, V.; Würthner, F. *Chem. Eur. J.* **2008**, *14*, 11343-11357.
- (10) Würthner, F.; Bauer, C.; Stepanenko, V.; Yagai, S. *Adv. Mater.* **2008**, *20*, 1695-1698.
- (11) Wicklein, A.; Kohn, P.; Ghazaryan, L.; Thurn-Albrecht, T.; Thelakkat, M. *Chem. Commun.* **2010**, *46*, 2328-2330.
- (12) Wicklein, A.; Lang, A.; Muth, M.; Thelakkat, M. *J. Am. Chem. Soc.* **2009**, *131*, 14442-14453.
- (13) Würthner, F.; Thalacker, C.; Diele, S.; Tschierske, C. *Chem. Eur. J.* **2001**, *7*, 2245-2253.
- (14) Che, Y.; Datar, A.; Balakrishnan, K.; Zang, L. *J. Am. Chem. Soc.* **2007**, *129*, 7234-7235.
- (15) Yang, X.; Xu, X.; Ji, H.-F. *J. Phys. Chem. B* **2008**, *112*, 7196-7202.
- (16) Balakrishnan, K.; Datar, A.; Oitker, R.; Chen, H.; Zuo, J.; Zang, L. *J. Am. Chem. Soc.* **2005**, *127*, 10496-10497.
- (17) Briseno, A. L.; Mannsfeld, S. C. B.; Reese, C.; Hancock, J. M.; Xiong, Y.; Jenekhe, S. A.; Bao, Z.; Xia, Y. *Nano Lett.* **2007**, *7*, 2847-2853.
- (18) Wicklein, A.; Ghosh, S.; Sommer, M.; Würthner, F.; Thelakkat, M. *ACS Nano* **2009**, *3*, 1107-1114.
- (19) Biron, E.; Otis, F.; Meillon, J.-C.; Robitaille, M.; Lamothe, J.; Van Hove, P.; Cormier, M.-E.; Voyer, N. *Bioorg. Med. Chem.* **2004**, *12*, 1279-1290.
- (20) Tsu, H.; Chen, X.; Chen, C.-T.; Lee, S.-J.; Chang, C.-N.; Kao, K.-H.; Coumar, M. S.; Yeh, Y.-T.; Chien, C.-H.; Wang, H.-S.; Lin, K.-T.; Chang, Y.-Y.; Wu, S.-H.; Chen, Y.-S.; Lu, I. L.; Wu, S.-Y.; Tsai, T.-Y.; Chen, W.-C.; Hsieh, H.-P.; Chao, Y.-S.; Jiaang, W.-T. *J. Med. Chem.* **2006**, *49*, 373-380.
- (21) Langhals, H.; Saulich, S. *Chem. Eur. J.* **2002**, *8*, 5630-5643.
- (22) Kaiser, H.; Lindner, J.; Langhals, H. *Chem. Ber.* **1991**, *124*, 529-35.
- (23) Wescott, L. D.; Mattern, D. L. *J. Org. Chem.* **2003**, *68*, 10058-10066.



## **LIST OF PUBLICATIONS**

1. R. Schobert, **A. Wicklein**:  
Short syntheses of (-)-(R)-pyrrolam A and (1S)-1-hydroxyindolizidin-3-one,  
*Synthesis*, **2007**, *10*, 1499-1502.
2. **A. Wicklein**, S. Ghosh, M. Sommer, F. Würthner, M. Thelakkat:  
Self-Assembly of Semiconductor Organogelator Nanowires for Photoinduced Charge  
Separation,  
*ACS Nano*, **2009**, *3* (5), 1107-1114.
3. **A. Wicklein**, A. Lang, M. Muth, M. Thelakkat:  
Swallow-Tail Substituted Liquid Crystalline Perylene Bisimides: Synthesis and Thermotropic  
Properties,  
*Journal of the American Chemical Society*, **2009**, *131* (40), 14442-14453.
4. **A. Wicklein**, P. Kohn, L. Ghazaryan, T. Thurn-Albrecht, M. Thelakkat:  
Synthesis and Structure Elucidation of Discotic Liquid Crystalline Perylene Imide  
Benzimidazole,  
*Chemical Communications*, **2010**, *46*, 2328-2330.
5. **A. Wicklein**, M. Muth, M. Thelakkat:  
Room Temperature Liquid Crystalline Perylene Diester Benzimidazoles with Extended  
Absorption,  
*Journal of Materials Chemistry*, DOI:10.1039/C0JM01626H.

---

*Die Natur gibt sich nicht einem jeden.  
Sie erweist sich vielmehr gegen viele  
wie ein neckisches junges Mädchen,  
das uns durch tausend Reize anlockt,  
aber in dem Augenblick, wo wir es zu  
fassen und zu besitzen glauben,  
unseren Armen ent schlüpft.*

(Gespräche mit Goethe, 1831)

## **DANKSAGUNG**

Ich möchte mich bei allen herzlichst bedanken, die auf vielfältige Art und Weise zum Gelingen dieser Arbeit beigetragen haben.

Ein besonderer Dank gilt meinem Doktorvater, Prof. Dr. Mukundan Thelakkat, für die Möglichkeit, auf einem sehr spannenden Themengebiet zu promovieren und unter seiner Leitung vollkommen frei forschen zu dürfen. Neben stetiger Diskussionsbereitschaft und vielen hilfreichen Anregungen bedanke ich mich speziell für einen sehr angenehmen Umgang im Miteinander sowie für die hervorragende und motivierende Betreuung, welche in dieser Form sicherlich nicht selbstverständlich ist. Die Möglichkeit zur Teilnahme an nationalen und internationalen Fachtagungen sowie der Forschungsaufenthalt in England waren eine große Bereicherung.

Prof. Dr. Hans-Werner Schmidt danke ich für die Bereitstellung eines sehr gut ausgestatteten Laborplatzes und für die Möglichkeit an seinem Lehrstuhl zu arbeiten.

Bei Prof. Dr. Neil Greenham bedanke ich mich für die Gelegenheit, 3 Monate in der Optoelectronics Group am Cavendish Laboratory in Cambridge verbringen zu dürfen.

Vielen Dank auch an alle Kooperationspartner für Messungen, fachliche Diskussionen und der Bereitstellung von Materialien. Prof. Dr. Frank Würthner (Universität Würzburg) und Dr. Suhrit Ghosh danke ich für die interessante Zusammenarbeit auf dem Gebiet der PBI-Organogelatoren. Prof. Dr. Thomas Thurn-Albrecht (Universität Halle-Wittenberg), Dr. Peter Kohn und Lilit Ghazaryan gebührt Dank für die Röntgenstreu-Experimente und die Diskussionen zum PIBI. Des Weiteren danke ich Dr. Devrim Atilla (Gebze Institute of Technology) für die Bereitstellung der CuPc's und die Diskussionen zu den PBI/CuPc Blends. Bei Anne Horn und Markus Hund (PC I) möchte ich mich für die AFM Aufnahmen bedanken. Dank gilt auch Melanie Pretzl (PC I) für die zahlreichen Untersuchungen an AW87.

Allen aktuellen und ehemaligen Mitarbeitern der MCI sage ich ein riesen Dankeschön für die allgegenwärtige Hilfsbereitschaft, die Unterstützung in fachlichen Angelegenheiten und noch viel mehr für die tolle Arbeitsatmosphäre und die lustige Zeit in unserer Gruppe (auch neben der Chemie) während der letzten Jahre. Danke vor allem an diejenigen, welche für mich relevante Messgeräte betreuten oder Messungen durchgeführt haben. Andreas Timme gilt Dank für die Einweisung und die Unterstützung bei der Betreuung der Guinier-Kamera, Michael Rothmann und Andreas Küst für die Unterstützung in Computerfragen, Benjamin Gössler und Martina Heider für die Einweisung am REM. Für die Unterstützung bei organisatorischen Angelegenheiten bedanke ich mich bei Petra Weiß und Gabriele Kassler.

Ein besonderes Dankeschön an meine Laborkollegin Helga Wietasch für ein unterhaltsames Klima in 583, das Vogelhaus, den Schnupperkurs im Golfen und die tatkräftige Unterstützung bei vielen Synthesen der „roten Seuche“.

## *Danksagung*

---

Danke auch an alle weiteren Mitglieder der AFuPo: Andreas Lang (Danke für den PEG-Schwabenschwanz, das viele Korrekturlesen von Manuskripten, das Bombardement mit flotten Sprüchen und die Hilfe beim Schleppen der Gasflaschen), Mathis-Andreas Muth (für die schönen Ergebnisse unserer gemeinsamen Forschung), Sebastián Maria (für den Urlaub in Besse sur Issole), Ruth Lohwasser (für die MALDI-TOF Messungen), Katja Willinger, Johannes Brendel, Anne Neubig, Michael Sommer (für das pvDMTPD) und Peter Bauer (für die Synthesediskussionen) für fachliche sowie moralische Unterstützung und vieler gemeinsamer Unternehmungen, wie z.B. Kochabende beim „Meister“.

Neben allem Fachlichen möchte ich mich ebenso bei all meinen Studienfreunden für unsere vielen gemeinsamen Erlebnisse und für die freundschaftliche Unterstützung ganz herzlich bedanken.

Bertram, Felix, Mike, Marc, Markus, Sandra, Tine, Florian, Dominik, Roland, Andreas, Kristina und Eva ohne euch wäre die Zeit in und um Bayreuth doch bei Weitem nicht so bunt gewesen!

Danke auch an alle Freunde in der Chemiker Spaß Gesellschaft für die tolle Gemeinschaft und die vielen Aktivitäten.

Herzlichen Dank an meine lieben Eltern, die mich auf jede erdenkliche Art und Weise unterstützt haben und mir während des Studiums und meiner Doktorarbeit den nötigen Rückhalt gegeben haben.

Und zuletzt Danke ich dir, Corinna, für die unermüdliche Unterstützung und dein Verständnis, in allen Lebenslagen, die notwendige Ablenkung und unseren gemeinsamen Weg.

## **ERKLÄRUNG**

Hiermit erkläre ich, dass ich die vorliegende Arbeit selbstständig verfasst und keine anderen als die von mir angegebenen Quellen und Hilfsmittel verwendet habe.

Ferner erkläre ich, dass ich weder anderweitig mit oder ohne Erfolg versucht habe, diese Dissertation einzureichen, noch eine gleichartige Doktorprüfung an einer anderen Hochschule endgültig nicht bestanden habe.

Bayreuth, den

André Wicklein